SYNTHESIS AND CHARACTERIZATION OF ZnO-CELLULOSE NANOCOMPOSITE (ZnO-CNF) FOR THE PHOTOCATALYTIC DEGRADATION OF ORGANIC DYE

A THESIS SUBMITTED IN PARTIAL FULFILLMENT OF THE REQUIREMENTS FOR THE DEGREE OF DOCTOR OF PHILOSOPHY

JYOTISHMA NATH

MZU REGISTRATION NO.: 1700078

Ph.D. REGISTRATION NO.: MZU/Ph.D./1405 of 14.08.2019

DEPARTMENT OF BOTANY

SCHOOL OF LIFE SCIENCES

DECEMBER, 2024

SYNTHESIS AND CHARACTERIZATION OF ZnO-CELLULOSE NANOCOMPOSITE (ZnO-CNF) FOR THE PHOTOCALYTIC DEGRADATION OF ORGANIC DYE

BY

JYOTISHMA NATH

DEPARTMENT OF BOTANY

Supervisor

Dr. SURYA KANT MEHTA

Submitted

In partial fulfillment of the requirement of the Degree of Doctor of Philosophy in Botany of Mizoram University, Aizawl

MIZORAM UNIVERSITY
MIZORAM: AIZAWL - 796 004

Botany Department

Dr. S. K. MEHTA
Professor

Post Box No. 190
Gram: MZU
Phone: 0389-2330733
Fax: 0389-2330532
Email: skmehta@mzu.edu.in

CERTIFICATE

This is to certify that **Miss Jyotishma Nath,** Registration No. **MZU/Ph.D./1405 of 14.08.2019** has submitted the thesis entitled **"Synthesis andCharacterization of ZnO-Cellulose Nanocomposite (ZnO-CNF) for the Photocatalytic Degradation of Organic Dye.**" under my supervision, for the requirement of the award of the Degree of Doctor of Philosophy in the Department of Botany, Mizoram University, Aizawl. The work is authentic, content of the thesis is the original work of the Research Scholar, and the nature and the presentation of the work are the first of its kind.

It is further certified that no portion(s) or part(s) of the content of the thesis has been submitted for any degree in Mizoram University or any other University or Institute.

Date: Your sincerely,

Place: Mizoram University

(Dr. SURYA KANT MEHTA)
Supervisor
Department of Botany
Mizoram University

DECLARATION

MIZORAM UNIVERSITY

DECEMBER, 2024

I **JYOTISHMA NATH**, hereby declare that the subject matter of this thesis is the record of work done by me, that the contents of this thesis did not form basis of the award of any previous degree to me or to do the best of my knowledge to anybody else, and that the thesis has not been submitted by me for any research degree in any other University/Institution.

This is being submitted to the Mizoram University for the **Degree of Doctor of Philosophy in Botany.**

Date:

Place: Aizawl, Mizoram

(Miss JYOTISHMA NATH)
Department of Botany
Mizoram University
Aizawl- 796004

(Prof. F. LALNUNMAWIA)
Head
Department of Botany
Mizoram University
Aizawl-796004

(Dr. SURYA KANT MEHTA)
Supervisor
Department of Botany
Mizoram University
Aizawl-796004

ACKNOWLEDGEMENT

It is my privilege to acknowledge all those, who helped and supported me throughout my research work.

First and foremost I am grateful to "Bhagwan", the author of knowledge and wisdom, for his countless love and blessing that have enabled me to complete this thesis.

It may not be possible to complete my research work without the proper supervision, guidance and cooperation of my esteemed supervisor Prof. Surya Kant Mehta, Department of Botany, Mizoram University. I am thankful to sir for introducing me to the emerging field of nanoscience. I will be forever in debt to sir for his persistent inspiration, keen interest, expert guidance and whole hearted help throughout the course of investigation till the preparation of the thesis.

I take this opportunity to thank Prof. F. Lalnunmawia Head of Botany Department, Mizoram University for providing necessary facilities and thankful to all the faculty members and non-teaching staff for their support and encouragement.

I would like to give my sincere gratitude to Dean of Life Science Prof. G. Gurusubramanianfor his kind support and cooperation. Particularly, I would like to acknowledge Prof. Y.T. Singh and Dr. K.S. Devi for allowing me to utilize their laboratory instruments for my experiments.

I express my gratefulness to Dr. Brojen Singh, Laboratory Technician, Chemistry Department, Mizoram University for FTIR facility, CSIR-NEIRST, Jorhat for XPS facility, CIC-Tripura University of SEM and EDX facility, SAIF-Gauhati University for TGA and DSC facility, SAIC- Tezpur University for SEM and XRD facility. I would also like to thank the Staff of Central Instrumentation Laboratory (Mrs. Sagarika Dash and Mr. C. Lalrinawma), Mizoram University for providing instrumentation facilities.

I am glad to have shared experiences with my labmates Mr. Sengjrang Ch. Momin, Miss Ruthi Lalmuanzeli, Mr. Lalremdika, Mrs. Chawngthantluangi, Mr. Ran Bahadur Pradhan, Mr. Agniv Kar, Miss Lalchhanhimi Khiangte and Miss Semima Farhin. It has been quite interesting to work with people from several specializations. Thanks to my all friends (especially to Barsha Kalita, Guna Kanta Ganju, Anima Borgohain, Janet Simte), who are very close to my heart, whose help, support, encouragement has always given me strength.

I am thankful to my family members, especially to my parents (Mr. Promod Nath and Mrs. Evamoni Nath), elder brother (Mr. Jiban Jyoti Nath), Sister-in-law (Mrs. Juthika Borah), cousin (Kalyan Kishur Nath) for their mental and financial support and being so nice to me at all times. I acknowledge my uncle Mr. Priya Kanta Borbora for accompanying me to University for the first time. Thanks to all my near and dear ones as well as my well-wishers for their encouragement during my research work.

This study has been financially supported by UGC-MZU (NON-NET) fellowship.

Date:

Jyotishma Nath

Mizoram University

CONTENTS

ABBREVIATION

AOP- Advanced oxidation process

BNF – Bacterial nanofibre

CVD-Chemical vapour deposition

CNC - Cellulose nanocomposite

CNF - Cellulose nanofiber

DSC - Differential scanning calorimetry

FTIR - Fourier iransform infrared spectroscopy

LIBs - Lithium-ion batteries

MB- Methylene blue

MO – Methyle orange

NPs – Nanoparticles

$^{\bullet}OH$ - Hydroxyl radicals

$^{\bullet}O_2^-$ - Superoxide anions

PVD- Physical vapour deposition

PVP - Polyvinylpyrrolidone

ROS - Reactive oxygen species

SEM - Scanning electron microscope

TEM - Transmission electron microscope

TGA - Thermogravimetric analysis

UV-VIS–Ultraviolet-visible spectroscopy

XPS - X-ray photoelectron spectroscopy

XRD - X-ray diffraction

LIST OF FIGURES

(α) as a function of photon energy (hν). The linear extrapolation of the plot yields an estimation of the band gap energy (*Eg*) of the ZnO-NPs.

Figure 14. UV-VIS absorption spectrum and tauc plot of ZnO-NPs synthesized from *C. vulgaris* (a) UV-VIS absorption spectrum of ZnO-NPs showing the absorption characteristics across a range of wavelengths. (b)Tauc plot of ZnO-NPs derived from the absorption spectrum. The plot displays the square of the absorption coefficient (α) as a function of photon energy (hν). The linear extrapolation of the plot yields an estimation of the band gap energy (*Eg*) of the ZnO-NPs.

Figure 15. Fourier transform infrared (FTIR) spectrum of ZnO-NPs (synthesized from the aqueous extract of *C. glomerata*) depicting characteristic absorption bands.

Figure 16. Fourier transform infrared (FTIR) spectrum of ZnO-NPs (synthesized from the aqueous extract of *C. vulgaris*) depicting characteristic absorption bands.

Figure 17. Scanning electron microscopy (SEM) images of ZnO-NPs synthesized from *C. glomerata* (a) at 2 µm, (b) at 200 nm, (c) at 100 nm (d) at 100 nm.

Figure 18. Scanning electron microscopy (SEM) images of ZnO-NPs synthesized from *C. vulgaris* (a) and (b) at 200 nm, (c) and (d) at 100 nm.

Figure 19. (a) EDX spectrum for the ZnO-NPs synthesized from *C. glomerata,* (b) Diameter of ZnO-NPs synthesized from *C. glomerata*, in Gaussian distribution.

Figure 20. (a) EDX spectrum for the ZnO-NPs synthesized from *C. vulgaris,* (b) Diameter of ZnO-NPs synthesized from *C. vulgaris* in Gaussian distribution.

Figure 21. XRD analysis of ZnO-NPs (a) synthesized using aqueous extract of *C. glomerata,* (b) synthesized using aqueous extract of *C. vulgaris.*

Figure 22. X-ray photoelectron spectroscopy (XPS) Analysis: (a) Provides the XPS survey spectra of ZnO-NPs synthesized from *C. glomerata*, offering an overview of the elemental composition and surface characteristics. (b) Presents an XPS core level scan of carbon (C1s) with a deconvoluted profile, allowing a closer examination of carbon's chemical environment and bonding states. (c) Offers an XPS core level scan of oxygen (O1s), giving insights into the chemical states and bonding of oxygen on

the sample's surface. (d) Shows the XPS core level scan of zinc (Zn 2p ½ and Zn 2p 3/2) with deconvoluted profiles.

Figure 23. X-ray photoelectron spectroscopy (XPS) Analysis: (a) Provides the XPS survey spectra of ZnO-NPssynthesized from *C. vulgaris*, offering an overview of the elemental composition and surface characteristics. (b) Presents an XPS core level scan of carbon (C 1s) with a deconvoluted profile, allowing a closer examination of carbon's chemical environment and bonding states. (c) Offers an XPS core level scan of oxygen (O 1s), giving insights into the chemical states and bonding of oxygen on the sample's surface. (d) Shows the XPS core level scan of zinc (Zn 2p ½ and Zn 2p 3/2) with deconvoluted profiles.

Figure 24. Fourier transform infrared (FTIR) spectrum of nanocellulose synthesized from *C. glomerata.*

Figure 25. Fourier transform infrared (FTIR) spectrum of nanocellulose synthesized from *C. vulgaris.*

Figure 26. Scanning electron microscopy (SEM) images of nanocellulose extracted from *C. glomerata* (a) at 20 µm (b) at 2 µm, (c) at 1 µm (d) at 200 nm.

Figure 27. (a) EDX spectrum of nanocellulose synthesized from *C. glomerata*, (b) Diameter of nanocellulose synthesized from *C. glomerata* in Gaussian distribution.

Figure 28. Scanning electron microscopy (SEM) images of nanocellulose extracted from *C. vulgaris* (a) at 20 µm, (b) at 2 µm, (c) at 2 µm and (d) at 200 nm.

Figure 29. (a) EDX spectrum of nanocellulose synthesized from *C. glomerata,* (b) Diameter of nanocellulose synthesized from *C. glomerata* in Gaussian distribution.

Figure 30. (a) Depicts the TGA curve of CNF isolated from *C. glomerata,* offering insights into their thermal stability and weight loss profile as a function of temperature. (b) Features the DTG curve of CNF, providing a detailed representation of the rate of weight change with respect to temperature for the CNF sample.

Figure 31. (a) The TGA curve of the CNC isolated from *C. vulgaris* revealing its thermal stability and weight loss characteristics under increasing temperature. (b)

Highlights the DTG curve of the CNC offering information about the rate of weight change with temperature for the CNC sample.

Figure 32. Depicts the DSC curve of isolated nanocelluose from *C. glomerata*, providing information on their thermal behaviour, including phase transitions and heat flow as a function of temperature.

Figure 33. Depicts the DSC curve of isolated nanocelluose *C. vulgaris*, providing information on their thermal behaviour, including phase transitions and heat flow as a function of temperature.

Figure 34. Fourier transform infrared (FTIR) spectrum of ZnO-CNF nanocomposite.

Figure35. Scanning electron microscopy (SEM) image of ZnO-CNFnanocomposite in different scale (a) at 1µm, (b) at 200 nm, (c) at 100 nm (d) at 100 nm.

Figure 36. (a) EDX spectrum for the ZnO-CNF nanocomposite, (b) Diameter of ZnO-CNF nanocomposite in Gaussian distribution.

Figure 37. (a) The TGA curve of the ZnO-CNF nanocompositerevealing its thermal stability and weight loss characteristics under increasing temperature. (b) Highlights the DTG curve of the ZnO-CNF nanocomposite offering information about the rate of weight change with temperature for this composite material.

Figure 38. The DSC curve of the ZnO-CNF nanocomposite, offering insights into its thermal characteristics, including any phase changes and heat absorption or release with changing temperature.

Figure 39. (a) Different concentration of MB before sunlight irradiance (b-d) Changes in colour of different concentration of methylene blue in absence and presence of differentcatalyst after 150 min of sunlight irrandiance (b) control without catalyst,(c)in presence of CNF,(d)in presence of ZnO-NPs and (e) in presence of ZnO-CNF nanocomposite.

Figure 40. Graphical representation of photocatalytic degradation of MB under sunlight irradiance in presence of ZnO-CNF nanocomposite.

Figure 41. Adsorption and removal of methylene blue (MB) catalyzed by ZnO-CNF nanocomposite under sunlight irradiance. (a) and (b) Demonstrate the time-dependent adsorption and removal (%) of MB respectively, from aqueous solutions under sunlight irradiance. The initial concentration of MB in the solutions was maintained at 5 mg L^{-1}.

Figure 42. Pseudo-first-order and pseudo-second-order kinetics for the adsorption of MB on (a) Control; (b) CNF; (c) ZnO-NPs and (d) ZnO-CNF nanocomposite. The initial concentration of MB was 5 mgL^{-1}.Vertical bars indicate the standard deviation (±SD).

Figure 43.(a) and (b) represent adsorption and removal (%) of MB respectively, at varying initial concentrations of MB under direct sunlight irradiance for a duration of 150 min. The data points are calculated as the means of three replicates, and the vertical bars accompanying them indicate the standard deviations (±SD).

Figure 44. Equilibrium isotherms for the biosorption of MB by the catalyst (A) CNF, (B) ZnO-NPs and (C) ZnO-CNF nanocomposite. The curves represent the fitting of the Langmuir, Freundlich, and Temkin isotherm models to the experimental data points.

LIST OF TABLES

CHAPTER-1

INTRODUCTION

1.1. Organic Dye:

Organic dyes are a class of colorant compounds primarily made of carbon-based molecules that can absorb light in the visible spectrum, thus imparting color. These dyes are typically derived from organic substances, including plants, animals, and synthetic chemical processes, rather than metals or minerals which are highly resistant to factors such as light, heat, and moisture This characteristic makes them particularly suitable for applications where colorfastness and longevity are crucial (Alegbe and Uthman, 2024).Some organic dyes and their chemical structure are shown in Figure 1.

Since prehistoric time human have used the natural dyes for coloring textiles and the other materials. Those dyes were extracted from the plants and animals (Morriss-Kay, 2010; Yadav et al., 2023). Mostly use early dyes were Indigo (extracted from indigo plants, widely used in India, Mesopotamia and Egypt), Tyrian Purple (made from sea snails, especially used by Romans and Phoenicians) and Madder (derived from the roots of *Rubia tinctorum*, used by ancient Romans, Greeks and Egyptians) (Alegbe and Uthman, 2024).Uses of natural dyes were expanded to the Middle East, Asia and Europe during the Middle ages (500-1500 CE).Woad, a blue dye extracted from *Isatis tinctoria* used in Europe. Some others yellow dyes such assaffron and turmeric were widely used in Europe, Asia and Middle East. Cochineal, a red dye derived from insects and used by Americans which was introduced to Europe in early modern period (1500-1800). Moreover, another black dye logwood was extracted from *Haematoxylum campechianum*, introduced into Europe (Abu-Ghosh et al., 2023).

In 1856, British chemist William Henry Perkin accidentally synthesized the first synthetic dye, mauveine while trying to create quinine for malaria treatment. This finding revolves around due to this breakthrough, the dye industry underwent a revolution and synthetic dyes with more vibrant colors, consistency, and affordability

were produced (Holme, 2006). In the late 19th century Azo dyes were developed based on nitrogen compounds and in 1890s, synthetic indigo replaced the natural dyes, making a major industrial shift. By the 20th century, synthetic dyes completely dominated the dye industry. Research in organic chemistry led to the creation of a wide range of dyes tailored for specific purposes, such as reactive dye and disperse dye (Abel, 2012; Welham, 1963).

1.2. Global Production of Organic Dyes: Major Dye Production Regions

China and India are the world's leading producers of organic dyes, with a significant presence in Asia, Europe, and North America (Alegbe and Uthman, 2024). China's manufacturing prowess, particularly in synthetic organic colorants and azo dyes, is a major contributor to its dominance. India, with its expertise in artificial organic coloring, is another key player. South Korea and Japan are known for their high-performance dye manufacturing, especially for innovative applications like solar cells and electronics (Yadav et al., 2023).

Germany, Switzerland, and Italy are renowned for producing high-quality organic dyes. Germany's dye and pigment industry, represented by companies like BASF, manufactures synthetic and natural dyes for various applications, including printing, textiles, medicine, and cosmetics. The North American dye industry, led by the US, focuses on producing high-value, specialized organic dyes for innovative materials, cosmetics, and pharmaceuticals. With increasing environmental regulations, there is a significant focus on developing eco-friendly dyes in North America (Ardila-Leal et al., 2021).

Other parts of the world, such as Brazil and other South American nations, have modest but developing capacities for producing dyes, with an emphasis on the food and textile industries. Middle Eastern nations produce dyes, particularly with growing investments in the chemical industry, although their market share is still lower than that of Asia or Europe.

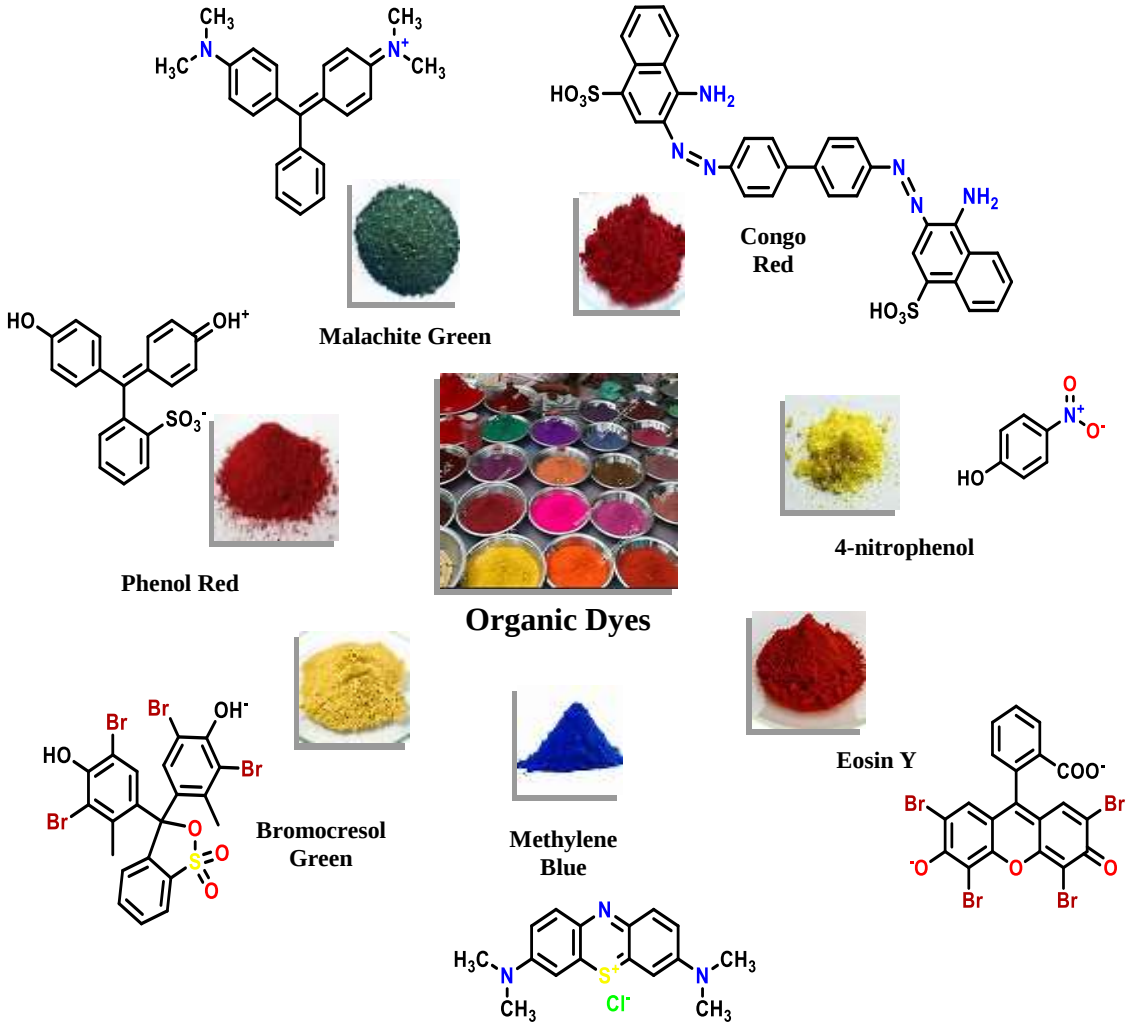

Figure 1: Different types of organic dyes and their chemical structures.

1.3. Leading Countries in Term of Dye Production

The dyes and pigments market are expected to be dominated by the Asia Pacific region. Due to the availability of inexpensive labour, the textile industry has expanded in nations like China and India, which is responsible for the expansion. China is the world's largest dye producer and exporter, primarily due to its textile production and extensive chemical manufacturing facilities. About 40% of the global textile market is controlled by China, while India accounts for about 5%. By 2027, the Indian technical textile industry is expected to reach $23.3 billion, according to the India Brand Equity Foundation. Further, in the forecast year of 2019-20, India's textiles and apparel exports accounted for 11% of total mercantile shipments. However, stricter environmental regulations have led to factory closures due to pollution concerns. India, the second-largest global dye producer and top exporter of textile dyes, is known for producing azo and reactive dyes. Figure 2 provides a visual representation of the regional growth rates in the global dyes and pigments market from 2021 to 2027. The map highlights the regions with high, medium, and low growth rates.

After India Germany is one of leading producer of high-quality specialty dyes, renowned for precision in chemical manufacturing. Leading chemical companies like BASF and Clariant dominate the sector, despite high production costs.South Korea, with its advanced textile and chemical industries, is a key producer of eco-friendly, high-performance dyes, particularly for export markets in Europe and the U.S.Japan produces high-quality, specialized dyes for electronics, automotive, and textiles, with advanced chemical engineering capabilities and leading producers like Sumitomo Chemical and DIC Corporation.The U.S., a major producer of specialty dyes and pigments, focuses on high-performance dyes for automotive, aerospace, and industrial coatings, with leading companies outsourcing production to Asia.Taiwan is a major dye producer, focusing on synthetic fibres and high-performance textiles due to its strong chemical and textile industries and high-quality control and precision manufacturing (Hagan and Poulin, 2021).

Figure 2: Regional growth rates in the global dyes and pigments market (2021-2027). (Source: OMR Global, Global Dyes and Pigments Market Size, Share and Trends Analysis Report, July 2023)

Several key trends are driving changes in the global production of organic dyes (Yadav et al., 2023). Stricter environmental regulations in Europe and North America are prompting a shift towards sustainable and eco-friendly dye production methods. India, with its rich agricultural heritage, is a major player in the natural dye industry (Islam et al., 2023).New production methods are being developed to improve efficiency and reduce environmental impact. The demand for biodegradable and non-toxic colors, especially in the food and cosmetics industries, is driving the growth of organic dye production. Significant investments in research and development are being made tocreate high-performance dyes for advanced applications.

The global synthetic dyes market is projected to reach USD 9.1 billion by 2029, growing at a CAGR of 5.0% during the forecast period (Figure 3). This growth is driven by factors such as increasing demand from various industries, including textiles, plastics, and coatings.The worldwide dyes market is projected to reach $15 billion by 2026, according to a research by Allied Market Research (2019) (Pereira et al., 2021). The worldwide synthetic dyes market is expected to develop at a

compound annual growth rate of 5.0% from 2024 to 2029, from a 2024 valuation of USD 7.1 billion to USD 9.1 billion (Figure 3), according to a Market Research Report (Report Code: CH8157, published in September 2024).Key companies operating in the synthetic dyes market include Archroma (Switzerland), Lanxess (Germany), Zhejiang Longsheng Group Co. Ltd (Dystar) (China), Heubach GmbH (Germany) Kiri Industries (India), Atul Ltd.(India), Bodal Chemicals (India), Chromascape (US), Henkel AG and Co (Germany), Kemira Oyj (Finland), Milliken and Company (US), Solenis LLC(US), Zhejiang Jihua Group (China) and Zhejiang Runtu Co. Ltd (China).

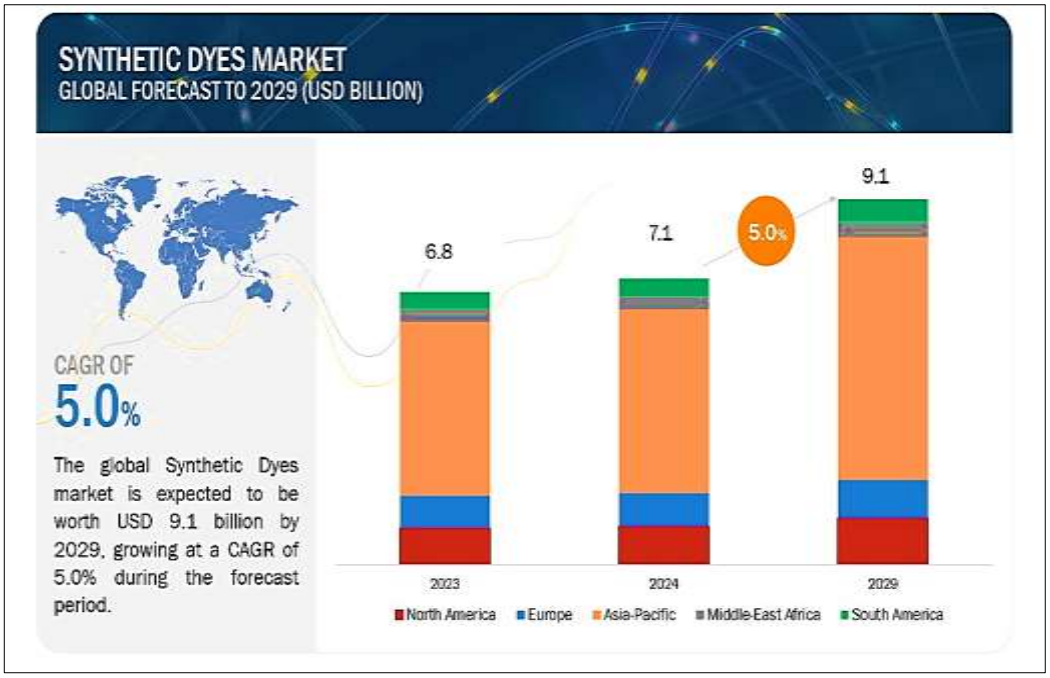

Figure 3: Global synthetic dyes market trends (Source: Market Research Report (Report Code: CH8157), published in September 2024)

1.4. Types of Organic Dyes:

Organic dyes are mainly divided into natural and synthetic dyes (Figure 4).

1.4.1. Natural Dyes

India, a land of diverse flora, is a rich source of natural dyes derived from plants like henna, indigo, madder, turmeric, marigold, tea, onion, and saffron (Sigurdson et al., 2017; Yadav et al., 2023; Arora et al., 2017). Animal-based dyes, such as cochineal, tyrian purple, sepia, and bone black, have historically been used but face challenges due to overharvesting and environmental concerns (Adeel et al., 2018; Alegbe and Uthman, 2024; Mahltig, 2024).

Cochineal, derived from the *Dactylopiuscoccus* insect, has been used for centuries as a natural food coloring and fabric dye (Galappaththi and Patabendige, 2022). Tyrian purple, a historically significant dye, was obtained from sea snails like *Murexbrandaris* and *Murextrunculus* (Daniels, 2006; Głowacki et al., 2012).

Mineral-based dyes, derived from minerals like ochre, malachite, and lapis lazuli, have been used for centuries due to their stability and durability. These dyes were often used in conjunction with natural dyes to enhance color fastness and provide a wider range of colors (Ngulube et al., 2017).

Natural dyes offer several advantages, including eco-friendliness, biodegradability, and potential health benefits. However, they can be challenging to extract, standardize, and reproduce, with limitations in color fastness and seasonal availability (Indraningsih, 2014; Ozturk et al., 2013).

1.4.2. Synthetic Dyes

Synthetic dyes, derived from various chemical compounds, offer a wide range of colors and are widely used in industries like textiles, plastics, and paper. They are chosen for their cost-effectiveness, durability, and color fastness. However, their production and disposal pose significant environmental and health risks. Synthetic dyes, particularly azo dyes, can release toxic chemicals like aromatic amines, which can contaminate water bodies and harm aquatic life. Moreover, exposure to these dyes can lead to health issues such as skin allergies, respiratory problems, and cancer. The non-biodegradable nature of many synthetic dyes further exacerbates

their environmental impact (Forgacs et al., 2004; Srivastava and Sofi, 2020; Millbern et al., 2024; Shabbir, 2019). Synthetic dyes are further classified as:

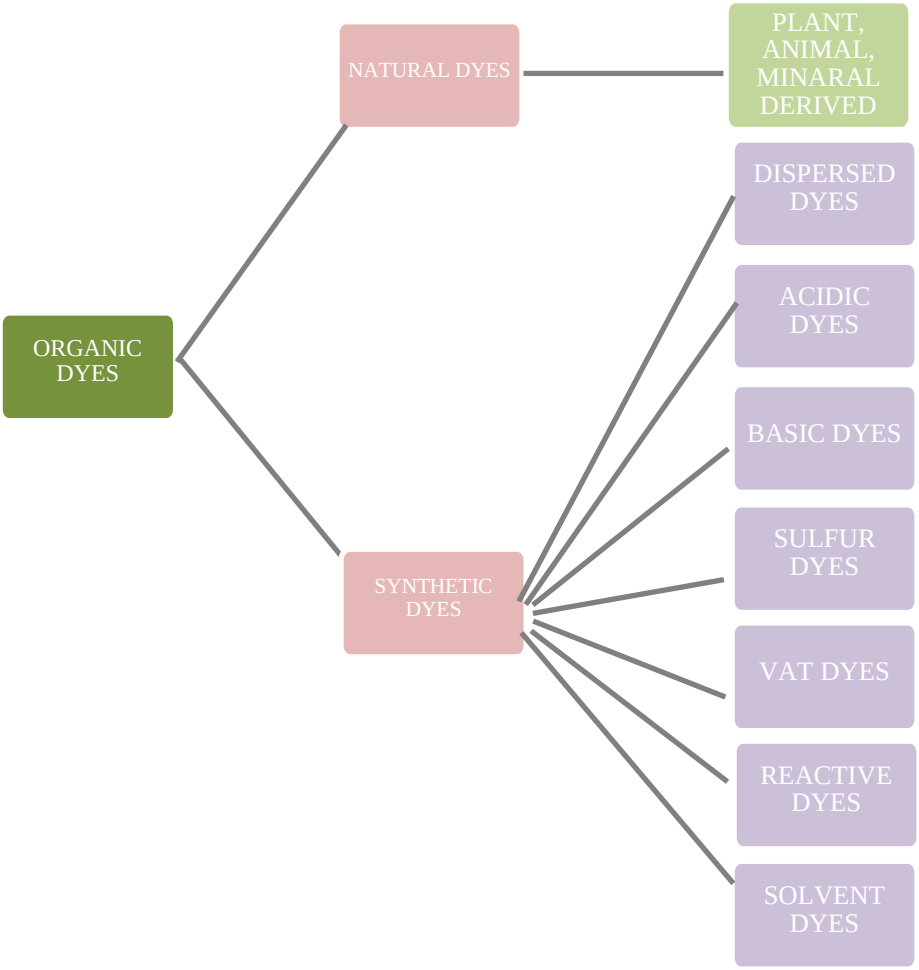

Figure 4: Classification of organic dyes

Water Soluble Dye

Acid Dyes are water-soluble dyes that are commonly used for dyeing protein fibers like wool, silk, and nylon. They are applied in acidic conditions, typically using acetic acid or sulfuric acid. Acid dyes offer a wide range of colors and are relatively easy to apply. However, their colorfastness may vary, and they are not suitable for cellulosic fibers (Benkhaya et al., 2020; Sharma et al., 2021).

Basic Dyes are water-soluble cationic dyes that are commonly used for dyeing acrylic fibers. They are also used for dyeing wool and silk, often in combination with a mordant. Basic dyes are known for their bright colors but have limited colorfastness, particularly to light and washing (Berradi et al., 2019).Direct Dyes are water-soluble dyes that have a strong affinity for cellulosic fibers like cotton and linen. They are applied directly to the fabric without the need for a mordant. Direct dyes are relatively easy to apply and offer a wide range of colors. However, their colorfastness to light and washing can be limited (Burkinshaw and Salihu, 2019). Reactive Dyes form covalent bonds with the fibers, resulting in excellent colorfastness. They are widely used for dyeing cellulosic fibers like cotton, linen, and viscose rayon. Reactive dyes offer a wide range of colors and are highly resistant to washing, light, and other environmental factors. They are often used in combination with other dyes to achieve complex color combinations (Barathi et al., 2020).

Water Insoluble Dye

Disperse dyes are used to dye hydrophobic synthetic fibers like polyester, acetate, nylon, and acrylic. These dyes are insoluble in water but can be dispersed into fine particles that can penetrate the fibers. They offer a wide range of colors and are commonly used in the textile industry (Al-Etaibi and El-Apasery, 2019; Bayramoglu et al., 2020; Meireles et al., 2018).Vat dyes are insoluble in water but become soluble in an alkaline reducing agent. This allows them to penetrate the fibers, where they are oxidized to form insoluble dye molecules. Vat dyes are known for their excellent colorfastness and are commonly used for dyeing cotton and other cellulosic fibers (Michie and Thornton, 1953; Morin, 2017). Sulfur dyes are a class of dyes that are insoluble in water but become soluble in alkaline sulfide solutions. They are used to dye cellulosic fibers and are known for their good colorfastness and economic viability. However, their application process can be complex and environmentally unfriendly (Khattab et al., 2020; Nguyen et al., 2010; Slama et al., 2021).Azo dyes are a large class of synthetic dyes that contain one or more azo groups (-N=N-). They are widely used in various industries, including textiles, paper, and plastics. Azo dyes

offer a wide range of colors and can be applied to a variety of fibers. However, some azo dyes can release toxic aromatic amines upon degradation, leading to environmental and health concerns. Therefore, there is a growing interest in developing safer and more sustainable alternatives to azo dyes (Louati et al., 2020; Singh et al., 2015; Li et al., 2019; Zhang et al., 2019).

1.5. Application of Organic Dyes

Dyes are essential in many industries due to their versatility, marketability, and efficacy. They enhance the appearance and functionality of products in sectors like food, healthcare, cosmetics, textiles, and pharmaceuticals, as well as cutting-edge technologies like solar energy and medical diagnostics (Repon et al., 2024; Dev et al., 2024). Their numerous and varied applications, ranging from utility to beauty, make them indispensable in contemporary industrial processes. A vast range of items, from textiles and paper to cosmetics, leather, food, pharmaceuticals, and plastics, are given color and functionality through the use of organic dyes (Li et al., 2022).

Synthetic dyes offer a wider range of colors and improved performance compared to natural dyes. They are used in various industries, including:

Textiles: Dyes are used to color fabrics like cotton, wool, silk, polyester, and nylon, enhancing their aesthetic appeal and providing functional properties like colorfastness and UV protection (Che and Yang, 2022).

Food: Dyes are used to enhance the appearance of food products and can indicate flavor. Common dyes include carotenoids, anthocyanins, chlorophyll, and curcumin (Dey and Nagababu, 2022; Novais et al., 2022).

Cosmetics: Dyes provide vibrant colors to cosmetics like lipsticks, eyeshadows, and blushes. Carmine, indigo, and henna are some common dyes used in cosmetics (Adeel et al., 2018; Guerra et al., 2018).

Pharmaceuticals: Dyes are used to color drugs and medical formulations for identification and aesthetic appeal. They are also used in diagnostic procedures (Fahad et al., 2024; Pérez-Ibarbia et al., 2016; Wainwright, 2008).

Printing and Packaging: Dyes are used in inks for printing on various materials. They enable high-resolution printing and provide vibrant colors (Kavyashree, 2020; Islam et al., 2024; Savvidis et al., 2014; Yeo and Shin, 2023).

Plastics: Dyes are used to color plastics, enhancing their appearance and providing functional properties like UV protection and heat resistance (Kumar et al., 2019; Patti and Acierno, 2022).

Solar Cells: Dyes are used in dye-sensitized solar cells to convert sunlight into electricity (Adedokun et al., 2016; Arkan et al., 2024; Diany et al., 2024; Mahajan et al., 2024).

Paper: Dyes are used to color paper products, enhancing their appearance and functionality (Reinhardt and Travis, 1997; Saakshy et al., 2016; Sugaya, 2003).

While synthetic dyes offer many advantages, their environmental impact is a significant concern. The textile industry, in particular, has been a major source of water pollution due to the release of untreated dye effluents. Therefore, there is a growing emphasis on developing sustainable and eco-friendly dyeing processes.

1.6. Environmental Impact of Dye Pollution

Dye pollution poses significant environmental and health risks. Dye effluents contain organic molecules, heavy metals, and hazardous chemicals that contaminate water bodies (Donkadokula et al., 2020). Dark-colored dyes can disrupt aquatic ecosystems by reducing sunlight penetration, affecting photosynthesis in plants and leading to oxygen depletion (Imran et al., 2015; Sakib et al., 2019). Many dyes are non-biodegradable and can persist in the environment for extended periods, causing long-term harm (Ito et al., 2016). Improper disposal of dye effluents can contaminate soil with heavy metals and hazardous compounds, affecting plant growth and microbial activity. Additionally, dye-contaminated soil can enter the food chain, posing risks to

animals and humans (Vikrant et al., 2018). Dyeing and drying processes release harmful air pollutants, including particulate matter, volatile organic compounds (VOCs), and nitrogen oxides (NOx), which can contribute to respiratory problems and climate change (Aldalbahi et al., 2021; Park et al., 2016). Exposure to dyes and chemicals can lead to various health issues, such as skin irritation, allergic reactions, respiratory problems, and eye problems. Consuming dye-contaminated water or food can have serious health consequences, including cancer, organ damage, and hormone imbalances (Rovira and Domingo, 2019; Khan and Malik, 2018; Wargala et al., 2021). Dye pollution in water bodies can harm aquatic life by reducing oxygen levels, altering water chemistry, and affecting the growth and survival of aquatic plants and animals (Al-Tohamy et al., 2022; Dutta et al., 2024).

1.7. Factors Contributing to Dye Pollution

The textile and chemical industries are major contributors to water pollution due to the discharge of dye-laden wastewater. Conventional wastewater treatment methods often struggle to effectively remove synthetic dyes, particularly those with complex chemical structures (Ranjit et al., 2021). The rapid growth of these industries has overloaded treatment infrastructure, leading to the discharge of untreated wastewater. This issue is exacerbated by incorrect operation and poor maintenance of treatment facilities (Singh et al., 2024).Many developing nations lack stringent environmental regulations and enforcement mechanisms for wastewater treatment and dye contamination. This allows industries to avoid legal obligations, discharge excessive dye concentrations, and contaminate water supplies. Some industries even resort to illegally releasing partially treated effluent to reduce costs (Plessis, 2022; Ferronato and Torretta, 2019).Improper disposal of dye-containing waste, including wastewater and solid waste, from industries like paper, textiles, leather, and dye manufacturing, can significantly contribute to soil, air, and water pollution. The incorrect disposal of solid waste containing dye residues in landfills or their improper burning can lead to air and soil pollution. Additionally, improper home disposal methods and inadequate infrastructure, particularly in developing nations, can exacerbate dye pollution (Chand et al., 2023; Kishor et al., 2021).

1.8. Mitigation Strategies for Dye Pollution

Physical Methods:

Adsorption: Adsorption is a process where molecules or atoms adhere to a surface. In the context of dye removal, adsorption involves binding of dye molecules onto the surface of a solid adsorbent material, such as activated carbon or agricultural waste. This process is effective in removing various types of dyes, including cationic and anionic dyes (Arora et al., 2020; Ghasemi et al., 2016). Adsorption offers several advantages, including its simplicity, low cost, and minimal maintenance requirements. However, adsorbents can become saturated, necessitating regeneration or disposal (Namasivayam et al., 1994; Chakraborty et al., 2005). Additionally, the effectiveness of adsorption can be influenced by factors like mass transfer and the properties of the dye and adsorbent (Aragaw and Bogale, 2021; Pellenz et al., 2023).

Membrane Filtration: Membrane filtration, particularly nanofiltration and reverse osmosis, is a highly effective method for removing dyes from wastewater. These processes filter out dyes based on their size and charge, allowing for the recovery and reuse of water. However, membrane filtration systems can be expensive to install and operate, and they require regular maintenance to prevent fouling (Aziz et al., 2024; Ahmad et al., 2022; Cevallos-Mendoza et al., 2022).

Nanofiltration is a pressure-driven membrane process that can remove dyes, salts, and other contaminants from water. It is particularly effective for removing dyes with a molecular weight greater than 200 Da. Reverse osmosis, on the other hand, is a more stringent process that can remove virtually all dissolved and suspended contaminants, including dyes, salts, and organic matter. However, it requires higher operating pressures and energy consumption compared to nanofiltration.The choice of membrane filtration process depends on various factors, including the type of dye, the desired level of treatment, and the available budget. For example, nanofiltration may be sufficient for removing dyes from textile wastewater, while reverse osmosis may be necessary for treating wastewater from other industries.Membrane fouling, caused by the accumulation of particles and organic matter on the membrane surface, can significantly reduce the efficiency of

membrane filtration. To mitigate fouling, various techniques, such as backwashing, chemical cleaning, and ultrasonic cleaning, can be employed. Additionally, optimizing operating conditions, such as transmembrane pressure and flow rate, can help minimize fouling and improve membrane performance (Mohammad et al., 2015; Yang et al., 2019).

Coagulation and flocculation: Coagulation and flocculation are cost-effective techniques for removing dyes from wastewater, especially in large-scale operations like textile and dye manufacturing plants (Saritha et al., 2017). By using suitable coagulants and flocculants, a wide range of dyes can be removed. This method is simple to implement and requires minimal equipment (Sher et al., 2013).For instance, Ihaddaden et al. (2022) used bentonite-based coagulants and cactus-based flocculants to remove methylene blue dye. Guibal and Roussy (2007) employed coagulation and flocculation to remove Reactive Black 5 using acetic acid and chitosan.However, coagulation and flocculation have limitations. Sludge generation can be costly and environmentally harmful (Gadekar and Ahammed, 2016). Additionally, chemical use can increase salinity and leave residues. The effectiveness of the process depends on factors like dye type, chemical properties, and pH. Proper dosage is crucial to avoid excessive sludge generation and insufficient color removal. Often, additional treatment methods, such as filtration or sedimentation, are required (Verma et al., 2012).

Ion Exchange: Ion exchange is a selective process that removes ionic dyes from wastewater by exchanging them with ions on a solid surface. This method is environmentally friendly and cost-effective, as ion exchange resins can be regenerated and reused (Satapanajaru et al., 2011). It is particularly suitable for small-scale wastewater treatment due to its compact nature.Various ion exchange resins have been used to remove different types of dyes. For example, Saruchi and Kumar (2019) synthesized a hybrid ion exchanger for rhodamine B and lead ion removal. Suteu et al. (2014) used Purolite resins to remove Basic Blue 9. Yanardağ and Edebali (2023) investigated malachite green dye removal using Diaion CR-11 and Amberlite IRC-748 resins. Wu et al. (2008) studied methyl violet 2B removal

using strong-acid cation exchange membranes.While ion exchange is effective, high-concentration wastewater may require pre-treatment. Additionally, the high cost of resins and regeneration chemicals can limit its application, especially for large-scale operations. Combining ion exchange with other methods can improve efficiency and cost-effectiveness (Raghu and Ahmed Basha, 2007)

Chemical Methods

Advanced Oxidation Processes (AOP): Advanced Oxidation Processes (AOPs) are powerful techniques for removing dyes from wastewater. They utilize highly reactive hydroxyl radicals to break down complex dye molecules into simpler, less harmful compounds or even mineralize them into carbon dioxide, water, and inorganic ions (Kalyani et al., 2009; Wang et al., 2009). Common AOPs include ozone oxidation, the Fenton process, and photo-Fenton process.

AOPs are environmentally friendly, relying on oxygen or UV light, and can degrade various organic pollutants, including pharmaceuticals and pesticides. They can be scaled for various wastewater treatment systems and achieve significant dye degradation quickly. For example, Nemr et al. (2018) used ozone and UV light to effectively degrade Acid Red 17 dye. Cuiping et al. (2011) investigated the oxidation of rhodamine B using different ozone-based processes, finding UV/ozone to be the most effective. Sauer et al. (2006) studied the photolysis of methylene blue using UV/H_2O_2 oxidation. However, AOPs have limitations. They can be energy-intensive and costly, especially those involving UV light or ozone generation. They require expensive chemicals like hydrogen peroxide or ozone, and precise control of reaction conditions. Additionally, AOPs require expensive equipment and regular maintenance, and are highly pH-sensitive (Kalyani et al., 2009; Wang et al., 2009).

Photocatalysis: Photocatalysis is an emerging technology that utilizes semiconductors to degrade organic pollutants, including dyes, into harmless substances like carbon dioxide and water. Semiconductors absorb light energy, generating electron-hole pairs that can initiate redox reactions, leading to the degradation of pollutants. Various semiconductor materials, such as TiO_2, ZnO, and

Cd-S, have been studied for photocatalytic dye degradation.For instance, Azimifar et al. (2022) developed a $Sb_2O_3/CuBi_2O_4$ composite photocatalyst for the removal of methylene blue and acid blue 25 dyes under visible light irradiation. Joseph and Elilarasi (2017) investigated the use of TiO_2-SiO_2 photocatalyst for the removal of methylene blue. Vaiano et al. (2016) studied the photocatalytic degradation of blue V using Au-TiO_2 and Pt-TiO_2 catalysts.While photocatalysis offers several advantages, including environmental friendliness and high efficiency, it also faces certain challenges. These include the need for UV light, which limits its practical applications, and potential catalyst deactivation due to factors like fouling and photo-corrosion. Additionally, the energy-intensive nature of UV light sources and the need for specialized reactors can increase the overall cost of photocatalytic systems (Kim et al., 2016; S. Zhu and Wang, 2017; Zia and Riaz, 2021; Li et al., 2022).

Biological Methods

*Biosorption***:** Biosorption is an eco-friendly and cost-effective method for removing contaminants from wastewater using biological materials. These materials, such as fungi, algae, and bacteria, can absorb, adsorb, or precipitate pollutants like heavy metals, dyes, and organic compounds (Bhatia et al., 2017; Donkadokula et al., 2020; Kathing and Saini, 2022).Various studies have demonstrated the effectiveness of biosorption for dye removal. For example, Maurya et al. (2006) used fungi like *Fomes fomentarius* and *Phellinus igniarius* to adsorb methylene blue and Rhodamine B. Aksu and Tezer (2005) used *C. vulgaris* to adsorb reactive dyes. Silva et al. (2019) employed weeds like *Cyanthilium cinereum* and *Paspalum maritimum* to remove methylene blue dye. Kumari and Abraham (2007) investigated the use of fungi like *Aspergillus niger*, *Aspergillus japonicus*, *Rhizopus nigricans*, *Rhizopus arrhizus*, and *Saccharomyces cerevisiae* for the removal of anionic reactive textile dyes.While biosorption offers several advantages, it also has limitations. The biological nature of biosorbents can lead to variations in performance and difficulty in controlling the process. Additionally, biosorbents can become saturated, reducing their effectiveness. To overcome these limitations, research is ongoing to develop

more efficient and reliable biosorbents and optimization techniques (Fomina and Gadd, 2014; Touliabah et al., 2022).

Bioaccumulation: Bioaccumulation is a process where organisms accumulate contaminants, such as heavy metals, pesticides, and synthetic dyes, from their environment over time. This can lead to high concentrations of toxins within individual organisms (Al-Tohamy et al., 2022; Chojnacka, 2010; Zhou et al., 2023).Various organisms, including bacteria, fungi, and plants, can be used for bioaccumulation of dyes. Sadettin and Dönmez (2006) studied the bioaccumulation of reactive dyes using cyanobacteria. Taskin and Erdal (2010) investigated the decolorization of Reactive Black-5 dye using *Aspergillusniger*. Xin et al. (2010) studied the bioaccumulation of Cu-complex reactive dye by *Penicillium oxalicum*. Saranya et al. (2011) investigated the bioaccumulation of Basic Violet 14 dye using *Hydrillaverticillata*.While specific dye-transporting proteins have not been extensively characterized, general membrane transport proteins and efflux pumps, like those in the ATP-binding cassette (ABC) superfamily, has been dhown to play play a role in dye uptake and efflux (Jindal et al., 2019).While bioaccumulation is an environmentally friendly and cost-effective method for removing pollutants, it has limitations. The effectiveness of bioaccumulation can be influenced by various factors, such as the type of organism, the concentration of the pollutant, and environmental conditions. Additionally, the potential for bioaccumulation in the food chain is a concern. Proper management and disposal of contaminated biomass are essential to minimize environmental risks (Rane and Joshi, 2021).

*Biotransformation***:** Biotransformation is a biological process that utilizes microorganisms or enzymes to break down complex organic compounds, including dyes, into simpler, less harmful substances. This process offers an environmentally friendly and cost-effective approach to dye degradation.A variety of microorganisms, including bacteria, fungi, and algae, can be used for biotransformation. For example, *Geotrichum* sp. has been shown to effectively degrade different types of azo dyes (Máximo et al., 2003). Bacterial consortia, such as those composed of *Pseudomonas* sp., *Brevibacillus* sp., and Stenotrophomonas strains, have also been used to degrade

dyes (Chattaraj et al., 2016). Additionally, enzymes, such as laccase, can be used to catalyze the degradation of dyes. Pereira et al. (2009) investigated the enzymatic biotransformation of Sudan Orange G using recombinant bacterial CotA-laccase. Surwase et al. (2013) studied the biotransformation of Remazol Orange 3R by *Pseudomonasaeruginosa*.While biotransformation offers several advantages, it has limitations. The process can be slow, especially for complex dyes. Additionally, the formation of toxic intermediates may occur during biotransformation. Therefore, careful monitoring and control of the process are essential (Fenner et al., 2021; Malla et al., 2018; Shertate and Thorat, 2014).

Biomineralization: Biomineralization is a biological process that involves the breakdown of complex dye molecules into simpler, non-toxic inorganic substances like carbon dioxide, water, and mineral salts. Microorganisms, such as bacteria and algae, play a crucial role in this process by utilizing enzymes to break down the complex dye molecules.For example, Subramanian et al. (2024) demonstrated the effective decolorization of dyes by a consortium of *Streptomyces* sp., *Rhodococcusruber*, and *Bacillus* sp., which induced biomineralization and produced well-crystallized calcium carbonate polymorphs. Bian et al. (2022) developed a novel approach for dye separation using a hybrid separation layer created through in-situ biomineralization, which improved the stability and anti-fouling properties of the membrane.While biomineralization is an environmentally friendly and sustainable approach to dye removal, it has certain limitations. The process can be relatively slow compared to chemical methods and may require specific environmental conditions. Additionally, biomineralization may produce intermediate byproducts that may require further treatment. However, it is a promising technique for reducing the environmental impact of dye pollution (Addadi and Weiner, 2014; Yan et al., 2023).

1.9. Development of Ecofriendly Dyes and Regulatory Measures:

The growing concern over the environmental impact of synthetic dyes has led to increased interest in developing eco-friendly alternatives. Advances in biotechnology and nanotechnology are driving the dye industry towards more sustainable solutions.

While traditional synthetic dyes offer a wide range of colors and excellent performance, they can contribute to water pollution and health risks. In contrast, eco-friendly dyes, derived from natural sources or synthesized using environmentally benign processes, provide a more sustainable option. However, the adoption of eco-friendly dyes is not without challenges. While they offer several advantages, such as reduced environmental impact and improved safety, they can be more expensive and difficult to scale up compared to traditional synthetic dyes.

To address the environmental impact of dye pollution, governments and regulatory agencies have implemented various measures. These include setting strict limits on pollutant concentrations in wastewater, requiring industries to use pre-treatment or advanced treatment techniques, and imposing penalties for non-compliance. Additionally, incentives are often provided to encourage the adoption of eco-friendly practices, such as zero-liquid discharge systems and the use of biodegradable dyes (Al-Tohamy et al., 2022; Lin et al., 2023; Periyasamy, 2024; Che and Yang, 2022; Yadav et al., 2023).

1.10. Methylene Blue:

Methylene blue (MB), a synthetic dye with the chemical formula $C_{16}H_{18}ClN_3S$ (Figure 5), is widely used in various industries, including textiles, paper, and pharmaceuticals (Khodaie et al., 2013).While MB has certain therapeutic applications, such as treating malaria and vasoplegia, its release into the environment poses significant health and environmental risks (Ginimuge and Jyothi, 2010; Meissner et al., 2006; Kofidis et al., 2001; Ahmad and Kumar, 2010). MB can cause various health issues in humans, including cyanosis, tissue necrosis, vomiting, jaundice, shock, and elevated heart rate. It can also negatively impact aquatic life, leading to growth suppression, pigment loss, and reduced protein content in algae like *Spirulina platensis* and *C. vulgaris* (Moorthy et al., 2021).Therefore, effective removal of MB from wastewater is crucial. Various techniques, including adsorption, biodegradation, and advanced oxidation processes, have been employed to remove MB from wastewater.Among these, polysaccharide-based composite hydrogels have emerged as a promising material for MB removal due to their large surface area,

excellent mechanical properties, swelling capability, and potential for large-scale production (Sivakumar and Lee, 2022).

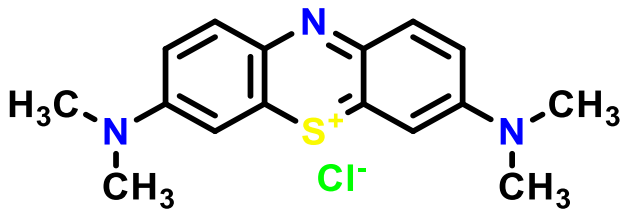

Figure 5: Chemical structure of methylene blue

1.11. Nanaoparticles

Nanoparticles, materials with at least one dimension in the nanometer range (1-100 nm), have unique properties that make them attractive for a wide range of applications. These properties include increased surface area-to-volume ratio and quantum confinement effects (Khan et al., 2019; Vallabani et al., 2023).The increased surface area of nanoparticles enhances their reactivity and interaction with other materials, making them effective catalysts for various processes (Baig et al., 2021; Sajid, 2022). Quantum confinement effects, which arise from the confinement of electrons and holes within the nanoparticle's dimensions, lead to unique optical, electronic, and magnetic properties (Ussia et al., 2024; Agarwal et al., 2023). However, it is important to note that the unique properties of nanoparticles also raise concerns about their potential environmental and health impacts. The increased surface area and reactivity of nanoparticles can lead to increased toxicity and reactivity, making them potentially harmful to the environment and human health.

Based on their dimensions, nanostructures are broadly categorized as shown in Table 1 (Joudeh and Linke, 2022).

Table 1: Classification of nanostructure according to their dimension.

Dimensionality	Nanostructure	Description
0D	Nanoparticles	Spherical or nearly spherical particles with unique properties like quantum confinement effects and LSPR.
0D	Nanoclusters	Small, tightly bound groups of atoms or molecules with unique electronic and magnetic properties.
0D	Fullerenes	Cage-like structures composed of carbon atoms arranged in a spherical or elliptical shape.
1D	Nanowires	Cylindrical or rod-shaped structures with anisotropic properties (Joudeh and Linke, 2022).
1D	Nanorods	Similar to nanowires but with a more irregular shape or smaller aspect ratio.
1D	Nanobelts	Flat, ribbon-like structures with unique optical and electronic properties.
2D	Graphene	A single layer of carbon atoms arranged in a hexagonal lattice.
2D	Transition metal dichalcogenides (TMDs)	Layered materials composed of transition metal atoms sandwiched between two layers of chalcogen atoms (e.g., sulfur, selenium).
2D	Black phosphorus	A layered material composed of phosphorus atoms arranged in a puckered honeycomb structure.
3D	Nanoporous	Materials with a porous structure on the

	materials	nanoscale.
3D	Nanostructured thin films	Thin films with a nanostructured morphology.
3D	Nanostructured bulk materials	Materials with a nanostructured internal structure.

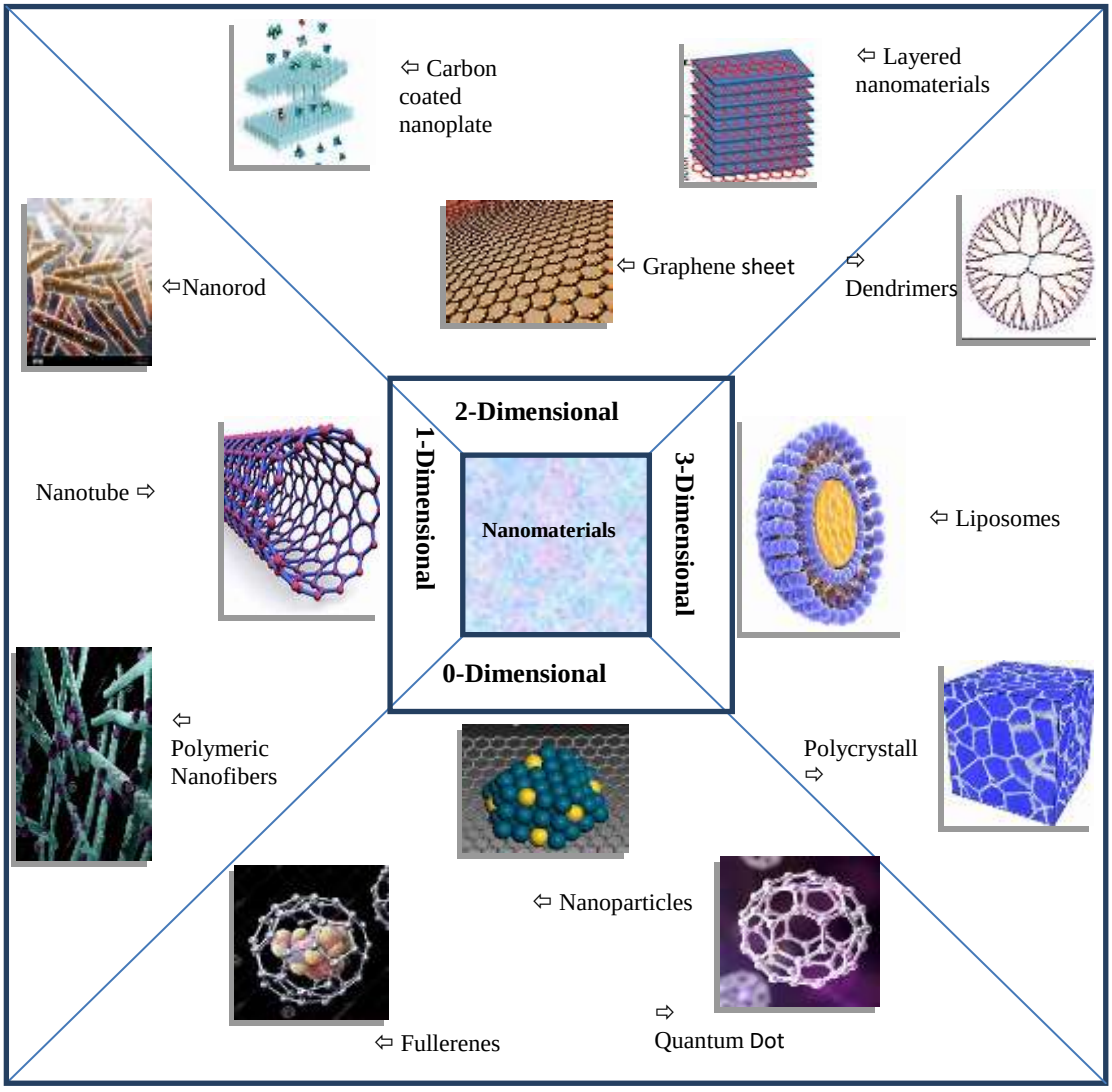

Figure 6: Classification of nanostructures on the basis of dimension.

Synthesis of Nanoparticles

Commonly top-down methods and botton-up synthesis are used to synthesize the metallic nanoparticles (Baig et al., 2021).Nanoparticles can be synthesized using various top-down and bottom-up approaches as summarized in Table 2:

Table 2: Synthesis of nanoparticles using various methods.

Synthesis Method	Advantages	Disadvantages
Top-Down		
Mechanical Milling	Simple, scalable, low cost	Introduces defects, limited control over particle size and shape
Nanolithography	Precise control over shape and size	Complex, time-consuming, and expensive
Laser Ablation	Versatile, high-purity nanoparticles	Energy-intensive, complex equipment, limited control over shape and size
Sputtering	Precise control over layer composition and thickness	Slow, complex equipment, inefficient material usage
Bottom-Up		
Sol-Gel	Versatile, low-temperature process, good control over particle size and shape	Time-consuming, potential for cracking, requires careful control of reaction conditions
Spinning	Simple, scalable, produces fibers with controlled diameter and morphology	Limited to fiber-shaped nanostructures, potential for low production rates
Chemical Vapor Deposition	High-quality nanoparticles, precise control over composition and structure	Complex equipment, high-temperature process, toxic precursors, potential for low deposition rates
Pyrolysis	Simple, scalable, rapid	High-temperature process, limited

	production of nanoparticles	control over particle size distribution, potential for toxic byproducts
Biosynthesis		
Biosynthesis	Eco-friendly, biocompatible, uses non-toxic chemicals	Slower reaction rates, limited control over nanoparticle properties, scaling challenges

Top-Down Approaches

Top-down approaches involve breaking down larger materials into smaller nanoparticles.

Mechanical Milling: This technique involves grinding materials to reduce particle size. It is a simple and widely used method, but it can introduce defects and impurities (Khan et al., 2022; Mekuye and Abera, 2023; Damonte et al., 2004; Aznan and Johan, 2012; Arbain et al., 2011; Yadav et al., 2012; Wei et al., 2023).

Nanolithography: This technique involves using lithographic techniques to create nanoscale patterns and structures. While it offers precise control over shape and size, it is complex, time-consuming, and expensive (Sharma et al., 2022; Colson et al., 2013; Pimpin and Srituravanich, 2012; Venugopal and Kim, 2013; Tiberto et al., 2015).

Laser Ablation: This technique involves using a laser to vaporize a target material, creating nanoparticles in the gas phase. It is a versatile method for producing various types of nanoparticles but can be energy-intensive and may introduce impurities (Kim et al., 2017; Naser et al., 2019; Gondal et al., 2009; Rashid et al., 2021; Amendola and Meneghetti, 2009).

Sputtering: This technique involves bombarding a target material with high-energy ions to eject atoms or molecules, which can then deposit onto a substrate or form nanoparticles. It offers precise control over layer composition and thickness but can be slow and requires complex equipment (Shah and Gavrin, 2006; Chung and Liu, 2004; Verma et al., 2018; Dreesen et al., 2009; Rane et al., 2018).

Bottom-Up Approaches

Sol-Gel: This method involves the hydrolysis and condensation of precursor materials to form a sol, which then gels and dries to form nanoparticles. It is a versatile technique for producing a variety of nanomaterials (Parashar et al., 2020; Bokov et al., 2021; Hasnidawani et al., 2016; Dubey et al., 2015; Chen and He, 2001; Alagiri et al., 2012; Guo et al., 2016; Navas et al., 2021).

Spinning: This technique involves spinning a liquid precursor to form nanofibers. It is suitable for producing fibrous materials but has limitations in terms of shape control and scalability (Stojanovska et al., 2016; Tai et al., 2008; Nguyen et al., 2010; Gu et al., 2017; Iskandar, 2009).

Chemical Vapor Deposition (CVD): This technique involves the deposition of a thin film of material from a gaseous precursor. It is a versatile method for producing high-quality nanoparticles but can be complex and energy-intensive (Manawi et al., 2018; Adachi et al., 2003; Lee et al., 2011; Gulino et al., 2005; Kumar and Ando, 2010; Saeed et al., 2020).

Pyrolysis: This technique involves the thermal decomposition of precursor materials to form nanoparticles. It is a simple and scalable method but can produce unwanted by-products and requires high temperatures (Odularu, 2018; Navaladian et al., 2007; Betancourt-Galindo et al., 2014; Davar et al., 2010; Ealia and Saravanakumar, 2017; Zahid et al., 2018; Din et al., 2019; Nemade and Waghuley, 2014; Mansour et al., 2017; Ismael et al., 2024; Jamkhande et al., 2019).

Biosynthesis.

Biosynthesis is an environmentally friendly approach to nanoparticle synthesis that utilizes biological entities like bacteria, fungi, plants, and algae. This method offers several advantages, including the use of non-toxic chemicals, mild reaction conditions, and the production of biocompatible nanoparticles.Various microorganisms have been used for the biosynthesis of nanoparticles. For example, *Pseudomonas aeruginosa* has been used to synthesize gold nanoparticles (Husseiny

et al., 2007), while *Bacillus subtilis* has been used to synthesize TiO_2 nanoparticles (Kirthi et al., 2011). Fungi like *Fusarium oxysporum* and *Aspergillus niger* can also be used to synthesize nanoparticles (Chaudhary et al., 2020). Plant extracts, such as those from tea leaves, neem leaves, and aloe vera, have also been employed for nanoparticle synthesis (Li et al., 2011).

Biosynthesis typically involves the reduction of metal ions to their corresponding nanoparticles using biological molecules such as enzymes, proteins, or metabolites. The biological agents act as reducing and capping agents, controlling the size, shape, and stability of the nanoparticles.While biosynthesis offers several advantages, it also has limitations. The process can be slower compared to chemical methods, and it can be challenging to achieve precise control over nanoparticle properties. Additionally, scaling up biosynthesis for industrial production can be difficult, and the potential for contamination from biological materials exists.Despite these challenges, biosynthesis remains a promising approach for the sustainable production of nanoparticles with various applications in fields such as medicine, catalysis, and materials science (Kulkarni and Muddapur, 2014; Vijayaraghavan and Ashokkumar, 2017; Selvarajan and Mohanasrinivasan, 2013; Elamawi et al., 2018; Jamkhande et al., 2019; Saravanan et al., 2021).

1.12. Cellulose Nanofibers: A Sustainable Material

Cellulose nanofibers (CNFs) are derived from cellulose, the most abundant organic polymer on Earth. Cellulose is a linear polymer composed of glucose units linked by β-1,4-glycosidic bonds (Figure 7). Each glucose unit has three hydroxyl groups (-OH) that can form hydrogen bonds with neighboring glucose units, contributing to the strong intermolecular forces and high crystallinity of cellulose. The linear chains of cellulose molecules can further aggregate into microfibrils, which are bundles of cellulose chains held together by hydrogen bonds. CNFs are obtained by breaking down these microfibrils into individual nanofibers.

CNFs can be used to reinforce composite materials, improving their mechanical properties. Their high surface area makes them ideal for use in barrier

films and coatings. Additionally, CNFs are biocompatible and biodegradable, making them suitable for biomedical applications like wound dressings, drug delivery, and tissue engineering scaffolds (Pennells et al., 2020; Lu et al., 2024; Benítez and Walther, 2017; Feng et al., 2014; Rodriguez et al., 2011).

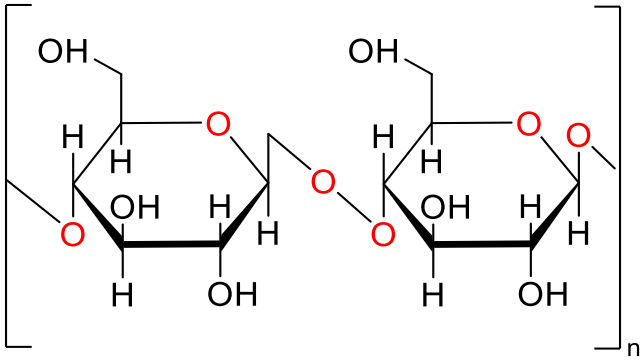

Figure 7: Chemical structure of cellulose (glucose units linked by β-1,4-glycosidic bonds)

Cellulose nanofibers (CNFs) are derived from cellulose, the most abundant organic polymer on Earth. CNFs are characterized by their high aspect ratio (length-to-diameter ratio) and nanoscale diameter, typically ranging from a few to hundreds of nanometers. These unique properties make CNFs attractive for a wide range of applications.

CNFs can be produced through various methods, including mechanical, chemical, and enzymatic processes. Mechanical methods involve breaking down cellulose fibers into smaller nanofibers through processes such as high-shear homogenization, ultrasonication, and microfluidization (Nagarajan et al., 2021; Widiarto et al., 2019; Stelte and Sanadi, 2009; Zhang et al., 2015). Chemical methods, such as acid hydrolysis and TEMPO oxidation, can be used to selectively remove non-cellulosic materials and modify the cellulose surface to enhance fibrillation (Soni et al., 2015; Onyianta et al., 2020; Madivoli et al., 2022; Menon et al., 2017). Enzymatic hydrolysis, a more environmentally friendly approach, uses enzymes to break down cellulose fibers into nanofibers (Djafari Petroudy et al.,

2021; Karim et al., 2017; De Campos et al., 2013; Martelli-Tosi et al., 2016; Hassan et al., 2021; Tibolla et al., 2014).

As mentioned below, CNFs have a wide range of applications due to their unique properties:

Water Treatment: CNFs can be used as adsorbents, membranes, and catalysts for water purification (Aoudi et al., 2022; Li et al., 2021; Mautner, 2020; Roy et al., 2021).

Energy Storage: CNFs can be used as electrode materials in supercapacitors and batteries, as well as proton exchange membranes in fuel cells (Fukuhara et al., 2021; Hasnidawani et al., 2016; Li et al., 2023; Maity et al., 2023).

Biomedical Applications: CNFs can be used in drug delivery, tissue engineering, and wound healing due to their biocompatibility and biodegradability (Heise et al., 2021; Moohan et al., 2019; Ong et al., 2023; Syed et al., 2023).

Electronics and Sensors: CNFs can be used as flexible substrates for electronic devices and as sensors for various analytes (Lahiri et al., 2021; Rivadeneyra et al., 2021; Teodoro et al., 2021; Ummartyotin and Manuspiya, 2015; Zhu et al., 2020).

Food Packaging: CNF-based packaging materials can improve the shelf life of food products and reduce plastic waste (Liu et al., 2021; Lu et al., 2024; Maresca and Mauriello, 2022; Sánchez-Gutiérrez et al., 2021).

1.13. Cellulose Nanofibers (CNFs) for Water Treatment

Cellulose nanofibers (CNFs) are emerging as a promising material for water treatment due to their unique properties, including high surface area, exceptional mechanical strength, biocompatibility, and environmental sustainability (Carpenter et al., 2015; Sayyed et al., 2021). Their high surface area enables them to effectively adsorb pollutants such as heavy metals, organic dyes, and pharmaceutical compounds (Norfarhana et al., 2024; Sueraya et al., 2024; Yu et al., 2020; Kurniawan et al., 2023). Additionally, CNFs can be used to create high-performance membranes for water filtration, removing bacteria, viruses, and

microplastics.Furthermore, CNFs can be functionalized to enhance their adsorption capacity and selectivity for specific pollutants. For example, CNFs can be modified with functional groups to selectively adsorb heavy metals like lead, cadmium, and mercury. The biodegradability and low environmental impact of CNFs make them a sustainable alternative to synthetic materials (Lamm et al., 2021; Wang, 2019; Gopakumar et al., 2017; Sharma et al., 2024).

In addition to water treatment, CNFs have applications in various other fields, including energy storage, tissue engineering, and composite materials (Yusuf et al., 2024; Hasnidawani et al., 2016; Li et al., 2023; Maity et al., 2023; Heise et al., 2021; Moohan et al., 2019; Ong et al., 2023; Syed et al., 2023; Lahiri et al., 2021; Rivadeneyra et al., 2021; Teodoro et al., 2021; Ummartyotin and Manuspiya, 2015; Zhu et al., 2020; Liu et al., 2021; Lu et al., 2024; Maresca and Mauriello, 2022; Sánchez-Gutiérrez et al., 2021). Their high surface area, mechanical strength, and biocompatibility make them a valuable material for addressing various challenges in these fields.

1.14. CNFs in Pollutant Removal:

CNFs have shown promise in water treatment for removing various pollutants due to their adaptability and customizable surface chemistry. They can be functionalized to target specific contaminants, such as heavy metals, organic dyes, and pharmaceutical compounds (Norfarhana et al., 2024; Sueraya et al., 2024; Yu et al., 2020). CNFs can adsorb heavy metals like lead, cadmium, and arsenic, reduce water toxicity, and adsorb industrial dyes, reducing water color and toxicity. Though industrial dyes present serious environmental risks, CNFs have shown promise in adsorbing these dyes, lowering their toxicity and color in water (Kurniawan et al., 2023). They also effectively adsorb pharmaceutical compounds, which are challenging to remove via conventional filtration, making them a promising solution for water treatment.

Cellulose nanofibers (CNFs) are versatile materials with high surface area, mechanical strength, biocompatibility, and renewability. They can be used in energy storage devices, tissue engineering, and composite materials (Yusuf et al., 2024).

CNFs enhance electrode stability, promote tissue regeneration, and are eco-friendly, making them a valuable asset in addressing water pollution challenges and supporting technological advancements in various fields. Their high surface area, biocompatibility, and renewability make them a promising material for advanced water treatment applications (Yadav et al., 2020; Zhang et al., 2023).

1.15. Algae: A Versatile Resource for Sustainability

Algae, a diverse group of photosynthetic organisms, offer a wide range of applications with significant potential to address global challenges. Their unique biochemical composition, rapid growth rate, and ability to thrive in diverse environments make them a valuable resource for various industries.

Biofuels and Renewable Energy: Higher lipid content and rapid growth rate of algae make them a promising source for biofuel production. Algae-derived biofuels, such as biodiesel, bioethanol, and biogas, offer a sustainable alternative to fossil fuels. By utilizing carbon dioxide as a carbon source, algae can contribute to carbon capture and sequestration. For example, species like *Botryococcusbraunii*, *Chlorella* sp., *Nannochloropsis* sp., and *Phaeodactylumtricornutum* are known for their high lipid content and are being extensively studied for biofuel production (Arora et al., 2021; Sarwer et al., 2022; Demirbas, 2011; Chisti, 2007).

Pharmaceuticals and Biomedicine: Algae produce a variety of bioactive compounds, including polysaccharides, polyunsaturated fatty acids, and pigments like phycocyanin, chlorophyll, and carotenoids. These compounds have potential applications in medicine, such as antiviral, anticancer, antioxidant, and antibacterial therapies. Algal-derived biomaterials are also being explored for drug delivery and tissue engineering (Rocha et al., 2007; Ale et al., 2011; Campos et al., 2012; Vishchuk et al., 2013; Abu et al., 2015; Velatooru et al., 2016; Kamei et al., 2009; Kok et al., 2016).

Nutraceuticals and Functional Foods: Algae, particularly species like *Chlorella* and *Spirulina*, are rich in essential nutrients, vitamins, minerals, and antioxidants. They are used as dietary supplements and functional food ingredients to promote health

and well-being (Ahmad et al., 2024; Wells et al., 2017; Domínguez, 2013; Escalante andPérez-Rico, 2021; Kiran and Venkata Mohan, 2021; Nehra, 2022; Udayan et al., 2017; Wells et al., 2017).

Bioplastics and Sustainable Materials: Algae-derived cellulose and other biopolymers can be used to produce biodegradable plastics and other sustainable materials. These bioplastics offer an environmentally friendly alternative to petroleum-based plastics (Mohan et al., 2022; Lim et al., 2021). Additionally, cellulose nanofibers (CNFs) derived from algae can be used to create advanced materials with unique properties (Chen et al., 2022; Lim et al., 2021).

Environmental Remediation: Algae can play a significant role in environmental remediation by removing pollutants from water and air. They can absorb nutrients like nitrogen and phosphorus from wastewater, reducing water pollution. Algae-based technologies are also being explored for carbon capture and sequestration (Hammed et al., 2016; Wang et al., 2023). Some algae species have the ability to absorb heavy metals from contaminated water (Lee et al., 2004; Mehta and Gaur, 2001; Karthikeyan et al., 2007; Arıca et al., 2005; Deng et al., 2006; Nuhoglu et al., 2002; Rincón et al., 2005; Singh et al., 2007; Rao et al., 2005; Onyancha et al., 2008).

Agriculture and Aquaculture: Algae can be used as biofertilizers and biostimulants in agriculture, improving soil health and crop yield. They can also be used as feed for fish and other aquatic organisms in aquaculture, promoting sustainable aquaculture practices (Abdel-Raouf, 2012; Trentacoste et al., 2015; Shields and Lupatsch, 2012).

Cosmetics and Personal Care: Algae-based ingredients, such as polysaccharides and fatty acids, are used in various cosmetic products, including skincare, haircare, and makeup. These ingredients offer numerous benefits, including moisturizing, antioxidant, and anti-aging properties (Ariede et al., 2017; Aslam et al., 2021; Dantas et al., 2019; Morikawa et al., 2018; Bedoux et al., 2014; Ahsan, 2019; Otero et al., 2019; Lafarga et al., 2019).

1.16. Algae: A Sustainable Source for Cellulose Nanofibers:

Cellulose nanofibers (CNFs) derived from algae offer a sustainable and environmentally friendly alternative to traditional CNF sources like wood pulp. Algae, a diverse group of photosynthetic organisms, can be cultivated in various settings, including wastewater treatment plants and marginal lands. This makes algae a renewable and abundant source of biomass for CNF production, reducing the reliance on non-renewable resources and minimizing environmental impact (Bhatt et al., 2022).

Algal CNFs possess unique properties such as high surface area, biodegradability, and tunable surface chemistry, making them suitable for a wide range of applications. These properties, combined with their sustainable production, make algal CNFs a promising material for various industries.

In water treatment, algal CNFs can be used as adsorbents to remove pollutants such as heavy metals, dyes, and organic compounds (Norfarhana et al., 2024; Sueraya et al., 2024; Yu et al., 2020; Kurniawan et al., 2023). They can also be used to create high-performance membranes for water filtration. In the biomedical field, algal CNFs can be used in tissue engineering, drug delivery, and wound healing due to their biocompatibility and biodegradability. Additionally, algal CNFs can be incorporated into composite materials to enhance their mechanical properties, thermal conductivity, and barrier properties.A variety of algae species, including macroalgae and microalgae, have been used as a source of CNFs. Some common algae species used for CNF production include *Ulva*, *Sargassum*, *Laminaria*, *Chlorella*, *Spirulina*, and *Nannochloropsis* (Table 3).

The Table 3 presents the yield (% dry weight) of cellulose nanofibers (CNFs) obtained from various algal species. The yield of CNFs varies significantly among different algal species. This variation can be attributed to several factors, including cell wall structure, the extraction method used, and growth conditions.Some species, such as *C.glomerata* and *Chaetomorpha melagonium*, showed relatively high yields (82% and 41%, respectively), indicating their potential as promising sources for CNF

production.However, the extraction method employed can significantly impact the yield. Different studies have used various methods, which could contribute to the observed variability in yields.

Table 3: Yield of cellulose nanofibers (CNFs) from dry biomass of different algae species.

Serial No.	Algae	Yield	Reference
1	*Ulva fasciata*	14.7±1.8%	Lakshmi et al., 2017
2	*Nannochloropsis gaditana*	25%	Samia et al., 2016
3	*Cystosphaera jacquinottii*	4.58% (±0.34)	Paniz et al., 2020
4	*Cladophora glomerata*	82%	Xiang et al., 2016
5	*Ulva lactuca*	43.07%	Jmel et al., 2019
6	*Cladophora rupestris*	28.5%	Cronshaw et al., 1958
7	*Chaetomorpha melagonium*	41%	Cronshaw et al., 1958
8	*Enteromorpha sp.*	21%	Cronshaw et al., 1958
9	*Halidrys siliquosa*	14%	Cronshaw et al., 1958
10	*Laminaria saccharina*	18%	Cronshaw et al., 1958
11	*Ptilota plumose*	24%	Cronshaw et al., 1958
12	*Griffithsia flosculosa*	22%	Cronshaw et al., 1958
13	*Laminaria digitate*	20%	Cronshaw et al., 1958
14	*Fucus serratus*	13.5%	Cronshaw et al., 1958

15	*Chaetomorpha antennina*	34±0.9%	Bhutiya et al., 2018
16	*Gelidiella acerosa*	13.65%	Siddhanta et al., 2009
17	*Cladophora glomerata*	21.6%	Xiang et al., 2016
18	Brown algae	18%	Gao et al., 2018
19	*Gelidium elegans*	15.5%	Chen et al., 2016
20	*Posidonia oceanica* brown algae	32.5%	Tarchoun et al., 2019

1.17. Nanocomposites

Nanocomposites are advanced materials engineered by combining two or more different materials at the nanoscale. This unique structural arrangement results in enhanced properties that often surpass those of their individual components (Nurazzi et al., 2021). By incorporating nanoscale reinforcements, such as carbon nanotubes or graphene, nanocomposites exhibit improved mechanical properties, including increased strength and durability. These materials also possess enhanced electrical conductivity, making them suitable for applications in electronics and sensors (Papageorgiou et al., 2020). Furthermore, nanocomposites offer superior thermal properties, making them ideal for use in aerospace and automotive industries. Some nanocomposites even exhibit catalytic properties, which can be beneficial for energy and environmental applications. Due to their advanced properties, nanocomposites find applications in a wide range of fields, including electronics, aerospace, automotive, and medicine. In the field of water treatment, nanocomposites are particularly effective in removing pollutants like heavy metals and pharmaceutical compounds due to their high surface area and tunable properties (Rahimi-Ahar and Ahar, 2024; Sonawane et al., 2018).

1.18. ZnO-CNFNanocomposites: A Synergistic Approach

The combination of cellulose nanofibers (CNFs) and zinc oxide nanoparticles (ZnO-NPs) in nanocomposites has gained significant attention due to their synergistic effects, which enhance the properties of both materials. This synergy can lead to improved performance in various applications, particularly in water treatment, where the removal of dyes and other pollutants is a major concern.

Enhanced Adsorption Capacity: CNFs, with their high surface area and active sites, can adsorb pollutants through various mechanisms, including electrostatic interactions, hydrogen bonding, and van der Waals forces. The incorporation of ZnO-NPs further enhances the adsorption capacity of the nanocomposite by providing additional adsorption sites and improving the accessibility of pollutants to the adsorbent surface (Chen et al., 2023; Hu et al., 2020; Wasim et al., 2021).

Enhanced Photocatalytic Activity: ZnO-NPs are well-known photocatalysts that can degrade organic pollutants under UV light by generating reactive oxygen species (ROS). CNFs can enhance the photocatalytic activity of ZnO-NPs by providing a stable support matrix, improving light absorption, and facilitating charge separation (Dehghani et al., 2020; Rabani et al., 2021; Shi et al., 2022, 2023).

Improved Mechanical Properties and Stability: CNFs can enhance the mechanical properties and stability of ZnO-based materials. The combination of these materials can lead to nanocomposites with improved strength, flexibility, and durability (Santos et al., 2024; Shi et al., 2019).

Antimicrobial Activity: ZnO-NPs exhibit antimicrobial properties, and their combination with CNFs can further enhance these properties. The synergistic effect of CNFs and ZnO-NPs can lead to improved antimicrobial activity against bacteria, fungi, and viruses (Arabkhani et al., 2023; Roy et al., 2021; Wu et al., 2023; Yan et al., 2023; Zhang et al., 2015).

Electrical and Sensing Applications: ZnO-NPs have semiconductor properties, making them useful for sensing applications. CNFs can enhance the electrical

conductivity and mechanical flexibility of ZnO-based sensors, leading to improved sensitivity and durability.

1.19. Synthesis of ZnO-CNF Nanocomposites:

Various techniques have been employed to create ZnO-CNF nanocomposites, each with its own advantages and limitations.*In-situ* synthesis involves the direct growth of ZnO nanoparticles onto the surface of CNFs, ensuring good dispersion and intimate contact. This method typically involves dispersing CNFs in a zinc salt solution, precipitating ZnO with a base, and then thermally treating the mixture to crystallize the nanoparticles. This method is advantageous as it prevents aggregation and enhances surface area for adsorption or photocatalysis (Lefatshe et al., 2017; Li et al., 2021; Yadollahi et al., 2015).

The sol-gel method involves the hydrolysis and condensation of a zinc precursor in the presence of CNFs. This method allows for precise control over the size and distribution of ZnO-NPs. The resulting nanocomposites exhibit high purity and homogeneity (Abdallah et al., 2024, 2024; Bokov et al., 2021; Liu et al., 2021).

Hydrothermal methods involve heating a mixture of CNFs and a zinc precursor in an autoclave under high temperature and pressure. This method can produce ZnO-CNF nanocomposites with controlled morphology, such as nanorods or nanospheres, which can enhance photocatalytic and antimicrobial properties (Guan et al., 2019; Narkpiban and Poonsawat, 2022; Wang et al., 2023). Chaurasia et al. (2010) utilized this method to synthesize cellulose acetate-ZnO NP composites for antibacterial applications.

Ultrasonic-assisted synthesis involves the use of ultrasound waves to disperse CNFs and Zn precursors, promoting the formation of ZnO-NPs on the CNF surface. This method can lead to rapid synthesis and improved dispersion of nanoparticles (Azizi et al., 2014; Kargarzadeh et al., 2017). Azizi et al. (2013) employed this technique to synthesize ZnO-NP-bacterial cellulose nanocomposites for antibacterial and thermal applications.The choice of synthesis method depends on various factors,

including the desired properties of the nanocomposite, the scale of production, and the cost-effectiveness of the process.

1.20. Methylene Blue Removal

ZnO-CNF nanocomposites offer a promising solution for the removal of methylene blue (MB) from wastewater. The high surface area and porous structure of CNFs, combined with the photocatalytic activity of ZnO-NPs, enhance the adsorption and degradation of MB (Ahmed et al., 2019; Dehghani et al., 2020; Rabani et al., 2021; Shi et al., 2022, 2023). Factors such as pH, contact time, dye concentration, and light intensity influence the efficiency of MB removal. ZnO-CNF nanocomposites, derived from renewable sources, offer a sustainable and cost-effective solution for wastewater treatment. However, challenges such as nanoparticle leaching and scalability need to be addressed to fully realize their potential (Nguyen et al., 2024).

Table 4 presents a comparative analysis of methylene blue (MB) removal efficiency using various ZnO-based composites reported in the literature.It is evident that the ZnO-CNF nanocomposites synthesized in this study demonstrate exceptional MB removal efficiency, exceeding 90% in many cases.A variety of materials, including CNFs, cellulose acetate, and bacterial cellulose, have been used to create ZnO-based composites.Pseudo-first-order and pseudo-second-order kinetics are commonly used to describe the adsorption process.Both UV light and Sun light

Table 4: Comparative analysis of MB removal efficiency by ZnO-based composites.

Sl No.	Material used for removal	Time (min)	Irradiation source	% removal of MB	Mechanism	Concentration of MB	References
1	ZnO-CNF nanocomposite	150	Sun light	88.13-94	Pseudo-second-order kinetic	10-1 mg L^{-1}	This work
2	Zno-CNF nano composite	10	UV light	>99	Pseudo-First-order kinetics	10 mg L^{-1}	Dehghani et al., 2020
3	Zno-CNF nano composite	10	UV light	94	Pseudo-First-order kinetics	10 mg L^{-1}	Dehghani et al., 2020
4	CNC–ZnO nanohybrids	200	UV light	95.21	Pseudo-First-order kinetics	5.0 9 *10^{-5} M	Abdalkarim et al., 2018
5	CNC/ZnO nanocomposite	1440	Sun light	97.5%	Pseudo-second-order kinetic,	100 mg L^{-1}	Oyewo et al., 2020

Sl No.	Material used for removal	Time (min)	Irradiation source	% removal of MB	Mechanism	Concentration of MB	References
6	Protein-capped ZnO nanoparticles	30	UV light	About 90%	Pseudo First-order kinetics	10 µM	Jain et al., 2014
7	Cellulose acetate ZnO-NPs (CA-ZnO-NP)	120	UV-light, Sunlight.	30%, 75%	Pseudo First-order kinetics	100 mg L^{-1}	Abu-Dalo et al., 2021
8	Zinc oxide/cellulose nanocomposite	300	UV light	79	Pseudo First-order kinetics	3.25 g L^{-1}	Lefatshe et al., 2017
9	ZnO/CNCs Nanocomposite	120	Sun light	88	Pseudo First-order kinetics	10 mg L^{-1}	Modi and Fulekar, 2020

Sl No.	Material used for removal	Time (min)	Irradiation source	% removal of MB	Mechanism	Concentration of MB	References
10	ZnO/CNC nanohybrids	240	Sun light	93.55	Pseudo-second-orderkinetics	50 mg L^{-1}	Guan et al., 2019
11	ZnO/Micro Crystalline Cellulose	120	UV light	97.4%	Pseudo-First-order kinetics	10 mg L^{-1}	Zuo et al., 2014
12	Fe-Doped ZnO/Bacterial Cellulose-Based Composite Aerogel	80	Sun light	90	Pseudo First-order kinetics	20 mg L^{-1}	Zhang et al., 2024
13	Fe-doped ZnO/nanocellulose	120	Sun light	98.84%	Pseudo First-order kinetics	5 mg L^{-1}	Farahani et al., 2022

CHAPTER – 2

MATERIALS AND METHOD

2.1. Collection and Identification of *Cladophora glomerata* (L.) Kutz

C.glomerata (L.) Kutz., a filamentous, branched freshwater green alga, was collected from the Tlawng River located at coordinates 23.48° N, 92.66° E in Aizawl, Mizoram, India during the month of April 2021 (Figure 8). In order to remove any contaminants, the collected algal biomass was thoroughly cleaned with tap water and then rinsed with distilled water. The collected sample were identified using established protocol and with the help of expert. The biomass was left to air-dry in the sun for three days.

2.2. Cultivation and Harvesting of *Chlorellavulgaris* Beijerinck

The identified test organism *C. vulgaris* Bijerinck was procured from the algal culture laboratory, Department of Botany, Mizoram University. The sample were cultured in Chu-10 medium (Chu, 1942) (Table 5). The culture was kept in anair-conditioned culture room at 17°C (Figure 9). The culture was grown in 250-, 500-, 1000- mL sterile Erlenmeyer flasks under fluorescent tubes (30 W) for 8 h (Gerloff et al., 1950). The medium's pH was maintained at 6.8±0.2 using 0.1N HCl and 0.1N NaOH. To ensure uniform growth, the cultures were shaken three times a day.

2.3. Preparation of Aqueous Extract of Algae

For the preparation of algal extract, to get rid of any traces of nutrients and cell debris, *C. vulgaris* Bijerinck was harvested by centrifugation at 2000 g for 10 min and then rinsed three times with sterile Milli-Q water. Then the biomass was kept for air dry and the dried biomass were collected. The biomass of *C. glomerata* (L.) Kutz. were collected from the field. On a hot plate, about 1g of dried biomass was re-suspended in 100 mL of Milli-Q water and heated to 80°C. After cooling down to room temperature, 0.45 µ Whatman's filter paper was used to filter the suspension. The filtrate was then stored for later use at 4°C.

Figure 8: (a) *C. glomerata* in natural habitat, (b) Photograph during collection

Figure 9: Laboratory cultivation of algae: from inoculation to harvesting.

Table 5: Nutrient composition of Chu-10 medium for algae cultivation.

Macronutrients	g L^{-1}	Micronutrients	g L^{-1}
KNO_3	0.04	$MnCl_2.4H_2O$	0.5
K_2HPO_4	0.01	$Na_2MoO_4.2H_2O$	0.01
$MgSO_4.7H_2O$	0.04	H_3BO_3	0.5
Na_2SiO_3	0.02	$CuSO_4.5H_2O$	0.02
Ferric citrate	0.003	$CoCl_2$	0.04
Citric acid	0.003	$ZnSO_4$	0.05

2.4. Ultrasoncation-assisted and Algal Extracellular Synthesis of ZnO-NPs

Biological synthesis of zinc oxide nanoparticles was done by using procedure as described by Mahana et al. (2020). Initially, after being cleaned with Milli-Q water, 1 g of fresh biomass was re-suspended in 100 mL of Milli-Q water and heated gradually for 30 min at 50ºC. Following cooling, 0.04 µm Whatman filter paper was used to filter the suspension, and the filtrate was then kept for nanoparticle formation at 4ºC. In a separate step, a 10 mL of 0.5 M $ZnCl_2 \cdot 2H_2O$ underwent an 8 min sonication process using an ultrasonicator (LABSONIC-P, Sartorius, Germany). The ultrasonic waves, emitted through a 3 mm diameter 100 mm long titanium horn, operated at a 24 kHz frequency and 40-70 % power amplitude. After Ultrasonication, equal amount of 1 % polyvinylpyrrolidone (PVP, %w/v) and the aqueous extract were added, yielding a white precipitate. This precipitate was further sonicated for 3 min at 70 % amplitude. After careful supernatant decanting, the white precipitate was dried until a consistent weight was reached.

2.5. Extraction of Cellulose from Algal Biomass

Cellulose extraction from the algal biomass was conducted following the methodology outlined by Chen et al., (2016). This multi-step process involved sequential treatments to remove impurities and isolate the cellulose component. Initially, 20 g of air-dried algal biomass were ground into a fine powder using a household grinder to facilitate subsequent processing. A 10 g portion of this powdered biomass was then subjected to Soxhlet extraction using a 2:1 v/v toluene: ethanol mixture for 7 h at 120°C. This step removed any lipid and wax components from the biomass. The extracted liquid was discarded, and the remaining insoluble fraction rinsed thoroughly with 99% ethanol to ensure complete removal of solvent. After that, the sample was air-dried for 24 h at 30°C to get rid of any remaining moisture. Following dewaxing and drying, samples were treated with a 2% NaOH solution at 80°C for 2 h. This alkaline treatment removed hemicellulose and lignin, leaving behind a cellulose-rich residue.

After cooling, the alkalized biomass was treated with 30% hydrogen peroxide (H_2O_2) at 50°C for 2 h to further purify the cellulose by removing any remaining lignin and other impurities. Following ten min of centrifugation at 2000 g, the treated material was discarded along with the supernatant.The insoluble fraction was washed repeatedly with Milli-Q water until it reached a pH of 7.0 to ensure complete removal of any residual chemicals. After another centrifugation, the insoluble fraction, which consisted primarily of cellulose, was collected and oven-dried at 50°C for 2 h. This final step yielded pristine white cellulose, ready for further analysis or use.

2.6. Preparation of Cellulose Nanofibers (CNF) and Cellulose Nanocrystal (CNC)

Cellulose nanofibers (CNF) and cellulose nanocrystals (CNC) were prepared from the extracted cellulose following a modified protocol adapted from Chen et al. (2016). About 1.0 g of bleached cellulose was dispersed in a 100 mL 20% sulphuric acid solution and stirred at 45°C for 45 min. This acid hydrolysis process selectively

cleaves the amorphous regions of the cellulose, resulting in the formation of nanofibers and nanocrystals. After centrifugation, the solid residue was treated with 4 mL of 1% NaOH to adjust the pH to 6-7. This step neutralizes the residual sulfuric acid and prevents further degradation of the cellulose nanostructures. The pH-adjusted cellulose was then subjected to sonication for 30 min, using an ultrasonicator (LABSONIC-P, Sartorius, Germany) with a 2-min on, 1-min off cycle. Sonication helps to disperse the cellulose nanofibers and nanocrystals, improving their homogeneity. Finally, the prepared CNF and CNC were lyophilized to remove any residual water and ensure their preservation. The resulting white fibers were stored at 4°C for subsequent analysis and applications.

2.7. Synthesis of ZnO-CNF Nanocomposite

The synthesis of the ZnO-CNF nanocomposite was carried out following a modified procedure adapted from Ali et al. (2016). Approximately 0.5 g of *C. glomerata* CNF were dispersed in 100 mL of MilliQ water and thoroughly mixed. To this dispersion, $ZnCl_2.2H_2O$ (1 mM) was added and stirred magnetically at 200 rpm for 1 h. This step allowed for the adsorption of zinc ions onto the surface of the CNF, Subsequently, the mixture was subjected to ultrasonication (LABSONIC-P, Sartorius, Germany) for 20 min to enhance the dispersion of the CNF and promote the interaction between the zinc ions and the cellulose nanofibers. Then, NaOH solution (10 mM) was added to the mixture, and the pH was adjusted to 10 using 1 M NaOH and 1 M HCl solutions. This alkaline environment facilitated the precipitation of zinc oxide (ZnO) nanoparticles onto the surface of the CNF. The mixture was continuously stirred at 200 g for 30 min to ensure complete precipitation of ZnO-NPs and to allow for their uniform distribution on the CNF surface. An additional 2 min of ultrasonication was performed to further improve the dispersion of the nanocomposite. After ultrasonication, the mixture was filtered to separate the solid nanocomposite from the liquid phase. The filter cake was thoroughly rinsed with 30% ethanol and distilled water to remove excess chemicals. The resulting nanocomposite was then dried overnight to remove residual moisture, the dried ZnO-CNF nanocomposite was cut

into approximately 5-mm piece using a sharp blade, preparing it for further analysis and applications.

2.8. Experimental Investigation of Methylene Blue (MB) Degradation and Catalyst Effects

Degradation studies were conducted using methylene blue (MB), which was procured from Himedia, India, without any additional purification.The study focused on two primary aspects: a time course study and a concentration-dependent investigation. This solution was then divided into four series: a control series without any catalyst, and three experimental series containing different catalysts: ZnO-NPs, CNF, and a ZnO-CNF nanocomposite. Each series received 10 mg of the respective catalyst and was mixed with 20 mL of the MB solution. The pH of each series was adjusted to 8 for standardization. To minimize photo-bleaching, the samples were shielded from light for 1 h before exposure to noon sunlight. The experiments were conducted under natural conditions with a temperature of 30±2°Cand a light intensity of 1120 LUX, as measured by a LUX meter. The time course study involved measuring the MB concentration at regular intervals over a period of 150 min. Samples were taken every 30 min and centrifuged at 4000 g for 10 min to remove the catalyst particles. The concentration of MB in the supernatant was then determined using a UV-VIS spectrophotometer at a wavelength of 663 nm, following the method described by Bano et al., (2021). The % removal of MB was determined using following equation:

$$Removal\ \% = \left(\frac{C_o - C}{C_o}\right) x100 \qquad (1)$$

Where,C_O represents the initial concentration, and C represents the final concentration of the MB solution.

2.9. Kinetics of Methylene Blue Degradation

To investigate the kinetics of methylene blue (MB) degradation, 20 mL of a 5 mg L^{-1} MB solution was prepared and exposed to direct sunlight irradiation. Various catalysts (ZnO-NPs, CNF, ZnO-CNF nanocomposite) were added to separate series,

while a control sample without any catalyst was maintained. The samples were subjected to different time intervals ranging from 0 to 150 min. Following each time interval, the catalyst was separated from the solution through centrifugation.

Kinetic Modelling

To characterize the adsorption kinetics of MB, the pseudo-first-order and pseudo-second-order models were employed. These models are widely used to describe adsorption processes and are based on the following equations:

A. Pseudo-first-order kinetic

The expression for the pseudo-first-order rate kinetics is the following, as described by Mahana et al. (2020).

$$q_t = q_e(1 - e^{-k_1 t}) \qquad (2)$$

Where:

q_e (mg g^{-1}) is equilibrium adsorption capacity
q_t (mg g^{-1}) is adsorbed capacity at time t (min)

k_1 (min^{-1}) is the rate constant.

B. Pseudo-second-order kinetics

The following equation provides the expression of the pseudo-second-order kinetics (Mahana et al., 2022):

$$q_t = \frac{q_e^2 k_2 t}{q_e k_2 t + 1} \qquad (3)$$

Where, k_2 (g^{-1} min^{-1}) is pseudo-second-order rate constant.

Data Analysis

The data analysis in the MB degradation kinetics study was conducted using non-linear curve fitting techniques applied to the pseudo-first-order and pseudo-second-order kinetic equations. The non-linear curve fitting, provides more precise estimates of the rate constants (k_1 and k_2) and equilibrium adsorption capacities (Qe) for each catalyst.

2.10. Adsorption Model

(i) *The Langmuir isotherm model*

The Langmuir equation (Langmuir 1918) describes monolayer sorption on a uniform surface without interaction between adsorbed molecules:

$$q_e = \frac{Q_m k_L C_e}{1+k_L C_e} \qquad (4)$$

Where:

q_e (mg g^{-1}) is the equilibrium adsorption of heavy metals
C_e (mg L^{-1}) is equilibrium concentration of the heavy metals
k_L (L mg^{-1}) denotes the constant relating to the free adsorption energy
Q_m (mg g^{-1}) is the maximum adsorption potential

The values of Q_m and k_L are determined by fitting experimental data to the Langmuir equation using non-linear curve fitting.

(ii) *The Freundlich isotherm model*

The correlation between the quantity of solute adsorbed on the surface of adsorbent and the solute concentration in the solution is described by an adsorption isotherm equation known as Freundlich model. When numerous layers are involved in the adsorption process, it is frequently used to describe the adsorption of solutes onto heterogeneous surfaces. Mathematically, the Freundlich equation is represented as(Freundlich 1907):

$$q_e = k_f C_e^{\frac{1}{n}} \quad (5)$$

where;

q_e represents the amount of solute adsorbed per unit mass of adsorbent at equilibrium (mg g^{-1}), k_f (mg g^{-1}) is the Freundlich constant related to the adsorption capacity, n is the Freundlich exponent (dimensionless).

The values of k_f and $\frac{1}{n}$ are determined by non-linear curve fitting of the equilibrium adsorption data to the Freundlich model.

(iii) *The Temkin isotherm*

Temkin isotherm describes adsorption interactions, assuming a linear decrease in the heat of adsorption with increasing surface coverage. This suggests non-uniform binding energies, with higher-energy sites becoming limited as more adsorbate molecules bind. Using the following equation the Temkin isotherm model is represented (Aharoni and Ungarish, 1977):

$$q_e = \frac{RT}{b_T} \ln (A_T C_e) \quad (6)$$

where:

q_e is the quantity of solute adsorbed per unit mass of adsorbent at equilibrium (mg g^{-1})

*R*is the universal gas constant (8.314 J $mol^{-1}K^{-1}$)

*T*is the absolute temperature (K)

b_T is the temkin isotherm constant related to the heat of adsorption (J mol^{-1})

A_T is the equilibrium binding constant corresponding to the maximum binding energy (L mol^{-1})

$C_e$is the equilibrium concentration of the solute in the solution (mg L^{-1})

2.11. Characterization and Energy Band Gap Analysis of ZnO-NPs

The 10 mg of ZnO nanopowder was dispersed in 10 mL of Milli-Q water with brief ultrasonication, and then a wavelength scan in the range of 180-600 nm was performed using UV-VIS-NIR spectrophotometer (Hitachi, U4100L).

Energy Band Gap Determination

i. *λmax Identification:* The wavelength at which the absorption was highest (λmax) was determined from the UV-Vis-NIR spectrum.
ii. *Band Gap Calculation:* The energy band gap (Eg) was calculated using the equation:

$$E_g(eV) = \frac{hxc}{\lambda_{max}} \quad (7)$$

iii.Tauc Plot Analysis

In addition, we employed a more precise method called the Tauc plot function to confirm the band gap energy. The absorption coefficient (α) was calculated using:

$$(\alpha h\nu)^n = A\left(h - E_g\right) \quad (8)$$

Where Eg represents the energy band gap, hv is the energy of the photon, A is a constant, and n is a value that depends on the type of transition. For ZnO, n equals 2, indicating direct and allowed transitions. The absorption coefficient (α) is determined using the following relationship:

$$\alpha = \frac{4\pi k}{\lambda_{max}} \quad (9)$$

By constructing a graph and extrapolating on the x-axis, we were able to determine the energy of the band gap, as described by Mahana et al. (2020).

2.12. FTIR Analysis of ZnO-NP, Nanocellulose and ZnO-CNF Nanocomposite

Fourier transform infrared spectroscopy (FTIR) was utilized to characterize the ZnO-NPs, CNF, and ZnO-CNF nanocomposite. A Bruker IFS 66/S spectrometer was employed to scan the spectral range from 4000 to 400 cm^{-1}. To prepare the sample, it was ground and mixed with a 1:100 (w/w) ratio of potassium bromide (KBr). Subsequently, the mixture was compressed into ultra-thin pellets for analysis. The FTIR spectra were compared with existing literature to identify the functional groups present in the samples. This analysis provided valuable information about the chemical composition and interactions between the components of the nanocomposite.

2.13. Morphological Examination and Size Distribution Analysis of Extracted ZnO-NP, Nanocellulose and ZnO-CNF Nanocomposite

In this study, the morphological structure of ZnO-NP, CNFs, and the ZnO-CNF nanocomposite were examined using a Scanning Electron Microscope (SEM) (JSM 6390LV model by JOEL, Japan) at the Central Instrumentation Centre, Tripura University, Tripura, India. The size distribution of particles was analysed using the Image J software. The Gaussian distribution method was employed to calculate the average particle size, providing a representative measure derived from the complex microstructure observed in the SEM images. Elemental compositions were analysed using EDX analysis in conjunction with SEM analysis.

2.14. X-ray Diffraction Analysis

The XRD analysis of ZnO nanopowder was conducted using an X-ray diffractometer (D8 FOCUS and MINIFIEX, BRUKER AXS, GERMANY and Rigaku Corporation, JAPAN) at wavelength of 1.540598 A°. Through continuous scanning mode with a 0.76 mm divergence slit, the scanning range for 2θ was 5-80° at 45 kV and 40 mA tube current. Both the previously published literature and the publicly accessible MATCH database were compared with the derived XRD pattern.

The crystalline size of the nanoparticles was calculated by using Scherer's equation (Cullity, 1956)

$$D = \frac{K\lambda}{\beta_{hkl} Cos\theta} \qquad (10)$$

Where:

K is the Debye-Scherer constant (the shape factor, typically 0.9)
λ (A^0) is the wavelength of incident CuKα radiation (i.e. λ=0.1540598)
β_{hkl} is the full width at half maximum (FWHM) of the diffraction peak (radians),
D (nm) is the crystalline size
θ is the Bragg diffraction angle (radian).

2.15. X-ray Photoelectron Spectroscopy (XPS) for Surface Elemental Characterization

In this study, we conducted surface elemental characterization of ZnO Nano-powder, using X-ray photoelectron spectroscopy (XPS). The XPS analysis was performed with an XPS instrument (Thermo Fisher UK, MODEL: ESCALAB Xi+). To determine the binding energies of the elements present, namely Zn, O, and C, we utilized Origin software, which allowed for precise measurement and analysis of the XPS data. This technique provided valuable insights into the surface composition and chemical states of the materials under examination.

2.16. Thermogravimetric Analysis (TGA)

Thermogravimetric analysis (TGA) and derivative thermogravimetric analysis (DTG) were employed to evaluate the thermal stability of the CNF, CNC, and ZnO-CNF nanocomposite. A Mettler Toledo TAG 2 thermal gravimetric analyzer was used for the analysis. For the analysis, 4.5 mg samples of CNF, CNC and the ZnO-CNF nanocomposite were selected. The analysis involved controlled heating, beginning at an initial temperature of 25°C and gradually increasing up to 500°C. To prevent thermal degradation and maintain the material's integrity, all experiments were conducted under a nitrogen atmosphere at a flow rate of 200 mL/min. in

conjunction with TGA, derivative thermogravimetric analysis (DTG) was employed. DTG allowed for the generation of derivative curves that precisely indicated the rate of weight change. This approach facilitated the identification of distinct temperature regions associated with decomposition or degradation processes within the samples.

2.17. Differential Scanning Calorimetry (DSC)

In this study, we investigated the thermal behaviour of cellulose nanofibers (CNF), cellulose nanocrystal (CNC) and the ZnO-CNF nanocomposite using a Differential Scanning Calorimeter DSC 3 (Mittler Toledo, Switzerland). The experimental procedure involved controlled heating, with the sample gradually heated from an initial temperature of 25°C to a maximum of 400°C. The heating rate was maintained at a constant 10°C per min. Through this analysis, we generated thermograms that provided critical information about the thermal properties of the materials. Specifically, we extracted two key parameters (i) onset melting temperature, and (ii) crystallization temperature.

CHAPTER -3

RESULT

3.1. Morphology of *C. glomerata* and *C. vulgaris*

C. glomerata is a green algae that is filamentous. Long, unbranched filaments make up its thallus (Figure 10), which frequently forms cottony mats. Large, elongated, multinucleated cells with distinct divisions, cellulose-based cell walls strengthened by a mucilaginous layer, and chloroplasts with several pyrenoids are some of its cellular features.

The morphology of *C. vulgaris*was small, spherical (Figure 11). They were bright green due to the presence of chlorophyll. Each cell has a rigid cell wall, a single large chloroplast, and is capable of photosynthesis.After one and half month of cultivation, 10 g±2 of dry biomass was harvested.

3.2. Synthesis of ZnO-NPs, Nanocellulose and ZnO-CNF Nanocomposite

The synthesis of ZnO-NPs is first confirmed by visualization technique. Ultrasonication-assisted synthesis takes short time period to produce nanoparticles. Synthesis was done in room temperature and the NaOH used as precursor to increase the pH to 10.2 and PVP used as reducing agent. In the visualization process, the ZnO nanostructure was established by the formation of white colour precipitation. The photograph showing the white colour precipitation of ZnO nanostructure synthesized using aqueous extract of *C. glomerata* (Figure 12a) and *C. vulgaris* (Figure 12b)

Cellulose was extracted from algal biomass using a multi-step process involving Soxhlet extraction to remove lipids and waxes, alkaline treatment to remove hemicellulose and lignin, and oxidative treatment with hydrogen peroxide for further purification. The final product was obtained after repeated washing and drying, yielding pure, white cellulose. Cellulose nanofibers (CNF) and nanocrystals (CNC) were prepared from the extracted cellulose by acid hydrolysis to cleave the amorphous regions. The resulting nanostructures were neutralized, sonicated to improve dispersion, and then lyophilized to obtain a white powder, which was stored

at 4°C. The nanocellulose derived from *C. glomerata* appeared as a cottony-soft, white substance (Figure 12c). In contrast, nanocellulose from *C. vulgaris* was an off-white powder (Figure 12d). Notably, *C. glomerata* yielded a significantly higher amount of nanocellulose (47%) compared to C. vulgaris (24%).

Given the higher yield of nanocellulose from *C. glomerata* compared to *C. vulgaris*, it was chosen as the preferred source for the preparation of ZnO-CNF nanocomposite.

The ZnO-CNF nanocomposite was synthesized by dispersing *C.glomerata*CNF in water and adding $ZnCl_2.2H_2O$. Ultrasonication improved the dispersion of the CNF and facilitated the interaction between the zinc ions and the cellulose nanofibers by breaking down aggregates and creating a more homogeneous mixture. This enhanced interaction led to a more uniform distribution of ZnO-NPs on the CNF surface. The pH was adjusted to 10 using NaOH solution, leading to the precipitation of ZnO-NPs onto the CNF surface. The resulting nanocomposite was filtered, washed, dried, and cut into 5-millimeter pieces for further analysis (Figure 12e).

3.3. Characterization of ZnO-NPs

3.3.1. UV-VIS Spectroscopy

The UV-Vis absorption spectrum of the synthesized ZnO-NPs using aqueous extract of *C. glomerata* exhibits a prominent absorption peak at approximately 350 nm (Figure 13a). This peak is characteristic of the band-to-band electronic transition within the ZnO crystal lattice. The Tauc plot analysis, a well-established method for determining the band gap of semiconductors, reveals an energy band gap of 3.18 eV for these nanoparticles (Figure 13b). This value is consistent with the reported band gap range of ZnO (2-5 eV), indicating a significant band gap that could potentially impact the electronic properties and applications of these nanoparticles. The observed band gap suggests that the synthesized ZnO-NPs possess a wide band gap, which is a desirable characteristic for various applications, including photocatalysis, optoelectronics, and energy storage.

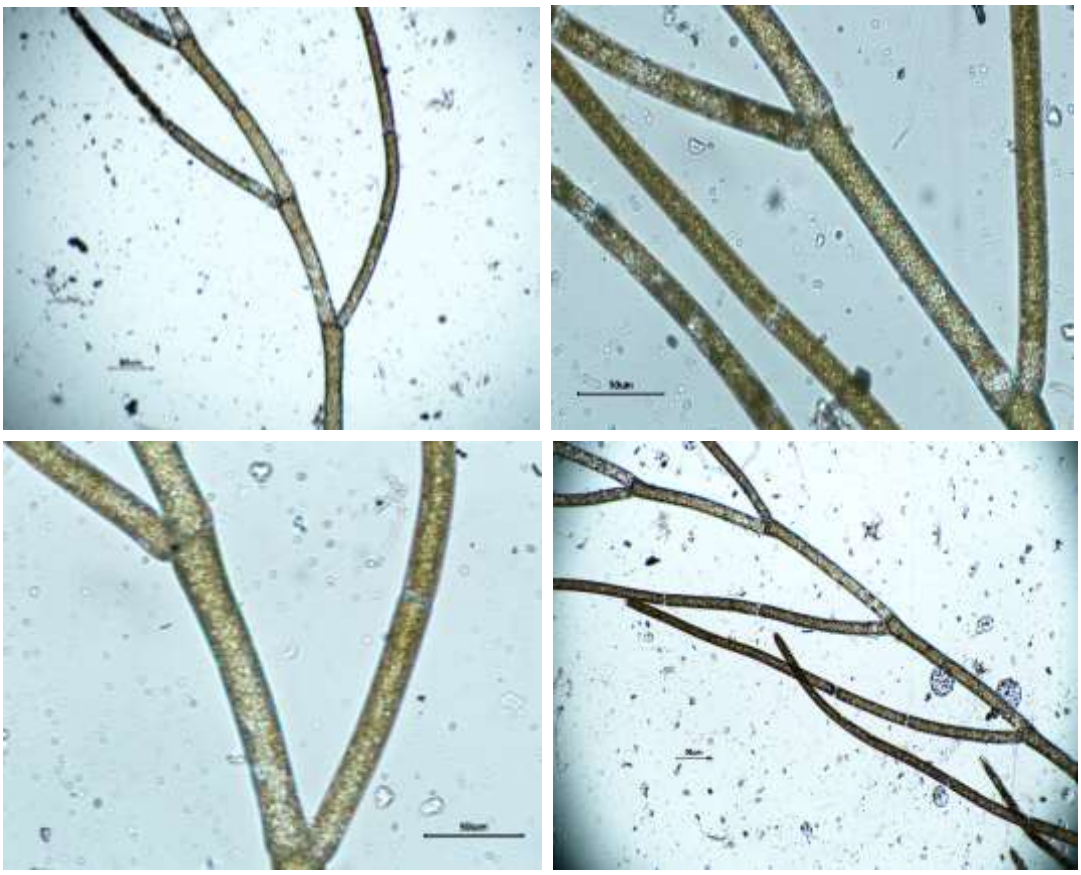

Figure 10: *C. glomerata* under microscope at 10x magnification.

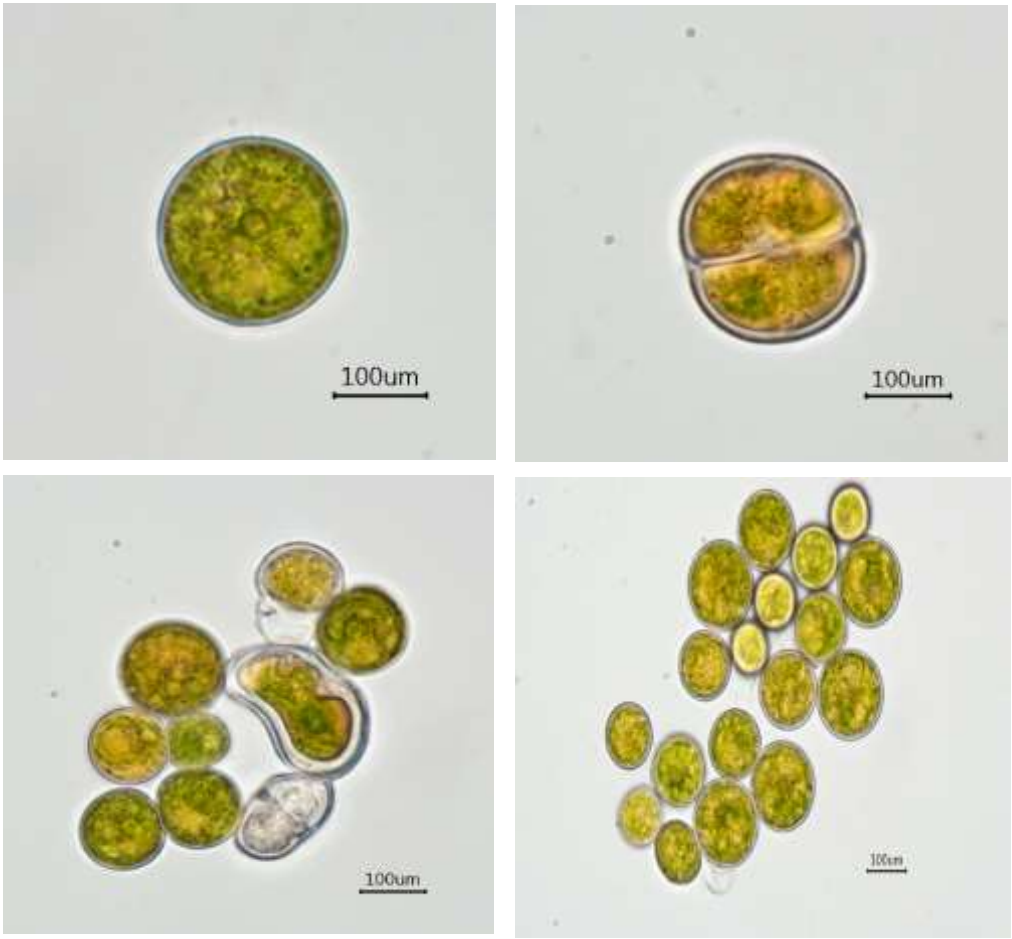

Figure 11.*C. vulgaris* under microscope at 40x and 10x magnification.

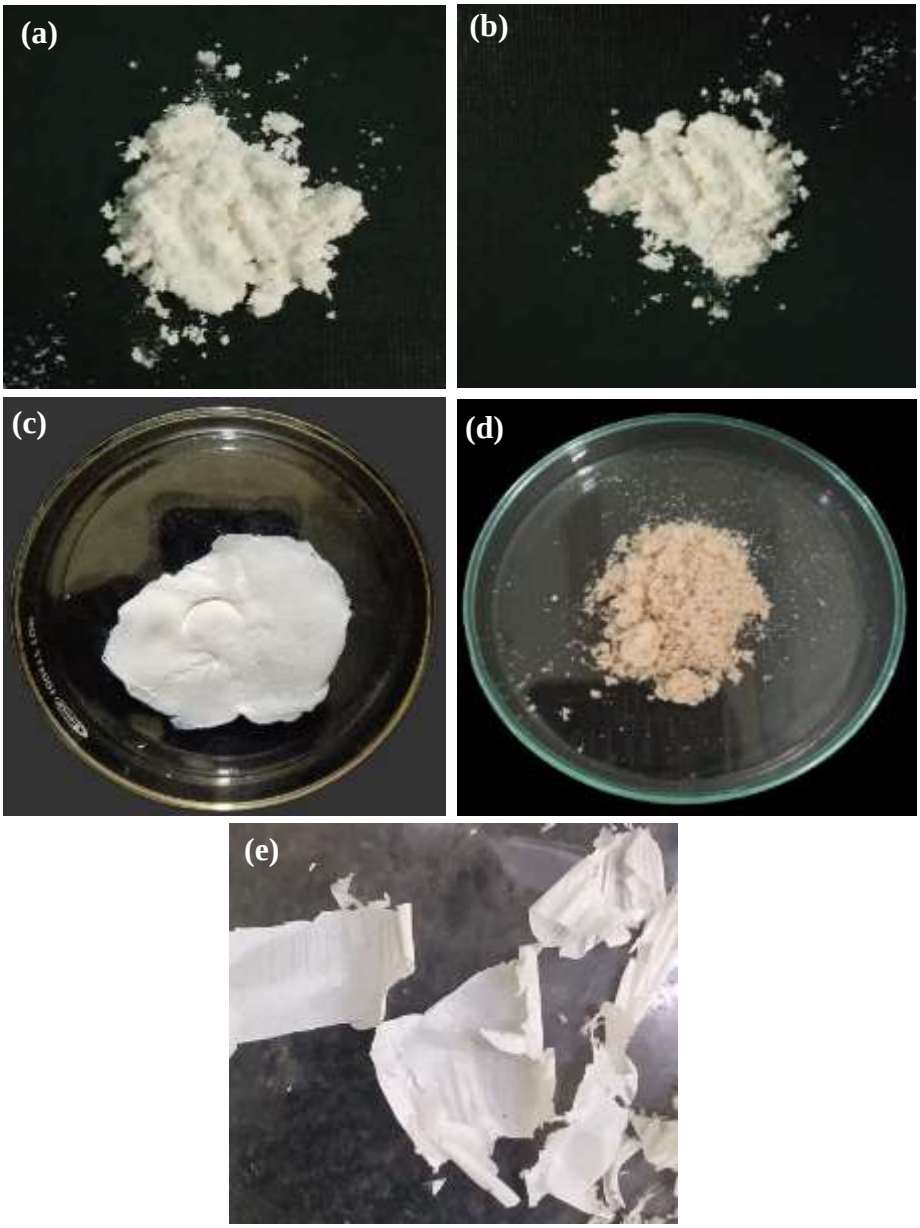

Figure 12. (a) Synthesized ZnO-NPs from the aqueous extract of *C. glomerata*, (b) Synthesized ZnO-NPs from the aqueous extract *C. vulgaris*, (c) Extracted nanocellulose from *C. glomerata*, (d) Extracted nanocellulose from *C. vulgaris*, (e) Thin sheet of ZnO-CNF nanocomposite.

The UV-Vis absorption spectrum of ZnO-NPs synthesized using aqueous extract of *C. vulgaris* shows a prominent absorption peak at around 335 nm, characteristic of the band-to-band electronic transition within the ZnO crystal lattice (Figure 14a). The Tauc plot analysis indicates a band gap of approximately 3.40 eV for these nanoparticles, which is consistent with the typical band gap range of ZnO (2-5 eV) (Figure 14b). This wide band gap could potentially impact their electronic properties and applications.

3.3.2. FTIR Analysis

FTIR analysis was conducted to identify the functional groups involved in the reduction and stabilization of ZnO-NPs synthesized using extracts from *C. glomerata* (Figure 15) and *C. vulgaris* (Figure 16). The FTIR spectra of the synthesized ZnO-NPs were recorded in the range of 4000-400 cm^{-1}.

For ZnO-NPs synthesized using *C. glomerata* extract (Table 6):

i. A broad peak at 3485 cm^{-1} indicates the presence of -OH groups, likely from phenolic compounds.
ii. A peak at 1655 cm^{-1} corresponds to the bending vibration of water molecules.
iii. Peaks at 1502 cm^{-1}, 1032 cm^{-1}, 901 cm^{-1}, 720 cm^{-1}, and 456 cm^{-1} suggest the presence of nitro groups, amines, aromatic compounds, alkenes, and Zn-O bonds, respectively.

For ZnO-NPs synthesized using *C. vulgaris* extract (Table 7):

i. A broad peak at 3399 cm^{-1} indicates the presence of -OH groups.
ii. A peak at 1655 cm^{-1} corresponds to the bending vibration of water molecules.
iii. Peaks at 1292 cm^{-1}, 1032 cm^{-1}, 901 cm^{-1}, 720 cm^{-1}, and 426 cm^{-1} suggest the presence of nitro groups, amines, aromatic compounds, alkenes, and Zn-O bonds, respectively.

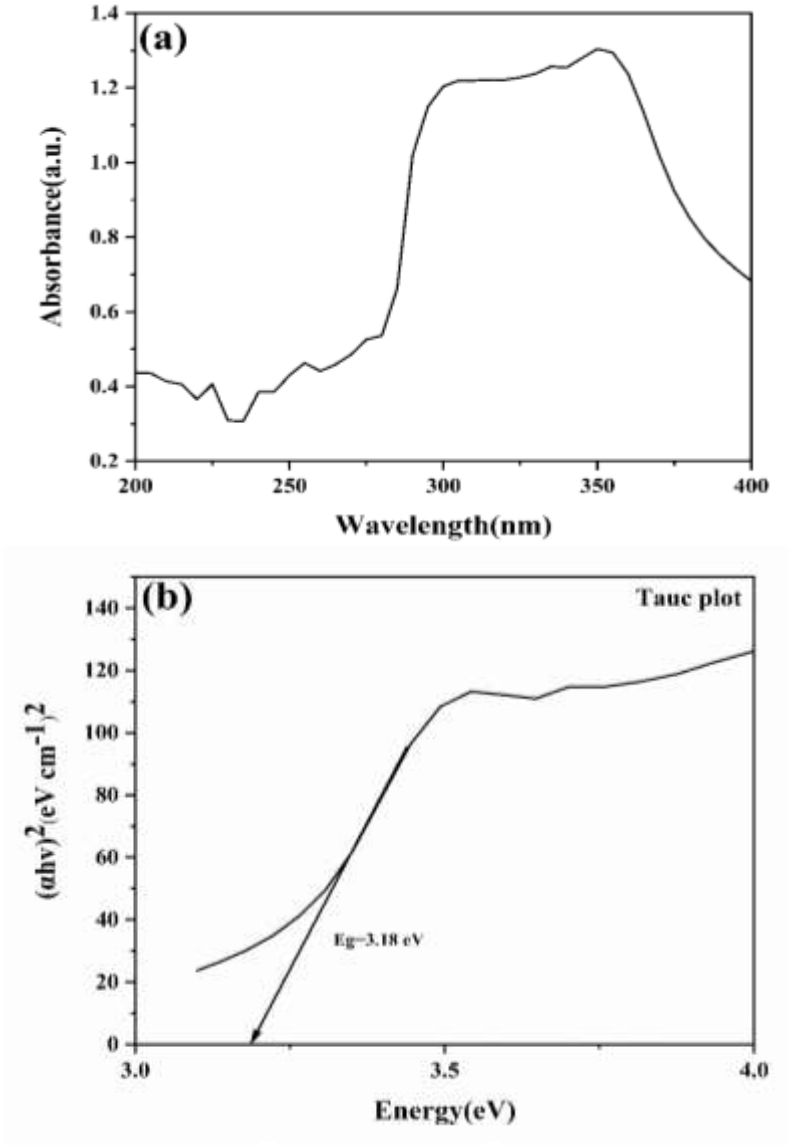

Figure 13. UV-VIS absorption spectrum and tauc plot of ZnO-NPs synthesized from *C. glomerata*(a) UV-VIS absorption spectrum of ZnO-NPs showing the absorption characteristics across a range of wavelengths. (b)Tauc plot of ZnO-NPs derived from the absorption spectrum. The plot displays the square of the absorption coefficient (α) as a function of photon energy (hν). The linear extrapolation of the plot yields an estimation of the band gap energy (*Eg*) of the ZnO-NPs.

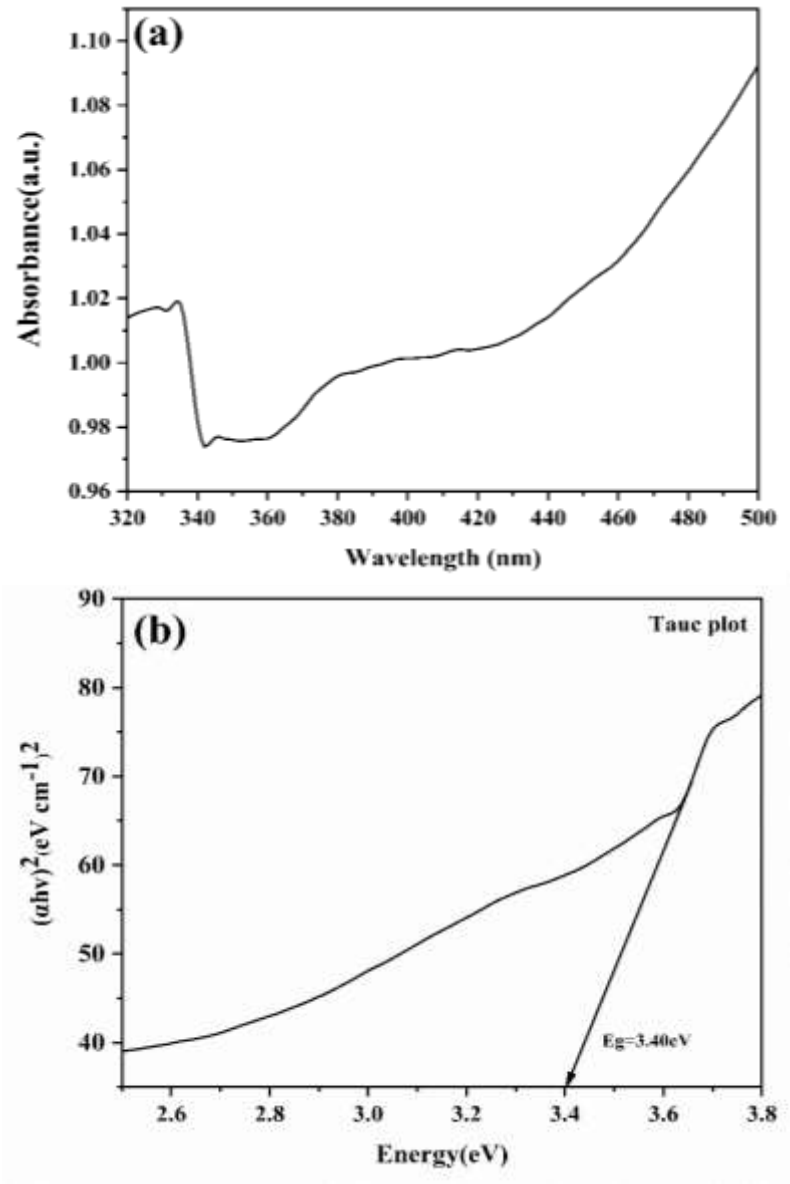

Figure 14. UV-VIS absorpn spectrum and Tauc Plot of ZnO-NPs synthesized from *C.vulgaris* (a) UV-VIS absorption spectrum of ZnO-NPs showing the absorption characteristics across a range of wavelengths. (b)Tauc plot of ZnO-NPs derived from the absorption spectrum. The plot displays the square of the absorption coefficient (α) as a function of photon energy (hν). The linear extrapolation of the plot yields an estimation of the band gap energy (*Eg*) of the ZnO-NPs.

The presence of above functional groups suggests that the biomolecules present in the algal extracts played a crucial role in the reduction of Zn^{2+} ions to ZnO-NPs and stabilized the resulting nanoparticles. Phenolic compounds, in particular, are known to have strong reducing and capping abilities.

Table 6: FTIR analysis showing functional groups and vibrations in ZnO-NPs synthesised from aqueous extract of *C. glomerata*.

Wavenumber (cm^{-1})	Functional groups	Vibrations
3490	Phenol and alcohol	O-H Stretching
1655	Hydroxyl	H-O-H Vibration
1502	Nitro group	N-O Stretching
1032	Amine	C-N Stretching
901	Aromatic compound	C-H Bending
720	Alkene	C=C Stretching
456	Metal oxide	Zn-O Stretching

3.3.3. SEM Analysis

The SEM images provide a detailed view of the morphology of ZnO-NPs synthesized from *C. glomerata* at various magnifications (Figure 17):

i. *Image (a):* This low-magnification image shows the overall distribution and agglomeration of the nanoparticles. The particles appear to be clustered together, forming larger aggregates.
ii. *Image (b):* At a higher magnification of 200 nm, the individual nanoparticles become more visible. They exhibit a spherical or slightly elongated shape.
iii. *Images (c) and (d):* These high-resolution images at 100 nm provide a closer look at the surface features of the nanoparticles. The particles appear to have

a rough surface with some irregularities. The surface roughness could be due to the presence of pores or defects in the nanoparticles. These pores and defects could increase the surface area of the nanoparticles, which could be beneficial for applications such as catalysis and sensing.

Overall, the SEM images suggest that the ZnO-NPs synthesized from *C. glomerata* exhibit a spherical morphology with some degree of agglomeration. The surface of the nanoparticles appears to be relatively rough, which could potentially increase their surface area and enhance their reactivity.

Table 7: FTIR analysis showing functional groups and vibrations in ZnO-NPs synthesised from aqueous extract of *C. vulgaris*.

Wavenumber (cm^{-1})	Functional groups	Vibrations
3399	Phenol and alcohol	O-H Stretching
1655	Alkane group	C=C Stretching
1292	Nitro group	N-O Stretching
1032	Amine	C-N Stretching
901	Aromatic compound	C-H Bending
720	Alkene	C=C Stretching
426	Metal oxide	Zn-O Stretching

The SEM images of ZnO-NPs synthesized from *C. vulgaris* reveal the following morphological features (Figure 18):

i. *Images (a) and (b):* These images, taken at a magnification of 200 nm, show that the nanoparticles exhibit a spherical or slightly elongated shape. They appear to be clustered together, forming agglomerates. The agglomeration of

the nanoparticles may be due to the presence of surface charges or interparticle forces. The size of the agglomerates varies, with some being larger than others. The variation in agglomerate size may be due to differences in the concentration of the algal extract or the synthesis conditions.

ii. *Images (c) and (d):* At a higher magnification of 100 nm, the individual nanoparticles become more distinct. The surface of the nanoparticles appears to be relatively smooth, with minimal surface roughness. The smooth surface of the nanoparticles may be due to the presence of biomolecules from the algal extract, which may have acted as capping agents during the synthesis process. Capping agents can help to prevent the nanoparticles from agglomerating and can also help to control their size and shape.

Overall, the SEM images suggest that the ZnO-NPs synthesized from *C. vulgaris* are primarily spherical in shape and tend to agglomerate. The relatively smooth surface of the nanoparticles might impact their surface area and reactivity compared to those synthesized from *C. glomerata*.

3.3.4. EDX Analysis

The elemental composition of ZnO-NPs synthesized from the aqueous extract of *C. glomerata* is presented in Figure 19(a) and Table 8. This spectrum provides elemental analysis of the synthesized ZnO-NPs from *C. glomerata*. The dominant peaks correspond to oxygen (O) and zinc (Zn), confirming the primary composition of the nanoparticles. The elemental composition of ZnO-NPs synthesized from the aqueous extract of *C. glomerata* is presented in Table 8. The table indicates that the nanoparticles are primarilycomposed of oxygen (O) and zinc (Zn), consistent with the expected composition of ZnO. However, the presence of chlorine (Cl) and gold (Au) in minor amounts suggests potential contamination or incorporation of these elements during the synthesis process. Further investigation is needed to determine the exact source of these elements and their impact on the properties of the nanoparticles.

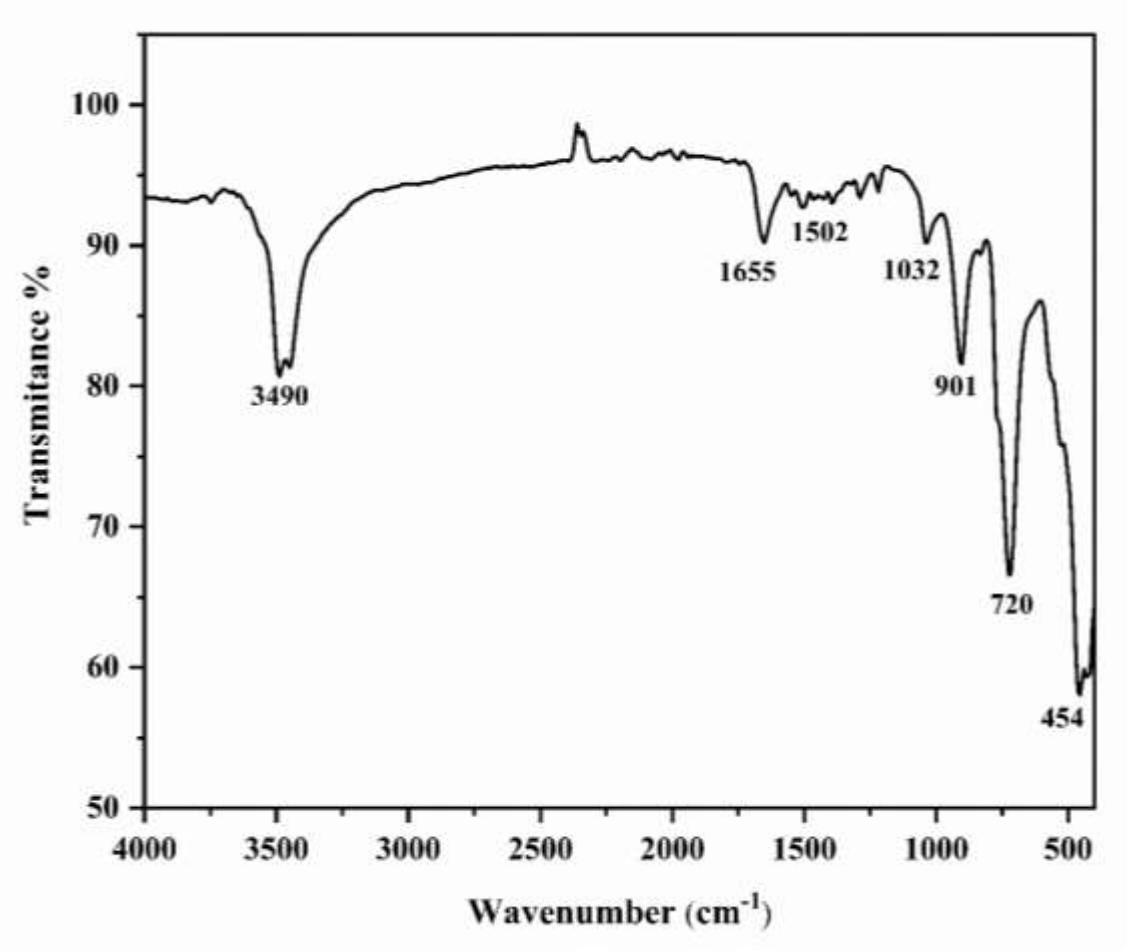

Figure 15. Fourier transform infrared (FTIR) spectrum of ZnO-NPs (synthesized from the aqueous extract of *C. glomerata*) depicting characteristic absorption bands.

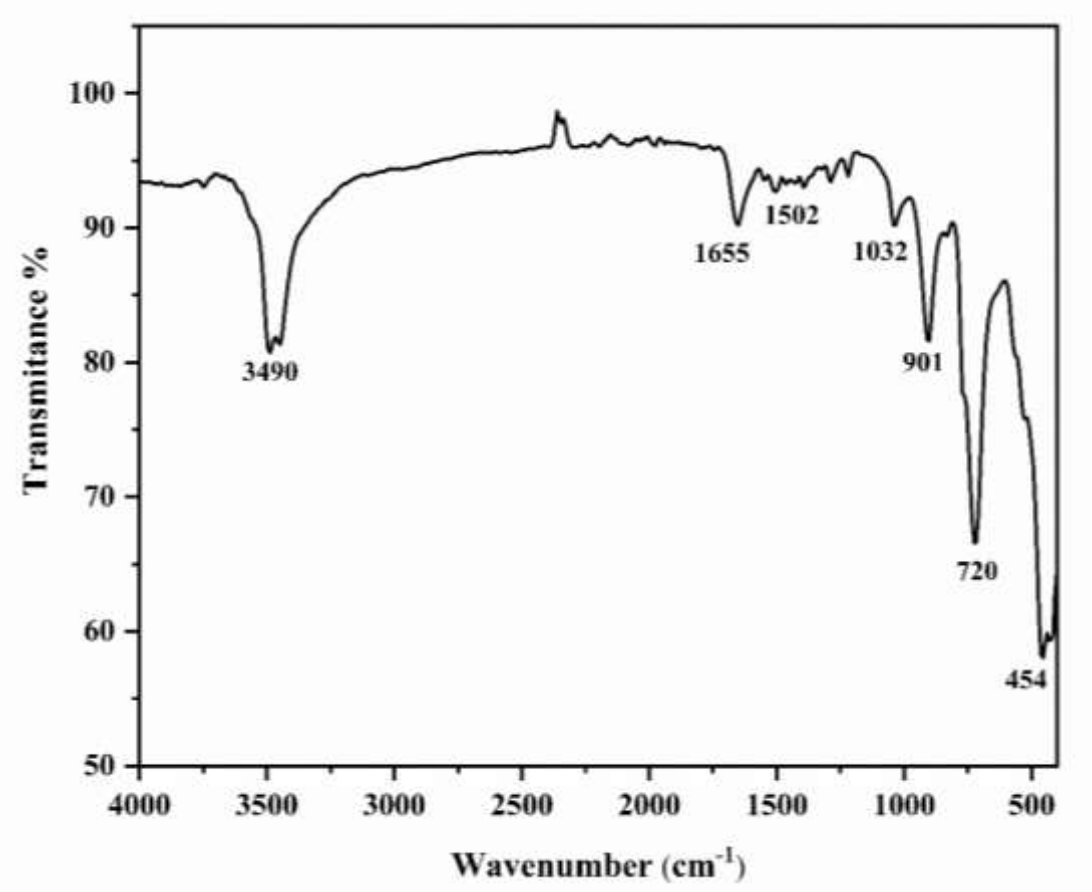

Figure 16. Fourier transform infrared (FTIR) spectrum of ZnO-NPs (synthesized from the aqueous extract of *C. vulgaris*) depicting characteristic absorption bands.

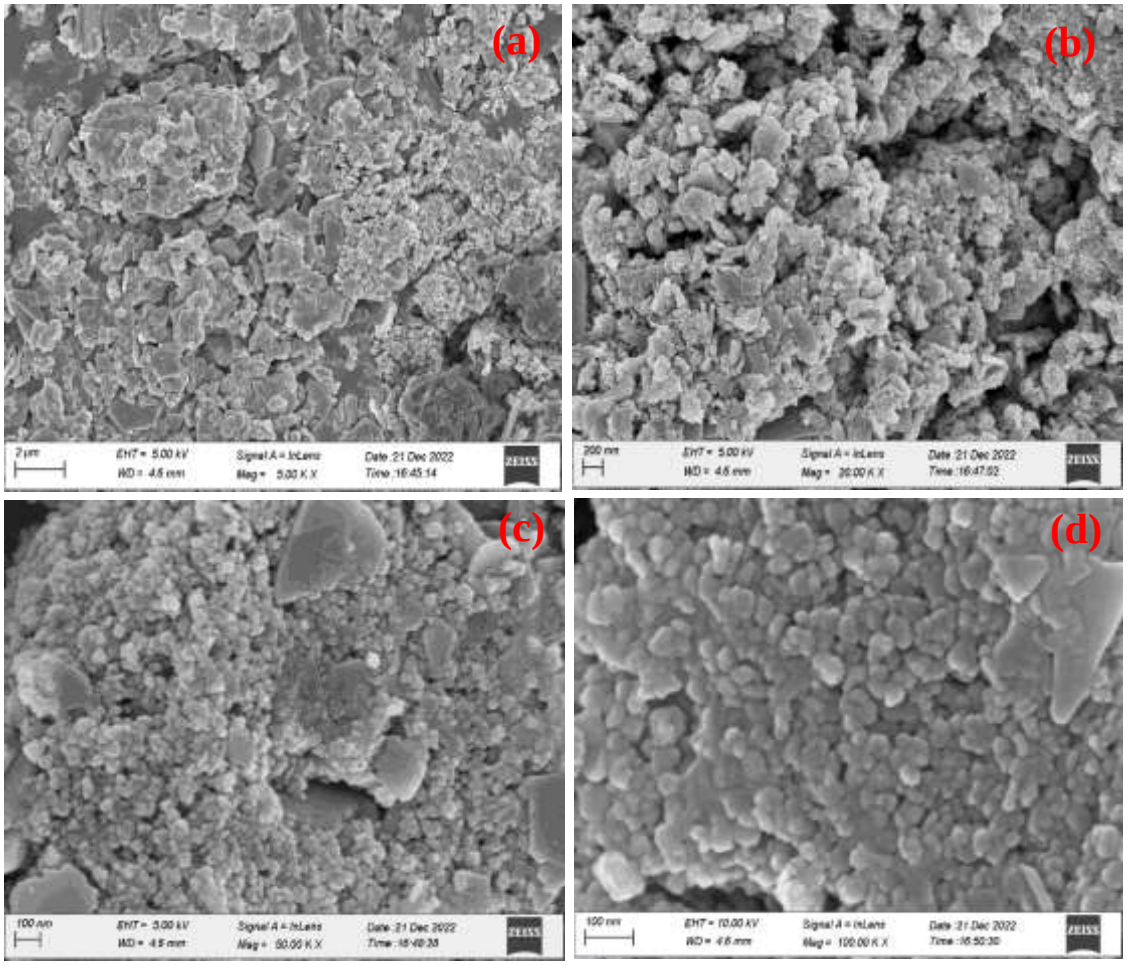

Figure 17. Scanning electron microscopy (SEM) images of ZnO-NPs synthesized from *C. glomerata* (a) at 2 µm, (b) at 200 nm, (c) at 100 nm (d) at 100 nm.

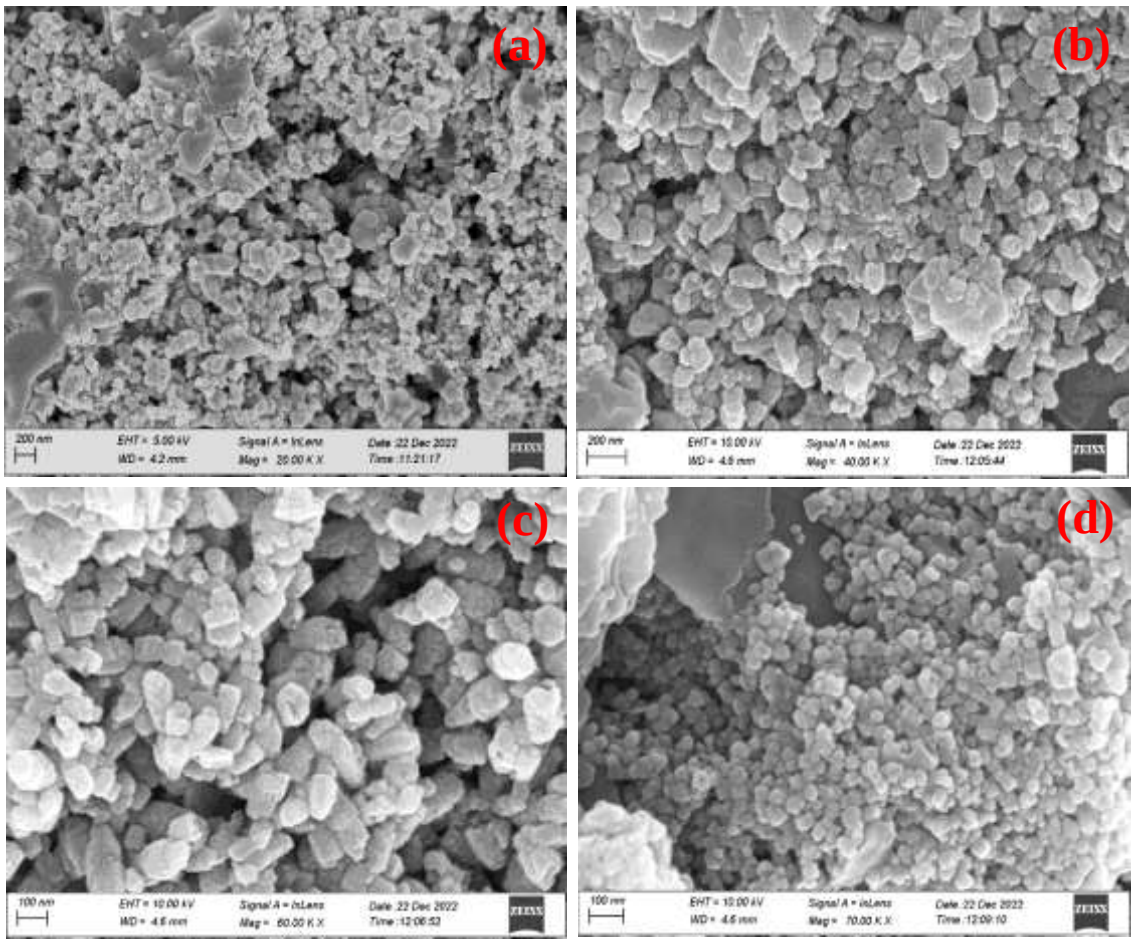

Figure 18. Scanning electron microscopy (SEM) images of ZnO-NPs synthesized from *C. vulgaris* (a) at 200 nm (b) at 200 nm, (c) at 100 nm (d) at 100 nm.

Table 8: Elemental composition of ZnO-NPs synthesized from aqueous extract of *C. glomerata*determined by EDX analysis.

Elements	Atomic %	Weight %
O K	29.50	62.56
Cl K	7.33	7.01
Zn K	56.40	29.27
Au L	6.77	1.17

The histogram (Figure 19 b) shows the distribution of particle sizes for ZnO-NPs synthesized from *C. glomerata*. The X-axis represents the particle diameter in nanometers, while the Y-axis represents the frequency or number of particles within a specific size range. The red curve overlaid on the histogram represents a Gaussian distribution, which is a common statistical distribution used to model the spread of data. The R^2 value of 0.96075 indicates a good fit between the experimental data and the Gaussian distribution, suggesting that the particle size distribution is relatively narrow andcentered around 30-35 nm.

The elemental composition of ZnO-NPs synthesized from the aqueous extract of *C. vulgaris* is presented in Figure 20(a) and Table 8.This spectrum shown in Figure 20a provides elemental analysis of the ZnO-NPs synthesized from *C. vulgaris*. The prominent peaks correspond to oxygen (O) and zinc (Zn), confirming the primary composition of the nanoparticles. Additionally, minor peaks for chlorine (Cl) and gold (Au) are observed. The presence of these elements could be attributed to the synthesis process or residual impurities.

Table 9 provides a detailed breakdown of the elemental composition of the ZnO-NPs synthesized from *C. vulgaris*. The dominant elements are oxygen (O) and zinc (Zn), which is expected for ZnO-NPs. However, the presence of chlorine (Cl)

and gold (Au) in minor amounts is noteworthy. These elements could be impurities from the synthesis process or from the algal extract itself.

Table 9: Elemental composition of ZnO-NPs synthesized from aqueous extract of *C. vulgaris*determined by EDX analysis.

Elements	Atomic %	Weight %
O K	33.21	64.40
Cl K	14.97	13.10
Zn K	45.20	21.45
Au L	6.61	1.04

This histogram (Figure 19b) shows the distribution of particle sizes for ZnO-NPs synthesized from *C. vulgaris*. The x-axis represents the particle diameter in nanometers, while the y-axis represents the frequency or number of particles within a specific size range. The red curve overlaid on the histogram represents a Gaussian distribution, whichis a common statistical distribution used to model the spread of data. The R^2 value of 0.99312 indicates a good fit between the experimental data and the Gaussian distribution, suggesting that the particle size distribution is relatively narrow and centered around 80-100 nm.

The characterization results indicate that ZnO-NPs were successfully synthesized from *C. vulgaris*. The nanoparticles are primarily composed of zinc oxide, but also contain minor amounts of chlorine and gold. The particle size distribution is relatively narrow, suggesting a homogeneous sample.

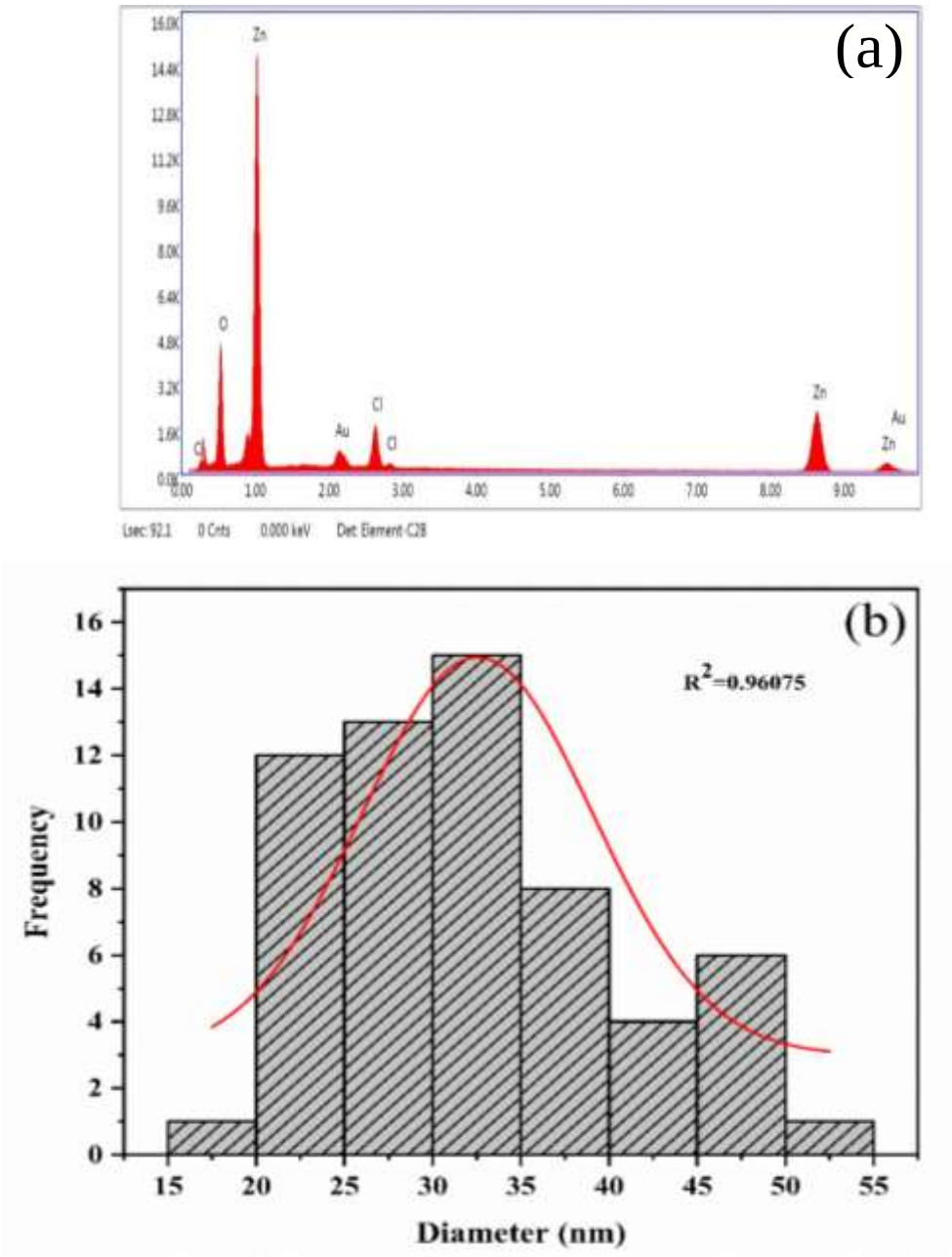

Figure 19. (a) EDX spectrum for the ZnO-NPs synthesized from *C. glomerata,* (b)Diameter of ZnO-NPs synthesized from *C. glomerata* in Gaussian distribution.

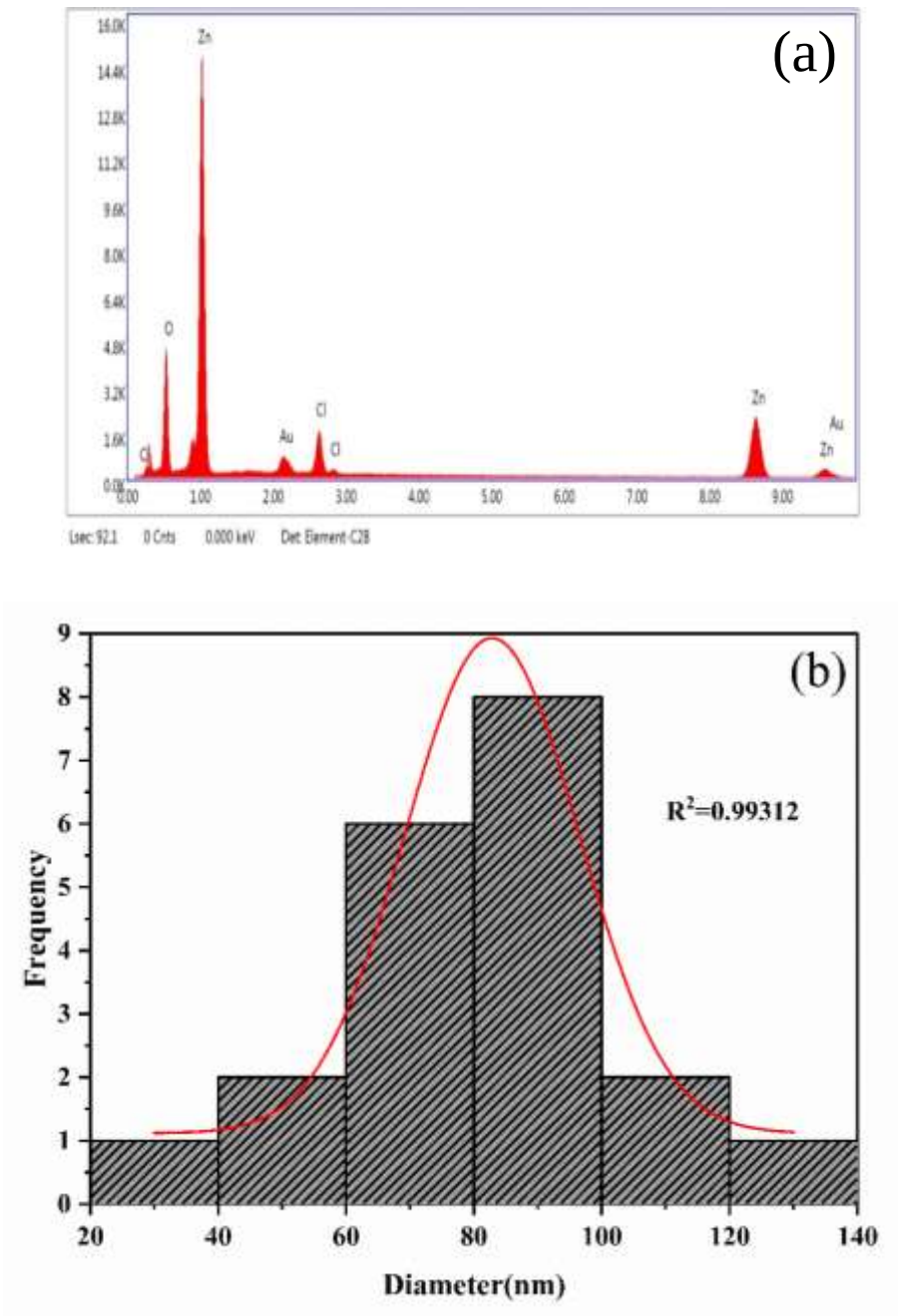

Figure 20. (a) EDX spectrum for the ZnO-NPs synthesized from *C. vulgaris*, (b) Diameter of ZnO-NPs synthesized from *C. vulgaris* in Gaussian distribution.

3.3.5. XRD Analysis

Figures 21a and 21b represent the X-ray diffraction (XRD) pattern of ZnO-NPs synthesized using an aqueous extract of *C. glomerata and C. vulgaris*. The presence of sharp, well-defined peaks in the XRD pattern indicates that the synthesized ZnO-NPs are highly crystalline. The XRD pattern of ZnO-NPs synthesized from both *C. glomerata* and *C. vulgaris* exhibits a similar set of diffraction peaks at approximately 31.66°, 34.06°, 36.31°, 47.17°, 56.64°, 62.86°, 66.81°, 67.17°, 69.11°, 72.5°, and 76.92°. These peaks can be indexed to the (100), (002), (101), (102), (110), (103), (200), (112), (201), (004) planes of the hexagonal wurtzite structure of ZnO-NPs, which is consistent with the standard XRD pattern of ZnO-NPs (MATCH card no. 00-900-4181). The provided lattice parameters (a = 3.2533 Å, c = 5.2073 Å) and space group (P63mc) correspond to the hexagonal wurtzite structure of ZnO-NPs. The calculated density of 5.663 g/cm³ is consistent with the theoretical density of ZnO-NPs with this crystal structure.

The broadening of the diffraction peaks can be attributed to the small crystallite size of the nanoparticles. Using the Scherrer equation, the average crystallite size can be estimated from the peak broadening.

The Scherrer equation is a widely used method to estimate the crystallite size of materials from X-ray diffraction (XRD) data. It relates the broadening of diffraction peaks to the size of the crystallites.

Where:

D: Crystallite size (nm)
K: Shape factor (typically 0.9)
λ: Wavelength of X-ray radiation (1.54 Å for Cu Kα)
β: Full Width Half Maximum (FWHM) of the diffraction peak in radians
θ: Bragg angle (degrees)

Scherrer Equation:

$$D = (K * \lambda) / (\beta * \cos\theta) \quad (11)$$

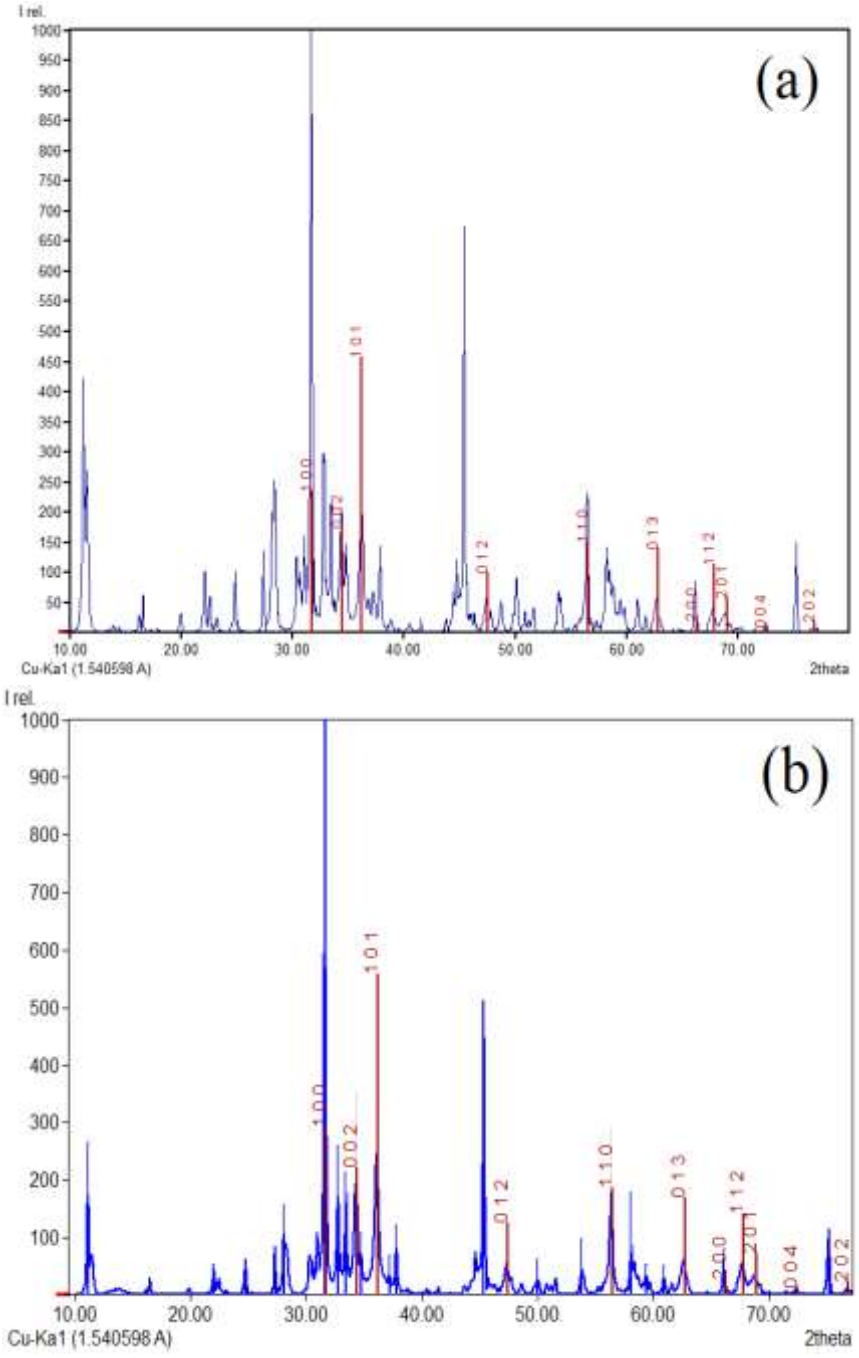

Figure 21. XRD analysis of ZnO-NPs (a) synthesized using aqueous extract of *C. glomerata*, (b) synthesized using aqueous extract of *C. vulgaris.*

The FWHM is a measure of the peak broadening, and it is inversely proportional to the crystallite size. A larger FWHM indicates smaller crystallite size. By measuring the FWHM of the diffraction peaks and using the Scherrer equation, the crystallite size of the ZnO-NPs was estimated to be in the range of 32-82 nm. This suggests that the synthesized nanoparticles are relatively small and may exhibit enhanced surface area and reactivity compared to larger particles.

3.3.6. XPS Analysis

X-ray Photoelectron Spectroscopy (XPS) is a powerful technique for analyzing the surface composition and chemical state of materials. In this study, XPS was used to investigate the surface properties of ZnO-NPs synthesized from *C. glomerata* and *C. vulgaris*. The XPS analysis revealed following:

i. *Elemental Composition:* The survey spectrum (Figure 22a and 23a) confirms the presence of Zn, O, and C elements in the nanoparticles. The absence of other significant peaks indicates the high purity of the synthesized ZnO.
ii. *Carbon (C 1s) Analysis:* The deconvoluted C 1s spectrum (Figure 22b and 23b) shows a peak at around 286.61 eV, which is attributed to C-C and C-H bonds in the organic residues from the synthesis process.
iii. *Oxygen (O 1s) Analysis:* The deconvoluted O 1s spectrum (Figure 22c and 23c) exhibits peaks at around 531.44 eV and 529.86 eV. The peak at 531.44 eV is assigned to the O-H bond, while the peak at 529.86 eV is attributed to the Zn-O bond in the ZnO lattice.
iv. *Zinc (Zn 2p) Analysis:* The deconvoluted Zn 2p spectrum (Figure 22d and 23d) shows two peaks at around 1045.69 eV and 1020.49 eV, corresponding to the Zn 2p1/2 and Zn 2p3/2 spin-orbit doublet, respectively. These peaks confirm the presence of Zn^{2+} ions in the ZnO lattice.

The binding energies obtained from the XPS analysis are in good agreement with the reference values for ZnO, with minor deviations (Table 10). These deviations may be attributed to the specific synthesis method, particle size, and surface properties of the nanoparticles.

Table 10. Binding energy of spectral line of ZnO-NPs synthesized from *C. glomerata* and *C. vulgaris*determined by XPS analysis.

Elements	Spectral line	Analysed binding energy(eV) *C. glomerata*	Analysed binding energy(eV) *C. vulgaris*	Binding energy from database(eV)
C	1s	286.61	285.68	286.63
O	1s	531.44	529.86	531.2
Zn	2p1/2	1045.69	1043.77	1044.7
Zn	2p3/2	1020.49	1021.11	1020.9
Zn	2s	1194.48	1194.43	1195.7
Zn	3d	11.85	10.21	11.8
Zn	3p	90.1	89.86	90.3
Zn	3s	140.44	140.76	140.3

In conclusion, the XPS analysis provides valuable insights into the surface composition and chemical state of the ZnO-NPs. The presence of Zn-O bonds confirms the formation of ZnO. The minor presence of carbon-based species suggests the presence of organic residues from the synthesis process, which may influence the properties of the nanoparticles. Further studies are needed to optimize the synthesis process and minimize the presence of impurities.

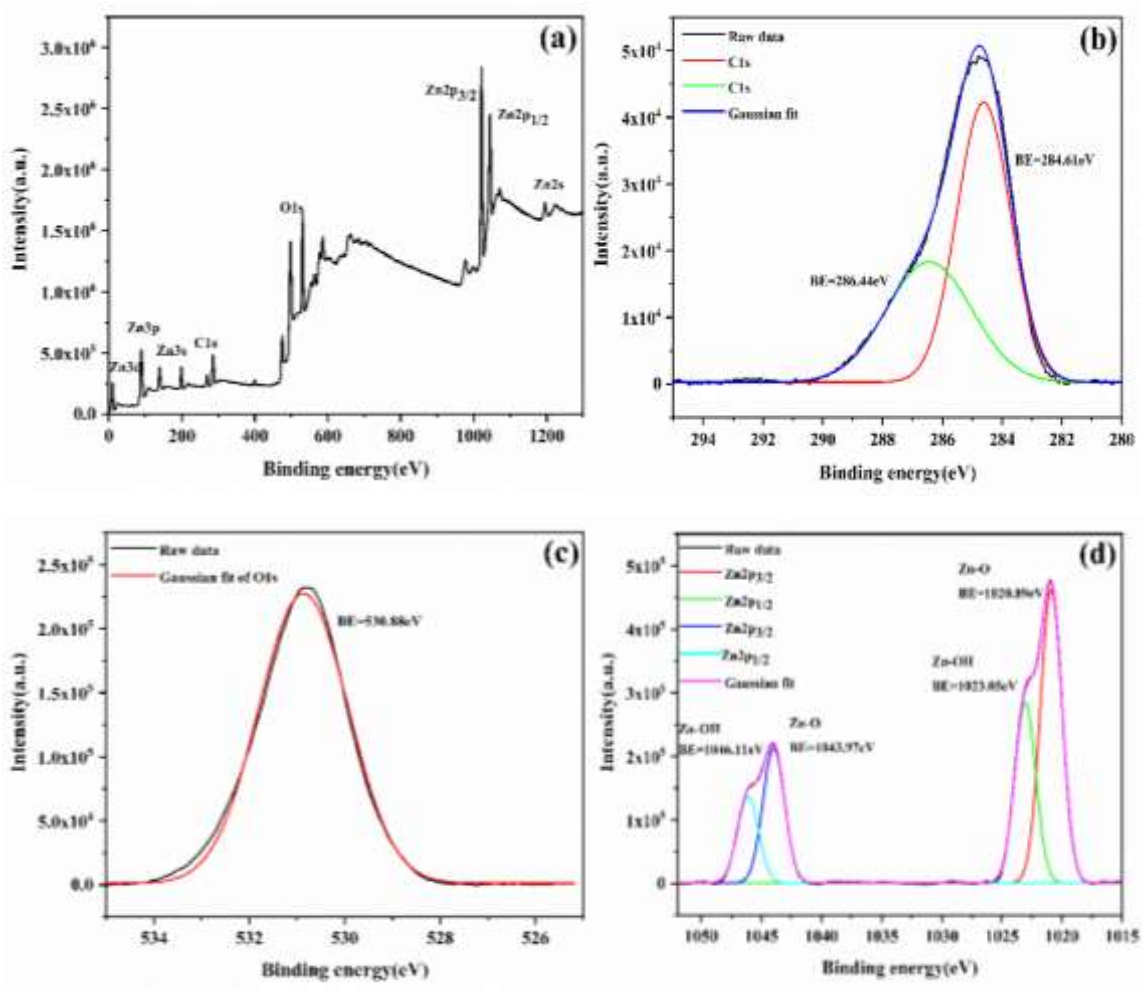

Figure 22. X-ray photoelectron spectroscopy (XPS) analysis: (a) Provides the XPS survey spectra of ZnO-NPs synthesized from *C. glomerata*, offering an overview of the elemental composition and surface characteristics. (b) Presents an XPS core level scan of carbon (C 1s) with a deconvoluted profile, allowing a closer examination of carbon's chemical environment and bonding states. (c) Offers an XPS core level scan of oxygen (O 1s), giving insights into the chemical states and bonding of oxygen on the sample's surface. (d) Shows the XPS core level scan of zinc (Zn 2p ½ and Zn 2p 3/2) with deconvoluted profiles.

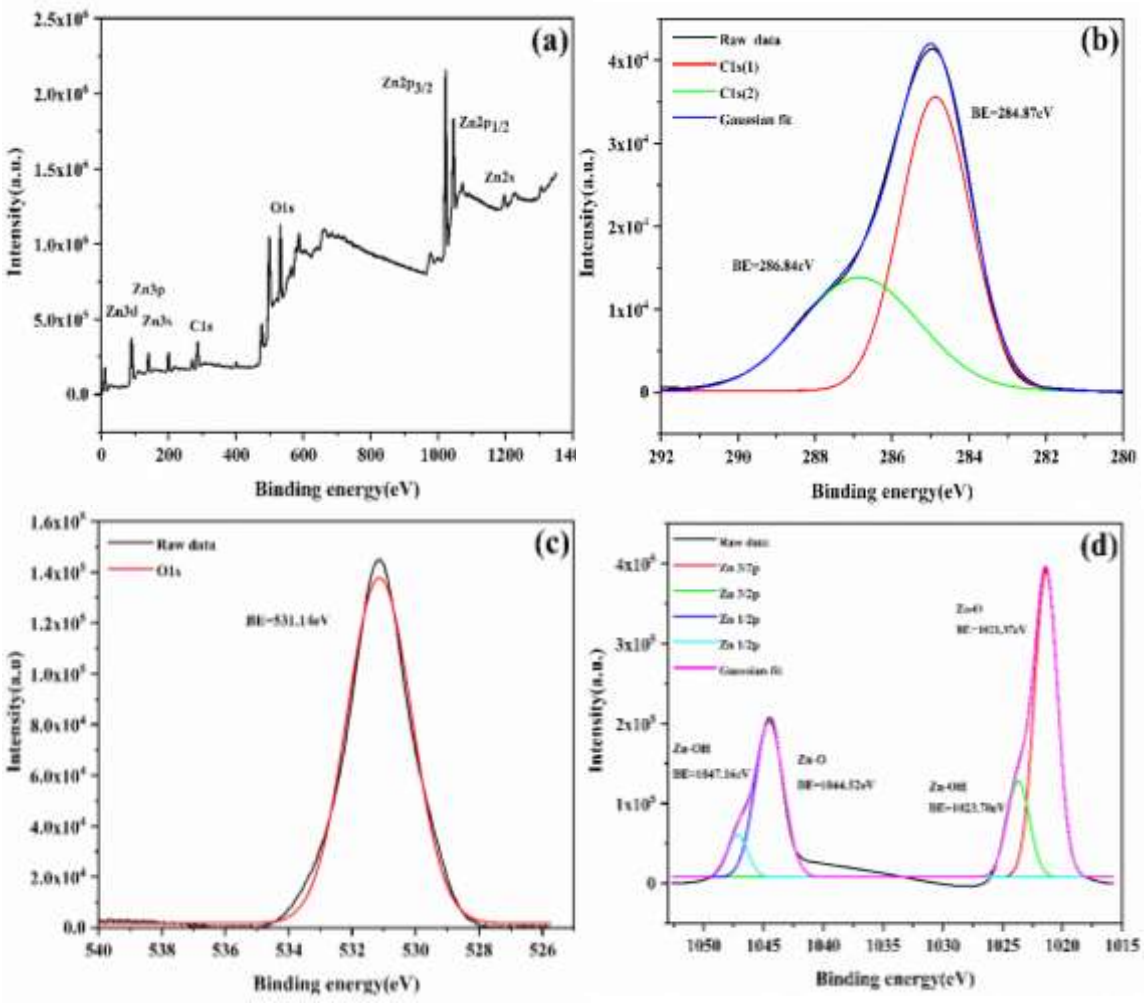

Figure 23. X-ray photoelectron spectroscopy (XPS) analysis: (a) Provides the XPS survey spectra of ZnO-NPs synthesized from *C. vulgaris*, offering an overview of the elemental composition and surface characteristics. (b) Presents an XPS core level scan of carbon (C 1s) with a deconvoluted profile, allowing a closer examination of carbon's chemical environment and bonding states. (c) Offers an XPS core level scan of oxygen (O 1s), giving insights into the chemical states and bonding of oxygen on the sample's surface. (d) Shows the XPS core level scan of zinc (Zn 2p ½ and Zn 2p 3/2) with deconvoluted profiles.

3.4. Characterization of Nanocellulose

3.4.1. FTIR Analysis

Fourier transform infrared (FTIR) spectroscopy was employed to identify the functional groups present in the nanocellulose extracted from *C. glomerata* and *C. vulgaris*. The spectra (Figure 24 and Figure 25) revealed the presence of various functional groups, including hydroxyl, carbonyl, and ether groups.

***C. glomerata*:**

i. A broad peak at 3345 cm^{-1} indicated the presence of O-H stretching vibrations from hydroxyl groups.
ii. A peak at 2905 cm^{-1} suggested C-H stretching vibrations from aliphatic groups.
iii. A peak at 1648 cm^{-1} indicated C=C stretching vibrations from alkenes or aromatic compounds.
iv. Peaks at 1160 cm^{-1}, 1110 cm^{-1}, 1060 cm^{-1}, and 1034 cm^{-1} were attributed to C-O stretching vibrations from various oxygen-containing functional groups.

***C. vulgaris*:**

i. A broad peak at 3310 cm^{-1} indicated O-H stretching vibrations.
ii. A peak at 2905 cm^{-1} suggested C-H stretching vibrations.
iii. A peak at 1676 cm^{-1} indicated C=C stretching vibrations.
iv. Peaks at 1417 cm^{-1}, 1110 cm^{-1}, 740 cm^{-1}, and 594 cm^{-1} were attributed to various functional groups, including C-O stretching, C-H bending, and aromatic ring vibrations.

The presence of these functional groups confers unique properties to nanocellulose, such as high surface area, strong hydrogen bonding, biodegradability, and excellent mechanical properties. These properties make nanocellulose a promising material for various applications in materials science, biomedicine, environmental remediation, and sustainable technologies

Detailed analysis of the functional groups and their corresponding vibrations is presented in Tables 11 and 12 for *C. glomerata* and *C. vulgaris*, respectively.

Table 11: FTIR analysis showing functional groups and vibrations in nanocellulose extracted from *C. glomerata*.

Wavenumber (cm^{-1})	Functional groups	Vibrations
3345	Alcohol	O-H Stretching
2905	Carboxylic acid	H-bending Stretching
1648	Alkene	C=C Stretching
1160	Tertiary alcohol	C-O Stretching
1110	Aliphatic ether	C-O Stretching
1060	Primary alcohol	C-O Stretching
1034	Sulfoxide	S=O Stretching
461		C-O-C Stretching

Table 12: FTIR analysis showing functional groups and vibrations in nanocellulose extracted from *C. vulgaris*.

Wavenumber (cm^{-1})	Functional groups	Vibrations
3310	Alcohol	O-H Stretching
2905	Carboxylic acid	H-bending Stretching
1676	Alkene	C=C Stretching
1417	Tertiary alcohol	C-O Stretching
1110	Aliphatic ether	C-O Stretching
740	Primary alcohol	C-O Stretching
594	Sulfoxide	S=O Stretching

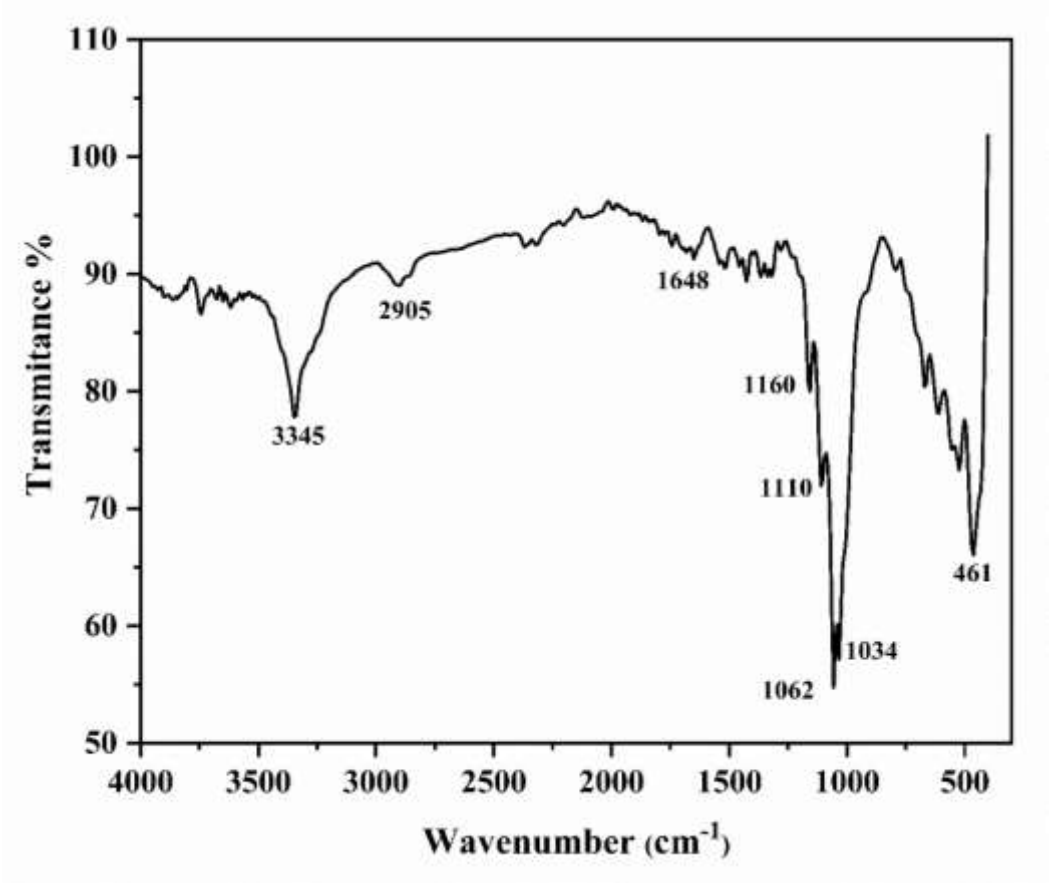

Figure 24. Fourier transform infrared (FTIR) spectrum of nanocellulose synthesized from *C. glomerata.*

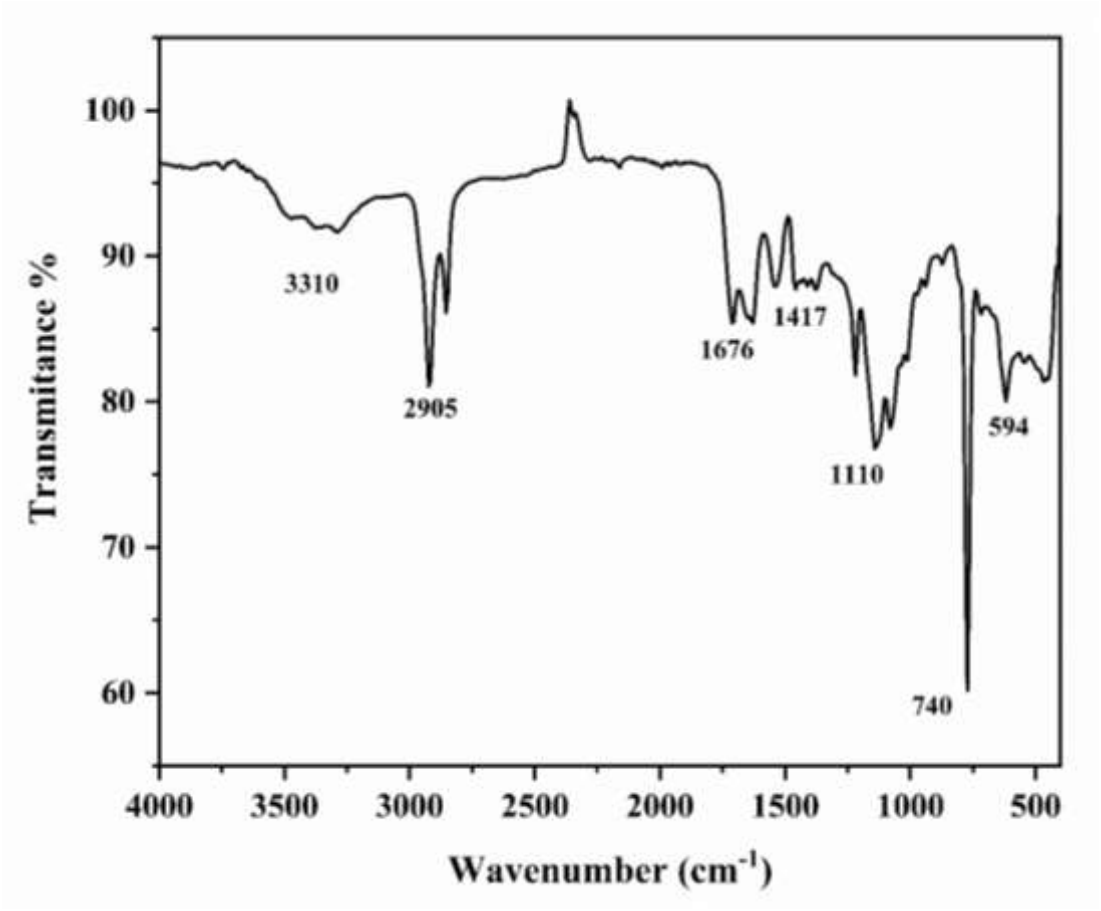

Figure 25. Fourier transform infrared (FTIR) spectrum of nanocellulose synthesized from *C. vulgaris.*

3.4.2. SEM and EDAX Analyses of Nanocellulose Obtained from *C. glomerata*

Figure 26 presents SEM images of nanocellulose extracted from *C. glomerata* at various magnifications.

i. *Image (a):* This low-magnification image provides an overview of the nanocellulose sample, showing a network-like structure with some agglomeration.
ii. *Image (b):* At a higher magnification, the fibrous nature of the nanocellulose becomes more apparent. Individual nanofibrils can be observed, although they are still somewhat aggregated.
iii. *Image (c):* At a higher magnification, the individual nanofibrils become more distinct. They appear to have a smooth surface and a relatively uniform diameter.
iv. *Image (d):* At the highest magnification, the nanofibrils appear to have a slightly rough surface, possibly due to the presence of surface functional groups or residual impurities.

Table 13: Elemental composition of nanocellulose extracted from *C. glomerata* determined by EDX analysis.

Elements	Atomic %	Weight %
C K	30.58	41.42
O K	49.32	50.16
Na K	2.53	1.52
Si K	10.56	6.11
K K	0.61	0.25
Au L	6.41	0.53

The average diameter of these nanofibrils was determined to be 22.5 ± 1.72 nm, indicating a relatively uniform size distribution. The observed morphology is characteristic of cellulose nanofibrils, which are known for their high aspect ratio and large surface area.

Energy-dispersive x-ray (EDX) spectroscopy was utilized to determine the elemental composition of the nanocellulose. The EDX spectrum (Figure 27a) confirmed the presence of carbon (C) and oxygen (O), which are the primary constituents of cellulose. Minor peaks corresponding to potassium (K), aluminum (Al), and gold (Au) were also observed (Table 13). These elements may be attributed to sample preparation techniques or residual impurities.

The particle size distribution of the nanocellulose was analyzed using image analysis techniques. The results showed a Gaussian distribution with an average particle size of approximately 22.5 nm (Figure 27b). This narrow particle size distribution is indicative of a relatively homogeneous sample.

3.4.3. SEM and EDAX Analyses of Nanocellulose Obtained from *C. vulgaris*

The SEM images (Figure 28) suggest that the cellulose nanocrystals extracted from *C. vulgaris* exhibit a complex morphology with varying features at different magnifications.

i. *Image (a):* At lower magnifications, the CNCs appear as plate-like structures with a rough surface.
ii. *Image (b) and (c):* As the magnification increases, the individual nanocrystals become more visible, revealing a rod-like morphology with a smooth surface. The presence of pores and irregularities on the surface of the nanocrystals can also be observed.
iii. *Image (d):* At the highest magnification, the crystalline nature of the nanocrystals becomes evident, with distinct lattice planes visible. The glittering edges observed in the SEM images are indicative of the crystalline nature of the cellulose nanocrystals.

The rod-like morphology and high aspect ratio of the CNCs make them suitable for various applications, including reinforcement in composite materials, drug delivery, and tissue engineering. The presence of pores on the surface of the nanocrystals can further enhance their adsorption and catalytic properties.

Elemental Composition (EDX) and Particle Size

EDXspectroscopy was utilized to determine the elementalcomposition of the nanocellulose. The EDX spectrum (Figure 29a) and Table 14 confirmed the presence of carbon (C) and oxygen (O), which are the primary constituents of cellulose. Minor peaks corresponding to sodium (Na), silicon (Si), sulfur (S), and gold (Au) were also detected. These elements may be attributed to sample preparation techniques or residual impurities.

Table 14: Elemental composition of nanocellulose extracted from *C. vulgaris*determined by EDX analysis.

Elements	Atomic %	Weight %
C K	61.71	74.91
O K	22.12	20.16
Na K	5.11	3.24
Si K	1.03	0.54
S K	1.07	0.49
Au L	8.96	0.66

The particle size distribution of the nanocellulose was analyzed using image analysis techniques. The results showed a Gaussian distribution with an average particle size of approximately 74.92±1.35 nm (Figure 29 b). This narrow particle size

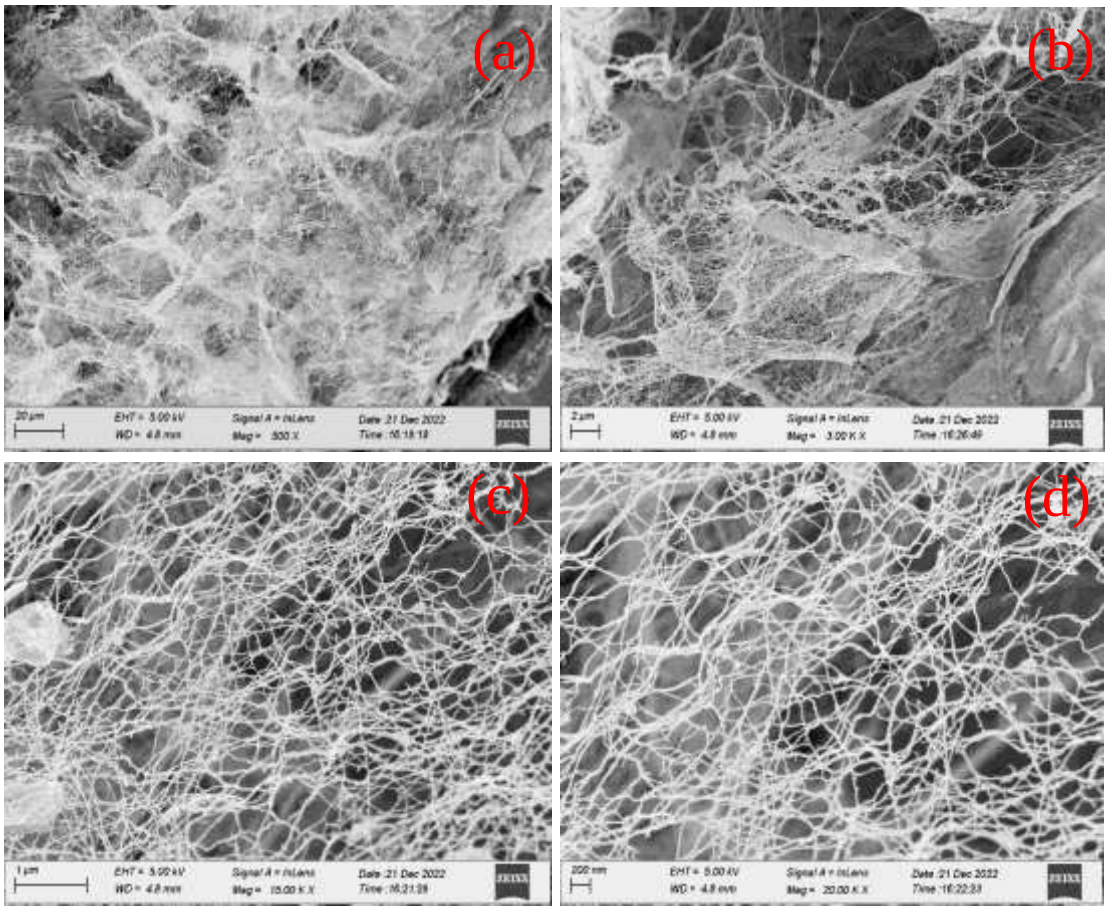

Figure 26. Scanning electron microscopy (SEM) images of nanocellulose extracted from *C. glomerata* (a) at 20 µm (b) at 2 µm, (c) at 1 µm (d) at 200 nm.

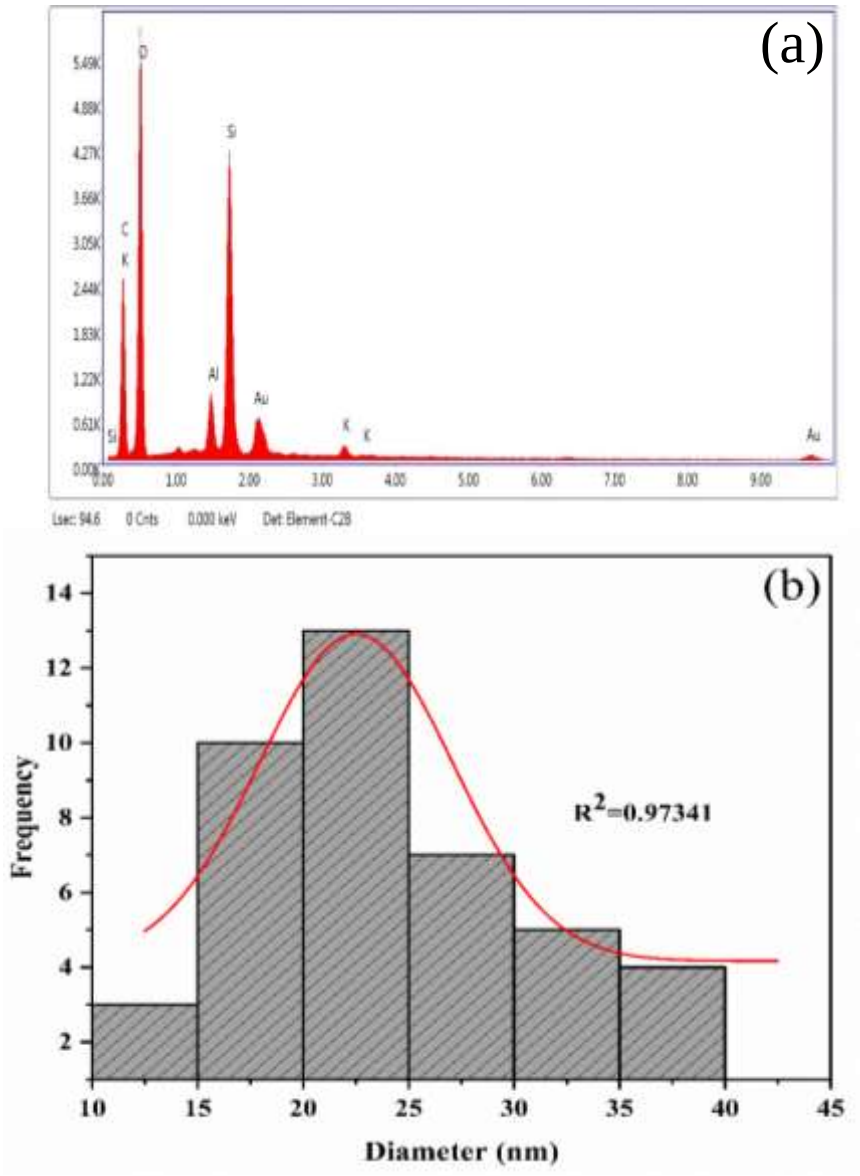

Figure 27. (a) EDX spectrum of nanocellulose synthesized from *C. glomerata,* (b)Diameter of nanocellulose synthesized from *C. glomerata* in Gaussian distribution.

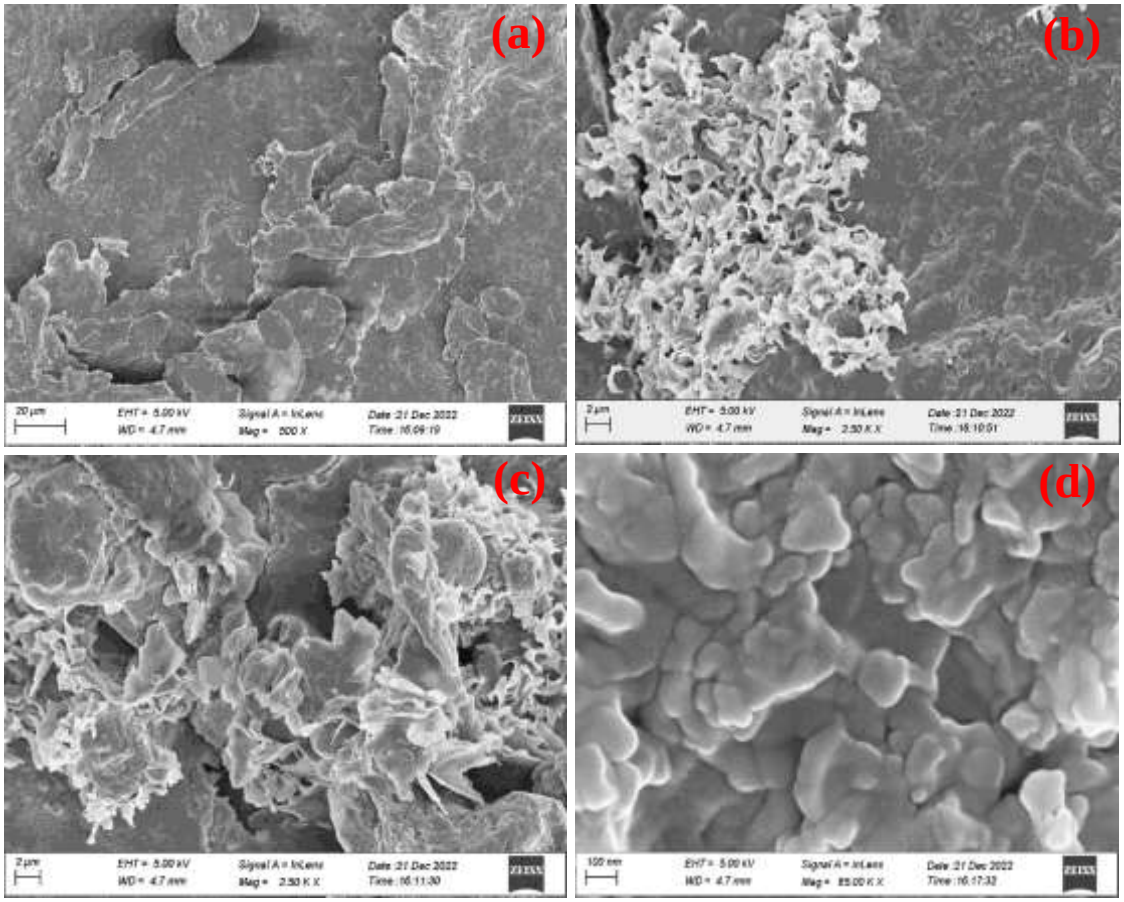

Figure 28. Scanning electron microscopy (SEM) images of nanocellulose extracted from *C. vulgaris* (a) at 20 µm, (b) at 2 µm, (c) at 2 µm and (d) at 200 nm.

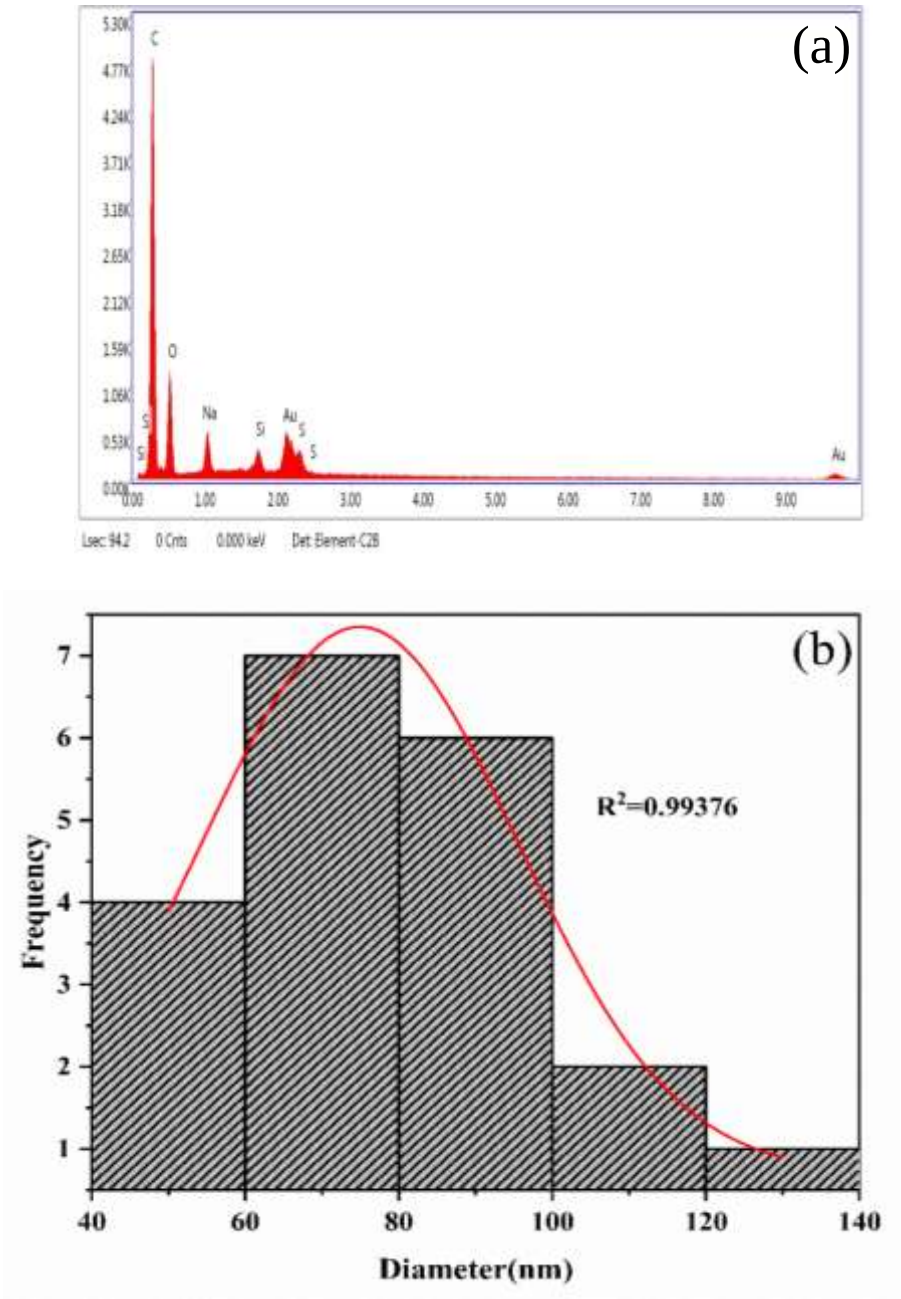

Figure 29. (a) EDX spectrum of nanocellulose synthesized from *C. glomerata*, (b) Diameter of nanocellulose synthesized from *C. glomerata* in Gaussian distribution.

distribution is indicative of a relatively homogeneous sample, which is desirable for many applications.

3.4.4. Thermogravimetric Analysis (TGA) of CNF Obtained from *C. glomerata*

Thermogravimetric analysis (TGA) was employed to evaluate the thermal stability and decomposition behavior of the extracted nanocellulose. The TGA curve (Figure 30a) exhibits three distinct weight loss stages:

i. *Initial Weight Loss (71°C to 171°C):* This initial weight loss of approximately 3.7% is attributed to the evaporation of moisture and the removal of surface-bound water, as supported by FTIR analysis.
ii. *Major Weight Loss (171°C to 365°C):* A significant weight loss of 42.7% occurs during this phase, primarily due to the thermal degradation of hemicellulose and the cleavage of glycosidic linkages within the cellulose chains.
iii. *Final Weight Loss (365°C to 500°C):* This final phase involves the decomposition of the remaining cellulose fibers, leading to a weight loss of 9.39%.

Derivative Thermogravimetric Analysis (DTG)

The DTG curve (Figure 30b) provides a more detailed view of the rate of weight loss during the thermal degradation process. The first peak in the DTG curve, observed at 44°C, corresponds to the removal of moisture and surface-bound water. The second peak, centered 348°C, is associated with the thermal degradation of hemicellulose and the cleavage of glycosidic linkages in cellulose. The third peak, occurring at around 437°C, corresponds to the decomposition of the remaining cellulose fibers. The shape and position of these peaks provide valuable information about the thermal stability and decomposition kinetics of the nanocellulose.

In conclusion, the TGA and DTG analysis indicate that the nanocellulose exhibits good thermal stability up to around 171°C. Beyond this temperature, the material undergoes significant thermal degradation, which limits its potential applications in high-temperature environments. However, the relatively high thermal

stability and controlled degradation behavior make nanocellulose a promising material for various applications, such as reinforcement in composite materials and drug delivery.

3.4.5. Thermogravimetric Analysis (TGA) of CNC Obtained from *C. vulgaris*

Thermogravimetric analysis (TGA) was employed to evaluate the thermal stability and decomposition behavior of the nanocellulose extracted from *C. vulgaris*. The TGA curve (Figure 31a) exhibits three distinct weight loss stages:

i. *Initial Weight Loss (33°C to 137°C):* This initial weight loss of approximately 5.17% is attributed to the evaporation of moisture and the removal of surface-bound water.
ii. *Major Weight Loss (137°C to 352°C):* A significant weight loss of 63% occurs during this phase, primarily due to the thermal degradation of hemicellulose and the cleavage of glycosidic linkages within the cellulose chains.
iii. *Final Weight Loss (352°C to 461°C):* This final phase involves the decomposition of the remaining cellulose fibers, leading to a weight loss of 11.62%.

Derivative Thermogravimetric Analysis (DTG)

The DTG curve (Figure 31b) provides a more detailed view of the rate of weight loss during the thermal degradation process. The DTG curve shows three distinct peaks, indicating three stages of weight loss:

i. *First Peak (40°C):* This peak corresponds to the removal of moisture and surface-bound water.
ii. *Second Peak (223°C):* This peak is associated with the thermal degradation of hemicellulose and the cleavage of glycosidic linkages in cellulose.
iii. *Third Peak (404°C):* This peak corresponds to the decomposition of the remaining cellulose fibers.

The TGA and DTG analysis indicate that the nanocellulose extracted from *C. vulgaris* exhibits good thermal stability up to around 137°C. Beyond this

temperature, the material undergoes significant thermal degradation, which limits its potential

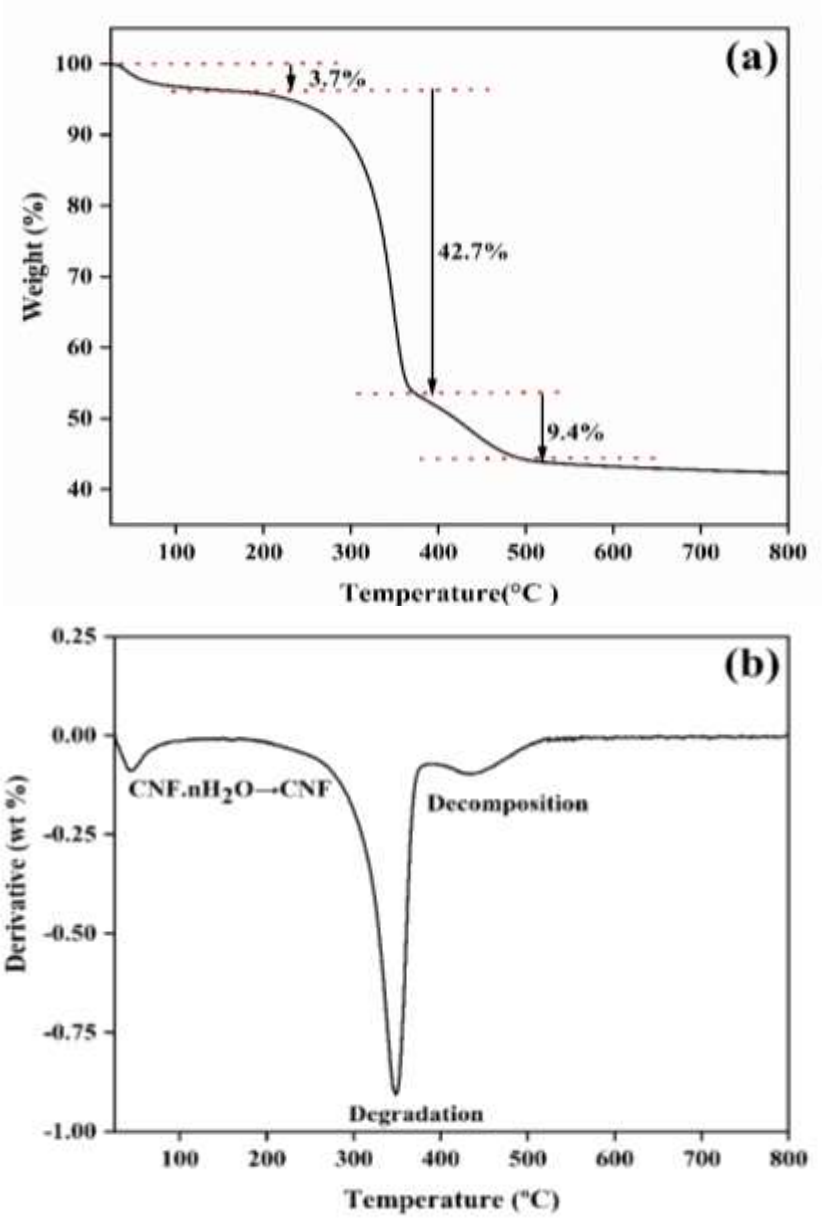

Figure 30. (a) Depicts the TGA curve of CNF isolated from *C. glomerata*, offering insights into their thermal stability and weight loss profile as a function of temperature. (b) Features the DTG curve of CNF, providing a detailed representation of the rate of weight change with respect to temperature for the CNF sample.

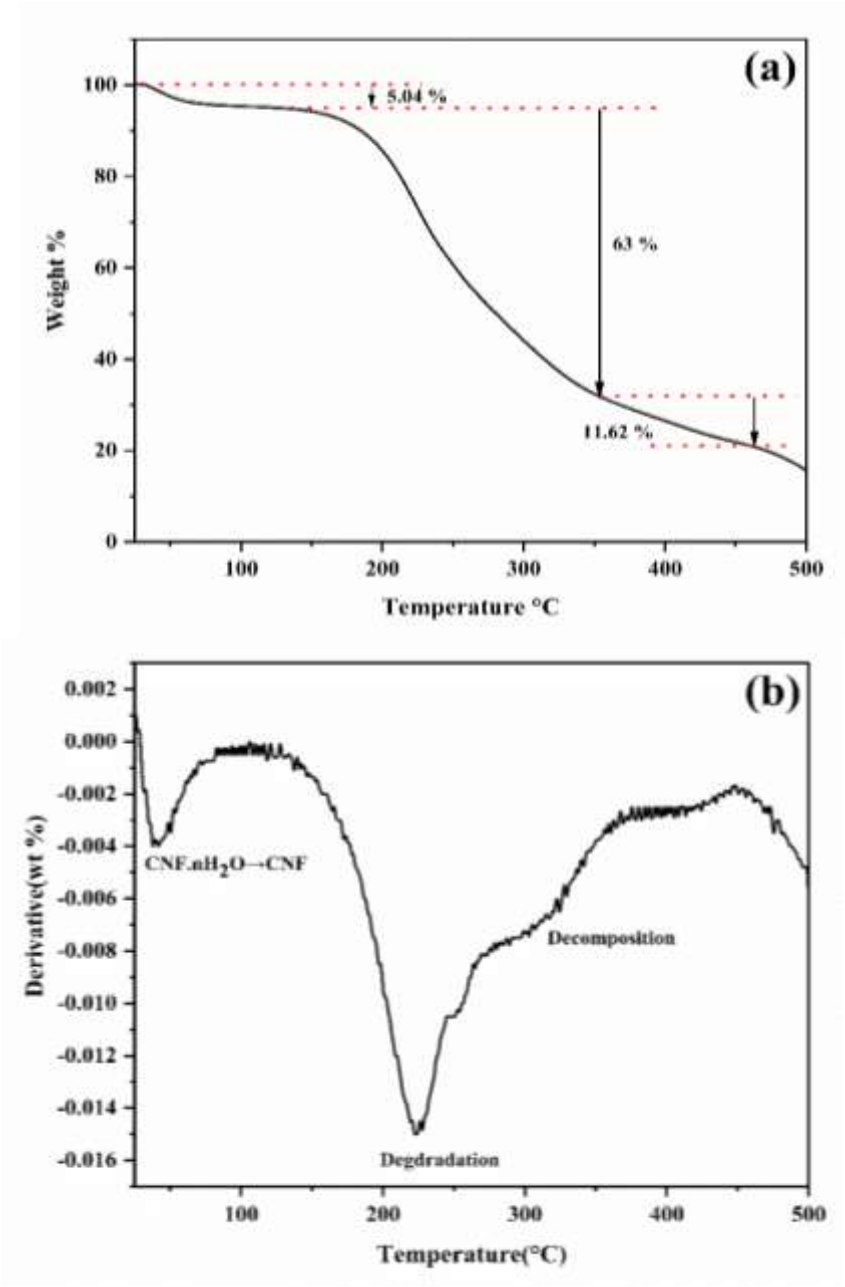

Figure 31. (a) The TGA curve of the CNC isolated from *C. vulgaris* revealing its thermal stability and weight loss characteristics under increasing temperature. (b) Highlights the DTG curve of the CNC offering information about the rate of weight change with temperature for theCNCsample.

applications in high-temperature environments. However, the relatively high thermal stability and controlled degradation behavior make nanocellulose a promising material for various applications, such as reinforcement in composite materials and drug delivery.

Overall, TGA and DTG analysis revealed that the nanocellulose from both algae sources exhibited good thermal stability upto certain temperature. Beyond thisstability and controlled degradation behavior make nanocellulose a promising material fortemperature, the material underwent thermal degradation, primarily due to the decomposition of hemicellulose and cellulose. The thermal stability of the nanocellulose can be attributed to the strong hydrogen bonding between cellulose chains.

3.4.6. DSC Analysis of Nanocellulose obtained from *C. glomerata*

Differential scanning calorimetry (DSC) was employed to investigate the thermal behavior of the nanocellulose extracted from *C. glomerata*. The DSC curve (Figure 32) reveals three distinct endothermic peaks, indicating the occurrence of phase transitions and energy absorption processes.

i. *First Endothermic Peak (72°C, 6.29 mW/mg):* This peak corresponds to the loss of moisture and surface-bound water. The relatively low temperature and heat flow associated with this peak suggest that the nanocellulose has a low moisture content and that the removal of water is a relatively easy process.

ii. *Second Endothermic Peak (227°C, 12.76 mW/mg):* This peak is attributed to the onset of thermal decomposition, likely involving the cleavage of glycosidic bonds within the cellulose chains. The higher temperature and heat flow associated with this peak indicate that the thermal degradation of cellulose is an endothermic process that requires significant energy input.

iii. *Third Endothermic Peak (382°C, 11.41 mW/mg):* This peak corresponds to the further degradation of cellulose and the formation of char. The lower heat flow compared to the second peak suggests that the remaining cellulose chains are more thermally stable and require higher temperatures to decompose.

Overall, the DSC analysis indicates that the nanocellulose extracted from *C. glomerata* exhibits good thermal stability up to around 226.58°C. Beyond this temperature, the material undergoes thermal degradation, which limits its potential applications in high-temperature environments. However, the relatively high thermal various applications, such as reinforcement in composite materials and drug delivery.

3.4.7. DSC Analysis of Nanocellulose Obtained from *C. vulgaris*

Differential scanning calorimetry (DSC) was employed to investigate the thermal behavior of the nanocellulose extracted from *C. vulgaris*. The DSC curve (Figure 33) reveals two distinct endothermic peaks, indicating the occurrence of phase transitions and energy absorption processes.

i. *First Endothermic Peak (51°C, 0.49 mW/mg):* This peak corresponds to the loss of moisture and surface-bound water. The relatively low temperature and heat flow associated with this peak suggest that the nanocellulose has a low moisture content and that the removal of water is a relatively easy process.

ii. *Second Endothermic Peak (187°C, 0.544 mW/mg):* This peak is attributed to the onset of thermal decomposition, likely involving the cleavage of glycosidic bonds within the cellulose chains. The higher temperature and heat flow associated with this peak indicate that the thermal degradation of cellulose is an endothermic process that requires significant energy input.

Overall, the DSC analysis indicates that the nanocellulose extracted from *C. vulgaris* exhibits good thermal stability up to around 187°C. Beyond this temperature, the material undergoes thermal degradation, which limits its potential applications in high-temperature environments. However, the relatively high thermal stability and controlled degradation behavior make nanocellulose a promising material for various applications, such as reinforcement in composite materials and drug delivery.

3.5.Characterization of ZnO-CNF (*C. glomerata*) Nanocomposite

For further investigation, the nanocellulose extracted from *C. glomerata* was selected due to its superior properties, including higher purity, better crystallinity, and larger

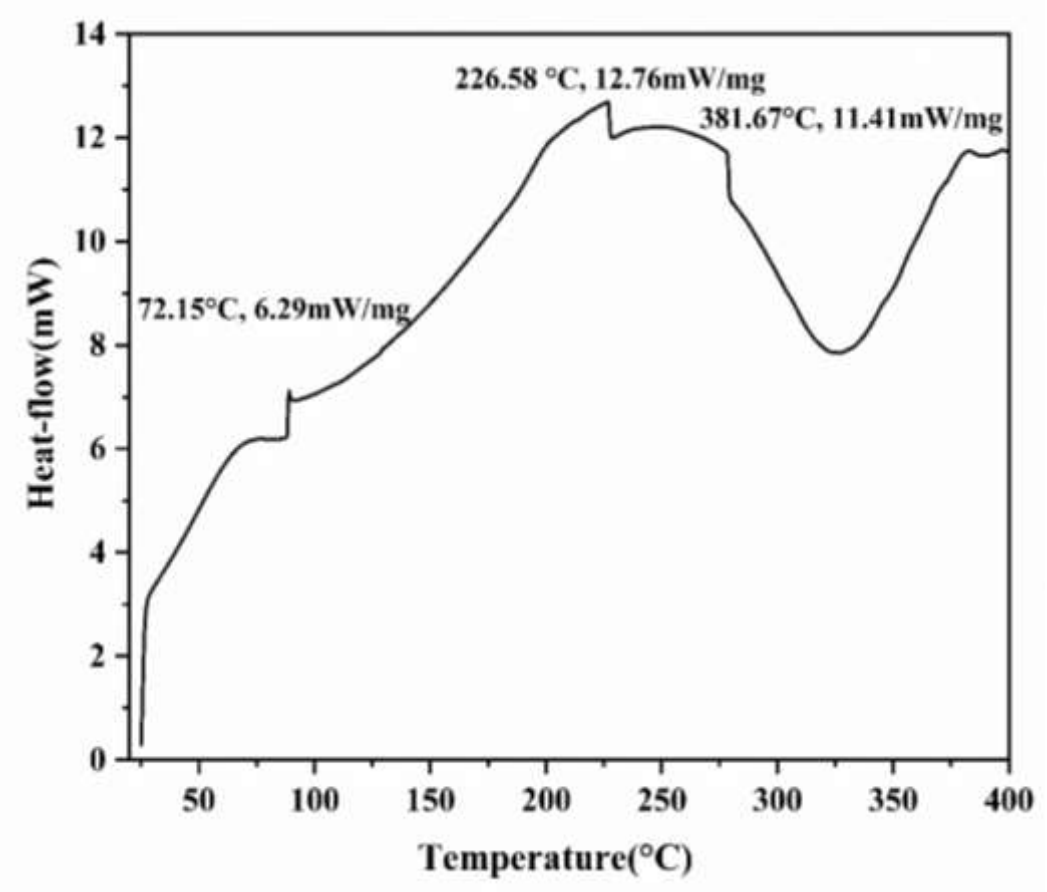

Figure 32. Depicts the DSC curve of isolated nanocelluose from *C. glomerata*, providing information on their thermal behaviour, including phase transitions and heat flow as a function of temperature.

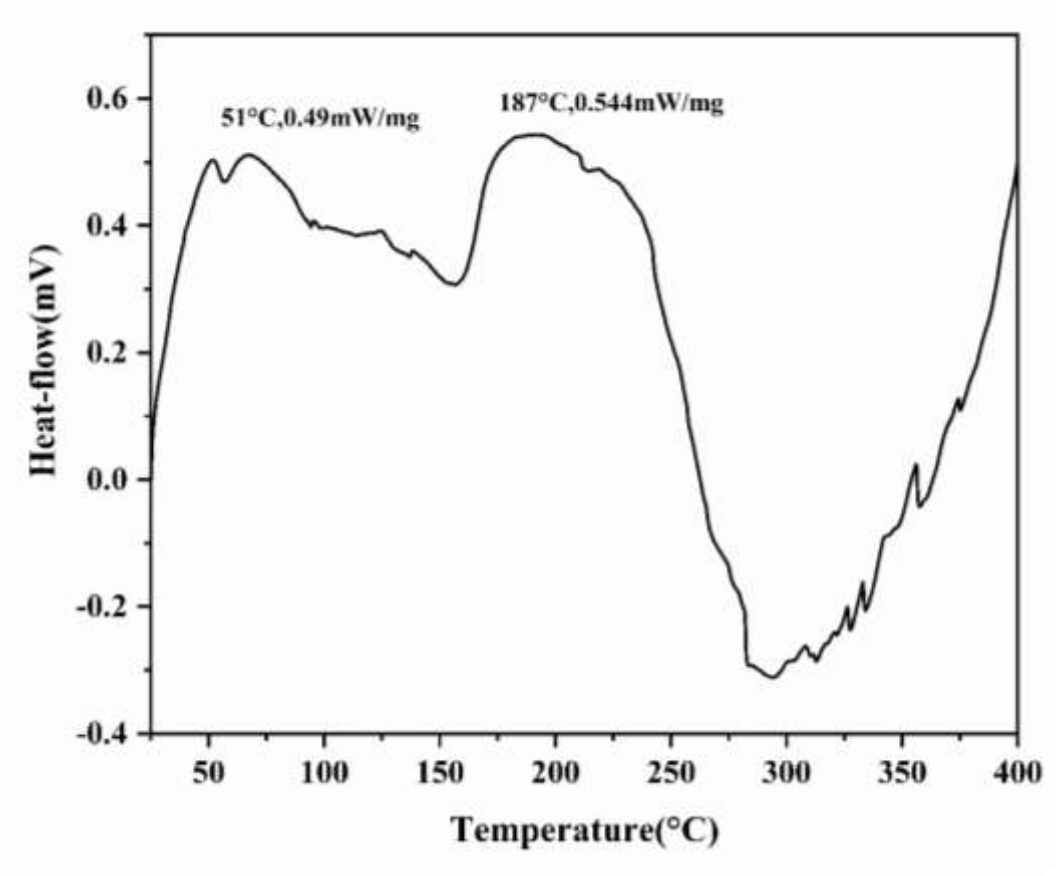

Figure 33. Depicts the DSC curve of isolated nanocelluose *C. vulgaris*, providing information on their thermal behaviour, including phase transitions and heat flow as a function of temperature.

particle size compared to the nanocellulose from *C. vulgaris*. These properties make it a more suitable candidate for various applications, particularly in the development of advanced materials.

To explore the potential of nanocellulose in material science, ZnO-CNF nanocomposites were synthesized. These nanocomposites were characterized using a variety of techniques, including FTIR, SEM, EDX, TGA, and DSC, to evaluate their structural, morphological, thermal, and mechanical properties.

3.5.1. FTIR Analysis of ZnO-CNF Nanocomposite

Fourier transform infrared (FTIR) spectroscopy was employed to investigate the functional groups present in the ZnO-CNF nanocomposite. The FTIR spectrum (Figure 34) revealed the presence of various functional groups, including hydroxyl, carbonyl, and ether groups, associated with the nanocellulose component (Table 15). Additionally, a peak at 531 cm^{-1} was observed, which is characteristic of the Zn-O bond in ZnO-NPs.

Table 15: FTIR analysis showing functional groups and vibrations in ZnO-CNF nanocomposite.

Wavenumber (cm^{-1})	Functional groups	Vibrations
3345	Alcohol	O-H Stretching
2905	Carboxylic acid	C-H bending Stretching
1160	Tertiary alcohol	C-O Stretching
1110	Aliphatic ether	C-O Stretching
1054	Sulfoxide	S=O Stretching
768	1,2-disubstituted	C-H bending
531	Metal oxide	Zn-O Stretching

The presence of the Zn-O bond peak in the FTIR spectrum confirms the successful incorporation of ZnO-NPs into the nanocellulose matrix. The other functional groups observed in the spectrum are associated with the nanocellulose component, indicating that the structure and properties of the nanocellulose have been preserved during the synthesis of the nanocomposite.

3.5.2. Morphological Analysis (SEM)

Scanning electron microscopy (SEM) was employed to investigate the morphology of the ZnO-CNF nanocomposite. The SEM images (Figure 35) revealed a network-like structure composed of nanofibrils with ZnO-NPs uniformly dispersed on their surface.

i. *Image (a):* This low-magnification image provides an overview of the nanocomposite, showing a porous and interconnected network structure. The nanofibrils appear to be randomly oriented and intertwined, forming a complex three-dimensional network. The pores within the network can provide pathways for the transport of ions and molecules, which is important for applications such as sensors and catalysts.
ii. *Image (b):* At a higher magnification, the individual nanofibrils become more visible, and the ZnO-NPs appear as small, spherical particles attached to the surface of the nanofibrils. The nanoparticles are well-dispersed and do not appear to be agglomerated, indicating good compatibility between the ZnO and nanocellulose components.
iii. *Images (c) and (d):* These high-magnification images provide a detailed view of the ZnO-NPs, which appear to be well-dispersed and tightly bound to the nanofibrils. The nanoparticles are relatively uniform in size and shape, and they do not appear to significantly disrupt the structure of the nanofibrils. The strong interaction between the ZnO-NPs and the nanofibrils is likely due to the presence of functional groups on the surface of the nanofibrils, such as hydroxyl and carboxyl groups, which can form bonds with the ZnO-NPs.

The uniform dispersion of ZnO-NPs on the surface of the nanofibrils is crucial for enhancing the mechanical, thermal, and electrical properties of the

nanocomposite. The interconnected network structure of the nanofibrils provides a large surface area for interaction with other materials, which can be beneficial for various applications.

Overall, the SEM analysis confirms the successful synthesis of ZnO-CNF nanocomposites with a well-defined morphology and uniform dispersion of ZnO-NPs.

3.5.3. Elemental Composition and Particle Size

EDX spectroscopy was utilized to determine the elemental composition of the ZnO-CNF nanocomposite. The EDX spectrum (Figure 36a) confirmed the presence of zinc (Zn), oxygen (O) along with silicon (Si), chlorine (Cl), and gold (Au) (Table 16). The presence of Zn and O elements suggests that the synthesis process was successful in incorporating ZnO-NPs into the nanocellulose matrix.

The particle size distribution of the ZnO-CNF nanocomposite was analysed using image analysis techniques. The results showed a Gaussian distribution with an average particle size of approximately 42.44 ± 1.72 nm(Figure 36b). This relatively narrow particle size distribution indicates a homogeneous sample, which is desirable for achieving consistent properties and performance.

Table 16: Elemental composition of ZnO-CNF nanocomposite determined by EDX analysis.

Elements	Atomic %	Weight %
O K	17.10	41.71
Si K	16.56	23.00
Cl K	1.63	1.79
Zn K	51.84	30.95
Au K	12.87	2.55

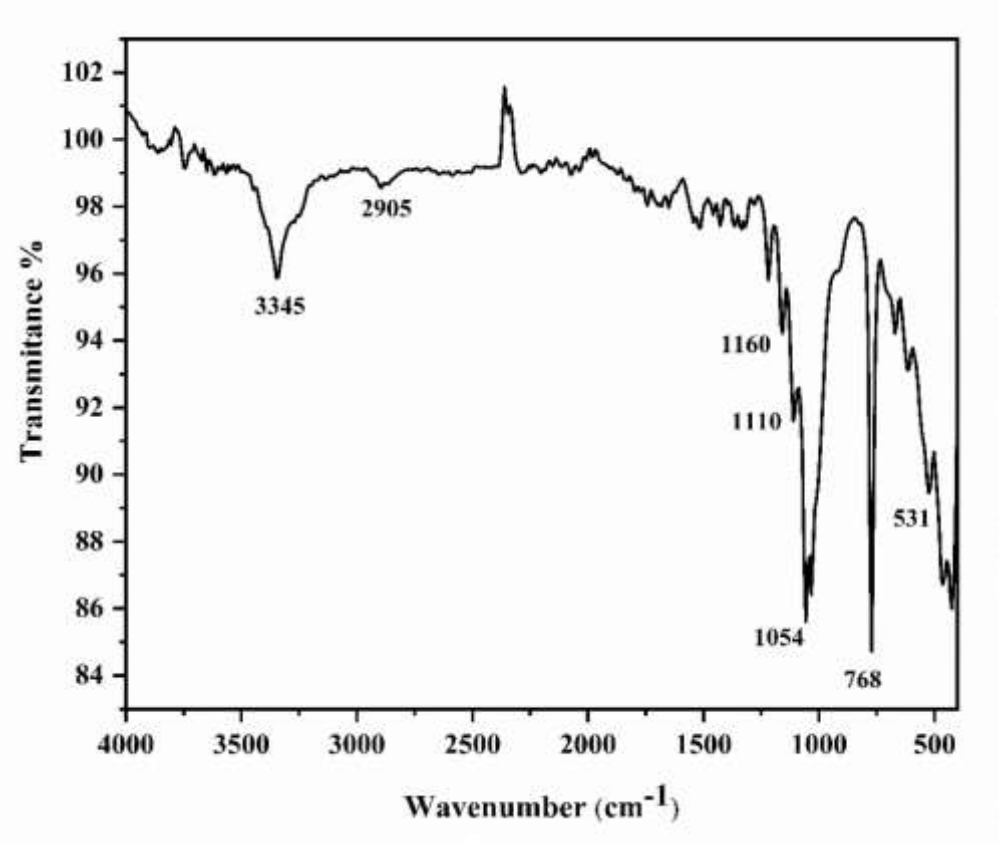

Figure 34. Fourier transform infrared (FTIR) spectrum of ZnO-CNF nanocomposite.

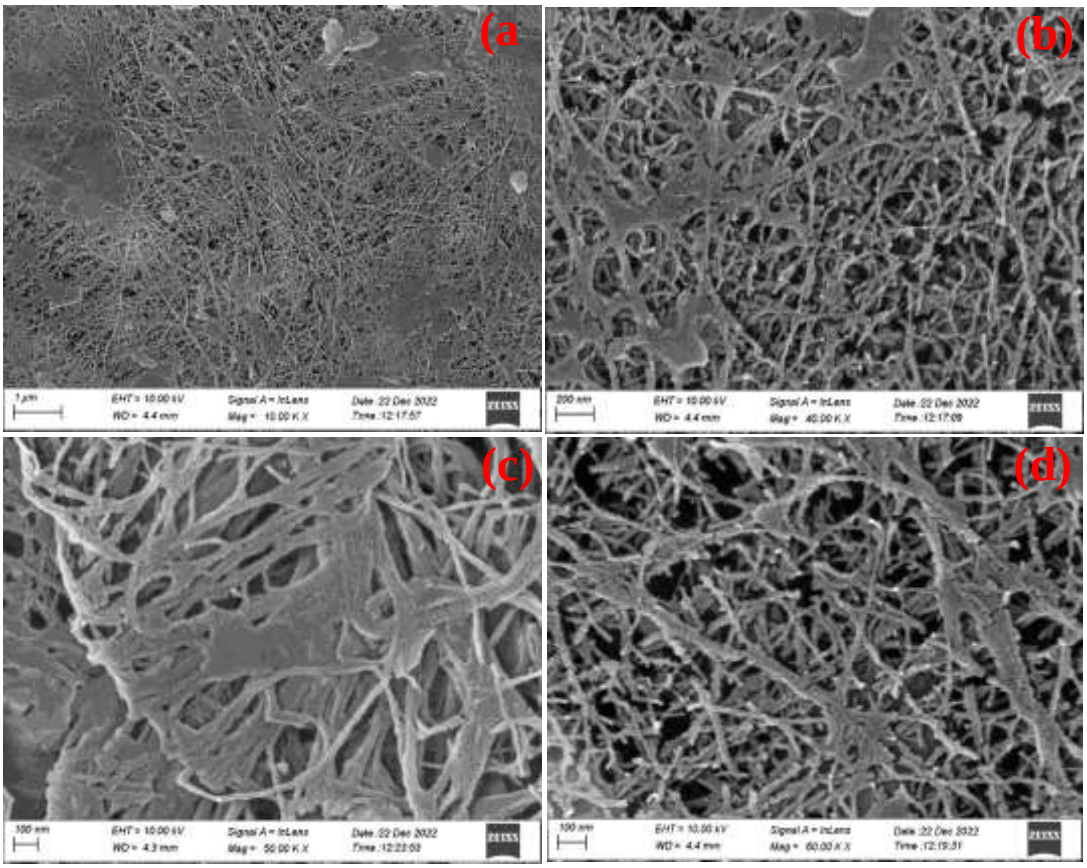

Figure 35. Scanning electron microscopy (SEM) image of ZnO-CNFnanocomposite in different scale (a) at 1µm, (b) at 200 nm, (c) at 100 nm (d) at 100 nm.

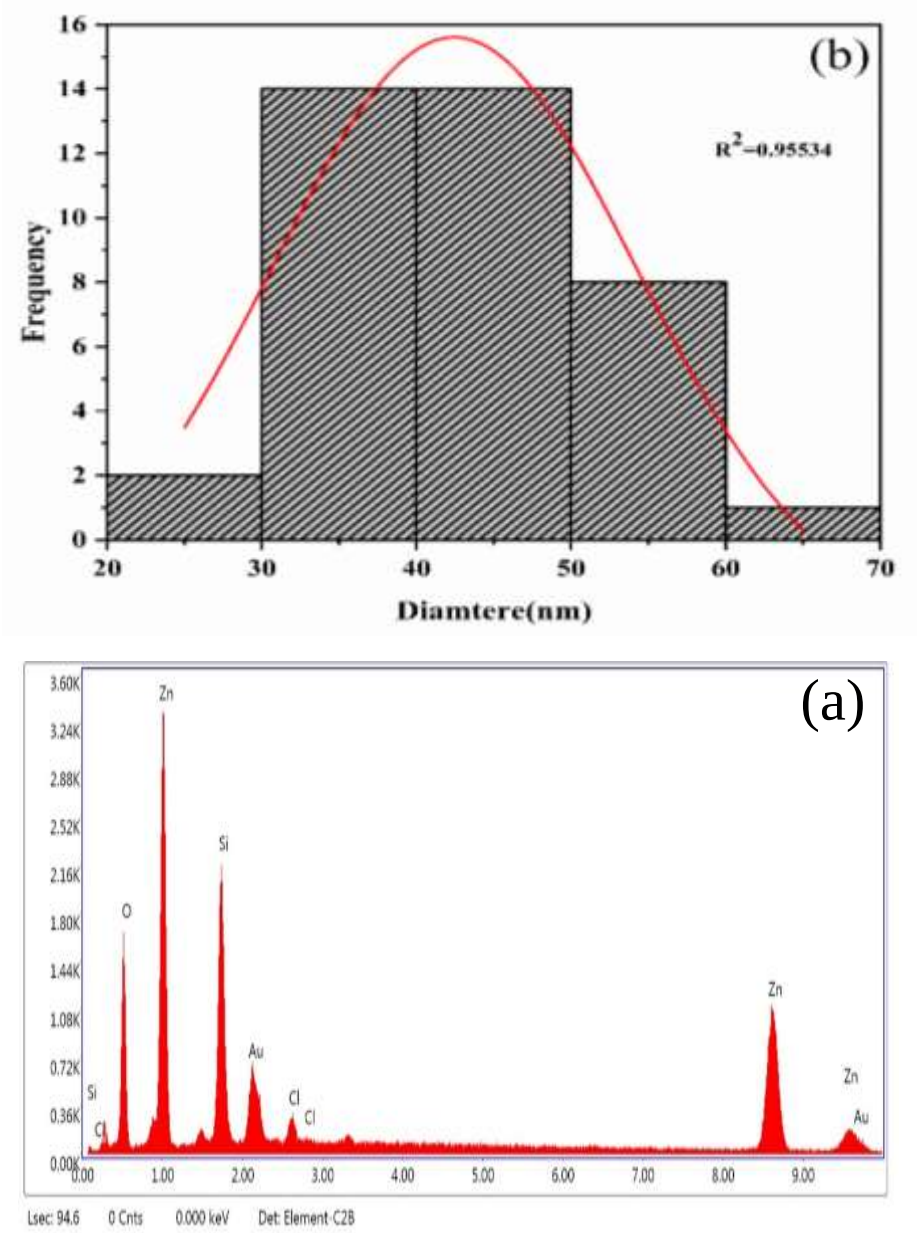

Figure 36. (a) EDX spectrum for the ZnO-CNF nanocomposite, (b) Diameter of ZnO-CNF nanocomposite in Gaussian distribution.

The elemental composition analysis indicates that the ZnO-CNF nanocomposite is primarily composed of zinc oxide and nanocellulose, with minor amounts of silicon, chlorine, and gold. The presence of these elements may be attributed to the synthesis process or residual impurities. Overall, the EDX and particle size distribution analyses provide valuable insights into the composition and size distribution of the ZnO-CNF nanocomposite. The successful incorporation of ZnO-NPs into the nanocellulose matrix is expected to enhance the mechanical, thermal, and electrical properties of the resulting nanocomposite.

3.5.4. Thermogravimetic Analysis (TGA)

Thermogravimetric analysis (TGA) was employed to evaluate the thermal stability and decomposition behavior of the ZnO-CNF nanocomposite. The TGA curve (Figure 37a) exhibits three distinct weight loss stages:

i. *Initial Weight Loss (33°C to 137°C):* This initial weight loss of approximately 3.77% is attributed to the evaporation of moisture and the removal of surface-bound water.
ii. *Major Weight Loss (137°C to 352°C):* A significant weight loss of 44.11% occurs during this phase, primarily due to the thermal degradation of hemicellulose and the cleavage of glycosidic linkages within the cellulose chains.
iii. *Final Weight Loss (352°C to 461°C):* This final phase involves the decomposition of the remaining cellulose fibers, leading to a weight loss of 17.76%.

Derivative Thermogravimetric Analysis (DTG)

The DTG curve (Figure 37b) provides a more detailed view of the rate of weight loss during the thermal degradation process. The DTG curve shows three distinct peaks, indicating three stages of weight loss:

i. *First Peak (43°C):* This peak corresponds to the removal of moisture and surface-bound water.

ii. *Second Peak (Around 348°C):* This peak is associated with the thermal degradation of hemicellulose and the cleavage of glycosidic linkages in cellulose.

iii. *Third Peak (Around 442°C):* This peak corresponds to the decomposition of the remaining cellulose fibers.

Overall, the TGA and DTG analysis indicate that the ZnO-CNF nanocomposite exhibits good thermal stability up to around 350°C. Beyond this temperature, the material undergoes significant thermal degradation, which limits its potential applications in high-temperature environments. However, the relatively high thermal stability and controlled degradation behavior make the nanocomposite a promising material for various applications, such as reinforcement in composite materials and drug delivery. The incorporation of ZnO-NPs into the nanocellulose matrix may further enhance the thermal stability of the nanocomposite.

3.5.5. Differential Scanning Calorimetry (DSC) Analysis

Differential scanning calorimetry (DSC) was employed to investigate the thermal behavior of the ZnO-CNF nanocomposite and compare it to the behavior of pure cellulose nanofibers (CNF). The DSC curve of the ZnO-CNF nanocomposite (Figure 38) reveals two distinct endothermic peaks, while the DSC curve of pure CNF (Figure 32) exhibits three endothermic peaks.

i. *First Endothermic Peak:*

This peak appears at 91.00°C, which is significantly higher than the corresponding peak in pure CNF (72°C). This shift in the peak temperature suggests that the presence of ZnO-NPs has altered the crystalline structure or thermal behavior of

the cellulose component. The increased melting point may be attributed to enhanced intermolecular interactions between the cellulose chains and the ZnO-NPs.

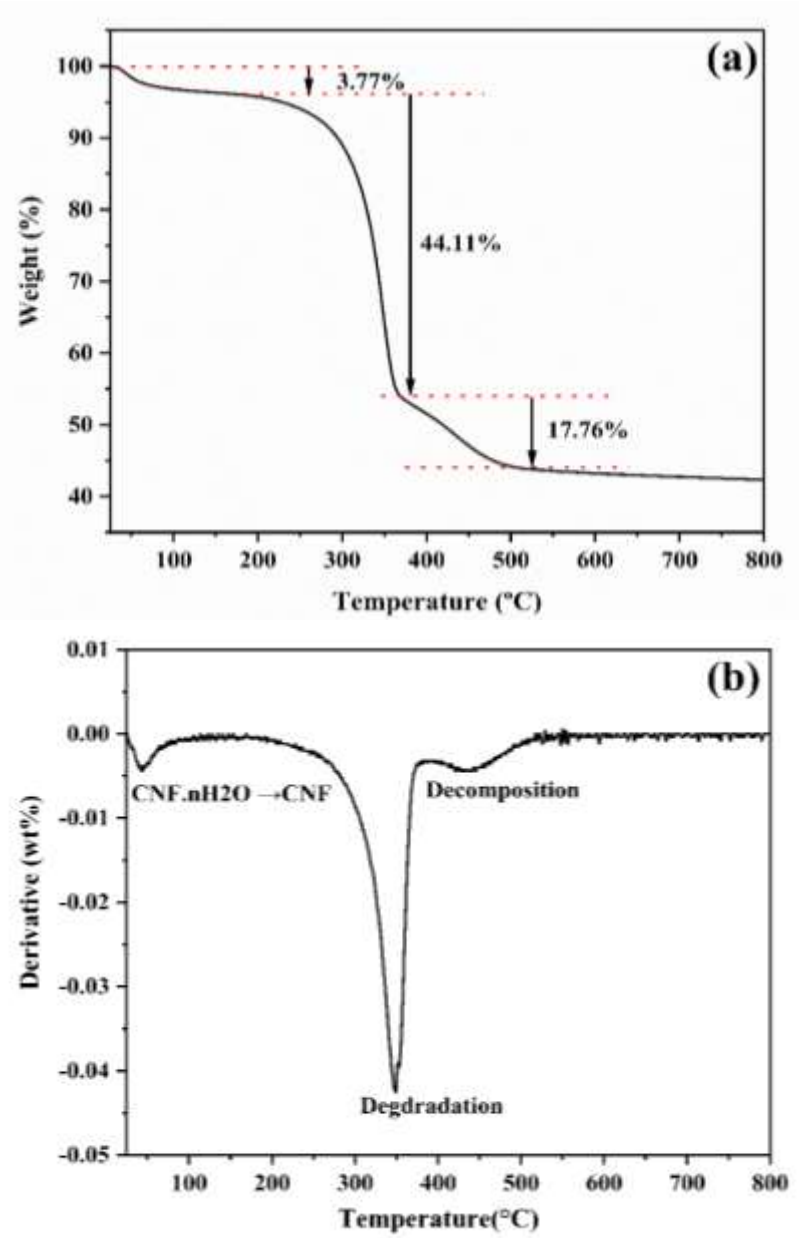

Figure 37. (a) The TGA curve of the ZnO-CNF nanocompositerevealing its thermal stability and weight loss characteristics under increasing temperature. (b) Highlights the DTG curve of the ZnO-CNF nanocomposite offering information about the rate of weight change with temperature for this composite material.

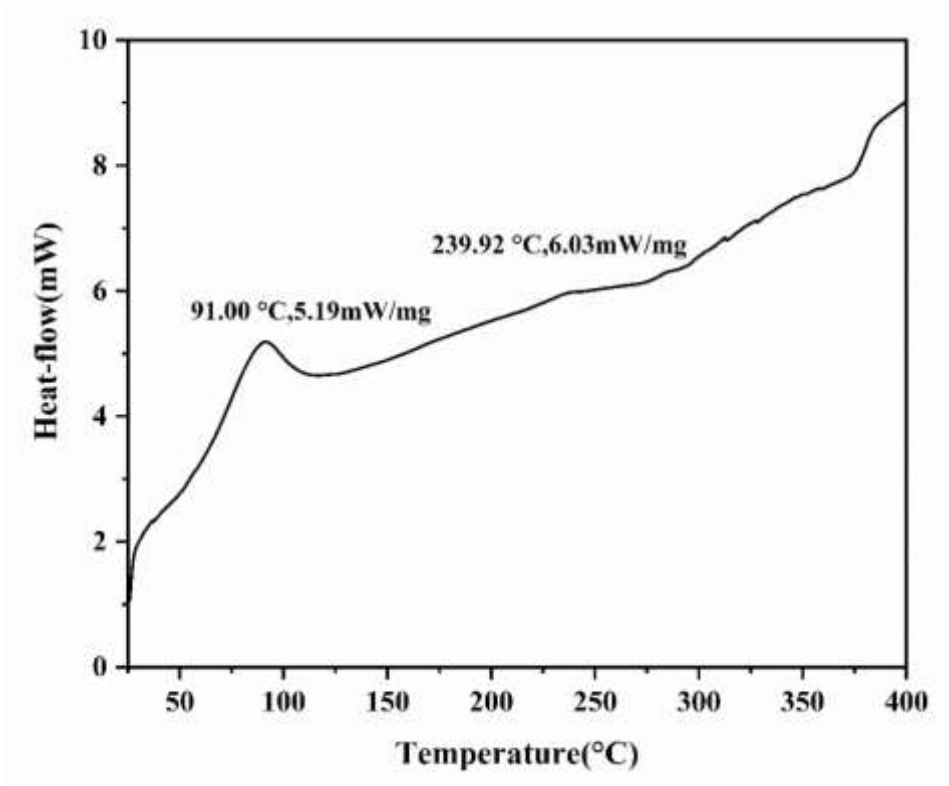

Figure 38. The DSC curve of the ZnO-CNF nanocomposite, offering insights into its thermal characteristics, including any phase changes and heat absorption or release with changing temperature.

ii. *Second Endothermic Peak:*

This peak appears at 240°C, which is slightly lower than the corresponding peak in pure CNF (227°C). However, the heat flow associated with this peak is also lower in the nanocomposite. This suggests that the presence of ZnO-NPs may have slowed down the decomposition process, possibly due to the formation of a protective layer around the cellulose fibers.

Overall, the DSC analysis indicates that the incorporation of ZnO-NPs into the nanocellulose matrix has a significant impact on the thermal behavior of the resulting nanocomposite. The increased melting point and reduced heat flow during decomposition suggest that the nanocomposite exhibits improved thermal stability compared to pure nanocellulose. This enhanced thermal stability can be attributed to the strong interfacial interactions between the ZnO-NPs and the cellulose nanofibrils, which can hinder the degradation process.

3.6. Photocatalytic Activity of ZnO-NPs, CNF, and ZnO-CNF Nanocomposite

The photocatalytic activity of ZnO-NPs, CNF, and ZnO-CNF nanocomposite was evaluated by monitoring the degradation of methylene blue (MB) dye under natural sunlight. The degradation efficiency of the different materials was assessed by measuring the decrease in the absorbance of the MB solution at a specific wavelength over time. Kinetic studies were performed to understand the mechanism of the photocatalytic degradation process. The experimental data were fitted to various kinetic models, including pseudo-first-order and pseudo-second-order kinetics. The rate constants and correlation coefficients were calculated to determine the nonlinear-fitting model. Adsorption isotherms were studied to investigate the adsorption behavior of MB dye onto the surface of the catalysts. Langmuir, Freundlich, and Temkin isotherm models were employed to analyze the adsorption data. The isotherm parameters, such as adsorption capacity and adsorption intensity, were calculated to gain insights into the adsorption mechanism.

3.6.1. Photocatalytic Degradation of Methylene Blue (MB)

The photocatalytic degradation of methylene blue (MB) was investigated using ZnO-NPs, CNF, and ZnO-CNF nanocomposite under natural sunlight irradiation. The

initial concentration of MB was varied from 1 mg $L^{-1}$to 10 mg L^{-1}, and the degradation was monitored over a period of 150 min.

Figure 39 shows the color change of MB solutions with different initial concentrations in the presence of various catalysts after 150 min of sunlight irradiation.

i. *Control Experiment (b):* In the absence of any catalyst, the color of the MB solution remained almost unchanged, indicating negligible photodegradation.
ii. *CNF (c):* The CNF alone exhibited limited photocatalytic activity, as evidenced by the slight color change of the MB solution, especially at higher initial concentrations.
iii. *ZnO-NPs (d):* The ZnO-NPs showed moderate photocatalytic activity, resulting in a significant reduction in the intensity of the blue color of the MB solution, particularly at lower initial concentrations.
iv. *ZnO-CNF Nanocomposite* (e): The ZnO-CNF nanocomposite demonstrated the highest photocatalytic activity, leading to almost complete decolorization of the MB solution, even at higher initial concentrations, within 150 min of sunlight irradiation.

The enhanced photocatalytic activity of the ZnO-CNF nanocomposite can be attributed to a synergistic effect between the ZnO-NPs and nanocellulose. The high surface area of nanocellulose provides more active sites for adsorption and degradation of MB molecules. The interface between ZnO and nanocellulose facilitates efficient charge separation, reducing recombination and enhancing photocatalytic activity. Additionally, the presence of ZnO-NPs improves light absorption, leading to increased generation of photoexcited charge carriers. These combined factors contribute to the superior performance of the ZnO-CNF nanocomposite compared to individual components. The photocatalytic degradation process of MB using ZnO-CNF nanocomposite under sunlight irradiance is graphically represented in Figure 40.

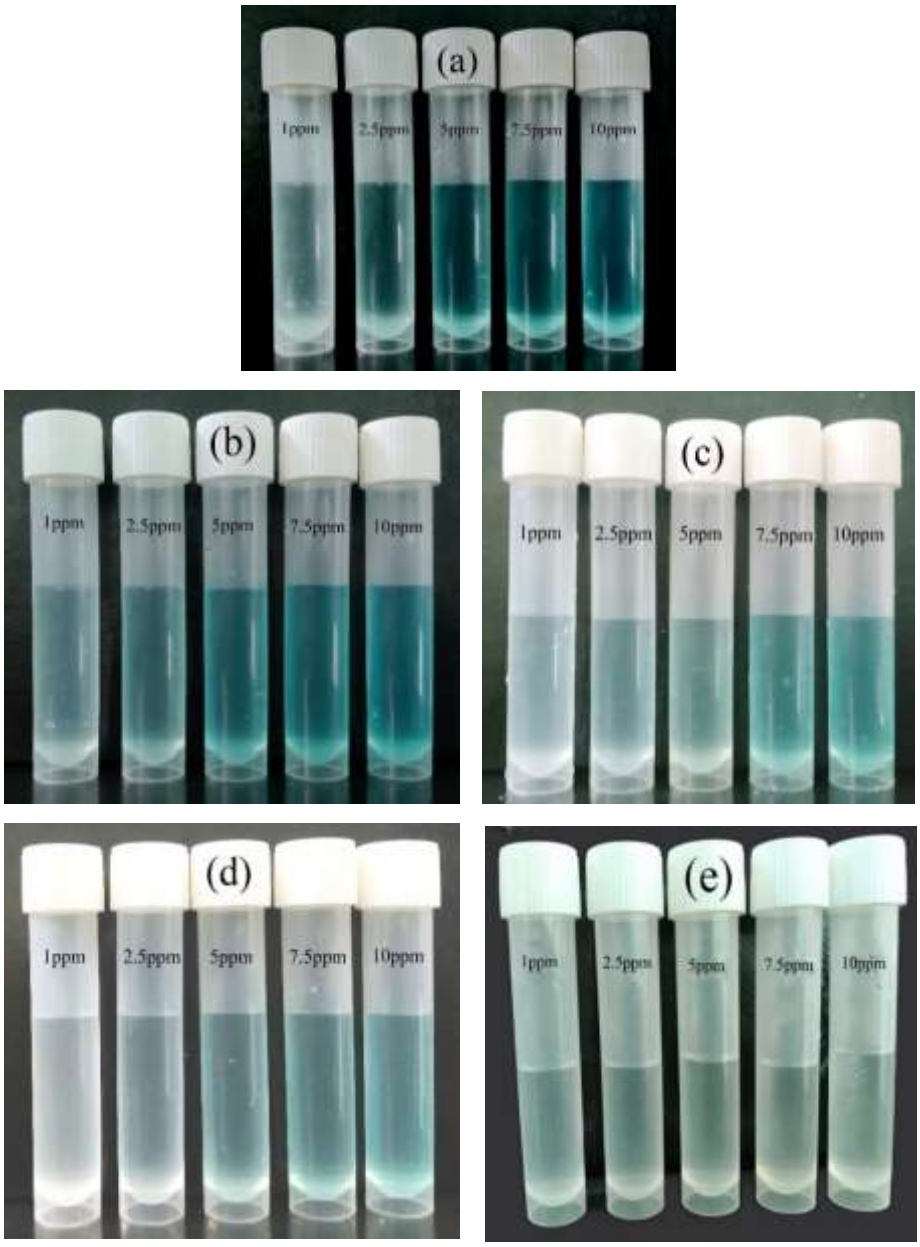

Figure 39. (a) Different concentration of MB before sunlight irradiance (b-d) Changes in colour of different concentration of methylene blue in absence and presence of differentcatalyst after 150 min of sunlight irrandiance (b) control without catalyst,(c)in presence of CNF,(d)in presence of ZnO-NPs and (e) in presence of ZnO-CNF nanocomposite.

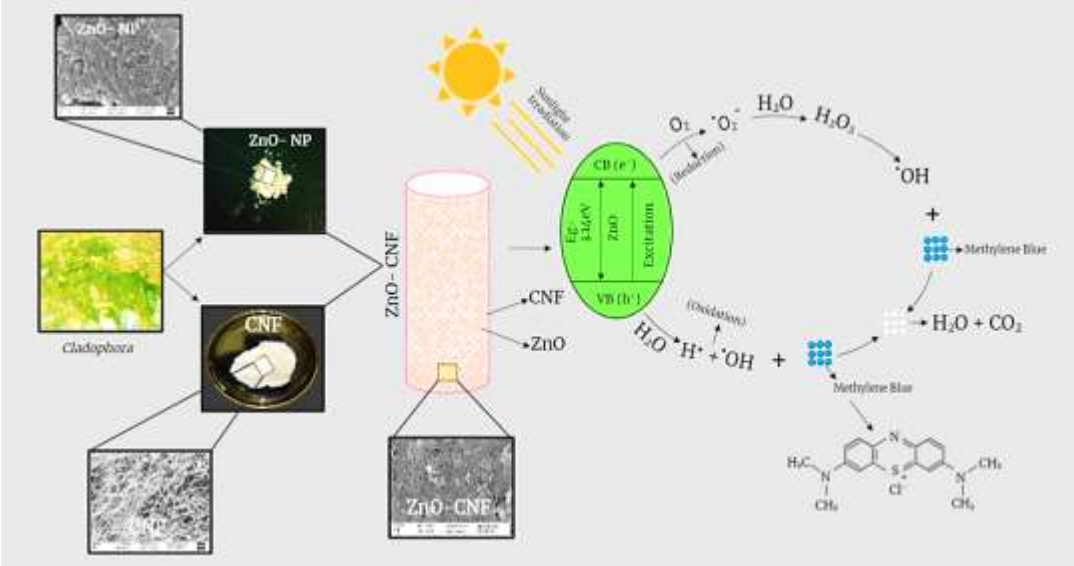

Figure 40. Graphical representation of photocatalytic degradation of MB under sunlight irradiance in presence of ZnO-CNF nanocomposite.

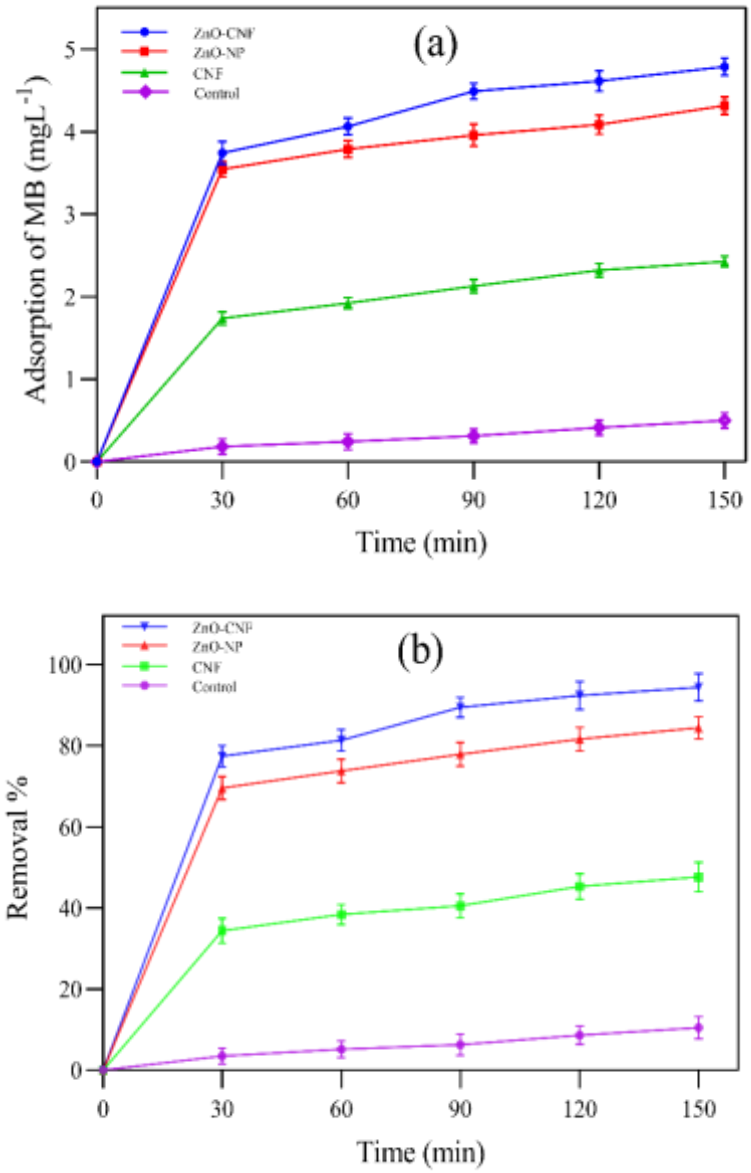

Figure 41. Adsorption and removal of methylene blue (MB) catalyzed by ZnO-CNF nanocomposite under sunlight irradiance. (a) and (b) Demonstrate the time-dependent adsorption and removal (%) of MB respectively, from aqueous solutions under sunlight irradiance. The initial concentration of MB in the solutions was maintained at 5 mg L^{-1}

3.6.2. Adsorption and Photocatalytic Activity of ZnO-CNF Nanocomposite: Time-Course Study

Figure 41(a) and 41(b) illustrate the time-dependent adsorption and photocatalytic removal of methylene blue (MB) from aqueous solutions under sunlight irradiation using ZnO-CNF nanocomposite, ZnO-NPs, CNF, and a control experiment. The initial concentration of MB was maintained at 5 mg L^{-1}.

The ZnO-CNF nanocomposite exhibited the highest adsorption capacity, reaching equilibrium within 60 min. Approximately 85% of MB was adsorbed within the first 30 min. ZnO-NPs showed moderate adsorption capacity, reaching equilibrium within 90 min. Approximately 60% of MB was adsorbed within the first 30 min. CNF exhibited the lowest adsorption capacity, with only about 20% of MB adsorbed within 150 min. In the absence of any catalyst, the adsorption of MB was negligible.

Above results showed that ZnO-CNF nanocomposite demonstrated significantly enhanced adsorption and photocatalytic activity compared to individual components (ZnO-NPs and CNF) and the control experiment.

3.6.3. Kinetics Studies

To gain insights into the mechanism of MB adsorption onto the different adsorbents, kinetic studies were performed. The time-course data were fitted to pseudo-first-order and pseudo-second-order kinetic models.

Figure 42 shows the adsorption kinetics of MB onto control (without catalyst), CNF, ZnO-NPs, and ZnO-CNF nanocomposite. The pseudo-second-order kinetic model provided a better fit to the experimental data for all adsorbents, indicating that chemisorption is the rate-limiting step in the adsorption process.

Table 17 summarizes the kinetic parameters obtained from the pseudo-first-order and pseudo-second-order models. The ZnO-CNF nanocomposite exhibited the highest adsorption capacity and the fastest adsorption rate, followed by ZnO-NPs, CNF, and the control.

Table 17: The kinetic constant of pseudo-first-order and pseudo-second-order rate of adsorption of MB under sunlight irradiance.

Kinetic models	Parameters	Control	CNF	ZnO-NPs	ZnO-CNF
Pseudo-first-order	q_e (mg g^{-1})	0.6344	2.1601	3.9719	4.5090
	k_1 (min^{-1})	0.0087	0.0505	0.0655	0.0613
	r^2	0.9518	0.7430	0.7393	0.7027
Pseudo-second-order	q_e (mg g^{-1})	0.9763	2.3938	4.2507	4.8641
	k_2 (g mg^{-1} min^{-1})	0.0062	0.0345	0.0325	0.0248
	r^2	0.9539	0.9091	0.9332	0.9086

.

The enhanced adsorption capacity and rate of the ZnO-CNF nanocomposite can be attributed to several factors. The combination of ZnO-NPs and nanocellulose in the nanocomposite can lead to a synergistic effect, where the individual components complement each other's properties. Further, the presence of functional groups on the surface of the nanocellulose, such as hydroxyl and carboxyl groups, can form strong interactions with MB molecules, leading to enhanced adsorption.

3.6.4. Adsorption and Removal of Methylene Blue: Equilibrium Study

Figure 43 presents the adsorption and removal of methylene blue (MB) at varying initial concentrations of methylene blue under direct sunlight irradiation using different materials: ZnO-CNF nanocomposite, ZnO-NPs, CNF, and a control.

The ZnO-CNF nanocomposite shows the highest adsorption capacity, increasing linearly with the initial concentration of MB (Figure 43a). This indicates

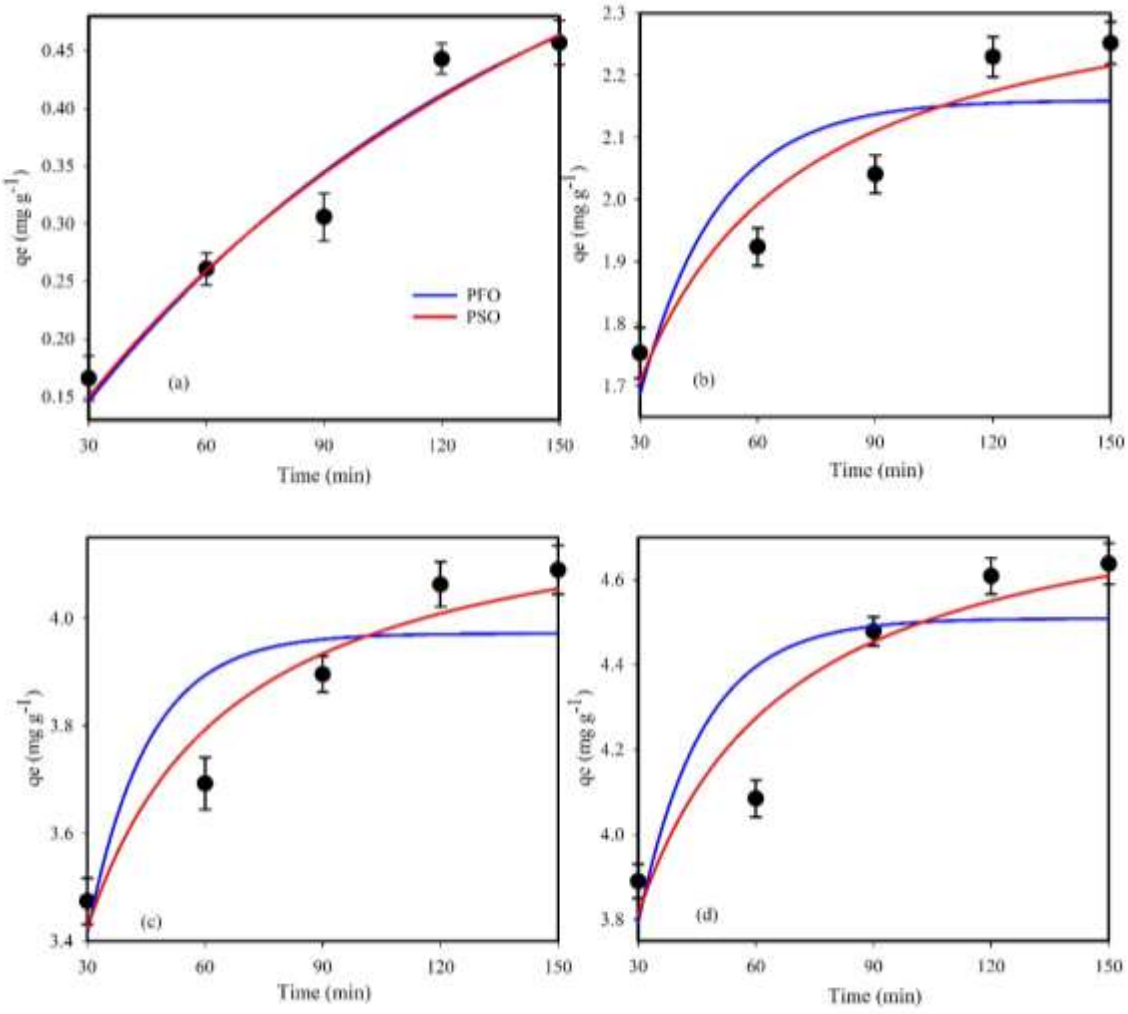

Figure 42. Pseudo-first-order and pseudo-second-order kinetics for the adsorption of MB on (a) Control; (b) CNF; (c) ZnO-NPs and (d) ZnO-CNF nanocomposite. The initial concentration of MB was 5 mgL^{-1}.Vertical bars indicate the standard deviation (±SD).

that the nanocomposite has a high affinity for MB molecules and can effectively adsorb them from solution. ZnO-NPs exhibit moderate adsorption capacity, lower than that of the ZnO-CNF nanocomposite (Figure 43a). CNF shows the lowest adsorption capacity among the tested materials.

The Figure 43b represents the removal of methylene blue at varying concentrations. The ZnO-CNF nanocomposite demonstrates the highest removal efficiency, achieving nearly 100% removal of MB at all initial concentrations. This superior performance is attributed to the synergistic effect between ZnO-NPs and nanocellulose, which enhances light absorption, charge separation, and the generation of reactive oxygen species. ZnO-NPs show moderate removal efficiency, with the percentage removal decreasing as the initial concentration of MB increases. CNF exhibits the lowest (about 50%) removal efficiency, with minimal removal of MB observed at all initial concentrations. The control experiment (absence of any catalyst) shows negligible removal of MB.

These results highlight the potential of ZnO-CNF nanocomposite as a promising material for the removal of organic pollutants from water.

3.6.5. Isotherm Study

Figure 44 presents the adsorption isotherms for MB onto CNF, ZnO-NPs, and ZnO-CNF nanocomposite. The experimental data were fitted to non-linear forms of Langmuir, Freundlich, and Temkin isotherm models.

The Langmuir isotherm assumes monolayer adsorption onto a homogeneous surface with a finite number of identical adsorption sites. The Freundlich isotherm is an empirical model that describes multilayer adsorption on heterogeneous surfaces. The Temkin isotherm assumes that the heat of adsorption decreases linearly with surface coverage.

Table 18 summarizes the parameters obtained from the different isotherm models. The ZnO-CNF nanocomposite consistently exhibited the highest adsorption capacity and the best fit to the Langmuir isotherm model. This indicates that the

adsorption of MB onto the ZnO-CNFnanocomposite is predominantly monolayer adsorption onto a homogeneous surface.

Table 18: Derived parameters for the biosorption of MB onto CNF, ZnO-NPs and ZnO-CNF nanocomposite.

Isotherm models	Model Parameters	CNF	ZnO-NPs	ZnO-CNF nanocomposite
Langmuir	q_{max}	9.18±0.55	21.38±1.28	43.11±2.58
	k_L	0.26±0.02	0.20±0.01	1.44±0.09
	r^2	0.9480	0.9964	0.9287
Freundlich	k_F	2.21±0.13	7.11±0.43	11.75±0.71
	1/n	0.52±0.03	0.76±0.05	0.54±0.03
	r^2	0.9932	0.9998	0.9364
Temkin	B_T	1.39±0.08	4.30±0.26	4.18±0.25
	A_T	7.18±0.43	7.69±0.46	19.84±1.19
	r^2	0.9005	0.8925	0.9194

Note: V*alues were determined using non-linear curve fitting techniques in accordance with the Langmuir, Freundlich, and Temkin isotherm.* q_{max} *(mg* g^{-1}*);* k_L *(L* mg^{-1}*);* B_T *(J* mol_{-1}*);* A_T *(L* mol^{-1}*).*

The ZnO-CNF nanocomposite exhibited the highest maximum adsorption capacity (q_{max}) of 43.11 mgg^{-1}, followed by ZnO-NPs (21.38 mgg^{-1}) and CNF (9.18 mgg^{-1}). The higher adsorption capacity of the ZnO-CNF nanocomposite can be attributed to its larger surface area, the synergistic effect between ZnO-NPs and nanocellulose, and the presence of various functional groups that can interact with MB molecules.

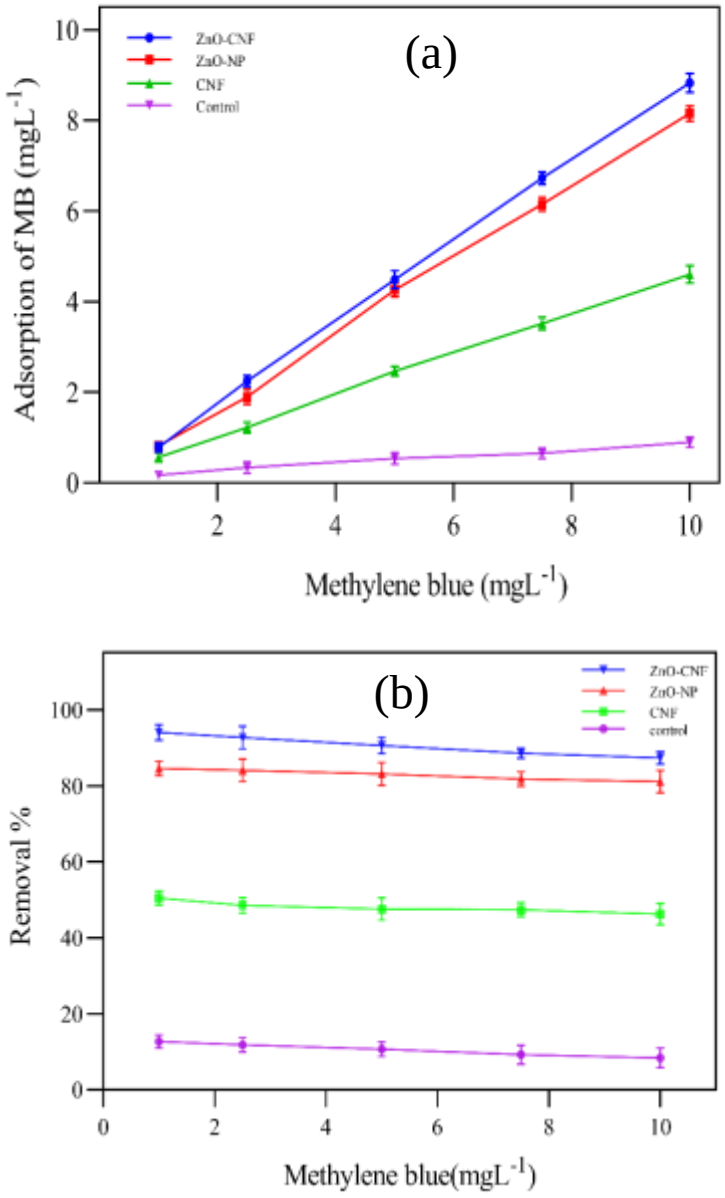

Figure 43. (a) and (b) represent adsorption and removal (%) of MB respectively, at varying initial concentrations of MB under direct sunlight irradiance for a duration of 150 min. The data points are calculated as the means of three replicates, and the vertical bars accompanying them indicate the standard deviations (±SD).

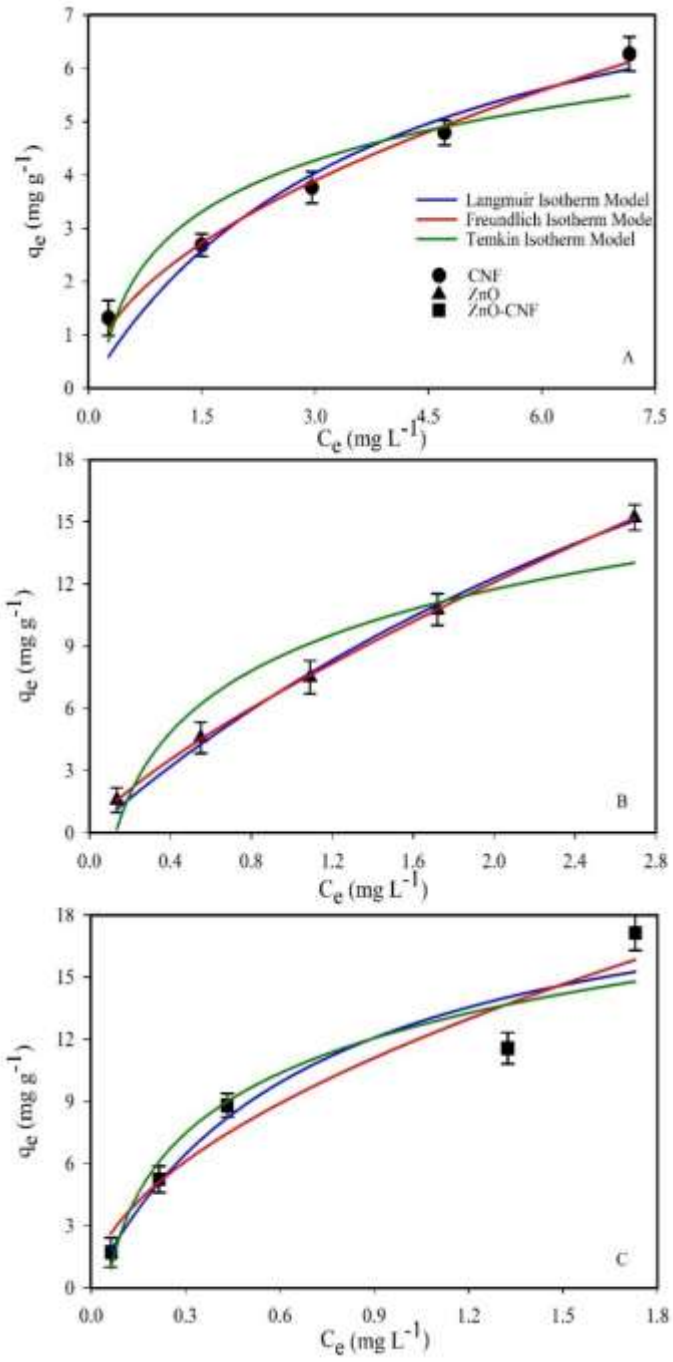

Figure 44. Equilibrium isotherms for the biosorption of MB by the catalyst (A) CNF, (B) ZnO-NPs and (C) ZnO-CNF nanocomposite. The curves represent the fitting of the Langmuir, Freundlich, and Temkin isotherm models to the experimental data points.

The Freundlich isotherm model provided the best fit for the experimental data, indicating multilayer adsorption on heterogeneous surfaces. The higher values of k_F and 1/n for the ZnO-CNF nanocomposite suggest a stronger affinity and higher adsorption capacity compared to CNF and ZnO-NPs.

The Temkin isotherm model suggests that the heat of adsorption decreases linearly with surface coverage. The higher values of B_T and A_T for the ZnO-CNF nanocomposite indicate a stronger interaction between MB molecules and the adsorbent surface.

CHAPTER - 4

DISCUSSION

*Cladophora glomerata*is a ubiquitous freshwater alga and can be found in various freshwater ecosystems around the world. As a primary producer, *C. glomerata* plays a crucial role in aquatic ecosystems by converting sunlight into energy through photosynthesis, thereby supporting the food web. Its dense mats provide habitat and shelter for various microorganisms, invertebrates, and small fish (Higgins et al., 2008). Additionally, *C. glomerata* contributes to nutrient cycling by assimilating and releasing nutrients. However, under nutrient rich conditions, such as excessive nutrient loading from agricultural runoff or wastewater discharge, *C. glomerata* can experience rapid growth, leading to harmful algal blooms. These blooms can have negative effects on water quality and aquatic life (Wu et al., 2024). Therefore, managing nutrient input and maintaining balanced ecosystems is crucial for controlling *C. glomerata* growth and preventing such blooms.*C. glomerata* is often used as a bioindicator of water quality. Research is ongoing to explore its potential applications in bioremediation and biofuel production (Çelekli and Alkan, 2024).

*C. vulgaris*is rich in proteins, containing all essential amino acids, making it a complete protein source containing all essential amino acids, vitamins (such as B-complex vitamins, vitamin C, and vitamin E) and minerals (including iron, magnesium, and zinc). As a primary producer, *C. vulgaris*plays a vital role in aquatic ecosystems by converting sunlight into energy and producing oxygen (Ru et al., 2020). It helps in nutrient cycling by assimilating inorganic nutrients and releasing organic matter upon decomposition. *C. vulgaris* is widely used as a dietary supplement due to its high nutritional value. It is available in various forms such as tablets, powders, and extracts (Bito et al., 2020).

C. vulgaris is used in bioremediation to remove contaminants, heavy metals, and excess nutrients from wastewater. Research is ongoing into using *C. vulgaris* for biofuel production, particularly biodiesel, due to its high lipid content. It is also used as a feed supplement in aquaculture and livestock due to its nutritional benefits. The chlorophyll in *C. vulgaris* is believed to help detoxify the body by binding to heavy

metals and other toxins (Al-Hammadi and Güngörmüşler, 2024). It has antioxidant properties that can help protect cells from damage caused by free radicals. Studies are being conducted toexplore the potential of *C. vulgaris* in pharmaceuticals for its anti-inflammatory, antimicrobial, and anticancer properties (Zhou et al., 2022). Due to its ability to grow in extreme conditions and provide essential nutrients and oxygen, *C. vulgaris* is being studied for use in life support systems for long-term space missions (Micco et al., 2023).

Organic dye pollution is a serious environmental problem brought on by industrial emissions, especially from the paper, leather, textile, and cosmetics industries. Due to their complex molecular structure, synthetic dyes are resistant to natural degradation processes.When discharged into water bodies, these synthetic dyes can obstruct sunlight, disrupting photosynthesis and aquatic ecosystems (Tkaczyk et al., 2020). Additionally, many dyes are harmful to human health, causing respiratory problems, skin irritation, and even cancer or mutagenesis (Al-Tohamy et al., 2022; Ismail et al., 2019). Due to their complex and persistent nature, dye molecules necessitate advanced remediation techniques, such as chemical, biological, or photocatalytic methods, to mitigate their environmental impact (Khan et al., 2024).

In our current study photocatalysis was employed for the remediation of organic dye (methylene blue) from aqueous solution. Photocatalysis has been demonstrated as a promising method for reducing organic dye pollution by using photocatalysts like zinc oxide, ZnO-CNF nanocomposite to degrade dye molecules under light irradiation (Lanjwani et al., 2024). ZnO-CNF catalysts generate reactive species, breaking down dye molecules into non-toxic components (Khan et al., 2020). Recent advancements in nanotechnology have improved photocatalyst efficiency, making it eco-friendly and cost-effective for large-scale wastewater treatment (Kuspanov et al., 2023). The estimated cost analysis for the synthesis and applications of ZnO-CNF nanocomposite using *Cladophora* biomass is listed in Table 19. Different studies were successfully done on organic dyes remediation employing photocatalysis (Chen et al., 2017; Golmohammadi et al., 2020; Luque-Morales et al., 2021; Mohammad et al., 2016; Porrawatkul et al., 2024; Ullah and

Dutta, 2008; Xu et al., 2010). There are different challenges in photocatalysis. These include low efficiency under visible light because of high band gaps in conventional photocatalysts like ZnO-NPs, rapid charge carrier recombination, high costs and stability issues for industrial use, secondary pollution from wrong photocatalyst handling, and complex wastewater matrices with competing substances that can reduce photocatalytic activity (Dong et al., 2015; Li et al., 2022; Romero et al., 1999).

Photocatalytic degradation using zinc oxide (ZnO) under sunlight is a sustainable approach to address environmental pollution. ZnO, when exposed to sunlight, generates electron-hole pairs that can initiate redox reactions, leading to the degradation of organic pollutants. This method offers a cost-effective and environmentally friendly solution to water and air pollution. ZnO-NPs possess a high surface area, offering a multitude of active sites that effectively adsorb dye (MB) molecules (Mandal et al., 2022; Wang et al., 2016). When the radiation of visible light hits on ZnO-NPs surface having equal to or higher than bandgap energy of the catalyst i.e., ZnO-NPs, initially electrons (e^-) at valence band gains energy and transfer to conduction band by leaving holes (h^+) at valence band. The generated holes (h^+) react with H_2O to form hydroxyl radicals ($^{\cdot}OH$). Similarly, photogenerated e^- migrates to surface of the catalyst, which act as an e^- acceptor. As a result, superoxide anion radicals ($^{\cdot}O_2$) are produced. Both hydroxyl and super anion radicals repeatedly attack the MB molecules and leads to the production of environment friendly carbon dioxide and water (Gowthambabu et al., 2021; Porrawatkul et al., 2024).

Cellulose nanofibers (CNF), known for their high surface area, porosity, and chemical stability, exhibit excellent adsorption properties (Surendran and Sherje, 2022; Trache et al., 2020). The combination of ZnO-NPs and CNFs creates a synergistic effect, enhancing adsorption and degradation capabilities, which results in higher MB removal efficiency in this study.The observed time-dependent increase in MB removal for all catalysts (ZnO-NPs, CNF and ZnO-CNF) can be attributed to the continuous adsorption and potential degradation of MB molecules. Adsorption occurs through interactions between the active sites on the ZnO-NPs, CNF, or ZnO-

CNF nanocomposite surfaces and MB molecules, effectively reducing their concentration in the solution.

Table 19: Estimated cost analysis for the synthesis and application of ZnO-CNF nanocomposite from *Cladophora* biomass (Lab scale)

Process Stage	Inputs and Operations	Estimated Cost (INR)	Remarks
1. Biomass collection	Manual collection from river, transport to lab	₹100–150/kg	Field labour and handling costs only; low infrastructure required
2. Nanocellulose extraction (CNF)	Solvent wash, NaOH, H_2O_2, acid hydrolysis (H_2SO_4), centrifugation, drying	₹400–600/kg	Eco-friendly bleaching and minimal chemical load reduce cost
3. ZnO-NPs Synthesis (Green route)	$ZnCl_2 \cdot 2H_2O$, algal extract, ultrasonication, centrifugation, drying	₹200–300/g	Low-cost Zn salt, no toxic solvents, low-energy ultrasonication-based process
4. ZnO-CNF nanocomposite fabrication (In-situ)	Zn^{2+} with CNF, NaOH-induced growth, mixing and drying	₹300–400/g	Efficient one-pot integration reduces energy and material consumption
5. Photocatalytic testing (MB degradation)	Methylene blue solution, sunlight irradiation, UV-Vis analysis	₹50–100/test	Sunlight use keeps energy cost zero; analytical cost minimal
Total approximate lab-scale cost	For 1 g ZnO-CNF nanocomposite + 1 degradation cycle	₹800–1200	Reflects a low-cost, eco-friendly synthesis pipeline at laboratory scale

Note: The total cost includes materials, energy, and basic instrumentation usage, but excludes fixed capital equipment. Industrial upscaling can further lower costs via solvent recovery, continuous processing, and bulk sourcing.

Traditionally, nano-sized particles have been synthesized using physical, chemical, mechano-chemical, and thermo-physical methods (Król et al., 2017). However, in recent years, there has been growing interest in exploring biological routes for the synthesis of metal oxide and magnetic nanoparticles (MNPs) using plants and microbes (Bandeira et al., 2020; Mahana et al., 2020; Narayanan and Sakthivel, 2011; Shaba et al., 2021). Further, ultrasonic-assisted biological methods have been reported to produce NPs with high purity, narrow particle size distribution, uniform shape, controllable reaction conditions, potentially low operating costs, and rapid reaction rates compared to conventional heating- and microwave-mediated biological methods (Amreddy et al., 2018).

In this study, ZnO-NPs were synthesized using an ultrasonication-assisted process with the aqueous extract of freshwater green algae *C. glomerata* and *C. vulgaris* as the primary reducing and capping agents.Previous studies have demonstrated the capability of *C. glomerata* extract to synthesize various metallic nanoparticles, including silver (Ag), zinc oxide (ZnO), and gold (Au) nanoparticles (Minhas et al., 2018; Alluri et al., 2018). The precursor used in the present study for the synthesis was $ZnCl_2.2H_2O$. Initially, $ZnCl_2.2H_2O$ dissolves in the water to form zinc ions (Zn^{2+}) and chloride ions (Cl^-). Subsequent hydrolysis reaction leads to the formation of zinc hydroxide precursors, represented by chemical equations such as:

$$Zn^{2+} + 2OH^- \rightarrow Zn(OH)_2 \qquad (12)$$

The zinc hydroxide precursors functioned as nucleation sites for the formation of zinc oxide nuclei. The aqueous extract of algaplays a dual role, serving both as a reducing agent and a stabilizing agent (Abdulwahid et al., 2019; Alluri et al., 2018; Colin et al., 2018; Minhas et al., 2018). The extract contains a variety of strong reducing molecules, including phenolic compounds, polysaccharides, proteins, and enzymes, which are capable of donating electrons to metal ions (e.g. Zn^{2+}) (Colin et al., 2018). This electron transfer process facilitates the reduction of the Zn^{2+} to their elemental state, leading to the formation of nanoparticles. Concurrently, the biomolecules present in the algal extract adsorb onto the surface of the formed nanoparticles, forming a capping layer that prevents their agglomeration and growth. PVP is a polymer commonly used as a capping agent or stabilizer in nanoparticle

synthesis processes. PVP molecules adsorb onto the surface of the zinc oxide nuclei formed during the nucleation stage and prevents the agglomeration and coalescence of the nuclei, thereby stabilizing them and inhibiting further growth. Ultrasonication was employed in the synthesis process to enhance mixing and promote uniform dispersion of reactants.

This study employed well-defined chemical processes to efficiently convert algal biomass into nanocellulose (CNF and CNC) while prioritizing environmental sustainability.Toluene and ethanol were used to remove fats and pigments from the biomass in the initial stage of the process.NaOH was used for alkalization, with optimized conditions to minimize cellulose degradation, notably by using lower concentrations and volumes than some previous studies. Chlorine-free H_2O_2 served as an environmentally conscious bleaching agent, transforming the biomass into a distinct white substance. Acid hydrolysis, employing concentrated H_2SO_4, broke down cellulose into nanofibers, with optimized conditions for yield and product quality. Environmental considerations, like solvent usage and waste management, align with sustainability practices.

In present studyZnO-NPs were grown *in-situ* on the surface of CNF. Initially, Zn^{2+} ions are introduced into the CNF suspension, where they interact with the hydroxyl groups of cellulose (Aladpoosh and Montazer, 2015). The adsorption of Zn^{2+} ions onto the surface of cellulosic fibers for pre-nucleation is primarily driven by electrostatic attraction (Li et al., 2019).The negatively charged hydroxyl groups (-OH) present on the surface of cellulosic fibers interact with the positively charged Zn^{2+} ions, leading to their adsorption onto the fiber surface. Subsequent addition of NaOH solution initiates the hydrolysis of Zn^{2+} ions, forming zinc hydroxide ($Zn(OH)_2$) precursors on the CNF surface (Supramaniam et al., 2021). Under alkaline conditions, zinc hydroxide precursors act as nucleation sites for the growth of ZnO-NPs (Wahab et al., 2009). The hydroxyl groups present on the cellulose surface facilitate the coordination and bonding with Zn^{2+} ions during the growth process, ensuring the attachment and uniform distribution of ZnO-NPs on the CNF surface.

The in-situ synthesis of ZnO-CNF nanocomposite eliminated the need for physically mixing pre-synthesized ZnO-NPs and CNFs.Firstly, the *in-situ* method ensures intimate contact and strong interaction between ZnO-NPs and CNF, leading to improved interfacial bonding and enhanced mechanical properties of the composite material. Secondly, the *in-situ* growth of ZnO-NPs on CNF surface allows for better dispersion and uniform distribution of nanoparticles within the CNF matrix, minimizing agglomeration and ensuring homogeneous properties throughout the composite material. Moreover, the one-pot synthesis approach of the *in-situ* method simplifies the fabrication process and reduces the number of processing steps, leading to potential cost savings and scalability for industrial production.

UV-VIS Spectroscopy is one of the widely applied primary techniques that reflect the wavelength and particularly in the calculation of band gap energy (Hamouda et al., 2019). Nanoparticles exhibit a characteristic absorption peak in the UV region due to electronic transitions from the valence band to the conduction band.The valence band consists of electrons tightly bound to atoms, while the conduction band comprises free electrons capable of conducting electricity. When a material absorbs energy, electrons can be excited from the valence band to the conduction band, leaving behind holes in the valence band.ZnO-NPs works as semiconductor and the absorption process involves direct transitions between the valence and conduction band. The ZnO-NPs synthesized in this study exhibited a band gap energy of approximately 3.2 eV, which is typical for bulk ZnO.Apart from the bandgap energy, ZnO-NPs frequently exhibit excitonic peaks in the ultraviolet spectrum. These peaks, arising from bound electron-hole pairs (excitons), provide insights into the exciton binding energy of the material.

ZnO-NPs is utilized in applications like transparent conductive coatings since it is often transparent in the visible spectrum (400–700 nm).Khalafi et al., 2019 reported 300-500 nm range of UV-spectra for ZnO-NPs synthesized using aqueous extract of *Chlorella* sp. Zinc oxide (ZnO) is a beneficial element for use in a variety of optoelectronic devices, including light-emitting diodes (LEDs), UV sensors, and photodetectors.The UV absorption of ZnO-NPs is important for photocatalysis as

well. Gaining insight into its UV-Vis spectrum allows for performance optimization in areas like environmental remediation.

Using Fourier-transform infrared (FTIR) spectroscopy, Zinc oxide nanoparticles (ZnO-NPs) can be effectively characterized for their functional groups and chemical bonds.This technique detects the amount of infrared radiation a sample absorbs, which results in molecular vibrations. The resulting spectrum offers details on the bonding environment and functional groups present in the sample.When compared to bulk zinc oxide, ZnO-NPs exhibit distinct physical and chemical characteristics, such as a high surface area to volume ratio and modified electrical properties.The Zn-O stretching vibration is generally the most prominent characteristic in the FTIR spectrum of ZnO-NPs (Khalil et al., 2014). Depending on the size of nanoparticles and surface modifications, the precise location of peaks may change.ZnO-NPs frequently exhibit absorption peaks at 3200–3600 cm^{-1}, which are related to surface hydroxyl groups (-OH) (Balogun et al., 2020). These peaks are the result of either hydroxyl groups generated during synthesis or water molecules adsorbed on the nanoparticle surface.A large peak at 3200–3600 cm^{-1} is frequently used to indicate the presence of adsorbed water or hydroxyl groups. It is possible that this peak and the O-H stretching vibrations overlap.The existence of these functional groups can be detected by FTIR if ZnO-NPs are synthesized or modified using organic compounds. For example, the spectrum will show the characteristic peaks (C-H stretching, C=O stretching) of surfactants and stabilizers if they are used in the synthesis (Mahamuni et al., 2019).Since surface interactions frequently control catalytic activity, it is crucial to comprehend the surface chemistry of ZnO-NPs using FTIR for catalytic applications (Hamouda et al., 2019; Zamiri et al., 2014).

β-D- glucose units are joined by β-1,4-glycosidic bonds to form a linear chain with hydroxyl groups that makes up cellulose (Trilokesh and Uppuluri, 2019). The cellulose structure is preserved in nanocellulose, although at a smaller size. The O-H stretching provides insight into the hydrogen bonding and moisture content, while the C-O-C stretching bands reflect the cellulose network (France et al., 2021). Shifts in the intensity or location of specific peaks may be a sign of modifications in the degree of crystallinity of nanocellulose. For example, the crystallinity index of

cellulose can be estimated by dividing the intensity of the peak at approximately 1420 cm^{-1} by the peak at approximately 1160 cm^{-1} (Randhawa et al., 2022;Thomas et al., 2020).

A strong peak between 400- 600 cm^{-1} range corresponding to the Zn-O stretching vibration. In the present study, the position as well as intensity of the distinctive peaks of both ZnO-NPs and CNF may be seen to have shifted or changed in the ZnO-CNF nanocomposite. Physical or hydrogen bonding interactions between ZnO and CNF may be the primary cause of these alterations (Ali et al., 2016; Saleh et al., 2024).

To study the crystalline parameters of nanoparticles, XRD technique was used in the present study. Results showed that synthesized ZnO-NP are hexagonal Wurtzite crystals. Similar to present study,several previous studies also reported the hexagonal structure of ZnO-NPs (Grace et al., 2023; Mahana et al., 2020).Islam et al., 2021 reported a Wurtzite structure with 25 nm mean size of chemically synthesized ZnO-NPs. Khalafi et al. (2019) and Khan et al. (2022) synthesized ZnO-NPs with hexagonal (Wurtzite) structure using aqueous extract of *Chlorella* sp.

The SEM analysis was used to study the shape and size of nanostructure. SEM image of ZnO-NPs shows an irregular shape in both samples having size 32nm and 82nm. As evident from SEM image, the surface of the ZnO-NPs was rough and agglomerated. It may due to the synthesis process. The size and shape variation of nanoparticles plays an important role on their different application like antibacterial activity. Some other algae used to ZnO-NPs synthesis are *Sargassum muticum* with 3nm to 57nm and hexagonal shape (Azizi et al., 2014), *Chlorella* sp. with 20nm to 50nm (Shokoofeh et al., 2019), *Agathosma betulina* with 15.8nm (Thema et al., 2015), *Ulva fasciata* with 77.81 nm and spherical shape (Alsaggaf et al., 2021).

Based on SEM imaging, our results showed that nanocellulose extracted from two different green algae showed different morphological structures. The nanocellulose extracted from *C. glomerata* exhibits long, smooth, fibrous structure forming a web. The fibers have 22 nm in diameter which is supported by the

previous study ofSalem and Ismail (2022) where theyreported the size range of nanofiber extracted from sea weed as 14.94-30.82 nm. The high aspect ration of nanofibers raises the possibility of benefits in areas like biomedical applications where structural flexibility and strength are essential, or reinforcement in composite materials. The nanofibers' high aspect ratio enhances the possibility of benefits in areas like biomedical applications where structural flexibility and strength are essential, or reinforcement in composite materials. In contrast, the nanocellulose extracted from *C. vulgaris* was crystalline, powdery with crystal size about 74.92 nm. Roman et al. (2010) observed rod shaped cellulose nanocrystal having size range from 50-200nm with average size between 100-150nm in length. The uniformity of the size and shape indicates purity of synthesis process which is an advantage for the practical application of cellulose nanocrystal.

The SEM image of ZnO-CNF nanocomposite obtained in the present study shows important aspects like interaction, distribution and overall structure. From the SEM image it was clear that the ZnO-NPs are nicely coated over the cellulose nanofiber and exhibits a rough surface. Our results showed that diameter of the nanofiber after coated with ZnO-NPs was 42±2 nm. This finding is supported by the previous study by Ali et al. (2016). The uniform distribution of ZnO-NPs over the nanofiber indicates the successful integration of the two components in the nanocomposite.The effective fusion of ZnO-NPs with CNFs has major implications for a number of activities. The uniform distribution and large surface area ofZnO particles can improve the catalytic, photocatalytic, or sensing properties ofnanocomposite. In applications such as energy storage, composites, and electronic devices, overall performance ofthe material can be enhanced by the mechanical reinforcement and conductivity offered by the CNFs (Wasim et al., 2021).The combination ofZnO-NPs and CNFs improve functionality and performance by utilizing the advantages of both materials (Farooq et al., 2020).

EDX analysis is consistent with the SEM analysis which revealed the percentage of elements present in the compound. The presence and relative quantity of different elements in the ZnO-NPs, nanocellulose and ZnO-CNF nanocomposite are shown by the EDX spectra. We found that the main component Zn and O in

ZnO-NPs, C and O in nanocellulose present in high percentage. In composite material both Zn, O and C are present which confirms the formation of composite material. Small amount of other elements were present in the sample possibly due to the synthesis processes. Presence of gold (Au) in the EDX data can be attributed to the sputter coating of material during the imaging process.

XPS is one of the powerful techniques for the analysis of surface chemistry of material.It interprets the binding energy of peaks in the XPS spectrum and determine the chemical state and elemental composition present in the material. Zinc (Zn) and oxygen (O) are the main components of ZnO-NPs. Due to spin-orbit splitting, the Zn 2p region usually exhibits two primary peaks, Zn 2p3/2 and Zn 2p1/2. ZnO, with the Zn 2p3/2 peak typically occurring at 1021.5 eV and the Zn 2p1/2 peak at 1044.8 eV on average (Al-Gaashani et al., 2013). These positions suggest that Zn is present in +2 oxidation state in ZnO. Information regarding the oxygen atmosphere within the nanoparticles is indicated by the O 1s region. Indicative of O_2^- ions in the ZnO lattice is indicated by a peak at 530.1 eV (Morozov et al., 2015; Zhou et al., 2018).The presence of carbon in algal-extract-synthesized ZnO-NPs introduces intriguing complexities. The C1s peak can be attributed to C-O and C=O bonds.Algal extractsare abundant in diverse biomolecules including proteins, lipids, carbohydrates, and other organic compounds (Ak et al., 2022; Geada et al., 2021).The additional peaks or shoulders suggest the existence of adsorbed water or hydroxyl groups (-OH) on the surface, which typically appear around 531.5 eV. During the synthesis process, biomolecules adsorb onto ZnO nanoparticle surfaces, potentially leading to the incorporation of carbon-based functional groups from these biomolecules (Latour, 2020).This complex interplay between organic components from the algal extract, surface passivation effects, potential contaminants, and the usage of carbon-based ligands or capping agents like PVP contributes to the observed carbon signal in X-ray photoelectron spectroscopy (XPS) analysis conducted in the present study.

ZnO-NPs formation is confirmed and any variations from the ideal stoichiometric compound are identified by the binding energy positions and peak morphologies, which reveal details about the chemical states of Zn and O.

Carbonates, other adsorbed species, and surface hydroxylation are all detectable by XPS and are essential for biomedical applications, sensor technologies, and catalysis. The electrical structure of ZnO-NPs, including the existence of flaws or vacancies that impact the material's characteristics, can be understood by an analysis of peak forms and positions (Chang et al., 2019). Size effects, charge, or variations in the immediate chemical environment can all cause slight changes in binding energy as observed. These shifts are especially significant for nanoparticles because they can reveal modifications in the electrical structure or surface chemistry brought on by quantum confinement phenomena. More widely spaced peaks may indicate a variety of chemical states or the existence of artifacts.

The thermogravimetric analysis of nanocellulose revealed the different thermal state like stability and decompositions. The first weight loss was observed below 100°C and can be attributed to removal of surface-bound moisture and chemisorbed water, also supported by FTIR analysis (C.S. et al., 2016; Lakshmi et al., 2017; Ray et al., 2002). This initial weight loss is normal for materials containing adsorbed water and consistent with the behaviour of nanocellulose. A large amount of weight loss was observed between 180-376°C which represent the decomposition process.In this process, glycosidic bond of cellulose break down which leads to the formation of volatile and char residues (Mandal and Chakrabarty, 2011; Trilokesh and Uppuluri, 2019). The last stage weight loss indicates the degradation process of the sample. The percentage of char residues indicate the purity of the sample and provides the information on the residual carbon content and the extent of thermal degradation.From our results it is evedent that the incorporation of ZnO-NPs into CNF, yielding the ZnO-CNF nanocomposite, does not compromise the thermal stability characteristic of CNF. Both CNF and ZnO-CNF demonstrate nearly identical thermal stabilities across all three weight loss phases observed, highlighting the nanocomposite's ability to preserve CNF's inherent thermal properties(Chen et al., 2016).

DSC analysis was performed to clarify the thermal stability of nanocellulose and nanocomposite, which is important for enhancing its use in a variety of applications. It shows three different endothermic peaks. The initial endothermic

peak represents an energy-absorbing process, consistent with literature indicating the typical melting point of cellulose nanofibers (Mandal and Chakrabarty, 2011). The second endothermic peak signifies another distinct thermal event within the cellulose nanofiber. It could be linked to further crystalline transitions, recrystallization, or possibly the initiation of thermal degradation (Madivoli et al., 2019). The third endothermic peak signifies a higher-temperature thermal event in cellulose nanofibers. This peak might be attributed to advanced stages of thermal degradation or chemical reactions within the CNF structure. Further investigations are required to precisely determine the nature of this event, as it may be related to the decomposition of residual organic matter, impurities, functional groups, secondary phase transitions, or reactions introduced during CNF production (Saba et al., 2017)

The DSC analysis of ZnO-CNF nanocomposite shows two distinct peaks. In the ZnO-CNF nanocomposite, the initial endothermic peak at 91.00°C is observed. This temperature is significantly higher than the first peak observed in pure CNF (72°C). The higher temperature suggests that the presence of ZnO-NPs within the nanocomposite may have altered the crystalline structure or thermal behavior of the cellulose component, leading to an increased melting point (Gan et al., 2020).It is possible that the nanoparticles have influenced cellulose crystallinity or introduced new interactions, resulting in the elevated melting point observed in the nanocomposite. The second prominent peak observed at 240°C in the ZnO-CNF nanocomposite is notably lower in magnitude compared to the second peak in pure CNF (227°C). This peak likely corresponds to the decomposition of the cellulose matrix and any organic components present within the nanocomposite. The lower heat flow associated with this peak suggests that the presence of ZnO-NPs might have enhanced the thermal stability of the nanocomposite, slowing down the decomposition process. Thus, the second peak in the ZnO-CNF nanocomposite occurring at a slightly higher temperature than in pure CNF, with a lower heat flow, possibly indicating improved thermal stability due to the presence of ZnO-NPs(Roy et al., 2021; Supramaniam et al., 2021).In conclusion, the lower melting point of the first peak in the nanocomposite suggests changes in cellulose crystallinity, while the altered characteristics of the second peak may signify improved thermal stability,

potentially beneficial for applications requiring enhanced thermal resistance, such as in electronics or coatings.

The pseudo-first-order kinetic model suggests that the equilibrium adsorption capacity (q_e) increased in the order: Control < CNF < ZnO-NP < ZnO-CNF. This indicates that the incorporation of ZnO-NPs and nanocellulose, either individually or in combination, significantly enhanced the adsorption capacity of the material compared to the untreated control. The rate constant (k_1) values also followed a similar trend, with the highest value observed for ZnO-NPs/CNF, suggesting that the composite material has the fastest adsorption rate among the tested samples. However, the determination coefficients (r^2) for the pseudo-first-order model were relatively low for all samples, indicating poor fitting of the experimental data to this kinetic model.

In contrast, the pseudo-second-order kinetic model provided a better fit to the experimental data, as indicated by the higher regression coefficients (r^2) for all samples. This suggests that chemisorption is the key rate-limiting step in the adsorption process. Similar to the pseudo-first-order model, the equilibrium adsorption capacity (q_e) values increased in the order: Control < CNF < ZnO-NP < ZnO-CNF. This further supports assumption that the incorporation of ZnO-NPs and nanocellulose enhances the adsorption capacity of the material.

However, the rate constant (k_2) values decreased for ZnO-CNFcompared to ZnO- NPs, indicating that the composite material has a slower adsorption rate than ZnO-NPs alone. This suggests that while the ZnO-CNF nanocomposite has a higher adsorption capacity, the rate at which adsorption occurs may be slightly slower compared to ZnO-NPs. This could be due to factors such as mass transfer limitations or changes in the surface properties of the composite material.The adsorption isotherm studies provided further insights into the adsorption mechanism and capacity of the different materials. In the present study, the Langmuir, Freundlich, and Temkin isotherm models were employed to analyze the experimental data.

The Langmuir isotherm assumes a monolayer adsorption onto a homogeneous surface with a finite number of identical and non-interacting

adsorption sites (Patiha et al., 2016). The maximum adsorption capacity (q_{max}) was found to be highest for the ZnO-CNF nanocomposite, followed by ZnO-NPs and CNF. This indicates that the ZnO-CNF nanocomposite has a higher number of available adsorption sites, which can be attributed to its larger surface area (Chaba and Nomngongo, 2019; Dehghani et al., 2020; Oyewo et al., 2020).

The Freundlich isotherm is an empirical model that describes a multilayer adsorption on heterogeneous surfaces. The Freundlich isotherm constants (k_F and 1/n) were determined for each adsorbent. A higher value of k_F indicates a stronger affinity between the adsorbent and adsorbate, while a higher value of 1/n suggests a more heterogeneous surface. The ZnO-CNF nanocomposite exhibited higher values of k_F and 1/n compared to CNF and ZnO-NPs, indicating stronger adsorption and a more heterogeneous surface.

The Temkin isotherm assumes that the heat of adsorption decreases linearly with surface coverage. The Temkin constants (B_T and A_T) were determined for each adsorbent. The higher values of B_T and A_T for the ZnO-CNF nanocomposite suggest a stronger interaction between MB molecules and the adsorbent surface.

SUMMARY

This study successfully synthesized ZnO-NPs and nanocellulose from the algae *C. glomerata* and *C. vulgaris*. The bioactive molecules present in the algal extracts played a crucial role in the biogenic synthesis of ZnO-NPs. The nanocellulose derived from *C. glomerata* exhibited higher yield compared to *C. vulgaris*.

Characterization techniques confirmed the successful synthesis of ZnO-NPs and ZnO-CNF nanocomposite. In this study, ZnO-based nanomaterials were synthesized using a facile green synthesis approach involving the aqueous extract of *C. glomerata* and *C. vulgaris*. The synthesized materials were characterized using various techniques, including X-ray diffraction (XRD), Fourier Transform Infrared Spectroscopy (FTIR), Scanning Electron

The characterization of ZnO-NPs synthesized using aqueous extracts of *C. glomerata* and *C. vulgaris* revealed several key insights. The absorption spectra exhibited distinct peaks at approximately 350 nm for *C. glomerata* and 335 nm for *C. vulgaris*, characteristic of the band-to-band electronic transition within the ZnO-NPs crystal lattice. Tauc plot analysis further revealed wide band gaps of 3.18 eV and 3.40 eV for the nanoparticles synthesized from *C. glomerata* and *C. vulgaris*, respectively. These band gaps fall within the typical range for ZnO-NPs and are promising for applications in photocatalysis, optoelectronics, and energy storage.

FTIR analysis identified functional groups like -OH, water molecules, and various organic compounds involved in the reduction and stabilization of theZnO-NPs. These biomolecules, particularly phenolic compounds, likely played a crucial role in the synthesis process. The presence of these groups suggests that the biomolecules acted as reducing agents, donating electrons to Zn^{2+} ions and facilitating their reduction to ZnO-NPs. Additionally, they may have acted as capping agents, binding to the surface of the nanoparticles and preventing their further growth and agglomeration. This stabilization effect is crucial for maintaining the desired properties of the nanoparticles.

SEM analysis provided information about the morphology of theZnO-NPs. Those synthesized from *C. glomerata* exhibited a spherical or slightly elongated shape with a rough surface, potentially beneficial for increasing surface area and reactivity. The rough surface may provide more active sites for catalytic reactions or adsorption of molecules. Additionally, the roughness could increase the effective surface area, which is important for applications like sensing and drug delivery.In contrast, nanoparticles from *C. vulgaris* were also spherical or elongated but had a relatively smooth surface, which might impact their reactivity. While a smooth surface may reduce non-specific interactions, it could also limit the number of active sites available for reactions. However, the smooth surface could be advantageous for applications where controlled release or targeted delivery is desired.

EDX analysis confirmed the primary composition of the nanoparticles as ZnO, with minor impurities. The particle size distribution, as determined by EDX analysis, was found to be relatively narrow, indicating a homogeneous sample. The narrow particle size distribution suggests that the synthesis process yielded nanoparticles with consistent dimensions, which can be crucial for optimizing their properties and performance in various applications.XRD analysis further confirmed the crystalline nature of the nanoparticles, revealing a hexagonal wurtzite structure. The Scherrer equation was used to estimate the average crystallite size, which was found to be in the range of 32-82 nm. The sharp, well-defined diffraction peaks in the XRD patterns indicated a high degree of crystallinity, which is desirable for many applications as it often correlates with improved material properties. The estimated crystallite size falls within the nanoscale range, which can significantly impact the optical, electronic, and catalytic properties of the nanoparticles. XPS analysis provided detailed information about the surface composition and chemical state of the nanoparticles. The presence of Zn-O bonds confirmed the formation of ZnO-NPs, while the minor presence of carbon-based species suggested the presence of organic residues from the synthesis process.

FTIR analysis confirmed the presence of key functional groups, including hydroxyl, carbonyl, and ether groups, in the nanocellulose extracted from both *C. glomerata* and *C. vulgaris*. These functional groups contribute to the unique

properties of nanocellulose, such as its high surface area, strong hydrogen bonding, and biodegradability.SEM analysis revealed the fibrous nature of the nanocellulose extracted from *C. glomerata*, with individual nanofibrils exhibiting a smooth surface and a relatively uniform diameter. In contrast, the nanocellulose from *C. vulgaris* exhibited a more complex morphology, with plate-like structures and rod-like nanocrystals.

EDX analysis confirmed the elemental composition of the nanocellulose, primarily consisting of carbon and oxygen. Minor impurities, such as sodium, silicon, and potassium, were also detected, likely originating from the extraction process or residual impurities in the algal biomass.TGA and DSC analysis provided insights into the thermal stability and decomposition behavior of the nanocellulose. Both algae-derived nanocellulose exhibited good thermal stability up to a certain temperature, beyond which thermal degradation occurred. The initial weight loss in TGA was attributed to the removal of moisture, while the subsequent weight loss was associated with the degradation of hemicellulose and cellulose. The DSC analysis confirmed the endothermic nature of these processes, with distinct peaks corresponding to the different stages of thermal degradation.

The characterization of ZnO-CNF nanocomposite revealed several key features. FTIR analysis confirmed the successful incorporation of ZnO-NPs into the nanocellulose matrix, as evidenced by the presence of the Zn-O bond peak. The presence of other functional groups associated with nanocellulose indicated the preservation of the nanocellulose structure during the synthesis process.SEM analysis revealed a network-like structure composed of nanofibrils with uniformly dispersed ZnO-NPs. The strong interaction between the ZnO-NPs and the nanofibrils is likely due to the presence of functional groups on the surface of the nanofibrils. This uniform dispersion is crucial for enhancing the properties of the nanocomposite.

EDX analysis of ZnO-CNFnanocomposite confirmed the presence of Zn and O, indicating the successful incorporation of ZnO-NPs. Minor impurities were also detected, which may be attributed to the synthesis process or residual impurities in the starting materials. The particle size distribution analysis revealed a relatively

narrow distribution, suggesting a homogeneous sample.Overall, the characterization results demonstrate the successful synthesis of ZnO-CNF nanocomposite with a well-defined structure and promising properties. These nanocomposites have the potential to be used in various applications, including sensors, catalysts, and advanced materials.

Thermogravimetric analysis (TGA) was employed to evaluate the thermal stability and decomposition behavior of the ZnO-CNF nanocomposite. The TGA curve exhibited three distinct weight loss stages. The initial weight loss, occurring between 33°C and 137°C, was attributed to the evaporation of moisture and removal of surface-bound water. The major weight loss, observed between 137°C and 352°C, was primarily due to the thermal degradation of hemicellulose and the cleavage of glycosidic linkages in cellulose. The final phase of weight loss, between 352°C and 461°C, corresponded to the decomposition of the remaining cellulose fibers.

The derivative thermogravimetric analysis (DTG) curve provided further insights into the rate of weight loss during thermal degradation. Three distinct peaks were observed, corresponding to the three stages of weight loss identified in the TGA curve.Overall, the TGA and DTG analysis indicated that the ZnO-CNF nanocomposite exhibited good thermal stability up to around 350°C. Beyond this temperature, significant thermal degradation occurred, limiting its potential applications in high-temperature environments. However, the relatively high thermal stability and controlled degradation behavior make the nanocomposite a promising material for various applications, including reinforcement in composite materials and drug delivery. The incorporation of ZnO-NPs into the nanocellulose matrix may further enhance the thermal stability of the nanocomposite.

The photocatalytic activity of ZnO-NPs, CNFs, and the ZnO-CNF nanocomposite was evaluated by monitoring the degradation of methylene blue (MB) dye under natural sunlight irradiation. The ZnO-CNF nanocomposite exhibited superior photocatalytic activity, achieving nearly 95% degradation of MB within 150 min, compared to 60% and 20% degradation by ZnO-NPs and CNFs, respectively.

Kinetic studies revealed that the adsorption of MB onto the ZnO-CNF nanocomposite followed pseudo-second-order kinetics, with a higher rate constant compared to individual components. The Langmuir isotherm model best fitted the adsorption data, indicating monolayer adsorption. The maximum adsorption capacity of the ZnO-CNF nanocomposite was found to be 45 mg g^{-1}, which is significantly higher than that of ZnO-NPs (35 mgg^{-1}) and CNFs (15 mgg^{-1}).These results demonstrate the potential of ZnO-CNF nanocomposites as efficient photocatalysts for water treatment. The synergistic effect between CNFs and ZnO-NPs enhances the adsorption and photocatalytic activity of the composite, leading to improved performance.

Future research should focus on optimizing the synthesis process to further enhance the properties of the ZnO-CNF nanocomposite, exploring its potential applications in various fields, and assessing its environmental impact.

REFERENCES

Abdalkarim, S. Y. H., Yu, H.-Y., Wang, C., Huang, L.-X., and Yao, J. (2018). Green synthesis of sheet-like cellulose nanocrystal–zinc oxide nanohybrids with multifunctional performance through one-step hydrothermal method. *Cellulose*, *25*(11), 6433–6446. https://doi.org/10.1007/s10570-018-2011-0

Abdallah, H., Tannous, J. H., and Abu-Jdayil, B. (2024). Cellulose and nanocellulose aerogels, their preparation methods, and potential applications: A review. *Cellulose*, 31(4), 2001–2029. https://doi.org/10.1007/s10570-024-05743-w

Abdel-Raouf N. (2012). Agricultural importance of algae. *African Journal ofBiotechnology*, 11(54). https://doi.org/10.5897/AJB11.3983

Abel, A. (2012). The history of dyes and pigments. In Colour Design (pp. 557–587). Elsevier. https://doi.org/10.1016/B978-0-08-101270-3.00024-2

Abu, R., Jiang, Z., Ueno, M., Isaka, S., Nakazono, S., Okimura, T., Cho, K., Yamaguchi, K., Kim, D., and Oda, T. (2015). Anti-metastatic effects of the sulfated polysaccharide ascophyllan isolated from *Ascophyllum nodosum* on B16 melanoma. *Biochemical and Biophysical Research Communications*, 458(4), 727–732. https://doi.org/10.1016/j.bbrc.2015.01.061

Abu-Dalo, M. A., Al-Rosan, S. A., and Albiss, B. A. (2021). Photocatalytic degradation of methylene blue using polymeric membranes based on cellulose acetate impregnated with ZnO nanostructures. *Polymers*, 13(19), 3451. https://doi.org/10.3390/polym13193451

Abu-Ghosh, S., Sukenik, N., Amar, Z., and Iluz, D. (2023). Yellow dyes in archaeological textiles: Sources, locations, identification, and challenges. *Journal of Archaeological Science:Reports*, 49, 104030. https://doi.org/10.1016/j.jasrep.2023.104030

Adachi, M., Tsukui, S., and Okuyama, K. (2003). Nanoparticle synthesis by ionizing source gas in chemical vapor deposition. *Japanese Journal of Applied Physics*, 42(Part 2, No.1A/B), L77–L79. https://doi.org/10.1143/JJAP.42.L77

Addadi, L., and Weiner, S. (2014). Biomineralization: Mineral formation by organisms. *Physica Scripta*, 89(9), 098003. https://doi.org/10.1088/0031-8949/89/9/098003

Adedokun, O., Titilope, K., and Awodugba, A. O. (2016). Review on natural dye-sensitized solar cells (DSSCs). *International Journal of Engineering Technologies*, IJET, 2(2), 34. https://doi.org/10.19072/ijet.96456

Adeel, S., Rafi, S., Mustaan, M. A., Salman, M., and Ghaffar, A. (2018). *Animal based natural dyes: A short review*. In M. Yusuf (Ed.), Handbook of renewable

materials for coloration and finishing (1st ed., pp. 41–74). Wiley. https://doi.org/10.1002/9781119407850.ch4

Agarwal, K., Rai, H., and Mondal, S. (2023). Quantum dots: An overview of synthesis, properties, and applications. *Materials Research Express*, 10(6), 062001. https://doi.org/10.1088/2053-1591/acda17

Ahmad, R., and Kumar, R. (2010). Adsorption studies of hazardous malachite green onto treated ginger waste. *Journal of Environmental Management*, 91(4), 1032–1038. https://doi.org/10.1016/j.jenvman.2009.12.016

Ahmad, S., Jan, K., Sahu, J. K., Habib, M., Jan, S., and Bashir, K. (2024). A comprehensive review on recent trends and utilization of algal β-glucan for the development of nutraceuticals and functional foods. *Food Reviews International*, 1–22. https://doi.org/10.1080/87559129.2024.2404222

Ahsan, H. (2019). The significance of complex polysaccharides in personal care formulations. *Journal of Carbohydrate Chemistry*, 38(4), 213–233. https://doi.org/10.1080/07328303.2019.1615498

Ak, İ., Koru, E., Türker, G., Çankırılıgil, E. C., and Dereli, M. G. (2022). *Biochemical compounds of algae: Sustainable energy sources for biofuel production*. In Handbook of Algal Biofuels (pp. 57–78). Elsevier. https://doi.org/10.1016/B978-0-12-823764-9.00026-1

Aksu, Z., and Tezer, S. (2005). Biosorption of reactive dyes on the green alga *Chlorella vulgaris*. *Process Biochemistry*, 40(3–4), 1347–1361. https://doi.org/10.1016/j.procbio.2004.06.007

Al Fahad, Md. A., Ahamed, R., Ahmed, T., Jahan, N., Mia, R., Toki, G. F. I., Mahmud, S. T., and Niloy, K. K. (2024). *Pharmaceutical applications of natural dyes and pigments*. InRenewable Dyes and Pigments (pp. 165–175). Elsevier. https://doi.org/10.1016/B978-0-443-15213-9.00011-9

Aladpoosh, R., and Montazer, M. (2015). The role of cellulosic chains of cotton in biosynthesis of ZnO nanorods producing multifunctional properties: Mechanism, characterizations and features. *Carbohydrate Polymers*, 126, 122–129. https://doi.org/10.1016/j.carbpol.2015.03.036

Alagiri, M., Ponnusamy, S., and Muthamizhchelvan, C. (2012). Synthesis and characterization of NiO nanoparticles by sol–gel method. *Journal of Materials Science: Materials in Electronics*, 23(3), 728–732. https://doi.org/10.1007/s10854-011-0479-6

Aldalbahi, A., El-Naggar, M., El-Newehy, M., Rahaman, M., Hatshan, M., andKhattab, T. (2021). Effects of technical textiles and synthetic nanofibers on environmental pollution. *Polymers*, 13(1), 155. https://doi.org/10.3390/polym13010155

Ale, M. T., Maruyama, H., Tamauchi, H., Mikkelsen, J. D.,and Meyer, A. S. (2011). Fucose-containing sulfated polysaccharides from brown seaweeds inhibit proliferation of melanoma cells and induce apoptosis by activation of caspase-3 in vitro. *Marine Drugs*, 9(12), 2605–2621. https://doi.org/10.3390/md9122605

Alegbe, E. O., and Uthman, T. O. (2024). A review of history, properties, classification, applications and challenges of natural and synthetic dyes. *Heliyon*, 10(13), e33646. https://doi.org/10.1016/j.heliyon.2024.e33646

Al-Etaibi, A. M., and El-Apasery, M. A. (2019). Dyeing performance of disperse dyes on polyester fabrics using eco-friendly carrier and their antioxidant and anticancer activities. *International Journal of Environmental Research and Public Health*, 16(23), 4603. https://doi.org/10.3390/ijerph16234603

Al-Gaashani, R., Radiman, S., Daud, A. R., Tabet, N., and Al-Douri, Y. (2013). XPS and optical studies of different morphologies of ZnO nanostructures prepared by microwave methods. *Ceramics International*, 39(3), 2283–2292. https://doi.org/10.1016/j.ceramint.2012.08.075

Al-Hammadi, M., and Güngörmüşler, M. (2024). New insights into *Chlorella vulgaris* applications. *Biotechnology and Bioengineering*, 121(5), 1486–1502. https://doi.org/10.1002/bit.28666

Ali, A., Ambreen, S., Maqbool, Q., Naz, S., Shams, M. F., Ahmad, M., Phull, A. R., and Zia, M. (2016). Zinc impregnated cellulose nanocomposites: Synthesis, characterization and applications. *Journal of Physics and Chemistry of Solids*, 98, 174–182. https://doi.org/10.1016/j.jpcs.2016.07.007

Alsaggaf, M. S., Diab, A. M., ElSaied, B. E. F., Tayel, A. A., and Moussa, S. H. (2021). Application of ZnO-NPs phycosynthesized with *Ulva fasciata* extract for preserving peeled shrimp quality. *Nanomaterials*, 11(2), 385. https://doi.org/10.3390/nano11020385

Al-Tohamy, R., Ali, S. S., Li, F., Okasha, K. M., Mahmoud, Y. A.-G., Elsamahy, T., Jiao, H., Fu, Y., and Sun, J. (2022). A critical review on the treatment of dye-containing wastewater: Ecotoxicological and health concerns of textile dyes and possible remediation approaches for environmental safety. *Ecotoxicology and Environmental Safety*, 231, 113160. https://doi.org/10.1016/j.ecoenv.2021.113160

Amendola, V., and Meneghetti, M. (2009). Laser ablation synthesis in solution and size manipulation of noble metal nanoparticles. *Physical Chemistry Chemical Physics*, 11(20), 3805. https://doi.org/10.1039/b900654k

Amreddy, N., Babu, A., Muralidharan, R., Panneerselvam, J., Srivastava, A., Ahmed, R., Mehta, M., Munshi, A., and Ramesh, R. (2018). Recent advances in nanoparticle-based cancer drug and gene delivery. *In Advances in Cancer Research*, 137,115–170. https://doi.org/10.1016/bs.acr.2017.11.003

Antony Lilly Grace, M., Veerabhadra Rao, K., Anuradha, K., Judith Jayarani, A., Arun Kumar, A., and Rathika, A. (2023). X-ray analysis and size-strain plot of zinc oxide nanoparticles by Williamson-Hall. *Materials Today: Proceedings*, 92, 1334–1339. https://doi.org/10.1016/j.matpr.2023.05.492

Anu Mary Ealia, S., and Saravanakumar, M. P. (2017). A review on the classification, characterisation, synthesis of nanoparticles and their application. IOP Conference Series: *Materials Science and Engineering*, 263, 032019. https://doi.org/10.1088/1757-899X/263/3/032019

Aoudi, B., Boluk, Y., and Gamal El-Din, M. (2022). Recent advances and future perspective on nanocellulose-based materials in diverse water treatment applications. *Science of The Total Environment*, 843, 156903. https://doi.org/10.1016/j.scitotenv.2022.156903

Arabkhani, P., Saeedi, N., Sadeghi, H., Nouripour-Sisakht, S., Gharaghani, M., and Asfaram, A. (2023). Plant extracts-mediated green synthesis of zinc oxide/carbon nanofiber nanocomposites with highly efficient photocatalytic and antimicrobial properties for wastewater treatment. *Journal of Water Process Engineering*, 54, 104020. https://doi.org/10.1016/j.jwpe.2023.104020

Aragaw, T. A., and Bogale, F. M. (2021). Biomass-based adsorbents for removal of dyes from wastewater: A Review. *Frontiers in Environmental Science*, 9, 764958. https://doi.org/10.3389/fenvs.2021.764958

Arbain, R., Othman, M., and Palaniandy, S. (2011). Preparation of iron oxide nanoparticles by mechanical milling. *Minerals Engineering*, 24(1), 1–9. https://doi.org/10.1016/j.mineng.2010.08.025

Ardila-Leal, L. D., Poutou-Piñales, R. A., Pedroza-Rodríguez, A. M., and Quevedo-Hidalgo, B. E. (2021). A brief history of colour, the environmental impact of synthetic dyes and removal by using laccases. *Molecules*, 26(13), 3813. https://doi.org/10.3390/molecules26133813

Arıca, M. Y., Tüzün, İ., Yalçın, E., İnce, Ö.and Bayramoğlu, G. (2005). Utilisation of native, heat and acid-treated microalgae *Chlamydomonas reinhardtii* preparations for biosorption of Cr(VI) ions. *Process Biochemistry*, 40(7), 2351–2358. https://doi.org/10.1016/j.procbio.2004.09.008

Ariede, M. B., Candido, T. M., Jacome, A. L. M., Velasco, M. V. R., De Carvalho, J. C. M., and Baby, A. R. (2017). Cosmetic attributes of algae—A review. *Algal Research*, 25, 483–487. https://doi.org/10.1016/j.algal.2017.05.019

Arkan, F., Pakravesh, F., Barati Darband, F., Sabagh, S., and Izadyar, M. (2024). Recent progress toward high-performance dye-sensitized solar cells: A review. *Journal of the Iranian Chemical Society*, 21(3), 577–638. https://doi.org/10.1007/s13738-024-02967-2

Arora, C., Kumar, P., Soni, S., Mittal, J., Mittal, A., and Singh, B. (2020). Efficient removal of malachite green dye from aqueous solution using *Curcuma*

*caesia*based activated carbon. *Desalination and Water Treatment*, 195, 341–352. https://doi.org/10.5004/dwt.2020.25897

Arora, J., Agarwal, P., and Gupta, G. (2017). Rainbow of Natural Dyes on Textiles Using Plants Extracts: Sustainable and Eco-Friendly Processes. *Green and Sustainable Chemistry*, 07(01), 35–47. https://doi.org/10.4236/gsc.2017.71003

Arora, K., Kumar, P., Bose, D., Li, X., and Kulshrestha, S. (2021). Potential applications of algae in biochemical and bioenergy sector. *3 Biotech*, 11(6), 296. https://doi.org/10.1007/s13205-021-02825-5

Aslam, A., Bahadar, A., Liaquat, R., Saleem, M., Waqas, A., and Zwawi, M. (2021). Algae as an attractive source for cosmetics to counter environmental stress. *Science of the Total Environment*, 772, 144905. https://doi.org/10.1016/j.scitotenv.2020.144905

Azimifar, M., Ghorbani, M., and Peyravi, M. (2022). Fabrication and evaluation of a photocatalytic membrane based on Sb_2O_3/CBO composite for improvement of dye removal efficiency. *Journal of Molecular Structure*, 1270, 133957. https://doi.org/10.1016/j.molstruc.2022.133957

Aziz, S., Mazhar, A. R., Ubaid, A., Shah, S. M. H., Riaz, Y., Talha, T., and Jung, D.-W. (2024). A comprehensive review of membrane-based water filtration techniques. *Applied Water Science*, 14(8), 169. https://doi.org/10.1007/s13201-024-02226-y

Azizi, S., Ahmad, M. B., Namvar, F., and Mohamad, R. (2014). Green biosynthesis and characterization of zinc oxide nanoparticles using brown marine macroalga *Sargassum muticum* aqueous extract. *Materials Letters*, 116, 275–277. https://doi.org/10.1016/j.matlet.2013.11.038

Azizi, S., Ahmad, M., Hussein, M., andIbrahim, N. (2013). Synthesis, antibacterial and thermal studies of cellulose nanocrystal stabilized ZnO-Ag heterostructure nanoparticles. *Molecules*, 18(6), 6269–6280. https://doi.org/10.3390/molecules18066269

Azizi, S., Ahmad, M., Ibrahim, N., Hussein, M., and Namvar, F. (2014). Cellulose nanocrystals/ZnO as a bifunctional reinforcing nanocomposite for poly (vinyl alcohol)/Chitosan blend films: fabrication, characterization and properties. *International Journal of Molecular Sciences*, 15(6), 11040–11053. https://doi.org/10.3390/ijms150611040

Aznan, N. A. K., and Johan, M. R. (2012). Quantum size effect in ZnO Nanoparticles via mechanical milling. *Journal of Nanomaterials*, 2012(1), 439010. https://doi.org/10.1155/2012/439010

Baig, N., Kammakakam, I., and Falath, W. (2021). Nanomaterials: A review of synthesis methods, properties, recent progress, and challenges. *Materials Advances*, 2(6), 1821–1871. https://doi.org/10.1039/D0MA00807A

Balogun, S. W., James, O. O., Sanusi, Y. K., and Olayinka, O. H. (2020). Green synthesis and characterization of zinc oxide nanoparticles using bashful (*Mimosa pudica*), leaf extract: A precursor for organic electronics applications. *SN Applied Sciences*, 2(3). https://doi.org/10.1007/s42452-020-2127-3

Bandeira, M., Giovanela, M., Roesch-Ely, M., Devine, D. M., and Da Silva Crespo, J. (2020). Green synthesis of zinc oxide nanoparticles: A review of the synthesis methodology and mechanism of formation. *Sustainable Chemistry and Pharmacy*, 15, 100223. https://doi.org/10.1016/j.scp.2020.100223

Barathi, S., Karthik, C., S, N., and Padikasan, I. A. (2020). Biodegradation of textile dye Reactive Blue 160 by *Bacillus firmus* (Bacillaceae: Bacillales) and non-target toxicity screening of their degraded products. *Toxicology Reports*, 7, 16–22. https://doi.org/10.1016/j.toxrep.2019.11.017

Bayramoglu, G., Kunduzcu, G., and Arica, M. Y. (2020). Preparation and characterization of strong cation exchange terpolymer resin as effective adsorbent for removal of disperse dyes. *Polymer Engineering and Science*, 60(1), 192–201. https://doi.org/10.1002/pen.25272

Bedoux, G., Hardouin, K., Burlot, A. S., and Bourgougnon, N. (2014). Bioactive components from seaweeds. *In Advances in Botanical Research* (Vol. 71, pp. 345–378). Elsevier. https://doi.org/10.1016/B978-0-12-408062-1.00012-3

Benítez, A. J., and Walther, A. (2017). Cellulose nanofibril nanopapers and bioinspired nanocomposites: A review to understand the mechanical property space. *Journal of Materials Chemistry A*, 5(31), 16003–16024. https://doi.org/10.1039/C7TA02006F

Benkhaya, S., M' Rabet, S., and El Harfi, A. (2020). A review on classifications, recent synthesis and applications of textile dyes. *Inorganic Chemistry Communications*, 115, 107891. https://doi.org/10.1016/j.inoche.2020.107891

Berradi, M., Hsissou, R., Khudhair, M., Assouag, M., Cherkaoui, O., El Bachiri, A., and El Harfi, A. (2019). Textile finishing dyes and their impact on aquatic environs. *Heliyon*, 5(11), e02711. https://doi.org/10.1016/j.heliyon.2019.e02711

Betancourt-Galindo, R., Reyes-Rodriguez, P. Y., Puente-Urbina, B. A., Avila-Orta, C. A., Rodríguez-Fernández, O. S., Cadenas-Pliego, G., Lira-Saldivar, R. H., and García-Cerda, L. A. (2014). Synthesis of copper nanoparticles by thermal decomposition and their antimicrobial properties. *Journal of Nanomaterials*, 2014(1), 980545. https://doi.org/10.1155/2014/980545

Bhatia, D., Sharma, N. R., Singh, J., and Kanwar, R. S. (2017). Biological methods for textile dye removal from wastewater: A review. *Critical Reviews in Environmental Science and Technology*, 47(19), 1836–1876. https://doi.org/10.1080/10643389.2017.1393263

Bhatt, P., Bhandari, G., Turco, R. F., Aminikhoei, Z., Bhatt, K., and Simsek, H. (2022). Algae in wastewater treatment, mechanism, and application of biomass for production of value-added product. *Environmental Pollution*, 309, 119688. https://doi.org/10.1016/j.envpol.2022.119688

Bhutiya, P. L., Misra, N., Abdul Rasheed, M., and Zaheer Hasan, S. (2018). Nested seaweed cellulose fiber deposited with cuprous oxide nanorods for antimicrobial activity. *International Journal of Biological Macromolecules*, 117, 435–444. https://doi.org/10.1016/j.ijbiomac.2018.05.210

Bian, L., Wei, Q., Li, J., Zhang, J., Qin, S., Yang, J., and Cui, Z. (2022). Hollow fiber composite membranes engineered via the combination of "anionic crosslinking and in-situ biomineralization" for dye removal. *European Polymer Journal*, 179, 111587. https://doi.org/10.1016/j.eurpolymj.2022.111587

Bito, T., Okumura, E., Fujishima, M., and Watanabe, F. (2020). Potential of *Chlorella* as a dietary supplement to promote human health. *Nutrients*, 12(9), 2524. https://doi.org/10.3390/nu12092524

Bokov, D., Turki Jalil, A., Chupradit, S., Suksatan, W., Javed Ansari, M., Shewael, I. H., Valiev, G. H., and Kianfar, E. (2021). Nanomaterial by Sol-Gel method: synthesis and application. *Advances in Materials Science and Engineering*, 2021(1), 5102014. https://doi.org/10.1155/2021/5102014

Burkinshaw, S. M., and Salihu, G. (2019). The role of auxiliaries in the immersion dyeing of textile fibres: Part 5 practical aspects of the role of inorganic electrolytes in dyeing cellulosic fibres with direct dyes. *Dyes and Pigments*, 161, 581–594. https://doi.org/10.1016/j.dyepig.2017.09.002

C.S., J. C., George, N., and Narayanankutty, S. K. (2016). Isolation and characterization of cellulose nanofibrils from arecanut husk fibre. *Carbohydrate Polymers*, 142, 158–166. https://doi.org/10.1016/j.carbpol.2016.01.015

Campos, A., Souza, C. B., Lhullier, C., Falkenberg, M., Schenkel, E. P., Ribeiro-do-Valle, R. M., and Siqueira, J. M. (2012). Anti-tumour effects of elatol, a marine derivative compound obtained from red algae *Laurencia microcladia*. *Journal of Pharmacy and Pharmacology*, 64(8), 1146–1154. https://doi.org/10.1111/j.2042-7158.2012.01493.x

Carpenter, A. W., De Lannoy, C.-F., and Wiesner, M. R. (2015). Cellulose nanomaterials in water treatment technologies. *Environmental Science and Technology*, 49(9), 5277–5287. https://doi.org/10.1021/es506351r

Çelekli, A., and Alkan, E. (2024). Effect of lead ions on biochemical behavior of *Cladophora glomerata* in sterilized and non-sterilized media. *Protoplasma*, 261(1), 77–87. https://doi.org/10.1007/s00709-023-01882-2

Cellulose Nanocrystals for Drug Delivery. (2010). In M. Roman, S. Dong, A. Hirani, and Y. W. Lee, ACS Symposium Series (pp. 81–91). *American Chemical Society*. https://doi.org/10.1021/bk-2009-1017.ch004

Cevallos-Mendoza, J., Amorim, C., Rodríguez-Díaz, J., and Montenegro, M. (2022). Removal of contaminants from water by membrane filtration: A review. *Membranes*, 12(6), 570. https://doi.org/10.3390/membranes12060570

Chaba, J. M., and Nomngongo, P. N. (2019). Effective adsorptive removal of amoxicillin from aqueous solutions and wastewater samples using zinc oxide coated carbon nanofiber composite. *Emerging Contaminants*, 5, 143–149. https://doi.org/10.1016/j.emcon.2019.04.001

Chakraborty, S., De, S., DasGupta, S., and Basu, J. K. (2005). Adsorption study for the removal of a basic dye: Experimental and modeling. *Chemosphere*, 58(8), 1079–1086. https://doi.org/10.1016/j.chemosphere.2004.09.066

Chand, S., Chand, S., and Raula, B. (2023). Textile and apparel industries waste and its sustainable management approaches. *Journal of Material Cycles and Waste Management*, 25(6), 3132–3143. https://doi.org/10.1007/s10163-023-01761-1

Chang, F.-M., Brahma, S., Huang, J.-H., Wu, Z.-Z., and Lo, K.-Y. (2019). Strong correlation between optical properties and mechanism in deficiency of normalized self-assembly ZnO nanorods. *Scientific Reports*, 9(1). https://doi.org/10.1038/s41598-018-37601-8

Chattaraj, S., Johnson, J., and Madamwar, D. (2016). Biotransformation of mixture of dyes by enriched bacterial consortium ASD. *Desalination and Water Treatment*, 57(45), 21585–21597. https://doi.org/10.1080/19443994.2015.1124345

Chaudhary, R., Nawaz, K., Khan, A. K., Hano, C., Abbasi, B. H., and Anjum, S. (2020). An overview of the algae-mediated biosynthesis of nanoparticles and their biomedical applications. *Biomolecules*, 10(11), 1498. https://doi.org/10.3390/biom10111498

Chaurasia, V., Chand, N.,and Bajpai, S. K. (2010). Water sorption properties and antimicrobial action of zinc oxide nanoparticles-loaded cellulose acetate films. *Journal of Macromolecular Science*, Part A, 47(4), 309–317. https://doi.org/10.1080/10601320903539207

Che, J., and Yang, X. (2022). A recent (2009–2021) perspective on sustainable color and textile coloration using natural plant resources. *Heliyon*, 8(10), e10979. https://doi.org/10.1016/j.heliyon.2022.e10979

Chen, B., Gu, Z., Wu, M., Ma, Z., Lim, H. R., Khoo, K. S., and Show, P. L. (2022). Advancement pathway of biochar resources from macroalgae biomass: A review. *Biomass and Bioenergy*, 167, 106650. https://doi.org/10.1016/j.biombioe.2022.106650

Chen, D.-H., and He, X.-R. (2001). Synthesis of nickel ferrite nanoparticles by sol-gel method. *Materials Research Bulletin*, 36(7–8), 1369–1377. https://doi.org/10.1016/S0025-5408(01)00620-1

Chen, X., Chen, Y., Zhang, L., Liu, Z., Qiu, E., Liu, Q., Regulacio, M. D., Lin, C., and Yang, D.-P. (2023). Hydrophilic ZnO/C nanocomposites with superior adsorption, photocatalytic, and photo-enhanced antibacterial properties for synergistic water purification. *Journal of Colloid and Interface Science*, 648, 535–550. https://doi.org/10.1016/j.jcis.2023.06.019

Chen, X., Wu, Z., Liu, D., and Gao, Z. (2017). Preparation of ZnO photocatalyst for the efficient and rapid photocatalytic degradation of azo dyes. *Nanoscale Research Letters*, 12(1), 143. https://doi.org/10.1186/s11671-017-1904-4

Chen, Y. W., Lee, H. V., Juan, J. C., and Phang, S.-M. (2016). Production of new cellulose nanomaterial from red algae marine biomass *Gelidium elegans*. *Carbohydrate Polymers*, 151, 1210–1219. https://doi.org/10.1016/j.carbpol.2016.06.083

Chisti, Y. (2007). Biodiesel from microalgae. *Biotechnology Advances*, 25(3), 294–306. https://doi.org/10.1016/j.biotechadv.2007.02.001

Chojnacka, K. (2010). Biosorption and bioaccumulation – the prospects for practical applications. *Environment International*, 36(3), 299–307. https://doi.org/10.1016/j.envint.2009.12.001

Chung, B.-X., and Liu, C.-P. (2004). Synthesis of cobalt nanoparticles by DC magnetron sputtering and the effects of electron bombardment. *Materials Letters*, 58(9), 1437–1440. https://doi.org/10.1016/j.matlet.2003.06.018

Colson, P., Henrist, C., and Cloots, R. (2013). Nanosphere lithography: A powerful method for the controlled manufacturing of nanomaterials. *Journal of Nanomaterials*, 2013(1), 948510. https://doi.org/10.1155/2013/948510

Cosgrove, W. J., and Loucks, D. P. (2015). Water management: Current and future challenges and research directions. *Water Resources Research*, 51(6), 4823–4839. https://doi.org/10.1002/2014WR016869

Cronshaw, J., Myers, A., and Preston, R. D. (1958). A chemical and physical investigation of the cell walls of some marine algae. *BBA - Biochimica et Biophysica Acta*, 27(C), 89–103. https://doi.org/10.1016/0006-3002(58)90295-6

Cuiping, B., Xianfeng, X., Wenqi, G., Dexin, F., Mo, X., Zhongxue, G., and Nian, X. (2011). Removal of rhodamine B by ozone-based advanced oxidation process. *Desalination*, 278(1–3), 84–90. https://doi.org/10.1016/j.desal.2011.05.009

Damonte, L. C., Mendoza Zélis, L. A., Marí Soucase, B., and Hernández Fenollosa, M. A. (2004). Nanoparticles of ZnO obtained by mechanical milling. *Powder Technology*, 148(1), 15–19. https://doi.org/10.1016/j.powtec.2004.09.014

Daniels, V. (2006). The light-fastness of textiles dyed with 6,6′-dibromoindigotin (Tyrian purple). *Journal of Photochemistry and Photobiology A: Chemistry*, 184(1–2), 73–77. https://doi.org/10.1016/j.jphotochem.2006.03.034

Dantas, D. M. D. M., Oliveira, C. Y. B. D., Costa, R. M. P. B., Carneiro-da-Cunha, M. D. G., Gálvez, A. O., and Bezerra, R. D. S. (2019). Evaluation of antioxidant and antibacterial capacity of green microalgae Scenedesmus subspicatus. *Food Science and Technology International*, 25(4), 318–326. https://doi.org/10.1177/1082013218825024

Davar, F., Salavati-Niasari, M., Mir, N., Saberyan, K., Monemzadeh, M., and Ahmadi, E. (2010). Thermal decomposition route for synthesis of Mn_3O_4 nanoparticles in presence of a novel precursor. *Polyhedron*, 29(7), 1747–1753. https://doi.org/10.1016/j.poly.2010.02.026

De Campos, A., Correa, A. C., Cannella, D., De M Teixeira, E., Marconcini, J. M., Dufresne, A., Mattoso, L. H. C., Cassland, P., and Sanadi, A. R. (2013). Obtaining nanofibers from curauá and sugarcane bagasse fibers using enzymatic hydrolysis followed by sonication. *Cellulose*, 20(3), 1491–1500. https://doi.org/10.1007/s10570-013-9909-3

De France, K., Zeng, Z., Wu, T., andNyström, G. (2021). Functional materials from nanocellulose: utilizing structure property relationships in bottom-up fabrication. *Advanced Materials*, 33(28), 2000657. https://doi.org/10.1002/adma.202000657

Dehghani, M., Nadeem, H., Singh Raghuwanshi, V., Mahdavi, H., Banaszak Holl, M. M., and Batchelor, W. (2020). ZnO/Cellulose nanofiber composites for sustainable sunlight-driven dye degradation. *ACS Applied Nano Materials*, 3(10), 10284–10295. https://doi.org/10.1021/acsanm.0c02199

Demirbas, M. F. (2011). Biofuels from algae for sustainable development. *Applied Energy*, 88(10), 3473–3480. https://doi.org/10.1016/j.apenergy.2011.01.059

Deng, L., Su, Y., Su, H., Wang, X., and Zhu, X. (2006). Biosorption of copper (II) and lead (II) from aqueous solutions by nonliving green algae *Cladophora fascicularis*: equilibrium, kinetics and environmental effects. *Adsorption*, 12(4), 267–277. https://doi.org/10.1007/s10450-006-0503-y

Dey, S., and Nagababu, B. H. (2022). Applications of food color and bio-preservatives in the food and its effect on the human health. *Food Chemistry Advances*, 1, 100019. https://doi.org/10.1016/j.focha.2022.100019

Diany, R., Kerraj, S., Aboulouard, A., Syed, A., Zeroual, A., Bahkali, A. H., El Idrissi, M., Salah, M., and Tounsi, A. (2024). Enhancing dye sensitized solar cells performance through quinoxaline based organic dye sensitizers. *Journal of Computational Electronics*. https://doi.org/10.1007/s10825-024-02211-3

Din, M. I., Raza, M., Hussain, Z., and Mehmood, H. A. (2019). Fabrication of magnetite nanoparticles (Fe_3O_4 -NPs) for catalytic pyrolysis of nutshells

biomass. *Soft Materials*, 17(1), 24–31. https://doi.org/10.1080/1539445X.2018.1542315

Djafari Petroudy, S. R., Chabot, B., Loranger, E., Naebe, M., Shojaeiarani, J., Gharehkhani, S., Ahvazi, B., Hu, J., and Thomas, S. (2021). Recent advances in cellulose nanofibers preparation through energy-efficient approaches: A Review. *Energies*, 14(20), 6792. https://doi.org/10.3390/en14206792

Domínguez, H. (2013). Algae as a source of biologically active ingredients for the formulation of functional foods and nutraceuticals. In Functional Ingredients from Algae for Foods and Nutraceuticals (pp. 1–19). Elsevier. https://doi.org/10.1533/9780857098689.1

Dong, H., Zeng, G., Tang, L., Fan, C., Zhang, C., He, X., and He, Y. (2015). An overview on limitations of TiO_2-based particles for photocatalytic degradation of organic pollutants and the corresponding countermeasures. *Water Research*, 79, 128–146. https://doi.org/10.1016/j.watres.2015.04.038

Donkadokula, N. Y., Kola, A. K., Naz, I., and Saroj, D. (2020). A review on advanced physico-chemical and biological textile dye wastewater treatment techniques. *Reviews in Environmental Science and Bio/Technology*, 19(3), 543–560. https://doi.org/10.1007/s11157-020-09543-z

Dreesen, L., Colomer, J.-F., Limage, H., Giguère, A., and Lucas, S. (2009). Synthesis of titanium dioxide nanoparticles by reactive DC magnetron sputtering. *Thin Solid Films*, 518(1), 112–115. https://doi.org/10.1016/j.tsf.2009.06.044

Du Plessis, A. (2022). Persistent degradation: Global water quality challenges and required actions. *One Earth*, 5(2), 129–131. https://doi.org/10.1016/j.oneear.2022.01.005

Dubey, R. S., Rajesh, Y. B. R. D., and More, M. A. (2015). Synthesis and characterization of SiO_2 nanoparticles via Sol-gel method for industrial applications. *Materials Today: Proceedings*, 2(4–5), 3575–3579. https://doi.org/10.1016/j.matpr.2015.07.098

Dutta, S., Adhikary, S., Bhattacharya, S., Roy, D., Chatterjee, S., Chakraborty, A., Banerjee, D., Ganguly, A., Nanda, S., and Rajak, P. (2024). Contamination of textile dyes in aquatic environment: Adverse impacts on aquatic ecosystem and human health, and its management using bioremediation. *Journal of Environmental Management*, 353, 120103. https://doi.org/10.1016/j.jenvman.2024.120103

El Nemr, A., Hassaan, M. A., and Madkour, F. F. (2018). Advanced oxidation process (AOP) for detoxification of Acid Red 17 dye solution and degradation mechanism. *Environmental Processes*, 5(1), 95–113. https://doi.org/10.1007/s40710-018-0284-9

Elamawi, R. M., Al-Harbi, R. E., and Hendi, A. A. (2018). Biosynthesis and characterization of silver nanoparticles using *Trichoderma longibrachiatum* and their effect on phytopathogenic fungi. *Egyptian Journal of Biological Pest Control*, 28(1), 28. https://doi.org/10.1186/s41938-018-0028-1

El-Sheekh, M. M., Yousuf, W. E., Kenawy, E.-R., and Mohamed, T. M. (2023). Biosynthesis of cellulose from *Ulva lactuca*, manufacture of nanocellulose and its application as antimicrobial polymer. Scientific Reports, 13(1), 10188. https://doi.org/10.1038/s41598-023-37287-7

Escalante, F. M. E., and Pérez-Rico, D. A. (2021). *Advancements in algae in nutraceutical and functional food*. In G. Rajauria and Y. V. Yuan (Eds.), Recent advances in micro and macroalgal processing (1st ed., pp. 506–536). Wiley. https://doi.org/10.1002/9781119542650.ch18

Farooq, A., Patoary, M. K., Zhang, M., Mussana, H., Li, M., Naeem, M. A., Mushtaq, M., Farooq, A., and Liu, L. (2020). Cellulose from sources to nanocellulose and an overview of synthesis and properties of nanocellulose/zinc oxide nanocomposite materials. *International Journal of Biological Macromolecules*, 154, 1050–1073. https://doi.org/10.1016/j.ijbiomac.2020.03.163

Feng, L., Xie, N., and Zhong, J. (2014). Carbon nanofibers and their composites: A Review of synthesizing, Properties and Applications. *Materials*, 7(5), 3919–3945. https://doi.org/10.3390/ma7053919

Fenner, K., Elsner, M., Lueders, T., McLachlan, M. S., Wackett, L. P., Zimmermann, M., and Drewes, J. E. (2021). Methodological advances to study contaminant biotransformation: new prospects for understanding and reducing environmental persistence? *ACS ESandT Water*, 1(7), 1541–1554. https://doi.org/10.1021/acsestwater.1c00025

Ferronato, N., and Torretta, V. (2019). Waste mismanagement in developing countries: A review of global issues. *International Journal of Environmental Research and Public Health*, 16(6), 1060. https://doi.org/10.3390/ijerph16061060

Fomina, M., and Gadd, G. M. (2014). Biosorption: current perspectives on concept, definition and application. *Bioresource Technology*, 160, 3–14. https://doi.org/10.1016/j.biortech.2013.12.102

Forgacs, E., Cserháti, T., and Oros, G. (2004). Removal of synthetic dyes from wastewaters: A review. *Environment International*, 30(7), 953–971. https://doi.org/10.1016/j.envint.2004.02.001

Fukuhara, M., Kuroda, T., Hasegawa, F., Hashida, T., Takeda, M., Fujima, N., Morita, M., and Nakatani, T. (2021). Amorphous cellulose nanofiber supercapacitors. *Scientific Reports*, 11(1), 6436. https://doi.org/10.1038/s41598-021-85901-3

Gadekar, M. R., and Ahammed, M. M. (2016). Coagulation/flocculation process for dye removal using water treatment residuals: Modelling through artificial neural networks. *Desalination and Water Treatment*, 57(55), 26392–26400. https://doi.org/10.1080/19443994.2016.1165150

Galappaththi, M., and Patabendige, N. (2022). Cochineal chemistry, related applications and problems: A mini review. *Academia Letters*. https://doi.org/10.20935/AL1792

Gan, P. G., Sam, S. T., Abdullah, M. F. B., and Omar, M. F. (2020). Thermal properties of nanocellulose-reinforced composites: A review. *Journal of Applied Polymer Science*, 137(11), 48544. https://doi.org/10.1002/app.48544

Gao, H., Duan, B., Lu, A., Deng, H., Du, Y., Shi, X., and Zhang, L. (2018). Fabrication of cellulose nanofibers from waste brown algae and their potential application as milk thickeners. *Food Hydrocolloids*, 79, 473–481. https://doi.org/10.1016/j.foodhyd.2018.01.023

Gaurav, K., Neeti, K., and Singh, R. (2024). Microalgae-based biodiesel production and its challenges and future opportunities: A review. *Green Technologies and Sustainability*, 2(1), 100060. https://doi.org/10.1016/j.grets.2023.100060

Geada, P., Moreira, C., Silva, M., Nunes, R., Madureira, L., Rocha, C. M. R., Pereira, R. N., Vicente, A. A., and Teixeira, J. A. (2021). Algal proteins: Production strategies and nutritional and functional properties. *Bioresource Technology*, 332, 125125. https://doi.org/10.1016/j.biortech.2021.125125

Ghasemi, M., Mashhadi, S., Asif, M., Tyagi, I., Agarwal, S., and Gupta, V. K. (2016). Microwave-assisted synthesis of tetraethylenepentamine functionalized activated carbon with high adsorption capacity for Malachite green dye. *Journal of Molecular Liquids*, 213, 317–325. https://doi.org/10.1016/j.molliq.2015.09.048

Ginimuge, P., and Jyothi, S. (2010). Methylene blue: Revisited. *Journal of Anaesthesiology Clinical Pharmacology*, 26(4), 517. https://doi.org/10.4103/0970-9185.74599

Głowacki, E. D., Voss, G., Leonat, L., Irimia-Vladu, M., Bauer, S., and Sariciftci, N. S. (2012). Indigo and tyrian purple – From ancient natural dyes to modern organic semiconductors. *Israel Journal of Chemistry*, 52(6), 540–551. https://doi.org/10.1002/ijch.201100130

Golmohammadi, M., Honarmand, M., and Ghanbari, S. (2020). A green approach to synthesis of ZnO nanoparticles using jujube fruit extract and their application in photocatalytic degradation of organic dyes. *Spectrochimica Acta Part A: Molecular and Biomolecular Spectroscopy*, 229, 117961. https://doi.org/10.1016/j.saa.2019.117961

Gondal, M. A., Drmosh, Q. A., Yamani, Z. H., and Saleh, T. A. (2009). Synthesis of ZnO_2 nanoparticles by laser ablation in liquid and their annealing

transformation into ZnO nanoparticles. *Applied Surface Science*, 256(1), 298–304. https://doi.org/10.1016/j.apsusc.2009.08.019

Gopakumar, D. A., Pasquini, D., Henrique, M. A., De Morais, L. C., Grohens, Y., and Thomas, S. (2017). Meldrum's acid modified cellulose nanofiber-based polyvinylidene fluoride microfiltration membrane for dye water treatment and nanoparticle removal. *ACS Sustainable Chemistry and Engineering*, 5(2), 2026–2033. https://doi.org/10.1021/acssuschemeng.6b02952

Gowthambabu, V., Balamurugan, A., Dhivya Bharathy, R., Satheeshkumar, S., and Kanmani, S. S. (2021). ZnO nanoparticles as efficient sunlight driven photocatalyst prepared by solution combustion method involved lime juice as biofuel. *Spectrochimica Acta Part A: Molecular and Biomolecular Spectroscopy*, 258, 119857. https://doi.org/10.1016/j.saa.2021.119857

Gu, D., Qin, Y., Wen, Y., Qin, L., and Seo, H. J. (2017). Photochemical and magnetic activities of $FeTiO_3$ nanoparticles by electro-spinning synthesis. *Journal of the Taiwan Institute of Chemical Engineers*, 78, 431–437. https://doi.org/10.1016/j.jtice.2017.04.003

Guan, Y., Yu, H.-Y., Abdalkarim, S. Y. H., Wang, C., Tang, F., Marek, J., Chen, W.-L., Militky, J., and Yao, J.-M. (2019). Green one-step synthesis of ZnO/cellulose nanocrystal hybrids with modulated morphologies and superfast absorption of cationic dyes. *International Journal of Biological Macromolecules*, 132, 51–62. https://doi.org/10.1016/j.ijbiomac.2019.03.104

Guerra, E., Llompart, M., and Garcia-Jares, C. (2018). Analysis of dyes in cosmetics: Challenges and recent developments. *Cosmetics*, 5(3), 47. https://doi.org/10.3390/cosmetics5030047

Guibal, E., and Roussy, J. (2007). Coagulation and flocculation of dye-containing solutions using a biopolymer (Chitosan). *Reactive and Functional Polymers*, 67(1), 33–42. https://doi.org/10.1016/j.reactfunctpolym.2006.08.008

Gulino, G., Vieira, R., Amadou, J., Nguyen, P., Ledoux, M. J., Galvagno, S., Centi, G., and Pham-Huu, C. (2005). C_2H_6 as an active carbon source for a large scale synthesis of carbon nanotubes by chemical vapour deposition. *Applied Catalysis A: General*, 279(1–2), 89–97. https://doi.org/10.1016/j.apcata.2004.10.016

Guo, X., Zhang, Q., Ding, X., Shen, Q., Wu, C., Zhang, L., and Yang, H. (2016). Synthesis and application of several sol–gel-derived materials via sol–gel process combining with other technologies: A review. *Journal of Sol-Gel Science and Technology*, 79(2), 328–358. https://doi.org/10.1007/s10971-015-3935-6

Hagan, E., and Poulin, J. (2021). Statistics of the early synthetic dye industry. *Heritage Science*, 9(1), 33. https://doi.org/10.1186/s40494-021-00493-5

Hameed, H., Waheed, A., Sharif, M. S., Saleem, M., Afreen, A., Tariq, M., Kamal, A., Al-onazi, W. A., Al Farraj, D. A., Ahmad, S., and Mahmoud, R. M. (2023). Green synthesis of zinc oxide (ZnO) nanoparticles from green algae and their assessment in various biological applications. *Micromachines*, 14(5), 928. https://doi.org/10.3390/mi14050928

Hammed, A. M., Prajapati, S. K., Simsek, S., and Simsek, H. (2016). Growth regime and environmental remediation of microalgae. *Algae*, 31(3), 189–204. https://doi.org/10.4490/algae.2016.31.8.28

Hamouda, R. A., Hussein, M. H., Abo-elmagd, R. A., and Bawazir, S. S. (2019). Synthesis and biological characterization of silver nanoparticles derived from the cyanobacterium *Oscillatoria limnetica*. *Scientific Reports*, 9(1), 13071. https://doi.org/10.1038/s41598-019-49444-y

Hasnidawani, J. N., Azlina, H. N., Norita, H., Bonnia, N. N., Ratim, S., and Ali, E. S. (2016). Synthesis of ZnO nanostructures using Sol-Gel method. *Procedia Chemistry*, 19, 211–216. https://doi.org/10.1016/j.proche.2016.03.095

Hassan, M. L., Berglund, L., Abou Elseoud, W. S., Hassan, E. A., and Oksman, K. (2021). Effect of pectin extraction method on properties of cellulose nanofibers isolated from sugar beet pulp. *Cellulose*, 28(17), 10905–10920. https://doi.org/10.1007/s10570-021-04223-9

Heise, K., Kontturi, E., Allahverdiyeva, Y., Tammelin, T., Linder, M. B., Nonappa, and Ikkala, O. (2021). Nanocellulose: Recent fundamental advances and emerging biological and biomimicking applications. *Advanced Materials*, 33(3), 2004349. https://doi.org/10.1002/adma.202004349

Higgins, S. N., Malkin, S. Y., Todd Howell, E., Guildford, S. J., Campbell, L., Hiriart-Baer, V., and Hecky, R. E. (2008). An ecological review of *Cladophora glomerata* (chlorophyta) in the laurentian great lakes. *Journal of Phycology*, 44(4), 839–854. https://doi.org/10.1111/j.1529-8817.2008.00538.x

Holme, I. (2006). Sir William Henry Perkin: A review of his life, work and legacy. *Coloration Technology*, 122(5), 235–251. https://doi.org/10.1111/j.1478-4408.2006.00041.x

Hu, C., Hu, X., Li, R., and Xing, Y. (2020). MOF derived ZnO/C nanocomposite with enhanced adsorption capacity and photocatalytic performance under sunlight. *Journal of Hazardous Materials*, 385, 121599. https://doi.org/10.1016/j.jhazmat.2019.121599

Husseiny, M. I., El-Aziz, M. A., Badr, Y., and Mahmoud, M. A. (2007). Biosynthesis of gold nanoparticles using *Pseudomonas aeruginosa*. *Spectrochimica Acta Part A: Molecular and Biomolecular Spectroscopy*, 67(3–4), 1003–1006. https://doi.org/10.1016/j.saa.2006.09.028

Ihaddaden, S., Aberkane, D., Boukerroui, A., and Robert, D. (2022). Removal of methylene blue (basic dye) by coagulation-flocculation with biomaterials

(bentonite and *Opuntia ficus indica*). *Journal of Water Process Engineering*, 49, 102952. https://doi.org/10.1016/j.jwpe.2022.102952

Imran, M., Crowley, D. E., Khalid, A., Hussain, S., Mumtaz, M. W., and Arshad, M. (2015). Microbial biotechnology for decolorization of textile wastewaters. *Reviews in Environmental Science and Bio/Technology*, 14(1), 73–92. https://doi.org/10.1007/s11157-014-9344-4

Indraningsih, A. W. (2014). Natural dyes from plants extract and its applications in indonesian textile small medium scale enterprise. *Eksergi*, 11(1), 16. https://doi.org/10.31315/e.v11i1.327

Iskandar, F. (2009). Nanoparticle processing for optical applications – A review. *Advanced Powder Technology*, 20(4), 283–292. https://doi.org/10.1016/j.apt.2009.07.001

Islam, A., Sharma, A., Chaturvedi, R., and Kumar Singh, P. (2021). Synthesis and structural analysis of zinc oxide nano particle by chemical method. *Materials Today: Proceedings*, 45, 3670–3673. https://doi.org/10.1016/j.matpr.2021.01.281

Islam, M., Wattoo, O. M., and Saleem, S. (2023). Environmental regulations and their implications for global sustainability. *Pakistan Journal of Humanities and Social Sciences*, 11(3). https://doi.org/10.52131/pjhss.2023.1103.0665

Ismael, M., Sharma, A., and Kumar, N. (2024). An extensive catalytic potential of sustainable TiO_2-based materials fabricated via flame spray pyrolysis: A comprehensive review. *Sustainable Materials and Technologies*, 40, e00826. https://doi.org/10.1016/j.susmat.2024.e00826

Ismail, M., Akhtar, K., Khan, M. I., Kamal, T., Khan, M. A., M. Asiri, A., Seo, J., andKhan, S. B. (2019). Pollution, toxicity and carcinogenicity of organic dyes and their catalytic bio-remediation. *Current Pharmaceutical Design*, 25(34), 3645–3663. https://doi.org/10.2174/1381612825666191021142026

Ito, T., Adachi, Y., Yamanashi, Y., and Shimada, Y. (2016). Long–term natural remediation process in textile dye–polluted river sediment driven by bacterial community changes. *Water Research*, 100, 458–465. https://doi.org/10.1016/j.watres.2016.05.050

Jain, N., Bhargava, A., and Panwar, J. (2014). Enhanced photocatalytic degradation of methylene blue using biologically synthesized “protein-capped” ZnO nanoparticles. *Chemical Engineering Journal*, 243, 549–555. https://doi.org/10.1016/j.cej.2013.11.085

Jamkhande, P. G., Ghule, N. W., Bamer, A. H., and Kalaskar, M. G. (2019). Metal nanoparticles synthesis: An overview on methods of preparation, advantages and disadvantages, and applications. *Journal of Drug Delivery Science and Technology*, 53, 101174. https://doi.org/10.1016/j.jddst.2019.101174

Jmel, M. A., Anders, N., Ben Messaoud, G., Marzouki, M. N., Spiess, A., and Smaali, I. (2019). The stranded macroalga *Ulva lactuca* as a new alternative source of cellulose: Extraction, physicochemical and rheological characterization. *Journal of Cleaner Production*, 234, 1421–1427. https://doi.org/10.1016/j.jclepro.2019.06.225

Joseph, C. G., and Elilarasi, L. (2017). Removal of methylene blue dye from aqueous solution using a newly synthesized TiO_2 -SiO_2 photocatalyst in the presence of active chlorine species. *IOP Conference Series: Materials Science and Engineering*, 206, 012090. https://doi.org/10.1088/1757-899X/206/1/012090

Joudeh, N., and Linke, D. (2022). Nanoparticle classification, physicochemical properties, characterization, and applications: A comprehensive review for biologists. *Journal of Nanobiotechnology*, 20(1), 262. https://doi.org/10.1186/s12951-022-01477-8

Kalyani, D. C., Telke, A. A., Dhanve, R. S., and Jadhav, J. P. (2009). Ecofriendly biodegradation and detoxification of Reactive Red 2 textile dye by newly isolated *Pseudomonas* sp. SUK1. *Journal of Hazardous Materials*, 163(2–3), 735–742. https://doi.org/10.1016/j.jhazmat.2008.07.020

Kamei, Y., Sueyoshi, M., Hayashi, K., Terada, R., and Nozaki, H. (2009). The novel anti-Propionibacterium acnes compound, Sargafuran, found in the marine brown alga *Sargassum macrocarpum*. *The Journal of Antibiotics*, 62(5), 259–263. https://doi.org/10.1038/ja.2009.25

Kargarzadeh, H., Ioelovich, M., Ahmad, I., Thomas, S., and Dufresne, A. (2017). *Methods for extraction of nanocellulose from various sources*. In H. Kargarzadeh, I. Ahmad, S. Thomas, and A. Dufresne (Eds.), Handbook of nanocellulose and cellulose nanocomposites (1st ed., pp. 1–49). Wiley. https://doi.org/10.1002/9783527689972.ch1

Karim, Z., Afrin, S., Husain, Q., and Danish, R. (2017). Necessity of enzymatic hydrolysis for production and functionalization of nanocelluloses. *Critical Reviews in Biotechnology*, 37(3), 355–370. https://doi.org/10.3109/07388551.2016.1163322

Karthikeyan, S., Balasubramanian, R., and Iyer, C. S. P. (2007). Evaluation of the marine algae *Ulva fasciata* and *Sargassum* sp. For the biosorption of Cu(II) from aqueous solutions. *Bioresource Technology*, 98(2), 452–455. https://doi.org/10.1016/j.biortech.2006.01.010

Kathing, C., and Saini, G. (2022). A review of various treatment methods for the removal of dyes from textile effluent. *Recent Progress in Materials*, 04(04), 1–15. https://doi.org/10.21926/rpm.2204028

Kavyashree, M. (2020). *Printing of textiles using natural dyes: A global sustainable approach*. In A. Kumar Samanta, N. S. Awwad, and H. Majdooa Algarni (Eds.), Chemistry and Technology of Natural and Synthetic Dyes and Pigments. IntechOpen. https://doi.org/10.5772/intechopen.93161

Khalafi, T., Buazar, F., and Ghanemi, K. (2019). Phycosynthesis and enhanced photocatalytic activity of Zinc Oxide nanoparticles toward organosulfur pollutants. *Scientific Reports*, 9(1), 6866. https://doi.org/10.1038/s41598-019-43368-3

Khalil, M. I., Al-Qunaibit, M. M., Al-zahem, A. M., and Labis, J. P. (2014). Synthesis and characterization of ZnO nanoparticles by thermal decomposition of a curcumin zinc complex. *Arabian Journal of Chemistry*, 7(6), 1178–1184. https://doi.org/10.1016/j.arabjc.2013.10.025

Khan, F., Shahid, A., Zhu, H., Wang, N., Javed, M. R., Ahmad, N., Xu, J., Alam, Md. A., and Mehmood, M. A. (2022). Prospects of algae-based green synthesis of nanoparticles for environmental applications. *Chemosphere*, 293, 133571. https://doi.org/10.1016/j.chemosphere.2022.133571

Khan, I., Saeed, K., and Khan, I. (2019). Nanoparticles: Properties, applications and toxicities. *Arabian Journal of Chemistry*, 12(7), 908–931. https://doi.org/10.1016/j.arabjc.2017.05.011

Khan, I., Saeed, K., Ali, N., Khan, I., Zhang, B., and Sadiq, M. (2020). Heterogeneous photodegradation of industrial dyes: An insight to different mechanisms and rate affecting parameters. *Journal of Environmental Chemical Engineering*, 8(5), 104364. https://doi.org/10.1016/j.jece.2020.104364

Khan, S., and Malik, A. (2018). Toxicity evaluation of textile effluents and role of native soil bacterium in biodegradation of a textile dye. *Environmental Science and Pollution Research*, 25(5), 4446–4458. https://doi.org/10.1007/s11356-017-0783-7

Khan, S., Noor, T., Iqbal, N., and Yaqoob, L. (2024). Photocatalytic dye degradation from textile wastewater: A review. *ACS Omega*, 9(20), 21751–21767. https://doi.org/10.1021/acsomega.4c00887

Khan, Y., Sadia, H., Ali Shah, S. Z., Khan, M. N., Shah, A. A., Ullah, N., Ullah, M. F., Bibi, H., Bafakeeh, O. T., Khedher, N. B., Eldin, S. M., Fadhl, B. M., and Khan, M. I. (2022). Classification, synthetic, and sharacterization approaches to nanoparticles, and their applications in various fields of nanotechnology: A review. *Catalysts*, 12(11), 1386. https://doi.org/10.3390/catal12111386

Khattab, T. A., Abdelrahman, M. S., and Rehan, M. (2020). Textile dyeing industry: Environmental impacts and remediation. *Environmental Science and Pollution Research*, 27(4), 3803–3818. https://doi.org/10.1007/s11356-019-07137-z

Khodaie, M., Ghasemi, N., Moradi, B., and Rahimi, M. (2013). Removal of methylene blue from wastewater by adsorption onto $ZnCl_2$ activated corn husk carbon equilibrium studies. *Journal of Chemistry*, 2013(1), 383985. https://doi.org/10.1155/2013/383985

Kim, M., Osone, S., Kim, T., Higashi, H., and Seto, T. (2017). Synthesis of nanoparticles by laser ablation: A review. *KONA Powder and Particle Journal*, 34(0), 80–90. https://doi.org/10.14356/kona.2017009

Kim, S. P., Choi, M. Y., and Choi, H. C. (2016). Photocatalytic activity of SnO_2 nanoparticles in methylene blue degradation. *Materials Research Bulletin*, 74, 85–89. https://doi.org/10.1016/j.materresbull.2015.10.024

Kiran, B. R., and Venkata Mohan, S. (2021). Microalgal cell biofactory—Therapeutic, nutraceutical and functional food applications. *Plants*, 10(5), 836. https://doi.org/10.3390/plants10050836

Kirthi, A. V., Rahuman, A. A., Rajakumar, G., Marimuthu, S., Santhoshkumar, T., Jayaseelan, C., Elango, G., Zahir, A. A., Kamaraj, C., and Bagavan, A. (2011). Biosynthesis of titanium dioxide nanoparticles using bacterium *Bacillus subtilis*. *Materials Letters*, 65(17–18), 2745–2747. https://doi.org/10.1016/j.matlet.2011.05.077

Kishor, R., Saratale, G. D., Saratale, R. G., Romanholo Ferreira, L. F., Bilal, M., Iqbal, H. M. N., and Bharagava, R. N. (2021). Efficient degradation and detoxification of methylene blue dye by a newly isolated ligninolytic enzyme producing bacterium *Bacillus albus* MW407057. *Colloids and Surfaces B: Biointerfaces*, 206, 111947. https://doi.org/10.1016/j.colsurfb.2021.111947

Kofidis, T., Strüber, M., Wilhelmi, M., Anssar, M., Simon, A., Harringer, W., and Haverich, A. (2001). Reversal of severe vasoplegia with single-dose methylene blue after heart transplantation. *The Journal of Thoracic and Cardiovascular Surgery*, 122(4), 823–824. https://doi.org/10.1067/mtc.2001.115153

Kok, J. M.-L., Jee, J.-M., Chew, L.-Y., and Wong, C.-L. (2016). The potential of the brown seaweed *Sargassum polycystum* against acne vulgaris. *Journal of Applied Phycology*, 28(5), 3127–3133. https://doi.org/10.1007/s10811-016-0825-4

Krishna Moorthy, A., Govindarajan Rathi, B., Shukla, S. P., Kumar, K., and Shree Bharti, V. (2021). Acute toxicity of textile dye Methylene blue on growth and metabolism of selected freshwater microalgae. *Environmental Toxicology and Pharmacology*, 82, 103552. https://doi.org/10.1016/j.etap.2020.103552

Król, A., Pomastowski, P., Rafińska, K., Railean-Plugaru, V., and Buszewski, B. (2017). Zinc oxide nanoparticles: Synthesis, antiseptic activity and toxicity mechanism. *Advances in Colloid and Interface Science*, 249, 37–52. https://doi.org/10.1016/j.cis.2017.07.033

Kulkarni, N., and Muddapur, U. (2014). Biosynthesis of metal nanoparticles: A review. *Journal of Nanotechnology*, 2014, 1–8. https://doi.org/10.1155/2014/510246

Kumar, M., and Ando, Y. (2010). Chemical vapor deposition of carbon nanotubes: A review on growth mechanism and mass production. *Journal of Nanoscience and Nanotechnology*, 10(6), 3739–3758. https://doi.org/10.1166/jnn.2010.2939

Kumar, P. S., Joshiba, G. J., Femina, C. C., Varshini, P., Priyadharshini, S., Karthick, M. S. A., and Jothirani, R. (2019). A critical review on recent developments in the low-cost adsorption of dyes from wastewater. *Desalination and Water Treatment*, 172, 395–416. https://doi.org/10.5004/dwt.2019.24613

Kumari, K., and Abraham, T. (2007). Biosorption of anionic textile dyes by nonviable biomass of fungi and yeast. *Bioresource Technology*, 98(9), 1704–1710. https://doi.org/10.1016/j.biortech.2006.07.030

Kurniawan, T. W., Sulistyarti, H., Rumhayati, B., and Sabarudin, A. (2023). Cellulose nanocrystals (CNCs) and cellulose nanofibers (CNFs) as adsorbents of heavy metal ions. *Journal of Chemistry*, 2023, 1–36. https://doi.org/10.1155/2023/5037027

Kuspanov, Z., Bakbolat, B., Baimenov, A., Issadykov, A., Yeleuov, M., and Daulbayev, C. (2023). Photocatalysts for a sustainable future: Innovations in large-scale environmental and energy applications. *Science of The Total Environment*, 885, 163914. https://doi.org/10.1016/j.scitotenv.2023.163914

Lafarga, T., Acién-Fernández, F. G., Castellari, M., Villaró, S., Bobo, G., and Aguiló-Aguayo, I. (2019). Effect of microalgae incorporation on the physicochemical, nutritional, and sensorial properties of an innovative broccoli soup. *LWT*, 111, 167–174. https://doi.org/10.1016/j.lwt.2019.05.037

Lahiri, D., Nag, M., Dutta, B., Dey, A., Sarkar, T., Pati, S., Edinur, H. A., Abdul Kari, Z., Mohd Noor, N. H., and Ray, R. R. (2021). Bacterial cellulose: Production, characterization, and application as antimicrobial agent. *International Journal of Molecular Sciences*, 22(23), 12984. https://doi.org/10.3390/ijms222312984

Lakshmi, D. S., Trivedi, N., and Reddy, C. R. K. (2017). Synthesis and characterization of seaweed cellulose derived carboxymethyl cellulose. *Carbohydrate Polymers*, 157, 1604–1610. https://doi.org/10.1016/j.carbpol.2016.11.042

Lamm, M. E., Li, K., Qian, J., Wang, L., Lavoine, N., Newman, R., Gardner, D. J., Li, T., Hu, L., Ragauskas, A. J., Tekinalp, H., Kunc, V., and Ozcan, S. (2021). Recent advances in functional materials through cellulose nanofiber templating. *Advanced Materials*, 33(12), 2005538. https://doi.org/10.1002/adma.202005538

Lanjwani, M. F., Tuzen, M., Khuhawar, M. Y., and Saleh, T. A. (2024). Trends in photocatalytic degradation of organic dye pollutants using nanoparticles: A review. *Inorganic Chemistry Communications*, 159, 111613. https://doi.org/10.1016/j.inoche.2023.111613

Latour, R. A. (2020). Fundamental principles of the thermodynamics and kinetics of protein adsorption to material surfaces. *Colloids and Surfaces B: Biointerfaces*, 191, 110992. https://doi.org/10.1016/j.colsurfb.2020.110992

Lee, H. S., Suh, J. H., Kim, I. B., and Yoon, T. (2004). Effect of aluminum in two-metal biosorption by an algal biosorbent. *Minerals Engineering*, 17(4), 487–493. https://doi.org/10.1016/j.mineng.2004.01.002

Lee, H., Song, M. Y., Jurng, J., and Park, Y.-K. (2011). The synthesis and coating process of TiO_2 nanoparticles using CVD process. *Powder Technology*, 214(1), 64–68. https://doi.org/10.1016/j.powtec.2011.07.036

Lefatshe, K., Muiva, C. M., and Kebaabetswe, L. P. (2017). Extraction of nanocellulose and in-situ casting of ZnO/cellulose nanocomposite with enhanced photocatalytic and antibacterial activity. *Carbohydrate Polymers*, 164, 301–308. https://doi.org/10.1016/j.carbpol.2017.02.020

Li, J., Bendi, R., Malla, R., Shah, K. J., Parida, K., and You, Z. (2021). Cellulose nanofibers-based green nanocomposites for water environmental sustainability: A review. *Emergent Materials*, 4(5), 1259–1273. https://doi.org/10.1007/s42247-021-00300-8

Li, N., Wang, Q., Zhou, J., Li, S., Liu, J., and Chen, H. (2022). Insight into the progress on natural dyes: Sources, structural features, health effects, challenges, and potential. *Molecules*, 27(10), 3291. https://doi.org/10.3390/molecules27103291

Li, R., Tian, D., Chen, L., Zhuang, B., Feng, H., Li, Q., Yu, L., and Ling, Y. (2023). The application of cellulose nanofibrils in energy systems. *Batteries*, 9(8), 399. https://doi.org/10.3390/batteries9080399

Li, W., Mu, B., and Yang, Y. (2019). Feasibility of industrial-scale treatment of dye wastewater via bio-adsorption technology. *Bioresource Technology*, 277, 157–170. https://doi.org/10.1016/j.biortech.2019.01.002

Li, X., Chen, Y., Tao, Y., Shen, L., Xu, Z., Bian, Z., and Li, H. (2022). Challenges of photocatalysis and their coping strategies. *Chem Catalysis*, 2(6), 1315–1345. https://doi.org/10.1016/j.checat.2022.04.007

Li, X., Li, H., Wang, X., Xu, D., You, T., Wu, Y., and Xu, F. (2021). Facile in situ fabrication of ZnO-embedded cellulose nanocomposite films with antibacterial properties and enhanced mechanical strength via hydrogen bonding interactions. *International Journal of Biological Macromolecules*, 183, 760–771. https://doi.org/10.1016/j.ijbiomac.2021.04.175

Li, X., Xu, H., Chen, Z.-S., and Chen, G. (2011). Biosynthesis of nanoparticles by microorganisms and their applications. *Journal of Nanomaterials*, 2011, 1–16. https://doi.org/10.1155/2011/270974

Li, Y., Sun, H., Zhang, Y., Xu, M., and Shi, S. Q. (2019). The three-dimensional heterostructure synthesis of ZnO/cellulosic fibers and its application for rubber composites. *Composites Science and Technology*, 177, 10–17. https://doi.org/10.1016/j.compscitech.2019.04.012

Lim, R., Kiew, P. L., Lam, M. K., Yeoh, W. M., and Ho, M. Y. (2021). Corn starch/PVA bioplastics—The properties and biodegradability study using *Chlorella vulgaris*cultivation. *Asia-Pacific Journal of Chemical Engineering*, 16(3), e2622. https://doi.org/10.1002/apj.2622

Lin, J., Ye, W., Xie, M., Seo, D. H., Luo, J., Wan, Y., and Van Der Bruggen, B. (2023). Environmental impacts and remediation of dye-containing wastewater. *Nature Reviews Earth and Environment*, 4(11), 785–803. https://doi.org/10.1038/s43017-023-00489-8

Liu, G., Li, J., Li, X., Pan, X., and Qian, C. (2021). Preparation and properties of novel superhydrophobic cellulose nanofiber aerogels. *Journal of Nanomaterials*, 2021, 1–8. https://doi.org/10.1155/2021/2631405

Liu, Y., Ahmed, S., Sameen, D. E., Wang, Y., Lu, R., Dai, J., Li, S., and Qin, W. (2021). A review of cellulose and its derivatives in biopolymer-based for food packaging application. *Trends in Food Science and Technology*, 112, 532–546. https://doi.org/10.1016/j.tifs.2021.04.016

Louati, I., Elloumi-Mseddi, J., Cheikhrouhou, W., Hadrich, B., Nasri, M., Aifa, S., Woodward, S., and Mechichi, T. (2020). Simultaneous cleanup of Reactive Black 5 and cadmium by a desert soil bacterium. *Ecotoxicology and Environmental Safety*, 190, 110103. https://doi.org/10.1016/j.ecoenv.2019.110103

Lu, Z., Zhang, H., Toivakka, M., and Xu, C. (2024). Current progress in functionalization of cellulose nanofibers (CNFs) for active food packaging. *International Journal of Biological Macromolecules*, 267, 131490. https://doi.org/10.1016/j.ijbiomac.2024.131490

Luque-Morales, P. A., Lopez-Peraza, A., Nava-Olivas, O. J., Amaya-Parra, G., Baez-Lopez, Y. A., Orozco-Carmona, V. M., Garrafa-Galvez, H. E., and Chinchillas-Chinchillas, M. D. J. (2021). ZnO semiconductor nanoparticles and their application in photocatalytic degradation of various organic dyes. *Materials*, 14(24), 7537. https://doi.org/10.3390/ma14247537

Madivoli, E. S., Kareru, P. G., Gachanja, A. N., Mugo, S. M., and Makhanu, D. S. (2019). Synthesis and characterization of dialdehyde cellulose nanofibers from *O. sativa* husks. *SN Applied Sciences*, 1(7), 723. https://doi.org/10.1007/s42452-019-0769-9

Madivoli, E. S., Kareru, P. G., Gachanja, A. N., Mugo, S. M., Sujee, D. M., and Fromm, K. M. (2022). Isolation of cellulose nanofibers from *Oryza sativa* residues via TEMPO mediated oxidation. *Journal of Natural Fibers*, 19(4), 1310–1322. https://doi.org/10.1080/15440478.2020.1764454

Mahajan, U., Prajapat, K., Dhonde, M., Sahu, K., and Shirage, P. M. (2024). Natural dyes for dye-sensitized solar cells (DSSCs): An overview of extraction, characterization and performance. *Nano-Structures and Nano-Objects*, 37, 101111. https://doi.org/10.1016/j.nanoso.2024.101111

Mahamuni, P. P., Patil, P. M., Dhanavade, M. J., Badiger, M. V., Shadija, P. G., Lokhande, A. C., and Bohara, R. A. (2019). Synthesis and characterization of zinc oxide nanoparticles by using polyol chemistry for their antimicrobial and antibiofilm activity. *Biochemistry and Biophysics Reports*, 17, 71–80. https://doi.org/10.1016/j.bbrep.2018.11.007

Mahana, A., Guliy, O. I., Momin, S. C., Lalmuanzeli, R., and Mehta, S. K. (2020). Sunlight-driven photocatalytic degradation of methylene blue using ZnO nanowires prepared through ultrasonication-assisted biological process using aqueous extract of *Anabaena doliolum*. *Optical Materials*, 108, 110205. https://doi.org/10.1016/j.optmat.2020.110205

Mahltig, B. (2024). Overview on natural dyes and their IR-spectra – Part II: Indigo containing plant dyes. *Communications in Development and Assembling of Textile Products*, 5(1), 66–80. https://doi.org/10.25367/cdatp.2024.5.p66-80

Maity, C. K., De, S., Verma, K., Moniruzzaman, M., and Sahoo, S. (2023). Nanocellulose: A versatile nanostructure for energy storage applications. *Industrial Crops and Products*, 204, 117218. https://doi.org/10.1016/j.indcrop.2023.117218

Malla, M. A., Dubey, A., Yadav, S., Kumar, A., Hashem, A., and Abd Allah, E. F. (2018). Understanding and designing the strategies for the microbe-mediated remediation of environmental contaminants using omics approaches. *Frontiers in Microbiology*, 9, 1132. https://doi.org/10.3389/fmicb.2018.01132

Manawi, Y. M., Ihsanullah, Samara, A., Al-Ansari, T., and Atieh, M. A. (2018). A Review of carbon nanomaterials' synthesis via the chemical vapor deposition (CVD) method. *Materials*, 11(5), 822. https://doi.org/10.3390/ma11050822

Mandal, A. K., Katuwal, S., Tettey, F., Gupta, A., Bhattarai, S., Jaisi, S., Bhandari, D. P., Shah, A. K., Bhattarai, N., and Parajuli, N. (2022). Current research on Zinc Oxide nanoparticles: Synthesis, characterization, and biomedical applications. *Nanomaterials*, 12(17), 3066. https://doi.org/10.3390/nano12173066

Mandal, A., and Chakrabarty, D. (2011). Isolation of nanocellulose from waste sugarcane bagasse (SCB) and its characterization. *Carbohydrate Polymers*, 86(3), 1291–1299. https://doi.org/10.1016/j.carbpol.2011.06.030

Mansour, S., Farha, A., and Kotkata, M. (2017). Synthesis and study of ZnO nanoparticles by polymer pyrolysis route using two different polymerization initiators. *International Journal of Applied Ceramic Technology*, 14(6), 1213–1221. https://doi.org/10.1111/ijac.12751

Maresca, D., and Mauriello, G. (2022). Development of antimicrobial cellulose nanofiber-based films activated with nisin for food packaging applications. *Foods*, 11(19), 3051. https://doi.org/10.3390/foods11193051

Marin, N. M., Pascu, L. F., Demba, A., Nita-Lazar, M., Badea, I. A., and Aboul-Enein, H. Y. (2019). Removal of the Acid Orange 10 by ion exchange and microbiological methods. *International Journal of Environmental Science and Technology*, 16(10), 6357–6366. https://doi.org/10.1007/s13762-018-2164-2

Martelli-Tosi, M., Torricillas, M. D. S., Martins, M. A., Assis, O. B. G. D., and Tapia-Blácido, D. R. (2016). Using commercial enzymes to poduce cellulose nanofibers from soybean straw. *Journal of Nanomaterials*, 2016, 1–10. https://doi.org/10.1155/2016/8106814

Maurya, N. S., Mittal, A. K., Cornel, P., and Rother, E. (2006). Biosorption of dyes using dead macro fungi: Effect of dye structure, ionic strength and pH. *Bioresource Technology*, 97(3), 512–521. https://doi.org/10.1016/j.biortech.2005.02.045

Mautner, A. (2020). Nanocellulose water treatment membranes and filters: A review. *Polymer International*, 69(9), 741–751. https://doi.org/10.1002/pi.5993

Máximo, C., Amorim, M. T. P., and Costa-Ferreira, M. (2003). Biotransformation of industrial reactive azo dyes by *Geotrichum* sp. CCMI 1019. *Enzyme and Microbial Technology*, 32(1), 145–151. https://doi.org/10.1016/S0141-0229(02)00281-8

Mehta, S. K., and Gaur, J. P. (2001). Removal of Ni and Cu from single and binary metalsolutions by free and immobilized *Chlorella vulgaris*. *European Journal of Protistology*, 37(3), 261–271. https://doi.org/10.1078/0932-4739-00813

Meireles, G., Daam, M. A., Sanches, A. L. M., Zanoni, M. V. B., Soares, A. M. V. M., Gravato, C., and Oliveira, D. P. D. (2018). Red disperse dyes (DR 60, DR 73 and DR 78) at environmentally realistic concentrations impact biochemical profile of early life stages of zebrafish (*Danio rerio*). *Chemico-Biological Interactions*, 292, 94–100. https://doi.org/10.1016/j.cbi.2018.07.007

Meissner, P. E., Mandi, G., Coulibaly, B., Witte, S., Tapsoba, T., Mansmann, U., Rengelshausen, J., Schiek, W., Jahn, A., Walter-Sack, I., Mikus, G., Burhenne, J., Riedel, K.-D., Schirmer, R. H., Kouyaté, B., and Müller, O. (2006). Methylene blue for malaria in Africa: Results from a dose-finding study in combination with chloroquine. *Malaria Journal*, 5(1), 84. https://doi.org/10.1186/1475-2875-5-84

Mekuye, B., and Abera, B. (2023). Nanomaterials: An overview of synthesis, classification, characterization, and applications. *Nano Select*, 4(8), 486–501. https://doi.org/10.1002/nano.202300038

Michie, A. G. H., and Thornton, R. (1953). The printing efficiency of vat dyes. *Journal of the Society of Dyers and Colourists*, 69(13), 629–647. https://doi.org/10.1111/j.1478-4408.1953.tb02806.x

Millbern, Z., Trettin, A., Wu, R., Demmler, M., and Vinueza, N. R. (2024). Synthetic dyes: A mass spectrometry approach and applications. *Mass Spectrometry Reviews*, 43(2), 327–344. https://doi.org/10.1002/mas.21818

Minhas, F. T., Arslan, G., Gubbuk, I. H., Akkoz, C., Ozturk, B. Y., Asıkkutlu, B., Arslan, U., and Ersoz, M. (2018). Evaluation of antibacterial properties on polysulfone composite membranes using synthesized biogenic silver nanoparticles with *Ulva compressa* (L.) Kütz. and *Cladophora glomerata* (L.) Kütz. extracts. *International Journal of Biological Macromolecules*, 107, 157–165. https://doi.org/10.1016/j.ijbiomac.2017.08.149

Mohammad, A. W., Teow, Y. H., Ang, W. L., Chung, Y. T., Oatley-Radcliffe, D. L., and Hilal, N. (2015). Nanofiltration membranes review: Recent advances and future prospects. *Desalination*, 356, 226–254. https://doi.org/10.1016/j.desal.2014.10.043

Mohammad, A., Kapoor, K., and Mobin, S. M. (2016). Improved photocatalytic degradation of organic dyes by ZnO-nanoflowers. *ChemistrySelect*, 1(13), 3483–3490. https://doi.org/10.1002/slct.201600476

Moohan, J., Stewart, S. A., Espinosa, E., Rosal, A., Rodríguez, A., Larrañeta, E., Donnelly, R. F., and Domínguez-Robles, J. (2019). Cellulose nanofibers and other biopolymers for biomedical applications. A review. *Applied Sciences*, 10(1), 65. https://doi.org/10.3390/app10010065

Morikawa, T., Uraguchi, Y., Sanda, S., Nakagawa, S., and Sawayama, S. (2018). Overexpression of DnaJ-like chaperone enhances carotenoid synthesis in *Chlamydomonas reinhardtii*. *Applied Biochemistry and Biotechnology*, 184(1), 80–91. https://doi.org/10.1007/s12010-017-2521-5

Morin, J.-F. (2017). Recent advances in the chemistry of vat dyes for organic electronics. *Journal of Materials Chemistry C*, 5(47), 12298–12307. https://doi.org/10.1039/C7TC03926C

Morozov, Iu. G., Belousova, O. V., Ortega, D., Mafina, M.-K., and Kuznetcov, M. V. (2015). Structural, optical, XPS and magnetic properties of Zn particles capped by ZnO nanoparticles. *Journal of Alloys and Compounds*, 633, 237–245. https://doi.org/10.1016/j.jallcom.2015.01.285

Morriss-Kay, G. M. (2010). The evolution of human artistic creativity. *Journal of Anatomy*, 216(2), 158–176. https://doi.org/10.1111/j.1469-7580.2009.01160.x

Nagarajan, K. J., Ramanujam, N. R., Sanjay, M. R., Siengchin, Suchart., Surya Rajan, B., Sathick Basha, K., Madhu, P., and Raghav, G. R. (2021). A comprehensive review on cellulose nanocrystals and cellulose nanofibers:

Pretreatment, preparation, and characterization. *Polymer Composites*, 42(4), 1588–1630. https://doi.org/10.1002/pc.25929

Namasivayam, C., Jeyakumar, R., and Yamuna, R. T. (1994). Dye removal from wastewater by adsorption on 'waste' Fe(III)/Cr(III) hydroxide. *Waste Management*, 14(7), 643–648. https://doi.org/10.1016/0956-053X(94)90036-1

Narayanan, K. B., and Sakthivel, N. (2011). Green synthesis of biogenic metal nanoparticles by terrestrial and aquatic phototrophic and heterotrophic eukaryotes and biocompatible agents. *Advances in Colloid and Interface Science*, 169(2), 59–79. https://doi.org/10.1016/j.cis.2011.08.004

Narkpiban, K., and Poonsawat, T. (2022). Optimizing cellulose extraction from kenaf (*Hibiscus Cannabinus* L.) fiber by selective retting and hydrothermal pretreatment. *Journal of Natural Fibers*, 19(2), 700–713. https://doi.org/10.1080/15440478.2020.1758982

Naser, H., Alghoul, M. A., Hossain, M. K., Asim, N., Abdullah, M. F., Ali, M. S., Alzubi, F. G., and Amin, N. (2019). The role of laser ablation technique parameters in synthesis of nanoparticles from different target types. *Journal of Nanoparticle Research*, 21(11), 249. https://doi.org/10.1007/s11051-019-4690-3

Navaladian, S., Viswanathan, B., Viswanath, R. P., and Varadarajan, T. K. (2007). Thermal decomposition as route for silver nanoparticles. *Nanoscale Research Letters*, 2(1), 44. https://doi.org/10.1007/s11671-006-9028-2

Navas, D., Fuentes, S., Castro-Alvarez, A., and Chavez-Angel, E. (2021). Review on Sol-Gel synthesis of perovskite and oxide nanomaterials. *Gels*, 7(4), 275. https://doi.org/10.3390/gels7040275

Nehra, M. (2022). Algae as a nutritional and functional food source. *Madridge Journal of Food Technology*, 7(1), 189–199. https://doi.org/10.18689/mjft-1000129

Nemade, K. R., and Waghuley, S. A. (2014). Synthesis of MgO nanoparticles by solvent mixed spray pyrolysis technique for optical investigation. *International Journal of Metals*, 2014, 1–4. https://doi.org/10.1155/2014/389416

Ngulube, T., Gumbo, J. R., Masindi, V., and Maity, A. (2017). An update on synthetic dyes adsorption onto clay based minerals: A state-of-art review. *Journal of Environmental Management*, 191, 35–57. https://doi.org/10.1016/j.jenvman.2016.12.031

Nguyen, N. T. T., Nguyen, T. T. T., Nguyen, D. T. C., and Tran, T. V. (2024). Recent advances and challenges of the green ZnO-based composites biosynthesized using plant extracts for water treatment. *Environmental Science and Pollution Research*. https://doi.org/10.1007/s11356-024-33748-2

Nguyen, T.-H., Lee, K.-H., and Lee, B.-T. (2010). Fabrication of Ag nanoparticles dispersed in PVA nanowire mats by microwave irradiation and electro-spinning. *Materials Science and Engineering: C*, 30(7), 944–950. https://doi.org/10.1016/j.msec.2010.04.012

Norfarhana, A. S., Khoo, P. S., Ilyas, R. A., Ab Hamid, N. H., Aisyah, H. A., Norrrahim, M. N. F., Knight, V. F., Rani, M. S. A., Septevani, A. A., Syafri, E., and Annamalai, P. K. (2024). Exploring of cellulose nanocrystals from lignocellulosic sources as a powerful adsorbent for wastewater remediation. *Journal of Polymers and the Environment*, 32(9), 4071–4101. https://doi.org/10.1007/s10924-024-03227-3

Novais, C., Molina, A. K., Abreu, R. M. V., Santo-Buelga, C., Ferreira, I. C. F. R., Pereira, C., and Barros, L. (2022). Natural food colorants and preservatives: A review, a demand, and a challenge. *Journal of Agricultural and Food Chemistry*, 70(9), 2789–2805. https://doi.org/10.1021/acs.jafc.1c07533

Nuhoglu, Y., Malkoc, E., Gürses, A., and Canpolat, N. (2002). The removal of Cu(II) from aqueous solutions by *Ulothrix zonata*. *Bioresource Technology*, 85(3), 331–333. https://doi.org/10.1016/S0960-8524(02)00098-6

Nurazzi, N. M., Sabaruddin, F. A., Harussani, M. M., Kamarudin, S. H., Rayung, M., Asyraf, M. R. M., Aisyah, H. A., Norrrahim, M. N. F., Ilyas, R. A., Abdullah, N., Zainudin, E. S., Sapuan, S. M., andKhalina, A. (2021). Mechanical performance and applications of CNTs reinforced polymer composites—A review. *Nanomaterials*, 11(9), 2186. https://doi.org/10.3390/nano11092186

Odularu, A. T. (2018). Metal nanoparticles: Thermal decomposition, biomedicinal applications to cancer treatment, and future perspectives. *Bioinorganic Chemistry and Applications*, 2018, 1–6. https://doi.org/10.1155/2018/9354708

Ong, X.-R., Chen, A. X., Li, N., Yang, Y. Y., and Luo, H.-K. (2023). Nanocellulose: Recent advances toward biomedical applications. *Small Science*, 3(2), 2200076. https://doi.org/10.1002/smsc.202200076

Onyancha, D., Mavura, W., Ngila, J. C., Ongoma, P., and Chacha, J. (2008). Studies of chromium removal from tannery wastewaters by algae biosorbents, *Spirogyra condensata* and *Rhizoclonium hieroglyphicum*. J*ournal of Hazardous Materials*, 158(2–3), 605–614. https://doi.org/10.1016/j.jhazmat.2008.02.043

Onyianta, A. J., O'Rourke, D., Sun, D., Popescu, C.-M., and Dorris, M. (2020). High aspect ratio cellulose nanofibrils from macroalgae *Laminaria hyperborea* cellulose extract via a zero-waste low energy process. *Cellulose*, 27(14), 7997–8010. https://doi.org/10.1007/s10570-020-03223-5

Otero, P., López-Martínez, M. I., and García-Risco, M. R. (2019). Application of pressurized liquid extraction (PLE) to obtain bioactive fatty acids and phenols from *Laminaria ochroleuca* collected in Galicia (NW Spain). *Journal of*

Pharmaceutical and Biomedical Analysis, 164, 86–92. https://doi.org/10.1016/j.jpba.2018.09.057

Oyewo, O. A., Adeniyi, A., Sithole, B. B., andOnyango, M. S. (2020). Sawdust-based cellulose nanocrystals incorporated with ZnO nanoparticles as efficient adsorption media in the removal of methylene blue dye. *ACS Omega*, 5(30), 18798–18807. https://doi.org/10.1021/acsomega.0c01924

Ozturk, M., Uysal, I., Gucel, S., Altundag, E., Dogan, Y., and Baslar, S. (2013). Medicinal uses of natural dye-yielding plants in Turkey. *Research Journal of Textile and Apparel*, 17(2), 69–80. https://doi.org/10.1108/RJTA-17-02-2013-B010

Paniz, O. G., Pereira, C. M. P., Pacheco, B. S., Wolke, S. I., Maron, G. K., Mansilla, A., Colepicolo, P., Orlandi, M. O., Osorio, A. G., and Carreño, N. L. V. (2020). Cellulosic material obtained from Antarctic algae biomass. *Cellulose*, 27(1), 113–126. https://doi.org/10.1007/s10570-019-02794-2

Papageorgiou, D. G., Li, Z., Liu, M., Kinloch, I. A., and Young, R. J. (2020). Mechanisms of mechanical reinforcement by graphene and carbon nanotubes in polymer nanocomposites. *Nanoscale*, 12(4), 2228–2267. https://doi.org/10.1039/C9NR06952F

Parashar, M., Shukla, V. K., and Singh, R. (2020). Metal oxides nanoparticles via sol–gel method: A review on synthesis, characterization and applications. *Journal of Materials Science: Materials in Electronics*, 31(5), 3729–3749. https://doi.org/10.1007/s10854-020-02994-8

Park, M., Lee, K. S., Shim, J., Liu, Y., Lee, C., Cho, H., Kim, M. J., Park, S.-J., Yun, Y. J., Kim, H. Y., and Son, D. I. (2016). Environment friendly, transparent nanofiber textiles consolidated with high efficiency PLEDs for wearable electronics. *Organic Electronics*, 36, 89–96. https://doi.org/10.1016/j.orgel.2016.05.030

Patiha, Heraldy, E., Hidayat, Y., and Firdaus, M. (2016). The langmuir isotherm adsorption equation: The monolayer approach. *IOP Conference Series: Materials Science and Engineering*, 107, 012067. https://doi.org/10.1088/1757-899X/107/1/012067

Patti, A., and Acierno, D. (2022). Towards the sustainability of the plastic industry through biopolymers: Properties and potential applications to the textiles world. *Polymers*, 14(4), 692. https://doi.org/10.3390/polym14040692

Pellenz, L., De Oliveira, C. R. S., Da Silva Júnior, A. H., Da Silva, L. J. S., Da Silva, L., Ulson De Souza, A. A., De Souza, S. M. D. A. G. U., Borba, F. H., and Da Silva, A. (2023). A comprehensive guide for characterization of adsorbent materials. *Separation and Purification Technology*, 305, 122435. https://doi.org/10.1016/j.seppur.2022.122435

Pennells, J., Godwin, I. D., Amiralian, N., and Martin, D. J. (2020). Trends in the production of cellulose nanofibers from non-wood sources. *Cellulose*, 27(2), 575–593. https://doi.org/10.1007/s10570-019-02828-9

Pereira, A. G. B., Rodrigues, F. H. A., Paulino, A. T., Martins, A. F., and Fajardo, A. R. (2021). Recent advances on composite hydrogels designed for the remediation of dye-contaminated water and wastewater: A review. *Journal of Cleaner Production*, 284, 124703. https://doi.org/10.1016/j.jclepro.2020.124703

Pereira, L., Coelho, A. V., Viegas, C. A., Santos, M. M. C. D., Robalo, M. P., and Martins, L. O. (2009). Enzymatic biotransformation of the azo dye Sudan Orange G with bacterial CotA-laccase. *Journal of Biotechnology*, 139(1), 68–77. https://doi.org/10.1016/j.jbiotec.2008.09.001

Pérez-Ibarbia, L., Majdanski, T., Schubert, S., Windhab, N., and Schubert, U. S. (2016). Safety and regulatory review of dyes commonly used as excipients in pharmaceutical and nutraceutical applications. *European Journal of Pharmaceutical Sciences*, 93, 264–273. https://doi.org/10.1016/j.ejps.2016.08.026

Periyasamy, A. P. (2024). Recent advances in the remediation of textile-dye-containing wastewater: Prioritizing human health and sustainable wastewater treatment. *Sustainability*, 16(2), 495. https://doi.org/10.3390/su16020495

Pimpin, A., and Srituravanich, W. (2012). Review on micro- and nanolithography techniques and their applications. *Engineering Journal*, 16(1), 37–56. https://doi.org/10.4186/ej.2012.16.1.37

Porrawatkul, P., Pimsen, R., Kuyyogsuy, A., Rattanaburi, P., and Nuengmatcha, P. (2024). Morphology-dependent photocatalytic performance of ZnO nanostructures in organic dye and antibiotic degradation. *International Journal of Environmental Science and Technology*, 21(11), 7397–7414. https://doi.org/10.1007/s13762-024-05530-x

Prakash Menon, M., Selvakumar, R., Suresh Kumar, P., and Ramakrishna, S. (2017). Extraction and modification of cellulose nanofibers derived from biomass for environmental application. *RSC Advances*, 7(68), 42750–42773. https://doi.org/10.1039/C7RA06713E

Prasad Yadav, T., Manohar Yadav, R., and Pratap Singh, D. (2012). Mechanical milling: A top down approach for the synthesis of nanomaterials and nanocomposites. *Nanoscience and Nanotechnology*, 2(3), 22–48. https://doi.org/10.5923/j.nn.20120203.01

Rabani, I., Lee, S.-H., Kim, H.-S., Yoo, J., Hussain, S., Maqbool, T., and Seo, Y.-S. (2021). Engineering-safer-by design ZnO nanoparticles incorporated cellulose nanofiber hybrid for high UV protection and low photocatalytic activity with mechanism. *Journal of Environmental Chemical Engineering*, 9(5), 105845. https://doi.org/10.1016/j.jece.2021.105845

Raghu, S., and Ahmed Basha, C. (2007). Chemical or electrochemical techniques, followed by ion exchange, for recycle of textile dye wastewater. *Journal of Hazardous Materials*, 149(2), 324–330. https://doi.org/10.1016/j.jhazmat.2007.03.087

Rahimi-Ahar, Z., and Rahimi Ahar, L. (2024). Thermal, optical, mechanical, dielectric, and electrical properties of nanocomposites. *European Polymer Journal*, 218, 113337. https://doi.org/10.1016/j.eurpolymj.2024.113337

Randhawa, A., Dutta, S. D., Ganguly, K., Patil, T. V., Patel, D. K., and Lim, K.-T. (2022). A review of properties of nanocellulose, its synthesis, and potential in biomedical applications. *Applied Sciences*, 12(14), 7090. https://doi.org/10.3390/app12147090

Rane, A. V., Kanny, K., Abitha, V. K., andThomas, S. (2018). *Methods for synthesis of nanoparticles and fabrication of nanocomposites*. In Synthesis of Inorganic Nanomaterials (pp. 121–139). Elsevier. https://doi.org/10.1016/B978-0-08-101975-7.00005-1

Rane, A., and Joshi, S. J. (2021). Biodecolorization and biodegradation of dyes: A review. *The Open Biotechnology Journal*, 15(1), 97–108. https://doi.org/10.2174/1874070702115010097

Ranjit, P., Jhansi, V., and Reddy, K. V. (2021). *Conventional wastewater treatment processes.* In N. R. Maddela, L. C. García Cruzatty, and S. Chakraborty (Eds.), Advances in the domain of environmental biotechnology (pp. 455–479). Springer Singapore. https://doi.org/10.1007/978-981-15-8999-7_17

Rashid, T. M., Nayef, U. M., Jabir, M. S., and Mutlak, F. A.-H. (2021). Synthesis and characterization of Au:ZnO (core:shell) nanoparticles via laser ablation. *Optik*, 244, 167569. https://doi.org/10.1016/j.ijleo.2021.167569

Ray, D., Sarkar, B. K., Basak, R. K., and Rana, A. K. (2002). Study of the thermal behavior of alkali-treated jute fibers. *Journal of Applied Polymer Science*, 85(12), 2594–2599. https://doi.org/10.1002/app.10934

Reinhardt, C., and Travis, A. S. (1997). The introduction of aniline dyes to paper printing and Queen Victoria's postage stamps. *Ambix*, 44(1), 11–18. https://doi.org/10.1179/amb.1997.44.1.11

Repon, Md. R., Dev, B., Rahman, M. A., Jurkonienė, S., Haji, A., Alim, Md. A., and Kumpikaitė, E. (2024). Textile dyeing using natural mordants and dyes: A review. *Environmental Chemistry Letters*, 22(3), 1473–1520. https://doi.org/10.1007/s10311-024-01716-4

Repon, Md. R., Islam, T., Paul, T. K., Jurkonienė, S., Haji, A., Shukhratov, S., and Toki, G. F. I. (2024). Natural dyes in textile printing: Parameters, methods, and performance. *Environmental Science and Pollution Research*, 31(35), 47552–47583. https://doi.org/10.1007/s11356-024-34424-1

Rincón, J., González, F., Ballester, A., Blázquez, M., and Muñoz, J. (2005). Biosorption of heavy metals by chemically-activated alga *Fucus vesiculosus*. *Journal of Chemical Technology and Biotechnology*, 80(12), 1403–1407. https://doi.org/10.1002/jctb.1342

Rivadeneyra, A., Marín-Sánchez, A., Wicklein, B., Salmerón, J. F., Castillo, E., Bobinger, M., and Salinas-Castillo, A. (2021). Cellulose nanofibers as substrate for flexible and biodegradable moisture sensors. *Composites Science and Technology*, 208, 108738. https://doi.org/10.1016/j.compscitech.2021.108738

Rocha, F. D., Soares, A. R., Houghton, P. J., Pereira, R. C., Kaplan, M. A. C., and Teixeira, V. L. (2007). Potential cytotoxic activity of some Brazilian seaweeds on human melanoma cells. *Phytotherapy Research*, 21(2), 170–175. https://doi.org/10.1002/ptr.2038

Rodriguez, A. J., Guzman, M. E., Lim, C.-S., and Minaie, B. (2011). Mechanical properties of carbon nanofiber/fiber-reinforced hierarchical polymer composites manufactured with multiscale-reinforcement fabrics. *Carbon*, 49(3), 937–948. https://doi.org/10.1016/j.carbon.2010.10.057

Romero, M., Blanco, J., Sánchez, B., Vidal, A., Sixto Malato, Cardona, A. I., and Garcia, E. (1999). Solar photocatalytic degradation of water and air pollutants: challenges and perspectives. *Solar Energy*, 66(2), 169–182. https://doi.org/10.1016/S0038-092X (98)00120-0

Rovira, J., and Domingo, J. L. (2019). Human health risks due to exposure to inorganic and organic chemicals from textiles: A review. *Environmental Research*, 168, 62–69. https://doi.org/10.1016/j.envres.2018.09.027

Roy, S., Kim, H. C., Panicker, P. S., Rhim, J.-W., and Kim, J. (2021). Cellulose nanofiber-based nanocomposite films reinforced with Zinc Oxide nanorods and grapefruit seed extract. *Nanomaterials*, 11(4), 877. https://doi.org/10.3390/nano11040877

Ru, I. T. K., Sung, Y. Y., Jusoh, M., Wahid, M. E. A., and Nagappan, T. (2020). *Chlorella vulgaris*: A perspective on its potential for combining high biomass with high value bioproducts. *Applied Phycology*, 1(1), 2–11. https://doi.org/10.1080/26388081.2020.1715256

Saakshy, Singh, K., Gupta, A. B., and Sharma, A. K. (2016). Fly ash as low cost adsorbent for treatment of effluent of handmade paper industry-Kinetic and modelling studies for direct black dye. *Journal of Cleaner Production*, 112, 1227–1240. https://doi.org/10.1016/j.jclepro.2015.09.058

Saba, N., Safwan, A., Sanyang, M. L., Mohammad, F., Pervaiz, M., Jawaid, M., Alothman, O. Y., and Sain, M. (2017). Thermal and dynamic mechanical properties of cellulose nanofibers reinforced epoxy composites. *International Journal of Biological Macromolecules*, 102, 822–828. https://doi.org/10.1016/j.ijbiomac.2017.04.074

Sadettin, S., and Dönmez, G. (2006). Bioaccumulation of reactive dyes by thermophilic cyanobacteria. *Process Biochemistry*, 41(4), 836–841. https://doi.org/10.1016/j.procbio.2005.10.031

Saeed, M., Alshammari, Y., Majeed, S. A., and Al-Nasrallah, E. (2020). Chemical vapour deposition of graphene-synthesis, characterisation, and applications: A review. *Molecules*, 25(17), 3856. https://doi.org/10.3390/molecules25173856

Sajid, M. (2022). Nanomaterials: Types, properties, recent advances, and toxicity concerns. *Current Opinion in Environmental Science and Health*, 25, 100319. https://doi.org/10.1016/j.coesh.2021.100319

Sakib, A., Masum, S., Hoinkis, J., Islam, R., and Molla, Md. (2019). Synthesis of CuO/ZnO nanocomposites and their application in photodegradation of toxic textile dye. *Journal of Composites Science*, 3(3), 91. https://doi.org/10.3390/jcs3030091

Saleh, A. K., Alessa, A. H., and Omran, A. M. E. (2024). Characterization of ex situ developed bacterial cellulose/ZnO-NPs nanocomposite for antimicrobial evaluation. *Biomass Conversion and Biorefinery*. https://doi.org/10.1007/s13399-023-05175-9

Salem, D. M. S. A., and Ismail, M. M. (2022). Characterization of cellulose and cellulose nanofibers isolated from various seaweed species. *Egyptian Journal of Aquatic Research*, 48(4), 307–313. https://doi.org/10.1016/j.ejar.2021.11.001

Sánchez-Gutiérrez, M., Bascón-Villegas, I., Espinosa, E., Carrasco, E., Pérez-Rodríguez, F., and Rodríguez, A. (2021). Cellulose nanofibers from olive tree pruning as food packaging additive of a biodegradable film. *Foods*, 10(7), 1584. https://doi.org/10.3390/foods10071584

Santos, P., Silva, A. P., and Reis, P. N. B. (2024). The effect of carbon nanofibers on the mechanical performance of epoxy-based composites: A review. *Polymers*, 16(15), 2152. https://doi.org/10.3390/polym16152152

Saranya, G., Saravanan, P., Dharmendira Kumar, M., and Renganathan, S. (2011). Equilibrium uptake and bioaccumulation of Basic Violet 14 using submerged macrophyte *Hydrilla verticillata*. *CLEAN - Soil, Air, Water*, 39(3), 283–288. https://doi.org/10.1002/clen.201000186

Saravanan, A., Kumar, P. S., Karishma, S., Vo, D.-V. N., Jeevanantham, S., Yaashikaa, P. R., and George, C. S. (2021). A review on biosynthesis of metal nanoparticles and its environmental applications. *Chemosphere*, 264, 128580. https://doi.org/10.1016/j.chemosphere.2020.128580

Saritha, V., Srinivas, N., and Srikanth Vuppala, N. V. (2017). Analysis and optimization of coagulation and flocculation process. *Applied Water Science*, 7(1), 451–460. https://doi.org/10.1007/s13201-014-0262-y

Saruchi, and Kumar, V. (2019). Adsorption kinetics and isotherms for the removal of rhodamine B dye and Pb^{+2} ions from aqueous solutions by a hybrid ion-exchanger. *Arabian Journal of Chemistry*, 12(3), 316–329. https://doi.org/10.1016/j.arabjc.2016.11.009

Sarwer, A., Hamed, S. M., Osman, A. I., Jamil, F., Al-Muhtaseb, A. H., Alhajeri, N. S., and Rooney, D. W. (2022). Algal biomass valorization for biofuel production and carbon sequestration: A review. *Environmental Chemistry Letters*, 20(5), 2797–2851. https://doi.org/10.1007/s10311-022-01458-1

Satapanajaru, T., Chompuchan, C., Suntornchot, P., and Pengthamkeerati, P. (2011). Enhancing decolorization of Reactive Black 5 and Reactive Red 198 during nano zerovalent iron treatment. *Desalination*, 266(1–3), 218–230. https://doi.org/10.1016/j.desal.2010.08.030

Sauer, T., Casaril, L., Oberziner, A., Jose, H., and Moreira, R. (2006). Advanced oxidation processes applied to tannery wastewater containing Direct Black 38-Elimination and degradation kinetics. *Journal of Hazardous Materials*, 135(1–3), 274–279. https://doi.org/10.1016/j.jhazmat.2005.11.063

Savvidis, G., Karanikas, E., Nikolaidis, N., Eleftheriadis, I., and Tsatsaroni, E. (2014). Ink-jet printing of cotton with natural dyes. *Coloration Technology*, 130(3), 200–204. https://doi.org/10.1111/cote.12087

Sayyed, A. J., Pinjari, D. V., Sonawane, S. H., Bhanvase, B. A., Sheikh, J., and Sillanpää, M. (2021). Cellulose-based nanomaterials for water and wastewater treatments: A review. *Journal of Environmental Chemical Engineering*, 9(6), 106626. https://doi.org/10.1016/j.jece.2021.106626

Selvarajan, E., and Mohanasrinivasan, V. (2013). Biosynthesis and characterization of ZnO nanoparticles using *Lactobacillus plantarum* VITES07. *Materials Letters*, 112, 180–182. https://doi.org/10.1016/j.matlet.2013.09.020

Shaba, E. Y., Jacob, J. O., Tijani, J. O., and Suleiman, M. A. T. (2021). A critical review of synthesis parameters affecting the properties of zinc oxide nanoparticle and its application in wastewater treatment. *Applied Water Science*, 11(2), 48. https://doi.org/10.1007/s13201-021-01370-z

Shabbir, M. (Ed.). (2019). Textiles and clothing (1st ed.). Wiley. https://doi.org/10.1002/9781119526599

Shah, P., and Gavrin, A. (2006). Synthesis of nanoparticles using high-pressure sputtering for magnetic domain imaging. *Journal of Magnetism and Magnetic Materials*, 301(1), 118–123. https://doi.org/10.1016/j.jmmm.2005.06.023

Sharma, E., Rathi, R., Misharwal, J., Sinhmar, B., Kumari, S., Dalal, J., andKumar, A. (2022). Evolution in lithography techniques: Microlithography to nanolithography. *Nanomaterials*, 12(16), 2754. https://doi.org/10.3390/nano12162754

Sharma, J., Sharma, S., and Soni, V. (2021). Classification and impact of synthetic textile dyes on aquatic flora: A review. *Regional Studies in Marine Science*, 45, 101802. https://doi.org/10.1016/j.rsma.2021.101802

Sharma, R., Nath, P. C., Mohanta, Y. K., Bhunia, B., Mishra, B., Sharma, M., Suri, S., Bhaswant, M., Nayak, P. K., and Sridhar, K. (2024). Recent advances in cellulose-based sustainable materials for wastewater treatment: An overview. *International Journal of Biological Macromolecules*, 256, 128517. https://doi.org/10.1016/j.ijbiomac.2023.128517

Sher, F., Malik, A., and Liu, H. (2013). Industrial polymer effluent treatment by chemical coagulation and flocculation. *Journal of Environmental Chemical Engineering*, 1(4), 684–689. https://doi.org/10.1016/j.jece.2013.07.003

Shertate, R. S., and Thorat, P. (2014). Biotransformation of textile dyes: a bioremedial aspect of marine environment. *American Journal of Environmental Sciences*, 10(5), 489–499. https://doi.org/10.3844/ajessp.2014.489.499

Shi, C., An, B., Zhang, L., Zai, Z., Shi, Z., Wang, Z., and Ma, J. (2023). Contribution of surface carboxyl of cellulose in the formation mechanism and interfacial catalysis activity of ZnO/cellulose nanocomposites. *Applied Surface Science*, 618, 156633. https://doi.org/10.1016/j.apsusc.2023.156633

Shi, C., Zhang, L., Shi, Z., Zai, Z., Ma, J., and Wang, Z. (2022). All-weather Ag–ZnO/cellulose photocatalysts tailored by surface groups and aspect ratios of cellulose nanofibers. *Cellulose*, 29(4), 2289–2304. https://doi.org/10.1007/s10570-022-04438-4

Shi, T., Li, Z., Guo, J., Gong, H., and Gu, C. (2019). Research progress on CNTs/CNFs-modified cement-based composites – A review. *Construction and Building Materials*, 202, 290–307. https://doi.org/10.1016/j.conbuildmat.2019.01.024

Shields, R., and Lupatsch, I. (2012). 5 Algae for aquaculture and animal feeds. In C. Posten and C. Walter (Eds.), Microalgal Biotechnology: Integration and Economy (pp. 79–100). DE GRUYTER. https://doi.org/10.1515/9783110298321.79

Shokoofeh, N., Moradi-Shoeili, Z., Naeemi, A. S., Jalali, A., Hedayati, M., and Salehzadeh, A. (2019). Biosynthesis of Fe_3O_4@Ag nanocomposite and evaluation of its performance on expression of norA and norB efflux pump genes in Ciprofloxacin-resistant *Staphylococcus aureus*. *Biological Trace Element Research*, 191(2), 522–530. https://doi.org/10.1007/s12011-019-1632-y

Siddhanta, A. K., Prasad, K., Meena, R., Prasad, G., Mehta, G. K., Chhatbar, M. U., Oza, M. D., Kumar, S., and Sanandiya, N. D. (2009). Profiling of cellulose content in Indian seaweed species. *Bioresource Technology*, 100(24), 6669–6673. https://doi.org/10.1016/j.biortech.2009.07.047

Sigurdson, G. T., Tang, P., and Giusti, M. M. (2017). Natural colorants: Food colorants from natural sources. *Annual Review of Food Science and Technology*, 8(1), 261–280. https://doi.org/10.1146/annurev-food-030216-025923

Silva, F., Nascimento, L., Brito, M., Da Silva, K., Paschoal, W., and Fujiyama, R. (2019). Biosorption of methylene blue dye using natural biosorbents made from weeds. *Materials*, 12(15), 2486. https://doi.org/10.3390/ma12152486

Singh, A., Kumar, D., and Gaur, J. (2007). Copper(II) and lead(II) sorption from aqueous solution by non-living *Spirogyra neglecta*. *Bioresource Technology*, 98(18), 3622–3629. https://doi.org/10.1016/j.biortech.2006.11.041

Singh, D., Singh, D., Mishra, V., Kushwaha, J., Sengar, M., Sinha, S., Singh, S., and Giri, B. S. (2024). Strategies for biological treatment of waste water: A critical review. *Journal of Cleaner Production*, 454, 142266. https://doi.org/10.1016/j.jclepro.2024.142266

Singh, R. L., Singh, P. K., and Singh, R. P. (2015). Enzymatic decolorization and degradation of azo dyes – A review. *International Biodeterioration and Biodegradation*, 104, 21–31. https://doi.org/10.1016/j.ibiod.2015.04.027

Sivakumar, R., and Lee, N. Y. (2022). Adsorptive removal of organic pollutant methylene blue using polysaccharide-based composite hydrogels. *Chemosphere*, 286, 131890. https://doi.org/10.1016/j.chemosphere.2021.131890

Slama, H. B., Chenari Bouket, A., Pourhassan, Z., Alenezi, F. N., Silini, A., Cherif-Silini, H., Oszako, T., Luptakova, L., Golińska, P., and Belbahri, L. (2021). Diversity of synthetic dyes from textile industries, discharge impacts and treatment methods. *Applied Sciences*, 11(14), 6255. https://doi.org/10.3390/app11146255

Sonawane, G. H., Patil, S. P., and Sonawane, S. H. (2018). *Nanocomposites and its applications*. In Applications of Nanomaterials (pp. 1–22). Elsevier. https://doi.org/10.1016/B978-0-08-101971-9.00001-6

Soni, B., Hassan, E. B., and Mahmoud, B. (2015). Chemical isolation and characterization of different cellulose nanofibers from cotton stalks. *Carbohydrate Polymers*, 134, 581–589. https://doi.org/10.1016/j.carbpol.2015.08.031

Srivastava, R., and Sofi, I. R. (2020). *Impact of synthetic dyes on human health and environment*: In K. A. Wani, N. K. Jangid, and A. R. Bhat (Eds.), Advances in Human Services and Public Health (pp. 146–161). IGI Global. https://doi.org/10.4018/978-1-7998-0311-9.ch007

Stelte, W., and Sanadi, A. R. (2009). Preparation and characterization of cellulose nanofibers from two commercial hardwood and softwood pulps. *Industrial and*

Engineering Chemistry Research, 48(24), 11211–11219. https://doi.org/10.1021/ie9011672

Stojanovska, E., Canbay, E., Pampal, E. S., Calisir, M. D., Agma, O., Polat, Y., Simsek, R., Gundogdu, N. A. S., Akgul, Y., and Kilic, A. (2016). A review on non-electro nanofibre spinning techniques. *RSC Advances*, 6(87), 83783–83801. https://doi.org/10.1039/C6RA16986D

Subramanian, A., Baskar, S., and Kadirvelu, K. (2024). Lab scale evaluation of biomineralization-assisted decolourization of reactive blue 4 and toxicity analysis. *Bioremediation Journal*, 1–12. https://doi.org/10.1080/10889868.2024.2414326

Sueraya, A. Z., Rahman, M. R., Kanakaraju, D., Said, K. A. M., James, A., Othman, A.-K. B., Bakri, M. K. B., and Uddin, J. (2024). A comprehensive review on nanocellulose-based membranes: Methods, mechanism, and applications in wastewater treatment. *Polymer Bulletin*, 81(9), 7519–7549. https://doi.org/10.1007/s00289-023-05084-x

Sugaya, K. (2003). The development of environmental consciousness with regard to the use of dyes and pharmaceuticals in the paper pulp industry. *Japan Tappi Journal*, 57(11), 1641-1645,016. https://doi.org/10.2524/jtappij.57.1641

Supramaniam, J., Low, D. Y. S., Wong, S. K., Tan, L. T. H., Leo, B. F., Goh, B. H., Darji, D., Mohd Rasdi, F. R., Chan, K. G., Lee, L. H., and Tang, S. Y. (2021). Facile synthesis and characterization of palm CNF-ZnO nanocomposites with antibacterial and reinforcing properties. *International Journal of Molecular Sciences*, 22(11), 5781. https://doi.org/10.3390/ijms22115781

Surendran, G., and Sherje, A. P. (2022). Cellulose nanofibers and composites: An insight into basics and biomedical applications. *Journal of Drug Delivery Science and Technology*, 75, 103601. https://doi.org/10.1016/j.jddst.2022.103601

Surwase, S. V., Deshpande, K. K., Phugare, S. S., and Jadhav, J. P. (2013). Biotransformation studies of textile dye Remazol Orange 3R. *3 Biotech*, 3(4), 267–275. https://doi.org/10.1007/s13205-012-0093-1

Suteu, D., Bilba, D., and Coseri, S. (2014). Macroporous polymeric ion exchangers as adsorbents for the removal of cationic dye basic blue 9 from aqueous solutions. *Journal of Applied Polymer Science*, 131(1), app.39620. https://doi.org/10.1002/app.39620

Syed, M. H., Zahari, M. A. K. M., Khan, M. M. R., Beg, M. D. H., and Abdullah, N. (2023). An overview on recent biomedical applications of biopolymers: Their role in drug delivery systems and comparison of major systems. *Journal of Drug Delivery Science and Technology*, 80, 104121. https://doi.org/10.1016/j.jddst.2022.104121

Syed, Z., Sogani, M., Rajvanshi, J., and Sonu, K. (2023). Microbial biofilms for environmental bioremediation of heavy metals: A review. *Applied Biochemistry and Biotechnology*, 195(9), 5693–5711. https://doi.org/10.1007/s12010-022-04276-x

Tahir, F., Ashfaq, H., Khan, A. Z., Amin, M., Akbar, I., Malik, H. A., Abdullah, M., Alessa, A. H., Alsaigh, A. A., Ralph, P. J., Mehmood, M. A., and Malik, S. (2024). Emerging trends in algae farming on non-arable lands for resource reclamation, recycling, and mitigation of climate change-driven food security challenges. *Reviews in Environmental Science and Bio/Technology*, 23(3), 869–896. https://doi.org/10.1007/s11157-024-09697-0

Tai, C. Y., Wang, Y., and Liu, H. (2008). A green process for preparing silver nanoparticles using spinning disk reactor. *AIChE Journal*, 54(2), 445–452. https://doi.org/10.1002/aic.11396

Tanaka, M., Murakami, S., Shinke, R., and Aoki, K. (2000). Genetic characteristics of cellulose-forming acetic acid bacteria identified phenotypically as *Gluconacetobacter xylinus*. *Bioscience, Biotechnology, and Biochemistry*, 64(4), 757–760. https://doi.org/10.1271/bbb.64.757

Tarchoun, A. F., Trache, D., and Klapötke, T. M. (2019). Microcrystalline cellulose from *Posidonia oceanica* brown algae: Extraction and characterization. International *Journal of Biological Macromolecules*, 138, 837–845. https://doi.org/10.1016/j.ijbiomac.2019.07.176

Taskin, M., and Erdal, S. (2010). Reactive dye bioaccumulation by fungus *Aspergillus niger*isolated from the effluent of sugar fabric-contaminated soil. *Toxicology and Industrial Health*, 26(4), 239–247. https://doi.org/10.1177/0748233710364967

Teodoro, K. B. R., Sanfelice, R. C., Migliorini, F. L., Pavinatto, A., Facure, M. H. M., and Correa, D. S. (2021). A review on the role and performance of cellulose nanomaterials in sensors. *ACS Sensors*, 6(7), 2473–2496. https://doi.org/10.1021/acssensors.1c00473

Thema, F. T., Manikandan, E., Dhlamini, M. S., and Maaza, M. (2015). Green synthesis of ZnO nanoparticles via *Agathosma betulina* natural extract. *Materials Letters*, 161, 124–127. https://doi.org/10.1016/j.matlet.2015.08.052

Thomas, P., Duolikun, T., Rumjit, N. P., Moosavi, S., Lai, C. W., Bin Johan, M. R., and Fen, L. B. (2020). Comprehensive review on nanocellulose: Recent developments, challenges and future prospects. J*ournal of the Mechanical Behavior of Biomedical Materials*, 110, 103884. https://doi.org/10.1016/j.jmbbm.2020.103884

Tiberto, P., Barrera, G., Celegato, F., Conta, G., Coïsson, M., Vinai, F., and Albertini, F. (2015). $Ni_{80}Fe_{20}$ nanodisks by nanosphere lithography for biomedical applications. *Journal of Applied Physics*, 117(17), 17B304. https://doi.org/10.1063/1.4913278

Tibolla, H., Pelissari, F. M., and Menegalli, F. C. (2014). Cellulose nanofibers produced from banana peel by chemical and enzymatic treatment. *LWT - Food Science and Technology*, 59(2), 1311–1318. https://doi.org/10.1016/j.lwt.2014.04.011

Tkaczyk, A., Mitrowska, K., and Posyniak, A. (2020). Synthetic organic dyes as contaminants of the aquatic environment and their implications for ecosystems: A review. *Science of The Total Environment*, 717, 137222. https://doi.org/10.1016/j.scitotenv.2020.137222

Touliabah, H. E.-S., El-Sheekh, M. M., Ismail, M. M., and El-Kassas, H. (2022). A review of microalgae- and cyanobacteria-based biodegradation of organic pollutants. *Molecules*, 27(3), 1141. https://doi.org/10.3390/molecules27031141

Trache, D., Tarchoun, A. F., Derradji, M., Hamidon, T. S., Masruchin, N., Brosse, N., and Hussin, M. H. (2020). Nanocellulose: From fundamentals to advanced applications. *Frontiers in Chemistry*, 8, 392. https://doi.org/10.3389/fchem.2020.00392

Trentacoste, E. M., Martinez, A. M., and Zenk, T. (2015). The place of algae in agriculture: Policies for algal biomass production. *Photosynthesis Research*, 123(3), 305–315. https://doi.org/10.1007/s11120-014-9985-8

Trilokesh, C., and Uppuluri, K. B. (2019). Isolation and characterization of cellulose nanocrystals from jackfruit peel. *Scientific Reports*, 9(1), 16709. https://doi.org/10.1038/s41598-019-53412-x

Udayan, A., Arumugam, M., and Pandey, A. (2017). *Nutraceuticals from algae and cyanobacteria*. In Algal Green Chemistry (pp. 65–89). Elsevier. https://doi.org/10.1016/B978-0-444-63784-0.00004-7

Ullah, R., and Dutta, J. (2008). Photocatalytic degradation of organic dyes with manganese-doped ZnO nanoparticles. *Journal of Hazardous Materials*, 156(1–3), 194–200. https://doi.org/10.1016/j.jhazmat.2007.12.033

Ummartyotin, S., and Manuspiya, H. (2015). A critical review on cellulose: From fundamental to an approach on sensor technology. *Renewable and Sustainable Energy Reviews*, 41, 402–412. https://doi.org/10.1016/j.rser.2014.08.050

Ussia, M., Privitera, V., and Scalese, S. (2024). Unlocking the potential and versatility of quantum dots: From biomedical to environmental applications and smart micro/nanorobots. *Advanced Materials Interfaces*, 11(17), 2300970. https://doi.org/10.1002/admi.202300970

Vaiano, V., Iervolino, G., Sannino, D., Murcia, J. J., Hidalgo, M. C., Ciambelli, P., and Navío, J. A. (2016). Photocatalytic removal of patent blue V dye on Au-TiO_2 and Pt-TiO_2 catalysts. *Applied Catalysis B: Environmental*, 188, 134–146. https://doi.org/10.1016/j.apcatb.2016.02.001

Vallabani, N. V. S., Gruzieva, O., Elihn, K., Juárez-Facio, A. T., Steimer, S. S., Kuhn, J., Silvergren, S., Portugal, J., Piña, B., Olofsson, U., Johansson, C., and Karlsson, H. L. (2023). Toxicity and health effects of ultrafine particles: Towards an understanding of the relative impacts of different transport modes. *Environmental Research*, 231, 116186. https://doi.org/10.1016/j.envres.2023.116186

Velatooru, L. R., Baggu, C. B., and Janapala, V. R. (2016). Spatane diterpinoid from the brown algae, *Stoechospermum marginatum* induces apoptosis via ROS induced mitochondrial mediated caspase dependent pathway in murine B16F10 melanoma cells. *Molecular Carcinogenesis*, 55(12), 2222–2235. https://doi.org/10.1002/mc.22463

Venugopal, G., and Kim, S.-J. (2013). *Nanolithography*. In K. Takahata (Ed.), Advances in Micro/Nano Electromechanical Systems and Fabrication Technologies. InTech. https://doi.org/10.5772/55527

Verma, A. K., Dash, R. R., and Bhunia, P. (2012). A review on chemical coagulation/flocculation technologies for removal of colour from textile wastewaters. *Journal of Environmental Management*, 93(1), 154–168. https://doi.org/10.1016/j.jenvman.2011.09.012

Verma, M., Kumar, V., and Katoch, A. (2018). Sputtering based synthesis of CuO nanoparticles and their structural, thermal and optical studies. *Materials Science in Semiconductor Processing*, 76, 55–60. https://doi.org/10.1016/j.mssp.2017.12.018

Vijayaraghavan, K., and Ashokkumar, T. (2017). Plant-mediated biosynthesis of metallic nanoparticles: A review of literature, factors affecting synthesis, characterization techniques and applications. *Journal of Environmental Chemical Engineering*, 5(5), 4866–4883. https://doi.org/10.1016/j.jece.2017.09.026

Vikrant, K., Giri, B. S., Raza, N., Roy, K., Kim, K.-H., Rai, B. N., and Singh, R. S. (2018). Recent advancements in bioremediation of dye: Current status and challenges. *Bioresource Technology*, 253, 355–367. https://doi.org/10.1016/j.biortech.2018.01.029

Vishchuk, O. S., Ermakova, S. P., and Zvyagintseva, T. N. (2013). The fucoidans from brown algae of Far-Eastern seas: Anti-tumor activity and structure–function relationship. *Food Chemistry*, 141(2), 1211–1217. https://doi.org/10.1016/j.foodchem.2013.03.065

Wahab, R., Ansari, S. G., Kim, Y. S., Song, M., and Shin, H.-S. (2009).The role of pH variation on the growth of zinc oxide nanostructures. *Applied Surface Science*, 255(9), 4891–4896. https://doi.org/10.1016/j.apsusc.2008.12.037

Wainwright, M. (2008). Dyes in the development of drugs and pharmaceuticals. *Dyes and Pigments*, 76(3), 582–589. https://doi.org/10.1016/j.dyepig.2007.01.015

Wang, D. (2019). A critical review of cellulose-based nanomaterials for water purification in industrial processes. *Cellulose*, 26(2), 687–701. https://doi.org/10.1007/s10570-018-2143-2

Wang, H., Su, J. Q., Zheng, X. W., Tian, Y., Xiong, X. J., and Zheng, T. L. (2009). Bacterial decolorization and degradation of the reactive dye Reactive Red 180 by *Citrobacter* sp. CK3. *International Biodeterioration and Biodegradation*, 63(4), 395–399. https://doi.org/10.1016/j.ibiod.2008.11.006

Wang, J., Xia, Y., Dong, Y., Chen, R., Xiang, L., and Komarneni, S. (2016). Defect-rich ZnO nanosheets of high surface area as an efficient visible-light photocatalyst. *Applied Catalysis B: Environmental*, 192, 8–16. https://doi.org/10.1016/j.apcatb.2016.03.040

Wang, X., Li, X., Sang, W., Peng, H., and Ma, G. (2023). Hydrothermal wheat straw-reinforced polyvinyl alcohol biodegradable mulch film. *Water, Air, and Soil Pollution*, 234(11), 695. https://doi.org/10.1007/s11270-023-06708-8

Wang, Y., Ma, C., Kong, D., Lian, L., and Liu, Y. (2023). Review on application of algae-based biochars in environmental remediation: Progress, challenge and perspectives. *Journal of Environmental Chemical Engineering*, 11(6), 111263. https://doi.org/10.1016/j.jece.2023.111263

Wargala, E., Sławska, M., Zalewska, A., and Toporowska, M. (2021). Health effects of dyes, minerals, and vitamins used in cosmetics. *Women*, 1(4), 223–237. https://doi.org/10.3390/women1040020

Wasim, M., Shi, F., Liu, J., Farooq, A., Khan, S. U., Salam, A., Hassan, T., and Zhao, X. (2021). An overview of Zn/ZnO modified cellulosic nanocomposites and their potential applications. *Journal of Polymer Research*, 28(9), 338. https://doi.org/10.1007/s10965-021-02689-6

Wei, L., Abd Rahim, S., Al Bakri Abdullah, M., Yin, A., Ghazali, M., Omar, M., Nemeș, O., Sandu, A., Vizureanu, P., and Abdellah, A. (2023). Producing metal powder from machining chips using ball milling process: A Review. *Materials*, 16(13), 4635. https://doi.org/10.3390/ma16134635

Welham, R. D. (1963). The early history of the synthetic dye industry. *Journal of the Society of Dyers and Colourists*, 79(4), 146–152. https://doi.org/10.1111/j.1478-4408.1963.tb02544.x

Wells, M. L., Potin, P., Craigie, J. S., Raven, J. A., Merchant, S. S., Helliwell, K. E., Smith, A. G., Camire, M. E., and Brawley, S. H. (2017). Algae as nutritional and functional food sources: Revisiting our understanding. *Journal of Applied Phycology*, 29(2), 949–982. https://doi.org/10.1007/s10811-016-0974-5

Widiarto, S., Pramono, E., Suharso, Rochliadi, A., and Arcana, I. M. (2019). Cellulose nanofibers preparation from Cassava peels via mechanical disruption. *Fibers*, 7(5), 44. https://doi.org/10.3390/fib7050044

Wu, J.-S., Liu, C.-H., Chu, K. H., and Suen, S.-Y. (2008). Removal of cationic dye methyl violet 2B from water by cation exchange membranes. *Journal of Membrane Science*, 309(1–2), 239–245. https://doi.org/10.1016/j.memsci.2007.10.035

Wu, W., Zhou, Y., Pan, J., Wu, Y., Goksen, G., and Shao, P. (2023). Multibranched flower-like ZnO anchored on pectin/cellulose nanofiber aerogel skeleton for enhanced comprehensive antibacterial capabilities. *Carbohydrate Polymers*, 322, 121320. https://doi.org/10.1016/j.carbpol.2023.121320

Wu, Z., Yuan, X., Xiong, X., Ao, H., Wu, C., Liu, G., and Zhu, H. (2024). *Cladophora* as ecological engineer: A new test from the largest lake of Qinghai-Tibet plateau with filamentous algal blooms. *Water Biology and Security*, 3(1), 100210. https://doi.org/10.1016/j.watbs.2023.100210

Xiang, Z., Gao, W., Chen, L., Lan, W., Zhu, J. Y., and Runge, T. (2016). A comparison of cellulose nanofibrils produced from *Cladophora glomerata* algae and bleached eucalyptus pulp. *Cellulose*, 23(1), 493–503. https://doi.org/10.1007/s10570-015-0840-7

Xin, B., Chen, G., and Zheng, W. (2010). Bioaccumulation of Cu-complex reactive dye by growing pellets of *Penicillium oxalicum* and its mechanism. *Water Research*, 44(12), 3565–3572. https://doi.org/10.1016/j.watres.2010.04.004

Xu, C., Cao, L., Su, G., Liu, W., Liu, H., Yu, Y., and Qu, X. (2010). Preparation of ZnO/Cu_2O compound photocatalyst and application in treating organic dyes. *Journal of Hazardous Materials*, 176(1–3), 807–813. https://doi.org/10.1016/j.jhazmat.2009.11.106

Yadav, D., Amini, F., and Ehrmann, A. (2020). Recent advances in carbon nanofibers and their applications – A review. *European Polymer Journal*, 138, 109963. https://doi.org/10.1016/j.eurpolymj.2020.109963

Yadav, S., Tiwari, K. S., Gupta, C., Tiwari, M. K., Khan, A., and Sonkar, S. P. (2023). A brief review on natural dyes, pigments: Recent advances and future perspectives. *Results in Chemistry*, 5, 100733. https://doi.org/10.1016/j.rechem.2022.100733

Yadollahi, M., Gholamali, I., Namazi, H., and Aghazadeh, M. (2015). Synthesis and characterization of antibacterial carboxymethyl cellulose/ZnO nanocomposite hydrogels. *International Journal of Biological Macromolecules*, 74, 136–141. https://doi.org/10.1016/j.ijbiomac.2014.11.032

Yan, M., An, B., Li, X., Zai, Z., Wu, S., Ma, J., and Zhang, L. (2023). Effect of different electronegative oxygen atoms of cellulose nanofibrils on the formation and photocatalytic property of ZnO/cellulose composite. *Applied Surface Science*, 637, 157974. https://doi.org/10.1016/j.apsusc.2023.157974

Yan, X., Zhang, Q., Ma, X., Zhong, Y., Tang, H., and Mai, S. (2023). The mechanism of biomineralization: Progress in mineralization from intracellular

generation to extracellular deposition. *Japanese Dental Science Review*, 59, 181–190. https://doi.org/10.1016/j.jdsr.2023.06.005

Yanardağ, D., and Edebali, S. (2023). Adsorptive removal of malachite green dye from aqueous solution by ion exchange resins. *Biomass Conversion and Biorefinery*. https://doi.org/10.1007/s13399-023-04839-w

Yang, Z., Zhou, Y., Feng, Z., Rui, X., Zhang, T., and Zhang, Z. (2019). A Review on reverse osmosis and nanofiltration membranes for water purification. *Polymers*, 11(8), 1252. https://doi.org/10.3390/polym11081252

Yeo, Y., and Shin, Y. (2023). Inkjet printing of textiles using biodegradable natural dyes. *Fibers and Polymers*, 24(5), 1695–1705. https://doi.org/10.1007/s12221-023-00162-3

Yu, Z., Hu, C., Dichiara, A. B., Jiang, W., and Gu, J. (2020). Cellulose nanofibril/carbon nanomaterial hybrid aerogels for adsorption removal of cationic and anionic organic Dyes. *Nanomaterials*, 10(1), 169. https://doi.org/10.3390/nano10010169

Yusuf, J., Firdaus, A. H. M., Sapuan, S. M., Rashid, U., Ilyas, R. A., Hassan, M. R., and Ansari, M. A. (2024). Nanocellulose-graphene hybrid composites: Fabrication, characterization, applications and environmental impact. *International Journal of Biological Macromolecules*, 137244. https://doi.org/10.1016/j.ijbiomac.2024.137244

Zahid, M. U., Pervaiz, E., Hussain, A., Shahzad, M. I., and Niazi, M. B. K. (2018). Synthesis of carbon nanomaterials from different pyrolysis techniques: A review. *Materials Research Express*, 5(5), 052002. https://doi.org/10.1088/2053-1591/aac05b

Zamiri, R., Rebelo, A., Zamiri, G., Adnani, A., Kuashal, A., Belsley, M. S., and Ferreira, J. M. F. (2014). Far-infrared optical constants of ZnO and ZnO/Ag nanostructures. *RSC Adv.*, 4(40), 20902–20908. https://doi.org/10.1039/c4ra01563k

Zhang, D., Jin, K., Lim, K. H., Jie, S., Wang, W.-J., and Yang, X. (2023). Eco-friendly cellulose nanofibrils with high surface charge and aspect ratio for nanopaper films with ultrahigh toughness and folding endurance. *Green Chemistry*, 25(12), 4696–4704. https://doi.org/10.1039/D3GC00632H

Zhang, L., Shao, Q., and Xu, C. (2019). Enhanced azo dye removal from wastewater by coupling sulfidated zero-valent iron with a chelator. *Journal of Cleaner Production*, 213, 753–761. https://doi.org/10.1016/j.jclepro.2018.12.183

Zhang, L., Tsuzuki, T., and Wang, X. (2015). Preparation of cellulose nanofiber from softwood pulp by ball milling. *Cellulose*, 22(3), 1729–1741. https://doi.org/10.1007/s10570-015-0582-6

Zhang, L., Yan, M., Li, X., Chen, C., Ma, J., and Wang, Z. (2024). Interfacial interaction between Zn^{2+} and surface functional groups impacting self-assembly of ZnO on cellulose nanofibrils. *Langmuir*, 40(44), 23415–23423. https://doi.org/10.1021/acs.langmuir.4c02710

Zhou, B., Zhang, T., and Wang, F. (2023). Microbial-based heavy metal bioremediation: toxicity and eco-friendly approaches to heavy metal decontamination. *Applied Sciences*, 13(14), 8439. https://doi.org/10.3390/app13148439

Zhou, L., Li, K., Duan, X., Hill, D., Barrow, C., Dunshea, F., Martin, G., and Suleria, H. (2022). Bioactive compounds in microalgae and their potential health benefits. *Food Bioscience*, 49, 101932. https://doi.org/10.1016/j.fbio.2022.101932

Zhou, Y., Jin, C., Li, Y., and Shen, W. (2018). Dynamic behavior of metal nanoparticles for catalysis. *Nano Today*, 20, 101–120. https://doi.org/10.1016/j.nantod.2018.04.005

Zhu, P., Ou, H., Kuang, Y., Hao, L., Diao, J., and Chen, G. (2020). Cellulose nanofiber/carbon nanotube dual network-enabled humidity sensor with high sensitivity and durability. *ACS Applied Materials and Interfaces*, 12(29), 33229–33238. https://doi.org/10.1021/acsami.0c07995

Zhu, S., and Wang, D. (2017). Photocatalysis: Basic principles, diverse forms of implementations and emerging scientific opportunities. *Advanced Energy Materials*, 7(23), 1700841. https://doi.org/10.1002/aenm.201700841

Zia, J., and Riaz, U. (2021). Photocatalytic degradation of water pollutants using conducting polymer-based nanohybrids: A review on recent trends and future prospects. *Journal of Molecular Liquids*, 340, 117162. https://doi.org/10.1016/j.molliq.2021.117162

Zuo, H.-F., Guo, Y.-R., Li, S.-J., and Pan, Q.-J. (2014). Application of microcrystalline cellulose to fabricate ZnO with enhanced photocatalytic activity. *Journal of Alloys and Compounds*, 617, 823–827.https://doi.org/10.1016/j.jallcom.2014.08.071

BIO-DATA

Name	:	Jyotishma Nath
Father's Name	:	Promod Nath
Mother's Name	:	Eva Moni Nath
Permanent Address	:	Hatighuli-785664,Gaurisagar,Sivasagar,Assam
Nationality	:	Indian
Date of Birth	:	26-11-1996
Sex	:	Female
Marital Status	:	Unmarried
Contact Number	:	9085495937
Email Address	:	jyotishmanath96@gmail.com

ACADEMIC QUALIFICATIONS (STARTING FROM THE HIGHEST DEGREE)

Sl. no.	Name of the degree/exam	Subject	Board/ University	Year of passing	% Marks/ Grade
1	M. Sc. Botany	Botany	Mizoram University (MZU)	2019	75.06 %
2	B. Sc. Botany	Botany	Moran College (Dibrugarh University)	2017	78.08 %
3	HS	Science	Jhanji HS School (AHSEC)	2014	66.4%
4	HSLC	-	Silpukhuri High School (SEBA)	2012	75%

LIST OF PUBLICATION

Paper Publication

1. Momin S Ch, Pradhan RB, **Nath J**, et al (2024b) Metal sequestration by *Microcystis* extracellular polymers: a promising path to greener water treatment. *Environmental Science and Pollution Research* 31:11192–11213. **(Impact Factor-5.8)**

2. Momin S Ch, **Nath J**, Mahana A, et al (2024a) Chemical activation of *Microcystis aeruginosa* biomass: a promising approach for enhanced diclofenac sorption and water treatment. *Journal of Chemical Technology and Biotechnology* 99:149–163. **(Impact Factor-3.4)**

3. Lalremdika R, Pradhan RB**,** Momin S Ch, **Nath J**, Lalmuanzeli R, & Mehta S K (2024). Carbon dioxide sequestration and sustainable domestic sewage bioremediation by *Microcystis aeruginosa* and *Chlorella vulgaris*. *Ecology, Environment and Conservation, 10, S108-S119*.http://doi.org/10.53550/EEC.2024.v30i06s.017

Patent

1. Mehta S. K, **Nath J** (2021) Method for making cellulose nanofiber (CNF) from Non-lignocellulogic feedstock green filamentous alga *Cladophora* sp. (*Cladophora glomerata* (L.) Kutz.Application No. 202131054233

PRESENTATION

1. Presented a paper on "Green filamentous alga *Cladophora* as source of cellulose nanofiber (CNF)" at Two-Day National Seminar on "Environment and Climate Change in North East India: Challenges and Sustainability" funded by Department of Science and Technology, Govt. of India. Organized by Sibsagar College, Joysagar (Autonomous), Sivasagar, Assam on 22nd and 23rd August, 2022.

2. Presented a paper on "Synthesis, Characterization and Applications of Cellulose Nanocrystal from lab grown alga *Chlorrella vulgaris*" at Science and Engineering Research Board (SERB), Indian National Academy of Science (INSA), Oil India Limited (OIL), IQAC, Tinsukia College Sponsored "National Conference on Current Trends in Basic Sciences and Applications (NCCTBSA24) organized by Department of Physics, Tinsukia College, Tinsukia, Assam, India on 22nd and 23rd January, 2024.

3. Presented a paper on "Sunlight-Driven Photocatalytic Removal of Methylene Blue by *Cladophora* Cellulose Nanofiber/Zinc Oxide (ZnO-NPs/CNF) Nanocomposites: Synthesis and Characterization" at the CACSRE-2024 and the NCCT-2024,joimtly organized by the Department of Chemistry, Industrial Chemistry, Chemistry (PUC), Mizoram University and the Association of Chemistry Teachers(ATC) during 6th-8th November, 2024 at Mizoram University.

MIZORAM UNIVERSITY (A Central University)

Ph.D. Thesis/M.Phil. Dissertation Certificate on Plagiarism Check

Name of Research Scholar/Student	Jyotishma Nath	
Ph.D./M.Phil. Registration Number	MZU/Ph.D./1405 of 14.08.2019	
Title of Ph.D. Thesis/M.Phil. Dissertation	Synthesis and Charaterization of ZnO-Cellulose Nanocomposite (ZnO-CNF) for Photocatalytic Degradation of Organic Dye	
Name & Institutional Address of the Supervisor/Joint Supervisor	Prof. S. K. Mehta, Department of Botany, Mizoram University, Tanhril-796004, Mizoram, India	
Name of the Department and School	Botany, School of Life Science	
Date of Submission		
Date of plagiarism check	07/12/2024	
Name of the software used	Turnitin	
Percentage of similarity detected by the **TURNITIN** software	**Core Areas**	0%
	Non-Core Areas	6%
Percentage of similarity permissible under MZU regulations	**Core Areas**	A common knowledge or coincidental terms **and/or *up to fourteen (14) consecutive words,* if option is available in the software.**
	Non-Core Areas	Up to 10%

I hereby declare/certify that the Ph.D. Thesis/M.Phil. Dissertation submitted by me is complete in all respect, as per the guidelines of the Mizoram University (MZU) for this purpose. I also certify that the Thesis/Dissertation (soft copy and print version) has been checked for plagiarism using **TURNITIN** similarity check software. Copy of the report generated by the **TURNITIN** software is also enclosed.

Place: (Name & Signature
of the Scholar) Date:

Name & Signature of
the Supervisor: with
seal

Name & Signature of the Joint Supervisor (if any): with seal

Name & Signature of the DRC Chairperson/Head: with seal

Plagiarism Verification Certificate

(This certificate should be submitted to the Examination Department at the time of submission of the Thesis/Dissertation)

This is to certify that the plagiarism check has been performed for Ph.D. Thesis/M.Phil. Dissertation **Synthesis and Charaterization of ZnO-Cellulose Nanocomposite (ZnO-CNF) for Photocatalytic Degradation of Organic Dye** submitted by **Ms. Jyotishma Nath**, under the supervision of Prof. S. K. Mehta, Department of Botany, School of Life Sciences, Mizoram University. The check performed by the Scholar/Student is found correct/adheres to MZU regulations and authentic software **TURNITIN** has been used for the similarity check.

Name, Signature & Seal of the Dean of the School:

PARTICULARS OF THE CANDIDATE

NAME	:	Jyotishma Nath
DEGREE	:	Ph.D.
DEPARTMENT	:	Botany
TITLE OF THESIS	:	Synthesis and Charaterization of ZnO-Cellulose Nanocomposite (ZnO-CNF) for the Photocatalytic Degradation of Organic Dye
DATE OF ADMISSION	:	14th August, 2019
DATE OF APPROVAL OF RESEARCH PROPOSAL		
1. DRC	:	21.05.2020
2. BOS	:	22.05.2020
3. SCHOOL BOARD	:	12.06.2020
MZU REGISTRATION NO.	:	1700078
PH. D REGISTRATION NO. and DATE	:	MZU/Ph.D./1405 of 14.08.2019
EXTENSION (IF ANY)	:	N/A

Head

Department of Botany

ABSTRACT

SYNTHESIS AND CHARACTERIZATION OF ZnO-CELLULOSE NANOCOMPOSITE (ZnO-CNF) FOR THE PHOTOCATALYTIC DEGRADATION OF ORGANIC DYE

AN ABSTRACT SUBMITTED IN PARTIAL FULFILLMENT OF THE REQUIREMENTS FOR THE DEGREE OF DOCTOR OF PHILOSOPHY

JYOTISHMA NATH

MZU REGISTRATION NO.: 1700078

Ph.D. REGISTRATION NO.: MZU/Ph.D./1405 of 14.08.2019

DEPARTMENT OF BOTANY

SCHOOL OF LIFE SCIENCES

DECEMBER, 2024

SYNTHESIS AND CHARACTERIZATION OF ZnO-CELLULOSE NANOCOMPOSITE (ZnO-CNF) FOR THE PHOTOCALYTIC DEGRADATION OF ORGANIC DYE

BY

JYOTISHMA NATH

DEPARTMENT OF BOTANY

Supervisor

Dr. SURYA KANT MEHTA

Submitted

In partial fulfillment of the requirement of the Degree of Doctor of Philosophy in Botany of Mizoram University, Aizawl

ABSTRACT

This research investigated the synthesis, characterization, and application of ZnO-NPs, Nanocellulose and ZnO-CNF nanocomposite derived from the algae *Cladophora glomerata* (L.) Kutz and *Chlorella vulgaris* Beijerinck. The primary objective was to explore the potential of these nanocomposites for water purification and environmental remediation.

Cellulose nanofibrils (CNF) and cellulose nanocrystal (CNC) were successfully extracted from both algal sources using a combination of mechanical and chemical treatments. The morphology and size distribution of the CNFs were characterized using scanning electron microscopy (SEM). The SEM images revealed a network-like structure composed of well-separated, rod-shaped nanocrystals with a high aspect ratio. The average length and width of the nanocrystals were found to be in the range of 100-200 nm and 5-10 nm, respectively.

The ZnO nanoparticles were synthesized using a biological approach, utilizing the bioactive compounds present in the algal extracts as reducing and stabilizing agents. The synthesis process involved the reduction of zinc ions to ZnO nanoparticles in the presence of algal extract. The size and morphology of the ZnO nanoparticles were controlled by adjusting the concentration of the algal extract and the reaction conditions. The synthesized ZnO nanoparticles were characterized using various techniques to determine their structural, optical, and morphological properties. X-ray diffraction (XRD) analysis confirmed the formation of crystalline ZnO nanoparticles with a hexagonal wurtzite structure. The average crystallite size of the ZnO nanoparticles was estimated to be around 20-30 nm.

Fourier Transform Infrared (FTIR) spectroscopy was used to identify the functional groups present in the ZnO nanoparticles and to investigate the possible interactions between the nanoparticles and the algal extract. The FTIR spectrum of ZnO nanoparticles showed characteristic peaks corresponding to the Zn-O stretching vibration at around 400-500 cm^{-1}. Additionally, the presence of other functional groups, such as hydroxyl, carbonyl, and amine groups, was observed, indicating the presence of organic residues from the algal extract.

UV-Vis spectroscopy was employed to study the optical properties of the ZnO nanoparticles. The UV-Vis spectrum showed a strong absorption band in the UV region, with an absorption peak around 380 nm. The band gap energy of the ZnO nanoparticles was estimated to be around 3.2 eV, which is consistent with the reported values for bulk ZnO.

SEM images revealed the morphology of the ZnO nanoparticles, showing spherical particles with a relatively uniform size distribution. The particle size was found to be in the range of 20-30 nm, consistent with the XRD results. XPS analysis confirmed the presence of Zn and O elements in the ZnO nanoparticles. The binding energies of Zn 2p3/2 and Zn 2p1/2 core levels were observed at around 1021.6 eV and 1045.0 eV, respectively, which are characteristic of Zn^{2+} ions in ZnO.

The ZnO-CNF nanocomposite was synthesized through a facile method involving the incorporation of ZnO nanoparticles into the nanocellulose (extracted from *C. glomerata*) matrix. This was achieved by mixing a dispersion of ZnO nanoparticles with a suspension of nanocellulose. The mixture was then subjected to various physical and chemical treatments, such as sonication, stirring, and drying, to ensure uniform dispersion of ZnO nanoparticles throughout the nanocellulose matrix. The successful incorporation of ZnO nanoparticles into the nanocellulose matrix was confirmed through various characterization techniques, including SEM, EDX and FTIR. The SEM images revealed the uniform dispersion of ZnO nanoparticles on the surface of the nanocellulose fibers, indicating strong interfacial interactions between the two components. The EDX analysis confirmed the presence of zinc, oxygen, and carbon elements in the nanocomposite, further supporting the successful integration of ZnO nanoparticles.

Thermogravimetric analysis (TGA) and differential scanning calorimetry (DSC) were employed to investigate the thermal stability and decomposition behaviour of the ZnO-CNF nanocomposite. The TGA curve showed a multi-step decomposition process, with the initial weight loss attributed to the evaporation of moisture and the subsequent weight loss corresponding to the decomposition of cellulose and ZnO nanoparticles. The DSC curve revealed endothermic peaks

associated with the loss of moisture and the decomposition of cellulose and ZnO. The incorporation of ZnO nanoparticles into the nanocellulose matrix slightly increased the thermal stability of the composite material.

The synergistic effect between ZnO nanoparticles and nanocellulose in the nanocomposite enhances its properties, such as increased surface area, improved adsorption capacity, and enhanced photocatalytic activity. The high surface area of the nanocellulose provides more active sites for adsorption and catalytic reactions, while the presence of ZnO nanoparticles facilitates efficient charge separation and light absorption, leading to improved photocatalytic performance.

The photocatalytic activity of the ZnO-CNF nanocomposite was evaluated using methylene blue (MB) as a model pollutant. The nanocomposite demonstrated superior photocatalytic degradation of MB compared to ZnO NPs and CNF alone, achieving nearly 100% degradation within 150 minutes under sunlight irradiation. The enhanced photocatalytic activity can be attributed to several factors, including:

i. Efficient charge separation: The interface between ZnO nanoparticles and nanocellulose facilitates efficient charge separation, reducing recombination of electron-hole pairs and increasing the generation of reactive oxygen species.

ii. Enhanced light absorption: The combination of ZnO nanoparticles and nanocellulose can enhance the absorption of light in the visible region, leading to increased photocatalytic activity.

iii. Synergistic effect: The synergistic effect between ZnO nanoparticles and nanocellulose can further enhance the photocatalytic activity by providing additional active sites for the adsorption and degradation of pollutants.

The adsorption and photocatalytic degradation kinetics were analyzed using pseudo-first-order and pseudo-second-order models. The pseudo-second-order kinetic model was found to be the best fit for both adsorption and photocatalytic degradation processes, indicating that chemisorption is the rate-limiting step. The

calculated rate constants (k_2) and equilibrium adsorption capacities (q_e) for the different materials are summarized in table below.

Material	k_2 (g mg^{-1} min^{-1})	q_e (mg/g)
Control	0.0062	0.9763
CNF	0.0345	2.3938
ZnO NPs	0.0325	4.2507
ZnO-CNF	0.0248	4.8641

Langmuir Isotherm showed the maximum adsorption capacity (q_{max}) of the ZnO-CNF nanocomposite as 43.11 mg/g, which is significantly higher than that of ZnO NPs (21.38 mg/g) and CNF (9.18 mg/g). This indicates that the ZnO-CNF nanocomposite has a higher number of available adsorption sites. The Freundlich isotherm constants (k_F and 1/n) were determined for each adsorbent. The higher values of k_F and 1/n for the ZnO-CNF nanocomposite suggest a stronger affinity and higher adsorption capacity compared to CNF and ZnO NPs. The Temkin isotherm suggests that the heat of adsorption decreases linearly with surface coverage. The higher values of B_T and A_T for the ZnO-CNF nanocomposite indicate a stronger interaction between MB molecules and the adsorbent surface.

This study highlights the potential of algae-derived nanocellulose and ZnO-CNF nanocomposites for sustainable and eco-friendly applications in water purification and environmental remediation. Future research should focus on optimizing the synthesis process, exploring novel applications, and assessing the long-term environmental impact of these materials.